NEW TEMPLATES FOR PORPHYRIN NANORINGS

A thesis submitted to the board of the Faculty of Physical Sciences in partial fulfillment of the requirements for the degree of

Doctor of Philosophy of the University of Oxford

By

Pengpeng Liu

The Chemistry Research Laboratory and Balliol College, Oxford

Hilary Term 2016

NEW TEMPLATES FOR PORPHYRIN NANORINGS

D.Phil Thesis, Michaelmas Term 2015
Pengpeng Liu, Balliol College, University of Oxford

Abstract

New templates based on the structures of cyclodextrin and ferrocene have been developed for porphyrin nanoring syntheses. Flexibility can be taken into account of the molecular template design. The flexibility of butadiyne bonds allow the formation of a 5-porphyrin nanoring, which is the smallest fully-conjugated porphyrin nanoring to date.

Chapter 1 describes the general information of porphyrin, cyclodextrin and ferrocene, which are used as basic structures in the thesis. The polymer chemistry of porphyrins is reviewed as the background knowledge of the work. Meanwhile, chelate cooperativity of supramolecular systems and the corresponding measurement method are introduced.

Chapter 2 presents the chemistry towards 6- and 7-porphyrin nanorings using molecular templates **T6*** and **T7***, which are based on the α- and β-cyclodextrin scaffolds. The cooperativity of respective template-nanoring complexes was investigated by UV-vis titrations. *Chapter 3* describes the Vernier-templated syntheses of porphyrin nanorings using **T7*** and different linear porphyrin oligomers (***l*-P2**, ***l*-P4** and ***l*-P8**). Both chapters focus on the influences of spatial preorganization and flexibility to the cooperativity of supramolecular systems.

Chapter 4 introduces the chemistry towards a ferrocene-based five-dentate template **T5** which successfully directed the syntheses of 5-porphyrin nanorings. Investigation of the cooperativity in the nanoring-template system is presented. *Chapter 5* investigates the cooperativity between **T5** and linear porphyrin oligomers in detail; and focuses on the contribution of partially-bound complexes in the measurement of equilibrium constants of the host-guest systems. Both chapters focus on the influences of intramolecular strain to the cooperativity in supramolecular systems.

Chapter 6 provides experimental procedures and characterization data of the known and novel compounds synthesized in the course of completing the thesis.

Abbreviations

Ar	Aryl
Bpin	4,4,5,5-Tetramethyl[1,3,2]dioxaborolan-2-yl
BQ	Benzoquinone
Bu	Butyl
CD	Cyclodextrin
COSY	Correlation spectroscopy
Cp	Cyclopentadienyl
d	Doublet (in NMR)
Da	Dalton
DABCO	1,4-Diazabicyclo[2.2.2]-octane
dba	Dibenzylideneacetone
DCC	*N*,*N*'-Dicyclohexylcarbodiimide
DCM	Dichloromethane
DCTB	*trans*-2-[3-(4-*tert*-Butylphenyl)-2-methyl-2-propenylidene]malononitrile
DDQ	2,3-Dichloro-5,6-dicyano-*para*-benzoquinone
DFT	Density functional theory
DMAP	4-Dimethylaminopyridine
DNA	Desoxyribonucleic acid
DOSY	Diffusion-ordered NMR spectroscopy
DPM	Dipyrromethane
EM	Effective molarity
ESI	Electrospray ionization
Et	Ethyl
Fc	Ferrocene, ferrocenyl
GPC	Gel permeation chromatography
h	Hour(s)
HOMO	Highest occupied molecular orbital
HSQC	Heteronuclear single-quantum correlation spectroscopy
i	Iso
IR	Infrared
LH	Light harvesting system
LUMO	Lowest unoccupied molecular orbital
MALDI	Matrix-assisted laser desorption ionization
m	multiplet (in NMR)
m	Meta
Me	Methyl
MM	Molecular mechanics

MW	Molecular weight
NBS	*N*-Bromosuccinimide
NIR	Near-infrared
NMO	*N*-Methylmorpholine *N*-oxide
NMR	Nuclear magnetic resonance
NOESY	Nuclear Overhauser effect spectroscopy
o	Ortho
p	Para
Ph	Phenyl
PL	Photoluminescence
PLE	Photoluminescence excitation
ppm	Parts per milliom
PS	Photosystem
Q band	Porphyrin S_0-S_1 absorption band
r.t.	Room temperature
s	Singlet (in NMR)
SEC	Size exclusion chromatography
SPhos	2-Dicyclohexylphosphino-2',6'-dimethoxybiphenyl
STM	Scanning tunneling microscopy
t	Triplet (in NMR)
t	Tertiary carbon
TBAF	Tetra-*n*-butylammonium fluoride
TBDMS	*tert*-Butyldimethylsilyl
TEA	Triethylamine
TFA	Trifluoroacetic acid
THF	Tetrahydrofuran
THS	Trihexylsilyl
TLC	Thin layer chromatography
TMEDA	Tetramethylethylenediamine
TMP	2,2,6,6-Tetramethylpiperidine
TOF	Time of flight
UV	Ultra-violet
vis	Visible
δ	Chemical shift
ε	Extinction coefficient
θ	Site occupancy of colored species
λ	Wavelength

Acknowledgements

First of all, I would like to thank my supervisor, Prof. Harry L. Anderson FRS, for his guidance on the projects in the course of completing my DPhil degree. It is a great experience working with Harry to be well trained as a chemist. His experience in chemistry, relentless effort to pursue the perfection of experimental results and academic writing, plus nice ideas in the molecular design, have all impressed me and they will be sure to give a long-lasting influence to my future research.

I would like to thank Clarendon Fund in collaboration with Jason-Hu Scholarship from Balliol College to provide funding to support my study in Oxford. Thanks to Prof. Tim Claridge, Dr. Barbara Odell, Ms. Tina Jackson and Mrs. Maria Marshall (Oxford Chemistry) for their help in the NMR measurement and the analysis of some of the NMR spectra. Thanks to Mr. Colin Sparrow (Oxford Chemistry) for his training in the MS instruments and EPSRC mass spectrometry service (Swansea) for MS spectra of some of the porphyrin nanoring samples. Thanks to Prof. T. Silviu Balaban (Aix-Marseille, France) for the measurements of circular dichroism spectra of the cyclodextrin-templated porphyrin nanorings and Juliane Gong (Laura M. Herz group, Oxford Physics) for measuring the photoluminescence and photoluminescence excitation spectra of ferrocene-templated porphyrin nanorings. Thanks to Dr. Qianfu Luo, Nuntaporn Kamonsutthipaijit, Dr. Cécile Roche, Dr. Ibrahim Bulut and Martin Peeks for sharing some of the starting materials for the reactions.

Thanks to Dr. Patrik Neuhaus, Dr. Dmitry Kondratuk and Dr. Christiane Knappke for their guidance and help in the starting one and half years of my DPhil study. It is a great experience working with them and asking for suggestions from them. Thanks to the members in HLA group, especially Nun, Dima, Patrik, Igor, Christiane, Cécile, Julien, James and Anjul, for the nice experiences working in the same lab.

I am grateful of the experience studying at Oxford, a place of old-fashioned fanciness and the residency of world-leading ideas. It is a great pleasure to visit the museums, libraries and concerts and to talk to people studying philosophy, classics, history, literature and all other versatile subjects in Oxford. Thanks to Balliol College people and University Counseling service for providing convenient living conditions and necessary help when I was in trouble.

Last but not least, I would like to thank my family and friends in China and in Oxford for their unconditional support in my life. All your support and help have given me motivations to work hard and to work smart. Many thanks to everyone.

Table of Contents

Chapter 1

Introduction

This chapter introduces the basic structures utilized in the whole thesis, including porphyrins, cyclodextrins and ferrocenes. As the whole work explores new possibilities in the template-directed syntheses of cyclic porphyrin oligomers, the chemistry of butadiyne-linked porphyrin oligomers is generally reviewed. Since a major part of the thesis involves the investigation of the cooperativity inside supramolecular systems, cooperativity itself, methods to investigate the cooperativity of supramolecular systems and related parameters, particularly effective molarity, are introduced.

1.1 Porphyrins – Properties and Applications

Porphyrins are a category of compounds consisting of four pyrrole units with α positions connected by methine bridges. Porphine is the simplest porphyrin.[1] As an aromatic macrocycle with many reactive sites,[2] the porphyrin structure can be chemically functionalized with various groups on both *meso*- and β-positions. The cavity of the structure contains four N atoms as ligands, making it possible to coordinate various metal atoms to form metalloporphyrins.

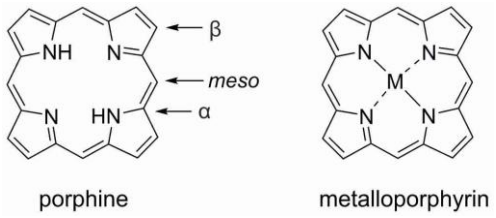

Figure 1.1 Structure of porphine and metalloporphyrin.

As a rigid structure with versatile chelating properties, metalloporphyrins and analogous structures are widely found in Nature, as they function in many biochemical processes. Haem is a group of iron porphyrin derivatives functioning as cofactors majorly in hemoglobin and myoglobin, which transfer oxygen in blood.[3] Cobalamin (vitamin B_{12}) is a group of cobalt porphyrinoids which function as cofactors transferring hydrogen or methyl in many metabolic processes.[4]

With rich delocalized π electron systems (total 26 delocalized π electrons), metalloporphyrins are readily excited by light and they are redox active. This photophysical property again makes porphyrins and their analogues the choice of Nature.

Light-harvesting complexes (LHC) and photosystems (PS) are the major molecular machines responsible for the light-induced charge separation and energy transfer, which is critical in photosynthesis in plants and in bacteria - the procedure of harvesting energy from the sun. The quantum efficiency of the photon-induced charge separation is extremely high because the concentration of dyes in PS and LHC is very high and the dyes cover a wide range of spectrum (even to the IR region). These dyes (cofactors in the membrane proteins) are often arranged in a circular pattern to facilitate the energy transfer between the subunits of LHC and PS.[5-7] As is shown in **Figure 1.2**, Shen, Kuang and co-workers have recently reported a high-resolution

structure of PSI-LHCI supercomplex of *Pisum sativum* (pea), which consists of 16 subunits (12 PS subunits and 4 LHC subunits).[8] The 600-kilodalton membrane protein supercomplex contains 155 chlorophylls (Chls) as cofactors, and 57 of them are located in LHCI. The high-resolution PSI-LHCI structure gives insight to the excitation and energy transfer in the light harvesting systems of Nature.

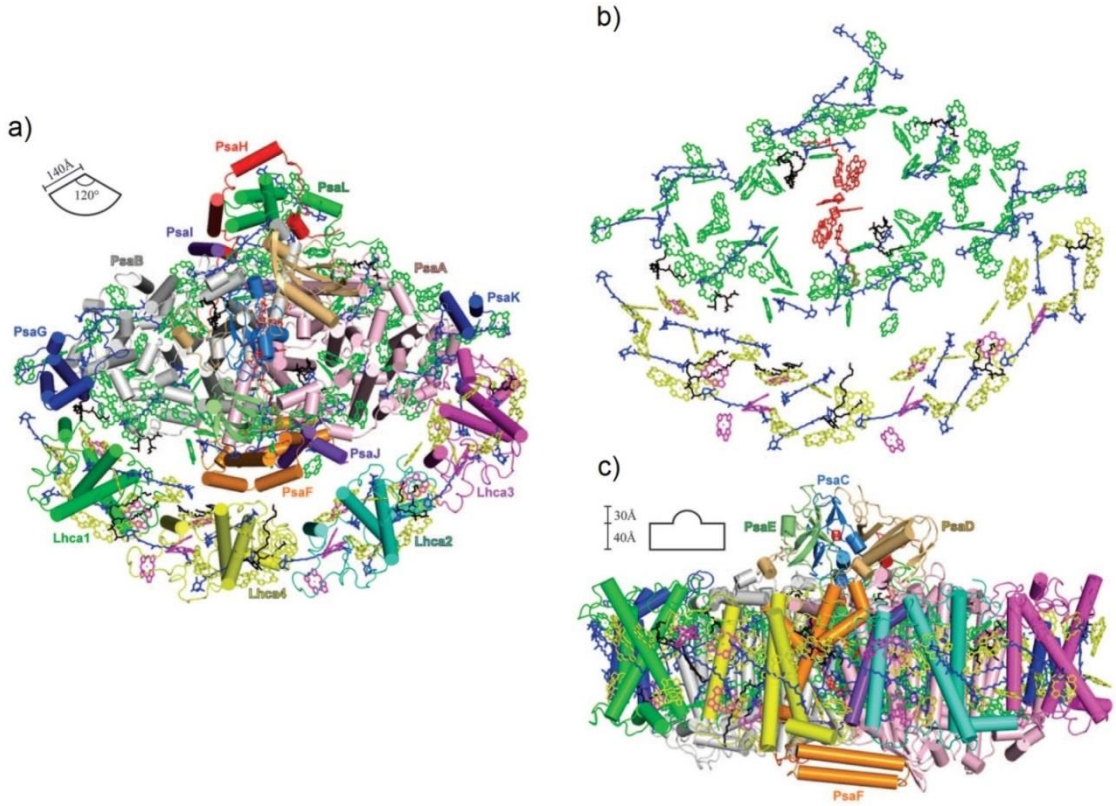

Figure 1.2 Structure of the PSI-LHCI supercomplex from *Pisum sativum* at a resolution of 2.8 Å. a) View along the membrane normal from the stromal side. b) Arrangement of pigments and other cofactors (lipids, Fe_4S_4 clusters and phylloquinones), with the view direction same as in a). For clarity, the protein backbones and phytol chains of Chls are omitted. c) Side view of the PSI-LHCI supercomplex from the LHCI side, with the phytol chains of Chls omitted. Color codes for cofactors: green, Chls a of PSI core complex; yellow, Chls a of LHCI; magenta, Chls b of LHCI; blue, carotenoids; black, lipids; red, cofactors of the electron transfer chain (Chls a, phylloquinones, and Fe_4S_4 clusters). Adapted with permission from ref. 8, Copyright 2015 American Association for the Advancement of Science.

The choice of Nature makes porphyrin structures interesting to many chemists and porphyrin chemistry has been thriving for decades as a result. Many artificial systems have been constructed using porphyrins. These include non-linear optical systems,[9] imaging in bio-systems,[10,11] photovoltaics[12,13] and other electro-optical systems.

An example of the applications of porphyrins in artificial systems is dye-sensitized solar cells

(DSSCs).[14] As is shown in **Figure 1.3**, The major components of DSSCs are sensitizing dyes, TiO_2 nanoparticles, conducting electrodes and electrolyte mediator. The dye is excited by the photon, with an electron injected into the TiO_2 nanoparticle, followed by the electron circulating in the outer circuit to generate electricity, and finally the electron goes back to the dye through the electrolyte mediator. The DSSC is a complex system and all components have been extensively investigated, including sensitizing dyes. In a report from Grätzel and co-workers in 2014, a porphyrin structure was functionalized into the "donor–π–acceptor" model (**Figure 1.3c**), with a bulky amine electron donor on the left and carboxylic acid electron acceptor on the right. The "donor–π–acceptor" model maximizes conjugation and facilitates charge transfer inside the molecule; the proquinoidal benzothiadiazole unit on the acceptor side functions as the co-sensitizer along with porphyrin; and the bulky alkyl chains minimize undesired charge recombination processes (dashed arrows in **Figure 1.3b**). As a result, the power conversion efficiency reaches a very high level at 13%.[15]

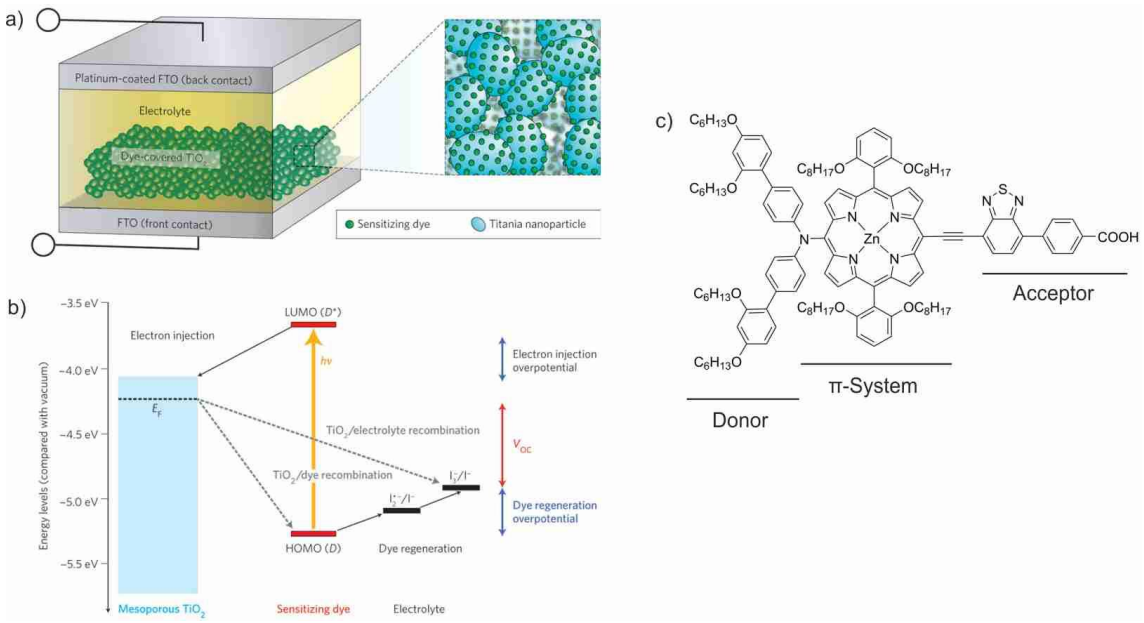

Figure 1.3 a) Composition of DSSCs. b) Energy level and device operation of DSSCs. c) A porphyrin dye used in dye-sensitized solar cell system giving high power conversion efficiency. Figures a) and b) are adapted from ref. 14 with permission, Copyright 2015 Nature Publishing Group.

To take a further step in the exploration of porphyrin chemistry and its applications, attempts have been made towards the construction of versatile oligomeric/polymeric porphyrin systems, which is presented in the following section of this chapter.

1.2 Conjugated Porphyrin Oligomers with Butadiyne Linkers

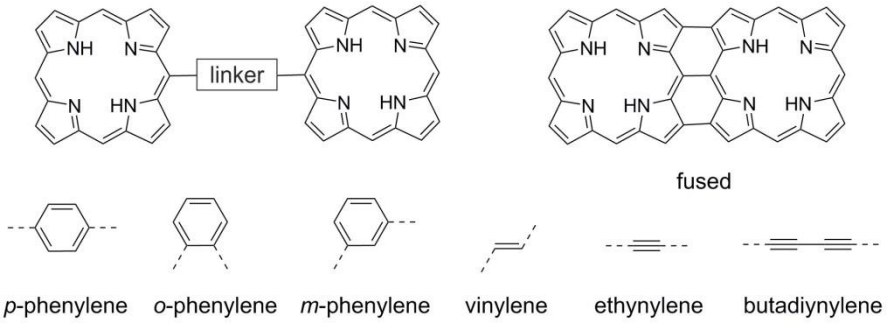

Figure 1.4 Common strategies to link porphyrin units.

Oligomeric and polymeric porphyrin structures are of much interest in molecular engineering since porphyrin units in multi-porphyrin systems can work hand in hand to create delocalization of excited states or charge separation states and function efficiently.[16,17] In fact, Nature's light harvesting systems are multi-porphyrin systems with porphyrin units interacting with each other through many types of interactions (H-bond, π-π interaction, etc.) including covalent bonding. As is shown in **Figure 1.4**, the linkers between porphyrin units are versatile; selected examples include C–C single bonds,[18] ethynylene (acetylene) bonds,[19] butadiynylene (butadiyne) bonds,[16] and phenylene (*ortho*-,[20] *meta*-[21,22] and *para*-[23]) groups. As the work presented in the thesis is based on the butadiyne-bridged porphyrin nanorings, this section focuses on the chemistry of butadiyne-linked porphyrin oligomers.

1.2.1 Optoelectronic Properties of Porphyrin Monomer and Oligomers

All porphyrins bear strong colors and the word "porphyrin" is derived from the Greek word πορφύρα, which means purple.[24] The absorption spectra of typical porphyrin monomers include a strong Soret band (B band), the transition to the second excited state ($S_0 \rightarrow S_2$), and a relatively weak Q band, the transition to the first excited state ($S_0 \rightarrow S_1$). As there is rapid internal transition from S_2 to S_1, fluorescence can only be detected from S_1.[16] Gouterman's four-orbital model is used to explain the phenomenon, with the two bands arising from π-π* transitions.[25] In D_{4h} symmetry porphyrins, the four frontier orbitals consist of two π orbitals a_{1u} (HOMO) and a_{2u} (HOMO-1), and a degenerate pair of π* orbitals e_{gx} and e_{gy} (both LUMO). The two highest occupied π orbitals a_{1u} and a_{2u} have about the same energy, so it might be expected that two peaks (generated from $a_{1u} \rightarrow e_g$

and $a_{2u} \rightarrow e_g$) with similar wavelengths and intensities would appear in the spectrum. However, the two transitions mix with each other by a process called configurational interaction, causing the two bands to differ substantially in wavelength and in intensity. **Figure 1.5** shows the structure, molecular orbitals, states and absorption spectrum of a model compound zinc octaethylporphyrin (ZnOEP). Modifications at *meso*- or β-positions could give alteration to the π/π* orbital systems and affect the porphyrin's optoelectronic properties. *meso*-Positions have higher frontier orbital coefficients compared to β-positions, so modifications at *meso*-positions usually give a more significant change compared to modifications at β-positions. The commonly used *meso*-aryl porphyrins do not have significant difference in optoelectronic properties compared to *meso*-unsubstituted porphyrins. This is caused by the large dihedral angles between porphyrin and aryl plane and conjugation is minimized.[16]

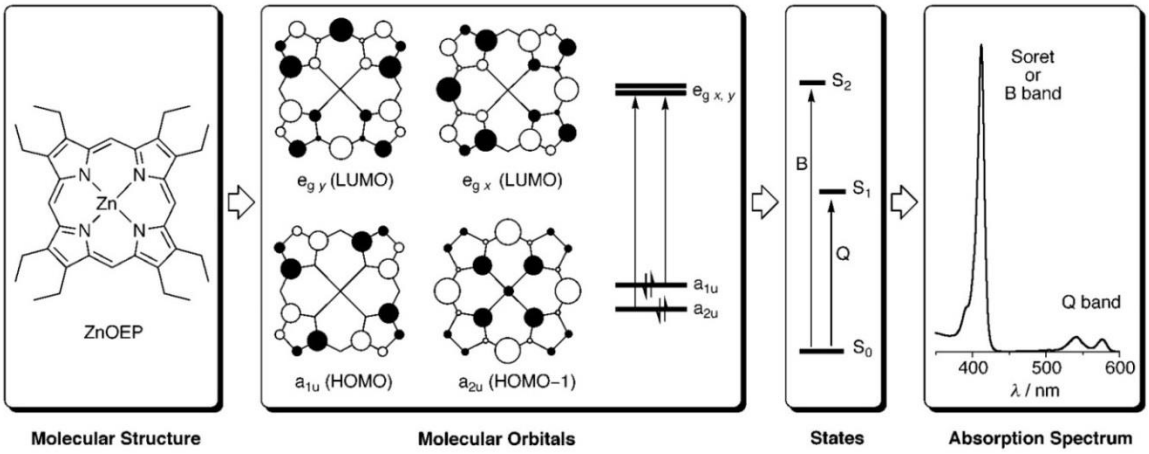

Figure 1.5 Structure, molecular orbitals, states and absorption spectrum of zinc octaethylporphyrin. Adapted with permission from ref. 16, Copyright 2015 Royal Society of Chemistry.

For linear porphyrin oligomers with butadiyne linkers, the Q bands have large red-shifts compared to porphyrin monomers.[26] DFT studies of the butadiyne-linked porphyrin dimers have revealed that the frontier orbitals responsible for the Q band spread over the butadiyne linker, which means conjugation has effects on Q band.[27] Also, the gaps between HOMO and LUMO decrease as the length of the oligomer increases.[28]

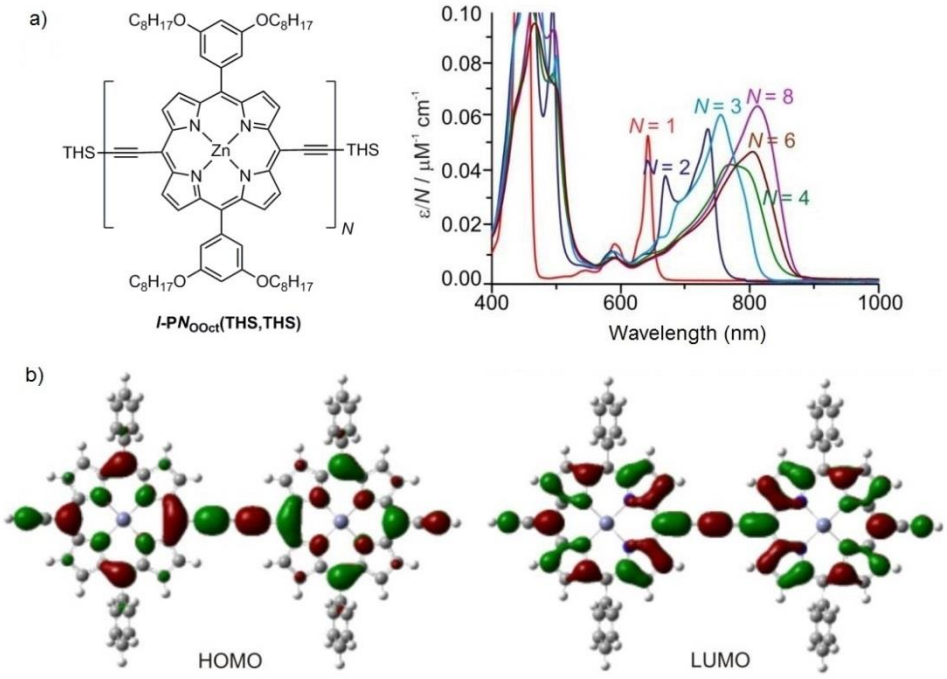

Figure 1.6 a) Absorption spectra in $CHCl_3$/1% pyridine of butadiyne-linked linear porphyrin oligomers **l-P*N*$_{OOct}$(THS,THS)**. Pyridine prevents the aggregation effects of porphyrins; spectra adapted with permission from ref. 26. b) HOMO and LUMO of butadiyne-linked porphyrin dimer. Adapted with permission from ref. 27, Copyright 2015 American Chemical Society.

1.2.2 Chemistry of Linear Butadiyne-Linked Porphyrin Oligomers

In the chemistry of butadiyne-linked porphyrin oligomers, butadiyne linkers can be easily constructed by Glaser coupling.[29] Johnson and co-workers reported the first butadiyne-linked porphyrin dimer in 1978, with the form of porphyrin units as octaethylporphyrins.[30] Ogawa and co-workers reported an example of butadiyne-linked porphyrin polymers being applied as molecular wire in 2006.[31]

Anderson's group has made major efforts in exploring this field of chemistry and the corresponding supramolecular chemistry based on porphyrin oligomers with butadiyne linkers. The first report investigated confined conformations of porphyrin dimer lattices by forming porphyrin ladders using bidentate ligands in 1994.[32] At this stage, the porphyrins had alkyl or alkyl-ester substituents on β-positions and the *meso*-positions were void if they were not connected to butadiyne linkers (**Figure 1.7a**). However, as the number of porphyrin units increase, their solubility decreases substantially and more solubilizing groups are needed to make the compounds soluble in ordinary solvents. The β-positions become unsubstituted and the previously void *meso*-positions are functionalized by aryl groups bearing bulky alkyl, alkyloxy, or alkylsilyl

substituents.[33-36] As is shown in **Figure 1.7b**, the *meso*-aryl groups perpendicular to the porphyrin plane are functionalized with bulky groups (R_2), which do not affect significantly on the electronic properties of the porphyrin units. This reduces the aggregation effects of the porphyrins and thus improves the solubility of the linear porphyrin oligomers.

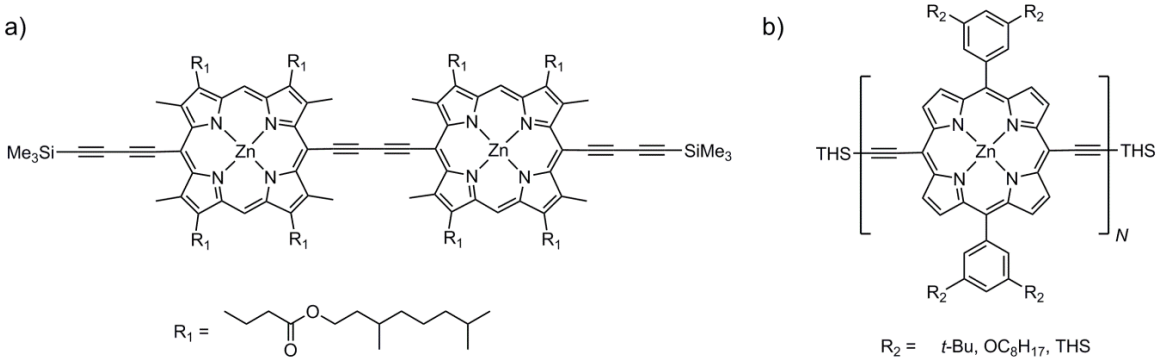

Figure 1.7 a) The structure of an early-stage butadiyne-linked porphyrin dimer in the Anderson group (ref. 32). b) The structure of linear butadiyne-linked porphyrin oligomers commonly used in the last 15 years.

As is shown in **Scheme 1.1**, the synthesis of acetylene-functionalized porphyrin monomer (***l*-P1**) has been well refined during the exploration of the chemistry of conjugated porphyrin oligomers in the Anderson group. Starting from pyrrole, dipyrromethane (DPM) is made as an intermediate for porphyrin synthesis.[37] DPM undergoes condensation with functionalized benzaldehydes[38,39] to form porphyrinogen; this is followed by DDQ oxidation to form free-base porphyrins (**$P1_{FB}$**).[40] **$P1_{FB}$** can be quantitatively converted into the corresponding zinc porphyrins (**$P1_{Zn}$**) by treating with $Zn(OAc)_2$. Electrophilic bromination on **$P1_{Zn}$** can selectively functionalize two *meso*-positions, giving dibrominated porphyrin (**P1(Br,Br)**).[41] Sonogashira coupling between **P1(Br,Br)** and trihexylsilylacetylene (THS-acetylene) gives the building block porphyrin monomer ***l*-P1(THS,THS)**, which is the starting point to construct conjugated porphyrin oligomers.

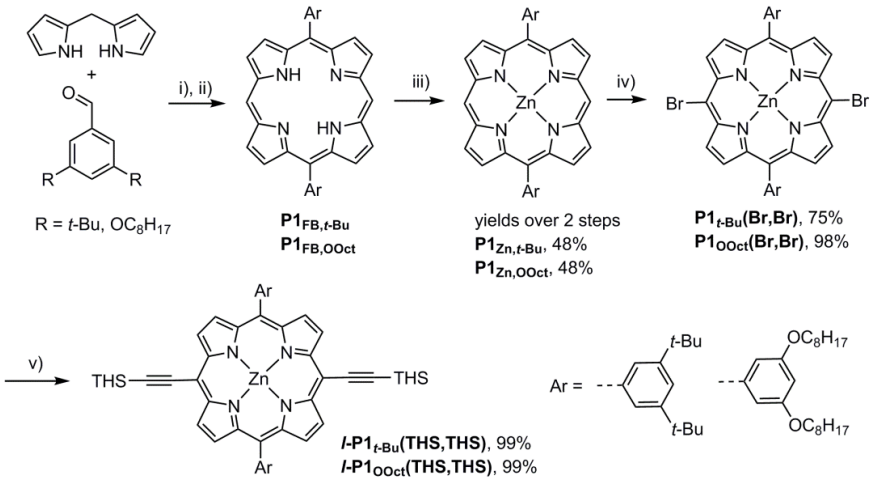

Scheme 1.1 The synthesis of building block porphyrin monomer ***l*-P1(THS,THS)**. i) TFA; ii) DDQ; iii) $Zn(OAc)_2$; iv) NBS; v) THS-acetylene, $Pd_2(dba)_3$, PPh_3, CuI, *i*-Pr_2NH.

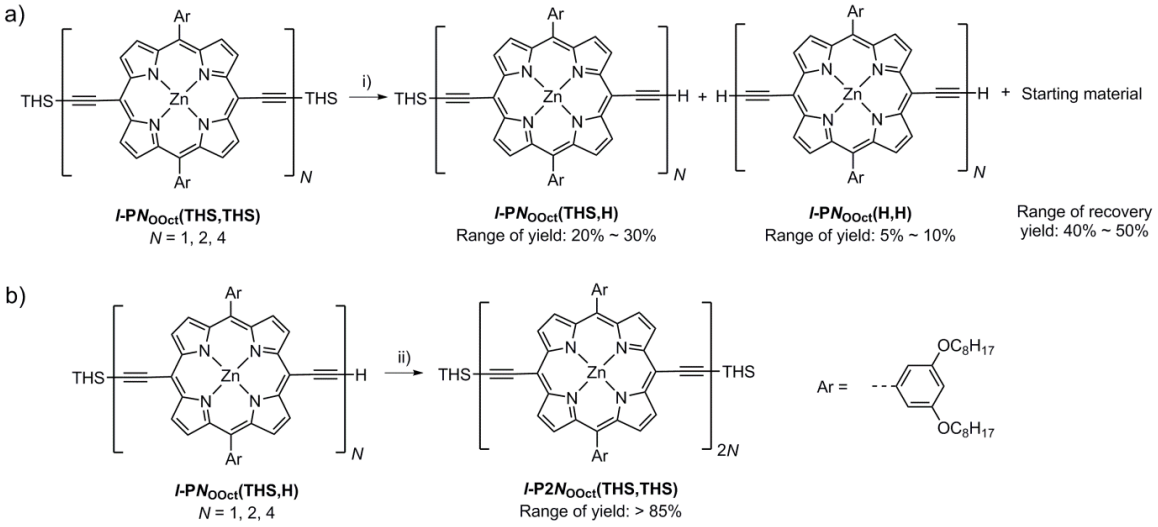

Scheme 1.2 a) Statistical deprotection of porphyrin oligomers, the yields come from ideal reaction results. b) Glaser coupling of mono-deprotected porphyrin oligomers to double the chain length. i) TBAF; ii) 1,4-benzoquinone, $Pd(PPh_3)_2Cl_2$, CuI, *i*-Pr_2NH.

The protecting THS groups on porphyrins can easily be removed by tetra-*n*-butylammonium fluoride (TBAF), which makes porphyrins available to couple into longer linear oligomers. Statistical deprotection, i.e. controlled deprotection of only one of the two THS groups to give ***l*-P*N*(THS,H)**, plays an important role in controlling the length of oligomer. Fully deprotected products ***l*-P*N*(H,H)** are formed as a byproduct. Pd/Cu co-catalyzed Glaser coupling of ***l*-P*N*(THS,H)** doubles the chain length in very high yield, as theoretically there is only one possible product ***l*-P2*N*(THS,THS)** (**Scheme 1.2**).[42]

As is shown in **Scheme 1.3**, a "capping" strategy can be used to produce linear porphyrin oligomers with versatile numbers of porphyrin units.[26] By coupling excess ***l*-P1(THS,H)** (the "cap") with fully deprotected porphyrin oligomers ***l*-P*N*(H,H)**, ***l*-P(*N*+2)(THS,THS)** could be obtained. The excess of the "cap" reduces the possibility of the self-coupling of ***l*-P*N*(H,H)**, making the product mixture less complicated. It should also be noted that if ***l*-P*N*(H,H)** is a long oligomer, the aggregation caused by π-π interaction will be strong and its reactivity will be low because of the aggregation. As a result, pyridine is added in the reaction to avoid the aggregation and to promote formation of the desired product.

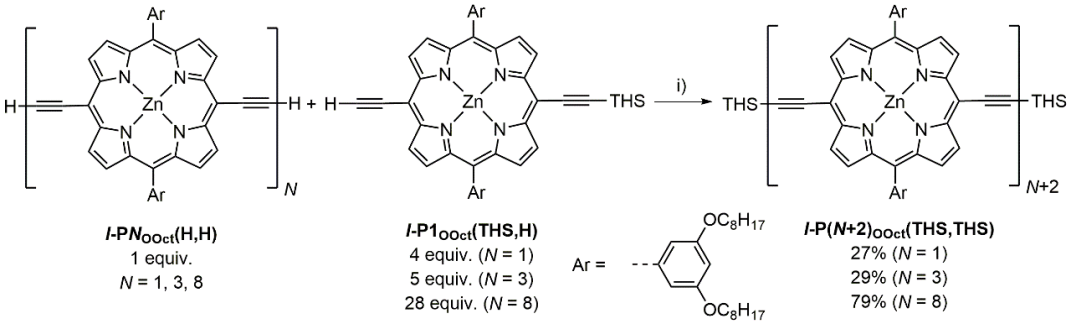

Scheme 1.3 "Capping" strategy to obtain linear porphyrin oligomers. The yields are cited from ref. 26 and calculated on the basis of ***l*-P*N*(H,H)**. i) 1,4-benzoquinone, $Pd(PPh_3)_2Cl_2$, CuI, *i*-Pr_2NH.

1.2.3 Chemistry of Cyclic Butadiyne-Linked Porphyrin Oligomers (Porphyrin Nanorings)

The construction of cyclic butadiyne-linked porphyrin oligomers is a further step towards the arrangement of porphyrins similar to the situation in Nature. The conjugated system of the porphyrin nanoring provides a primitive model for the study of excited state delocalization[43-45] and energy transfer[46] of the light harvesting process in plants and in bacteria.

Templates have a pivotal role in the chemistry of porphyrin nanorings, since both porphyrins and butadiyne linkers have straight linear π-conjugated conformations and we need influences from outside to endow the system with curvature. As metalloporphyrins bear possibilities to coordinate with axial ligands, multi-dentate molecules with ideal geometry could be used as templates. Molecular templates for the synthesis of cyclic porphyrin oligomers have been reported over 20 years ago by Sanders, although in that case the cyclic porphyrin oligomer systems were not fully conjugated.[21,47]

As is shown in **Scheme 1.4**, the first π-conjugated porphyrin nanoring was ***c*-P8$_{OOct}$·T8** reported in 2007.[48] The core of the template **T8** is a porphyrin with all eight β-positions linked to

pyridyl groups in a suitable distance. The starting material on the porphyrin side is a linear porphyrin octamer ***l*-P8$_{OOct}$(H,H)**; so the ring formation requires only one butadiyne bond formed in the reaction.

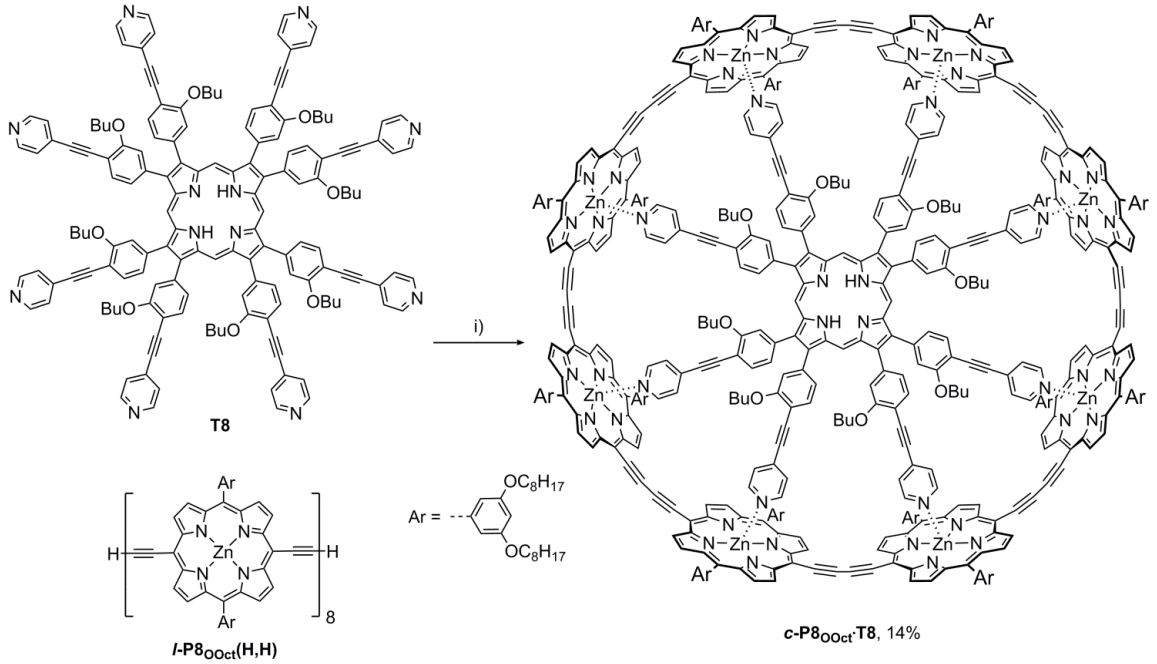

Scheme 1.4 The synthesis of the first porphyrin nanoring ***c*-P8$_{OOct}$·T8**. i) 1,4-benzoquinone, $Pd(PPh_3)_2Cl_2$, CuI, *i*-Pr_2NH.

Soon people found that molecular templates are more potent than expected, if the geometry is right and the structure is robust. **T6**, with its core as hexaphenylbenzene, has very good efficiency in synthesizing a wide scope of porphyrin nanorings which include ***c*-P6**,[43,49] ***c*-P12**,[50,51] ***c*-P24**,[52] ***c*-P30**,[53] and also a porphyrin nanotube.[54] Some highlights in this series of chemistry include: up to 62% yield of ***c*-P6$_{t\text{-Bu}}$·T6** from ***l*-P2$_{t\text{-Bu}}$(H,H)** and **T6** using the optimized Pd/Cu co-catalyst coupling condition (**Scheme 1.5a**);[42,43] 39% isolated yield of ***c*-P12$_{t\text{-Bu}}$·(T6)$_2$** from the Vernier-templating synthesis between ***l*-P4$_{t\text{-Bu}}$(H,H)** and **T6** (**Scheme 1.5b** and **Scheme 1.5c**);[50] the crystal structures of ***c*-P6$_{t\text{-Bu}}$·T6** and ***c*-P12$_{t\text{-Bu}}$·(T6)$_2$** being analyzed in detail;[43,51] a ring nesting inside another ring in the STM image of very large porphyrin nanorings such as ***c*-P40$_{OOct}$** (**Figure 1.8**, note that this compound is prepared through the Vernier-templating synthesis between ***l*-P10$_{OOct}$(H,H)** and **T8**); and a 12-porphyrin nanotube (**Figure 1.9**).[53]

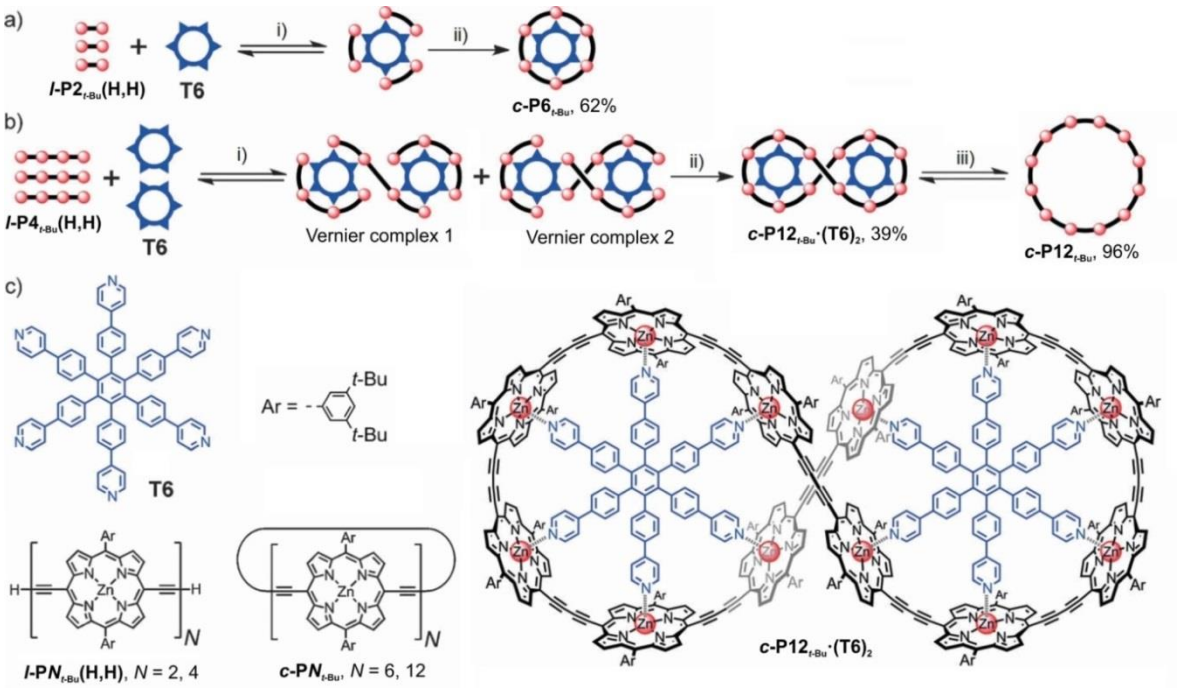

Scheme 1.5 a) Classical template-directed synthesis of ***c*-P6$_{t\text{-Bu}}$·T6** from ***l*-P2$_{t\text{-Bu}}$(H,H)** and **T6**. b) Vernier-templating synthesis of ***c*-P12$_{t\text{-Bu}}$·(T6)$_2$** from ***l*-P4$_{t\text{-Bu}}$(H,H)** and **T6**. c) Chemical structures. i) Self-assembly; ii) 1,4-Benzoquinone, $Pd(PPh_3)_2Cl_2$, CuI, *i*-Pr_2NH; iii) Pyridine. Adapted with permission from ref. 51, Copyright 2015 John Wiley and Sons.

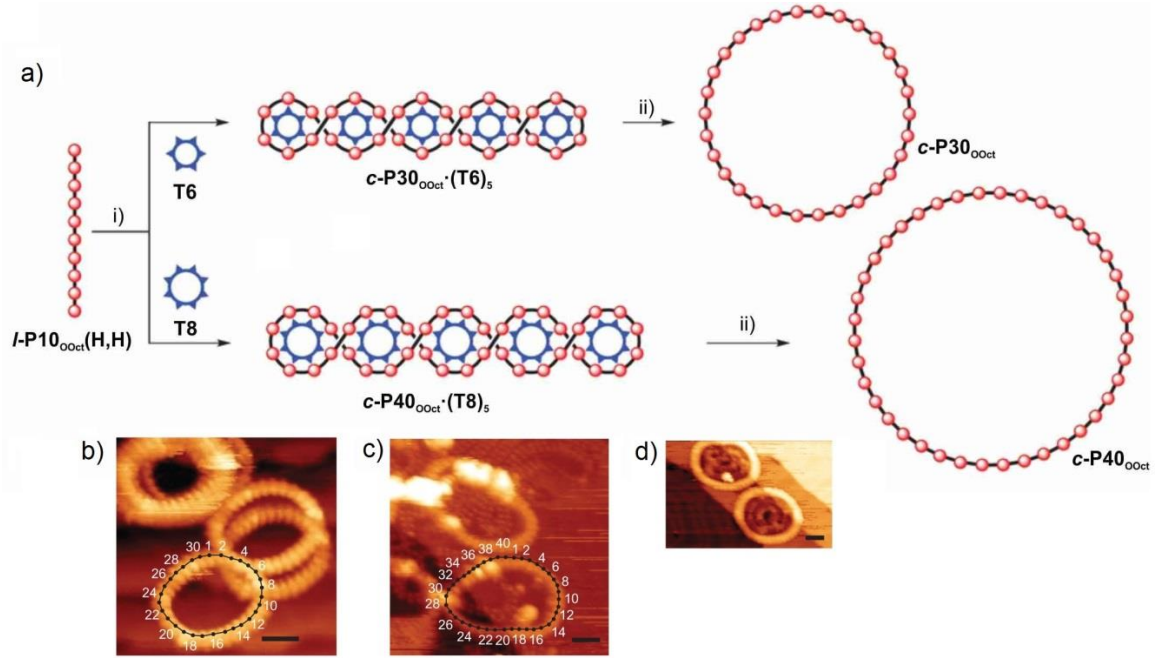

Figure 1.8 a) Vernier-templating syntheses of ***c*-P30$_{OOct}$** (from ***l*-P10$_{OOct}$** and **T6**) and ***c*-P40$_{OOct}$** (from ***l*-P10$_{OOct}$** and **T8**). i) 1,4-Benzoquinone, $Pd(PPh_3)_2Cl_2$, CuI, *i*-Pr_2NH; ii) Pyridine. STM images of b) ***c*-P30$_{OOct}$** and c) ***c*-P40$_{OOct}$**. d) Nested nanoring complexes of ***c*-P40$_{OOct}$**. All scale bars: 5 nm. Adapted with permission from ref. 53, Copyright 2015 Nature Publishing Group.

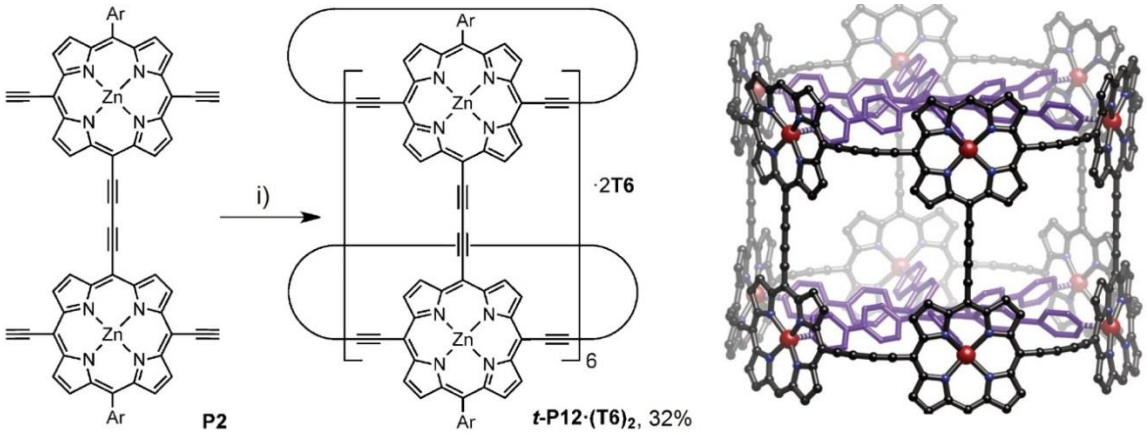

Figure 1.9 Synthesis of a porphyrin nanotube ***t*-P12·(T6)$_2$** and its calculated structure from molecular mechanics. i) **T6**, 1,4-benzoquinone, $Pd(PPh_3)_2Cl_2$, CuI, *i*-Pr_2NH. Ar = 3,5-di(trihexylsilyl)phenyl. In calculated structure, aryls and hydrogens are omitted for clarity. Adapted with permission from ref. 54, Copyright 2015 John Wiley and Sons.

Vernier-templating methodology is the foundation for the success of this chemistry.[55-57] For a template with *m* binding sites and a porphyrin oligomer with *n* binding sites, the Vernier product is the porphyrin nanoring with the number of porphyrin units as the lowest common multiple of *m* and *n*. The efficiency of Vernier-templating synthesis is very delicate, since the two components have influences on each other in the reactions and they have to be a perfect match in design.

In the template-directed synthesis of porphyrin nanorings, multiple ligands in the template work hand in hand to chelate to the porphyrin binding sites, making the binding between the template (guest) and the linear/cyclic porphyrin oligomer (host) very different from isolated binding processes. Thus the chelation in the host-guest system decides the efficiency of the synthesis. As is shown in the following section, the method to investigate chelate cooperativity inside supramolecular system is introduced.

1.3 Chelate Cooperativity of Supramolecular Systems

1.3.1 Entropy-Related Chelate Cooperativity

Cooperativity is a general concept reflecting the interplay between the interactions inside a multivalent supramolecular system,[58-60] and is thus crucial for understanding molecular recognition and supramolecular self-assembly which widely exist in bio-molecular systems such as the cooperative binding of oxygen by hemoglobin,[61] self-assembly of polypeptides into proteins,[62] and

cooperative supramolecular polymerization of biomolecules.[63]

For a specific binding, i.e. the binding between A and B in **Figure 1.10**, the bindings in the isolated state can be very different from the situation in the self-assembly system. In the chelate system shown in **Figure 1.10b**, the first binding forms an open complex (*o*-AA·BB); and this process can give changes to the second binding as compared to the isolated state (**Figure 1.10a**).

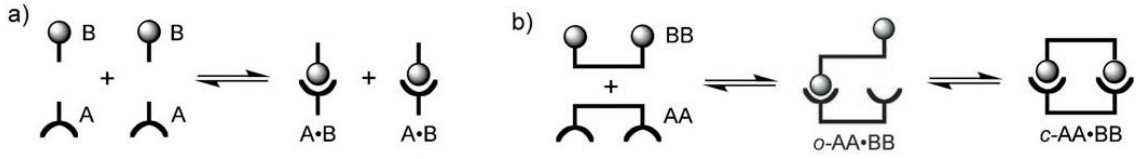

Figure 1.10 Chelate cooperativity inside a two-site closed self-assembly system. a) Isolated bindings (reference system). b) Closed self-assembly (chelate) systems. Adapted with permission from ref. 59, Copyright 2015 John Wiley and Sons.

Entropy change is the origin of chelate cooperativity. In the figure above, the first binding confines the second binding to a specific conformation, which generates entropy change and makes the binding more favored/disfavored. Many artificial chelate systems have been constructed to investigate the phenomenon: the contributions include works from Lehn (self-sorting in helicate self-assembly),[64] Williams (bindings between cell wall precursor analogs and antibiotics),[65] Anderson (preorganization in template-directed syntheses, also a theme in this thesis)[66] and Hunter (solvent effects on chelate cooperativity).[67]

1.3.2 Effective Molarity

Effective molarity (EM) is the critical parameter in evaluating the cooperativity of chelated systems at the microscopic level. It is a concept originally generated in physical chemistry to explain the reaction rate increase caused by proximity/orientation effects in intramolecular reactions. The theory was introduced into the area of biochemistry to explain the mechanisms of enzyme catalysis.[68] As is shown in **Figure 1.11**, the proximity effect causes a much faster intramolecular reaction, which is reflected from k_2/k_1, the kinetic effective molarity. As EM reflects the difference between intramolecular and intermolecular processes, its unit is molar for both thermodynamic and kinetic processes.

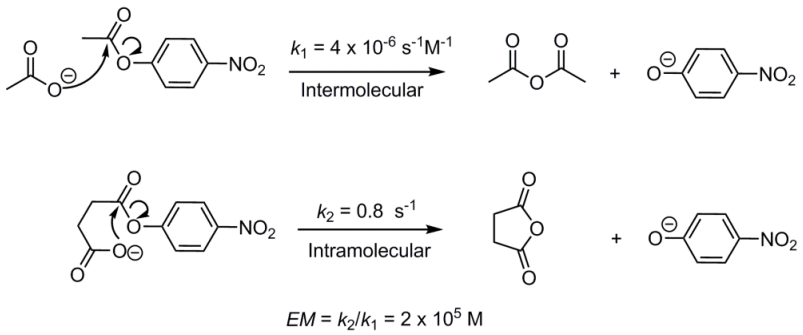

Figure 1.11 Kinetic effective molarity caused by proximity/orientation effects in intramolecular reactions. Figure adapted from ref. 68, Copyright 2015 W. H. Freeman and Company.

In supramolecular chemistry, the affinity between host and guest inside closed self-assembly system is related to thermodynamic effective molarity. As is shown in **Figure 1.12**, the 2-site 1:1 binding model shows the relationship between bindings in isolated states (intermolecular, K_A and K_B) and bindings in chelate states (intramolecular, EMK_A and EMK_B), and this difference is reflected by thermodynamic effective molarity.

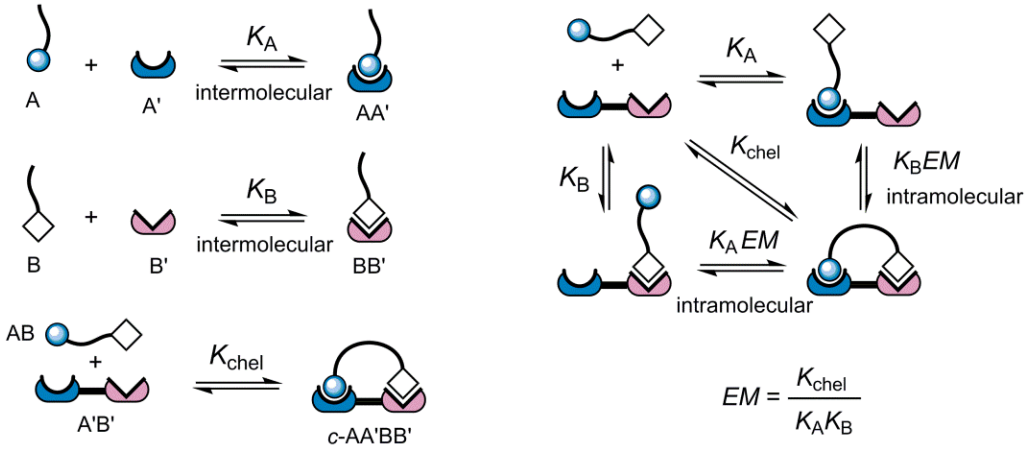

Figure 1.12 Thermodynamic effective molarity inside a 2-site 1:1 binding model system. Adapted with permission from ref. 66, Copyright 2015 American Chemical Society.

The physical meaning of EM is the free-energy change caused by the chelation process in the system. The free-energy of the formation of AA' and BB' (isolated states) are:

$$\Delta G_{\mathrm{AA'}} = -RTlnK_{\mathrm{A}} \quad (1.1)$$

$$\Delta G_{\mathrm{BB'}} = -RTlnK_{\mathrm{B}} \quad (1.2)$$

The free-energy of the formation of *c*-AA'BB' (chelate state) is:

$$\Delta G_{c-\mathrm{AA'\,BB'}} = -RTlnK_{\mathrm{chel}} = -RTlnEMK_{\mathrm{A}}K_B = \Delta G_{\mathrm{AA'}} + \Delta G_{\mathrm{BB'}} - RTlnEM \quad (1.3)$$

Thus EM directly reveals the free-energy change caused by the chelation process, which indicates that EM is an entropy-related term.

For systems constructed by templates and linear/cyclic porphyrin oligomers, every additional chelating ligand's binding generates a new EM. As is illustrated in **Figure 1.13**, the process from 2-site chelation to 4-site chelation involves two EMs. For a chelating system with *n* sites of binding, there are (*n* - 1) EMs involved in the process starting from single-site binding.

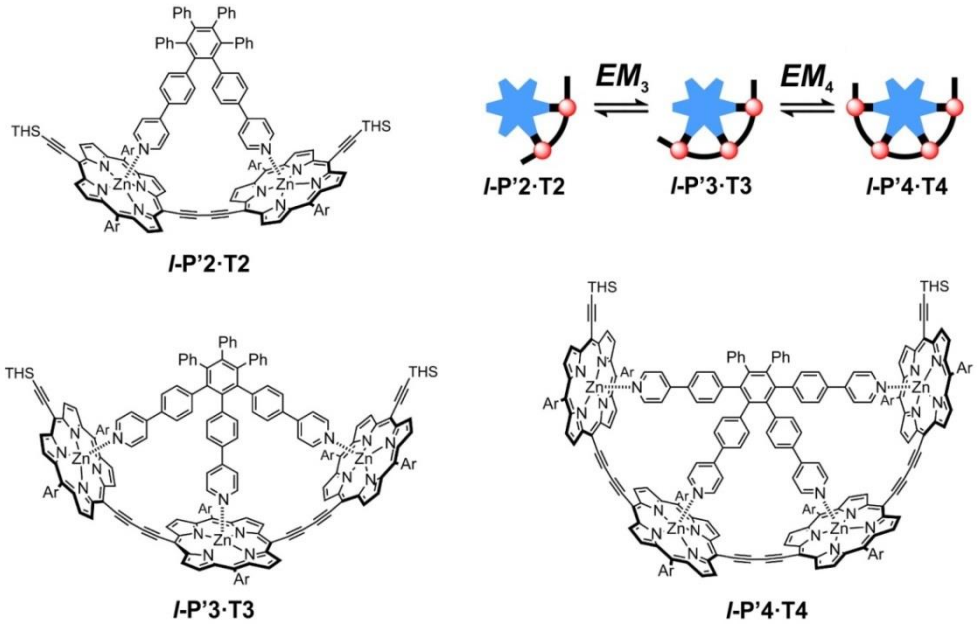

Figure 1.13 Effective molarities involved in the part of chelating process between templates and linear porphyrin oligomers. Ar = 3,5-bis(octyloxy)phenyl. Adapted with permission from ref. 66, Copyright 2015 American Chemical Society.

1.3.3 Measurement of Effective Molarities

Thermodynamic effective molarity is determined by the association constants of related complexes; so measurement of EM is essentially the measurement of the association constants of related complexes. For metalloporphyrins which bear strong color, their electronic properties change as they bind to ligands, which leads to color change and this property can be utilized for UV-vis titrations.

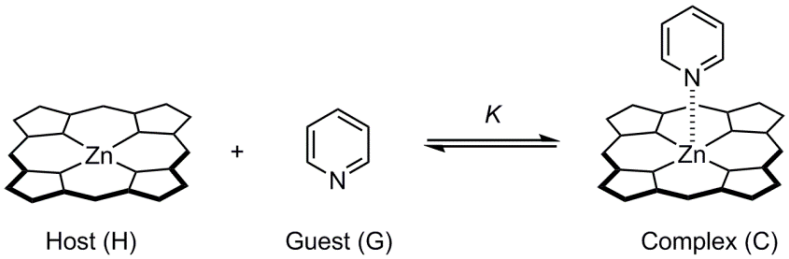

Scheme 1.6 Formation of a host-guest complex by a zinc-porphyrin (host) and pyridine (guest). The nitrogen atoms, double bonds and substituents are omitted for clarity.

For the formation of single-site 1:1 complex, the association constant K between host and guest is:

$$K = \frac{[\mathrm{C}]}{[\mathrm{H}][\mathrm{G}]} \tag{1.4}$$

In the titration experiments of the host-guest systems, the host porphyrin concentration usually stays constant and guest ligands are added into the system stepwise to give a series of spectral changes, which reflect the site-occupancy states (θ, indicating the proportions of the porphyrins in bound state) of colored porphyrin units. We can deduce the relationship between K and θ through equation (1.4) and fit the isotherm to generate the value of K. The detailed calculation steps will be shown in relevant chapters.

As equation (1.4) is only relevant to the stoichiometry between host and guest, the association constant of a multi-site binding complex can be generated from the equation provided the stoichiometry is 1:1 and the measured association constants do not exceed 10^7 M^{-1} so that they can be measured accurately.[69] For the multidentate binding in cyclic/linear porphyrin oligomer-template systems, the binding stoichiometry is 1:1; but the association constants are usually very high (higher than 10^7 M^{-1}) to give a square 1:1 binding isotherm and the error range is too high.[69] Indirect measurements through denaturation cycle are needed to determine the association constants.[59,66] The detailed description of the denaturation cycle will be shown in **Chapter 2**.

1.3.4 Preorganization and Template Design

In my DPhil projects, the preorganization properties of templates and their influences on the supramolecular systems are the main focus of investigation. The previously reported templates all have rigid structure and the preorganization effect gives high effective molarity in ***c*-P6$_{t\text{-Bu}}$·T6** and this causes the high performance of **T6** in the template-directed synthesis.[66] A question is raised: Does a template always need to be totally rigid to be successful for porphyrin nanoring synthesis? What is the role of flexibility in supramolecular systems? Cyclodextrins were chosen as a candidate in the template design for porphyrin nanoring syntheses to answer the questions since they are intrinsically symmetric (D_{6h} for α-cyclodextrin, D_{7h} for β-cyclodextrin) and structurally flexible.

In the porphyrin nanoring synthesis, formation of a cyclic porphyrin oligomer requires the

curvature of butadiyne bonds and this induces a free energy cost since the preorganization form of butadiyne bonds is linear. The free energy cost is compensated by chelation between ligands and porphyrin units. Another question is raised as follows: What is the limit to bend the butadiyne linker in porphyrin nanoring system? How poor can spatial preorganization be and how does it influence the cooperativity in the system? Based on butadiyne linkers, how small can a porphyrin nanoring be? To answer this question, we attempted to synthesize a 5-porphyrin nanoring using template-directed synthetic methodology and the D_{5h} symmetric ferrocene structure was chosen for template design.

In the following section, the chemistry of cyclodextrin and ferrocene towards porphyrin nanoring templates is introduced. Apart from the exploration of cooperativity, discovery of new templates will also be an incentive to expand the scope of porphyrin nanoring library and Vernier-templating synthetic methodology.

1.4 Cyclodextrin and Ferrocene Chemistry towards Templates

1.4.1 Cyclodextrin Chemistry

Cyclodextrin (CD) is a group of cyclic polysaccharides (dextrins) generated from degradation of starch by enzymes. The discovery of CD dates back to 1891 when the French pharmacist and chemist Antoine Villiers used the butyric ferment *Bacillus amylobacter* (*Clostridium butyricum*) to degrade potato starch.[70] Villiers found that a large proportion of the degradation product which can no longer be digested by the bacteria had the properties of dextrins (being stained red by iodine). They were difficult to hydrolyze any further, had "very different optical rotation properties" (chirality) and their crystals were resistant to the action of acid and water.

Such is the general chemical property of CDs. They are chemically robust and they contain useful hydroxyl groups which can be potentially functionalized. Common CDs include α-, β- and γ-CDs: the denomination is based on the number of the constituting sugar units.

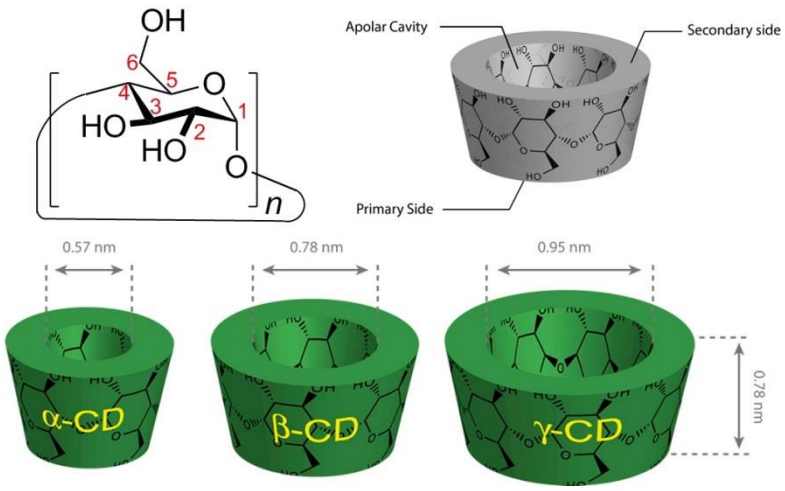

Figure 1.14 Top: Functional structural scheme of α-CD (*n* = 6), β-CD (*n* = 7) and γ-CD (*n* = 8). Bottom: Geometric dimensions of CDs. Adapted with permission from ref. 70, Copyright 2015 American Chemical Society.

The barrel-like CD molecule is rich in hydroxyl groups on the rim, making it soluble in many polar solvents. The cavity majorly contains glycosidic oxygen and C–H bonds, and is less polar (apolar, hydrophobic) and compatible with many organic molecules that are not soluble in water. The pharmaceutical industry applies the amphiphilicity of CDs in drug delivery.[71] Chemists focusing on the supramolecular properties of CDs usually thread its cavity to form rotaxanes, polyrotaxanes and catenanes.[72-76] In this thesis, however, we are focusing on the symmetry of CDs and their use as cores for the construction of porphyrin nanoring templates. This section introduces a synthetic route for functionalizing the hydroxyl groups while retaining the symmetry.[77]

In each sugar unit of CDs, there are three hydroxyl groups: two secondary hydroxyl on 2- and 3-positions (secondary side) and one primary hydroxyl on 6-position (primary side). Modification of CDs takes place on the nucleophilic hydroxyl groups, and the reactivity of the three positions are different. 6-Position hydroxyl (6-OH) is the most basic and usually the most nucleophilic; 2-OH is the most acidic; and 3-OH is the most inaccessible.[78,79] In our design of the template, as will be shown in **Chapter 2**, the linkers between CDs and pyridyl ligands are made through 6-OH. At the same time, we would like the 2- and 3-positions to be inactive in the process of template synthesis. We adopted the reported compound per-2,3-di-*O*-methylcyclodextrin as the precursor for the CD templates.[80]

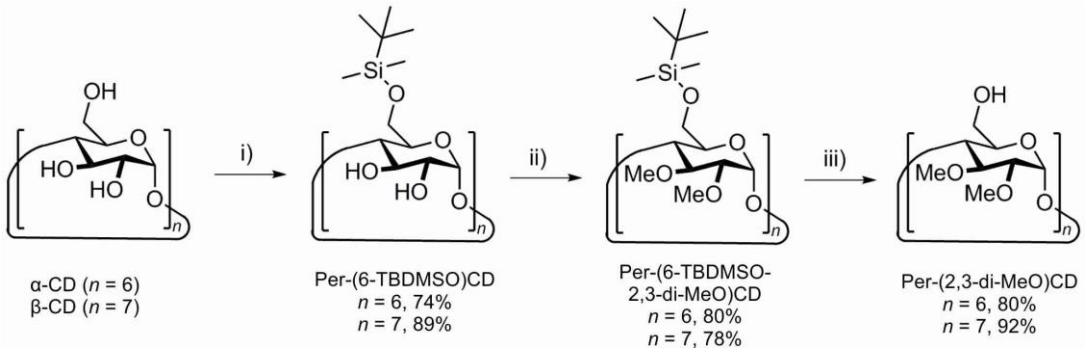

Scheme 1.7 Synthetic route to per-2,3-di-O-methylcyclodextrins as precursors for CD templates. i) TBDMSCl, imidazole; ii) NaH, MeI; iii) TBAF.

tert-Butyldimethylsilyl chloride (TBDMSCl) was found to be a selective protecting reagent on the 6-OH groups on CDs.[81] Trimethylsilyl chloride is too reactive and can react with all positions indiscriminately.[82] After the protection, all the 2-OH and 3-OH groups are "capped" by methyl groups by Williamson ether synthesis. The TBDMS group can be easily removed by TBAF, which gives the precursor per-2,3-di-*O*-methylcyclodextrins for use in the synthesis of the templates.[80]

1.4.2 Ferrocene Chemistry

Discovered in 1951,[83] ferrocene (Fc) is the archetypal organometallic sandwich compound constructed by the π-bonds between cyclopentadienyl (Cp) anion and iron(II). The two five-membered rings in the sandwich compound have aromaticity, thus ferrocene can undergo certain types of aromatic reactions, such as Friedel-Crafts acylation.[84] However, as the π-electrons are stabilized by the iron(II) cation, the reactivity of the π-system is quite low compared to a cyclopentadienyl anion. Functionalization on the Cp groups often needs rigorous reaction conditions: lithiation with *n*-BuLi or *t*-BuLi, then substitution.[85,86] As for application, ferrocene phosphine functionalized by chiral substituents can serve as chiral ligands in asymmetric catalysis.[87,88] Also, the reversible redox behavior of ferrocene has made it a standard in electrochemistry as Fc^{+}/Fc (0.64 V vs. the standard hydrogen electrode).

Two synthetic routes for modifying ferrocene into 5-fold symmetric Fc derivatives drew our attention since they provide potential precursors to build Fc-based molecular templates for porphyrin nanoring synthesis. In 2002, Hartwig reported a type of 1,2,3,4,5-pentaphenylferrocene phosphine as the ligand for asymmetric catalysis.[89] The synthetic strategy is to use the existing phosphine group to direct palladium metal into activating the five positions on the Cp ring opposite

to the ring that the phosphine group is positioned. In 2009, Williams changed the phenyl substituents into *para*-pyridyl substituents and used the product to build football-like supramolecular assemblies with metal ions.[90]

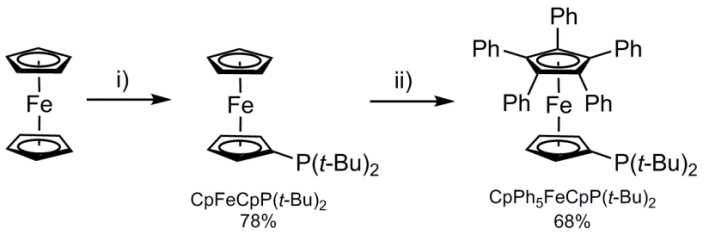

Scheme 1.8 The synthesis of a 1,2,3,4,5-pentaphenylferrocene phosphine by Hartwig Group. The yields are cited from ref. 89. i) *t*-BuLi, then $ClP(t\text{-}Bu)_2$; ii) $Pd(OAc)_2$, *t*-BuONa, chlorobenzene.

In 2008, Butler reported a stepwise method to synthesize 1,2,3,4,5-pentabromoferrocene.[91,92] The key to this method is 2,2,6,6-tetramethylpiperidine (TMP) ligand, which directs the lithiation position to the *ortho*-position of an existing substituent on the Cp ring.[93]

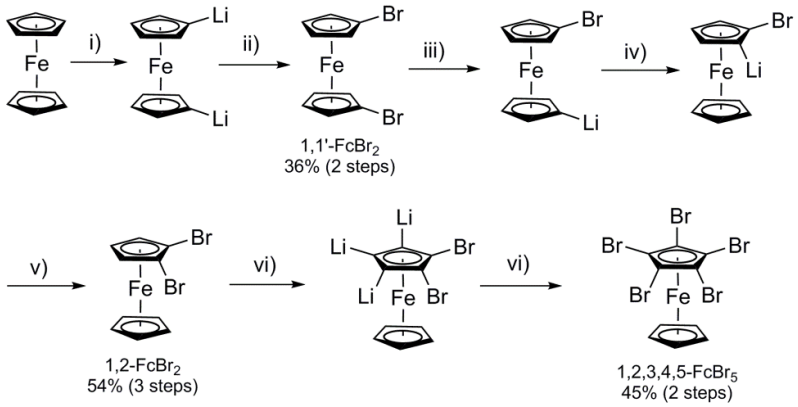

Scheme 1.9 The synthesis of 1,2,3,4,5-pentabromoferrocene. i) *n*-BuLi, TMEDA; ii) Tetrabromoethane; iii) *n*-BuLi (1 equiv.); iv) TMP; v) Tetrabromoethane; vi) LiTMP (10 equiv.); vii) Tetrabromoethane. TMEDA = tetramethylethylenediamine; TMP = 2,2,6,6-tetramethylpiperidine.

Both synthetic strategies give us inspiration to connect the Cp ring with functional groups of the suitable sizes to give a template for porphyrin nanoring synthesis. As will be shown in **Chapter 4**, the molecular design and chemistry towards templates for porphyrin nanoring synthesis are based on the synthetic strategies introduced above.

1.5 Project Aims and Highlights

This thesis sets out to answer these questions:

Do flexible templates work for porphyrin nanoring synthesis? Cyclodextrin templates are designed and synthesized for the preparation of porphyrin nanorings.

How small can a porphyrin nanoring be, based on butadiyne linkers? Ferrocene templates are designed and synthesized to prepare a 5-porphyrin nanoring.

Cooperativity of the nanoring-template complexes is investigated in parallel, revealing the influences of flexibility and intramolecular strain to the supramolecular systems.

There are also several highlights in the process of exploration:

Chirality of porphyrin nanoring. Chiral cyclodextrin templates have transferred their chirality to the nanoring-template complexes and one of them gave a strong Cotton effect.

Template-directed synthesis from prime-numbered template. A 7-dentate template has been obtained from β-cyclodextrin and has been successful to add new components in the porphyrin nanoring library.

Partial chelation induced by strain. The geometry of ferrocene-based 5-dentate template has given a large curvature to linear porphyrin oligomers: the induced intramolecular strain caused an observable equilibrium between full chelation and partial chelation in the supramolecular system.

1.6 References

[1] M. O. Senge, M. Davis, *J. Porphyrins Phthalocyanines* **2010**, *14*, 557–567.
[2] H. Fliegl, D. Sundholm, *J. Org. Chem.* **2012**, *77*, 3408–3414.
[3] T. Omura, R. Sato, *J. Biol. Chem.* **1964**, *239*, 2370–2378.
[4] R. Banerjee, S. W. Ragsdale, *Annu. Rev. Biochem.* **2003**, *72*, 209–247.
[5] G. McDermott, S. M. Prince, A. A. Freer, A. M. Hawthornthwaite-Lawless, M. Z. Papiz, R. J. Cogdell, N. W. Isaacs, *Nature* **1995**, *374*, 517–521.
[6] A. Ben-Shem, F. Frolow, N. Nelson, *Nature* **2003**, *426*, 630–635.
[7] R. Croce, *Science* **2015**, *348*, 970–971.
[8] X. Qin, M. Suga, T. Kuang, J.-R. Shen, *Science* **2015**, *348*, 989–995.
[9] M. O. Senge, M. Fazekas, E. G. A. Notaras, W. J. Blau, M. Zawadzka, O. B. Locos, E. M. N. Mhuircheartaigh, *Adv. Mater.* **2007**, *19*, 2737–2774.
[10] K. Maxwell, G. N. Johnson, *J. Exp. Bot.* **2000**, *51*, 659–668.
[11] M. Ethirajan, Y. Chen, P. Joshi, R. K. Pandey, *Chem. Soc. Rev.* **2011**, *40*, 340–362.
[12] M. V. Martínez-Díaz, G. de la Torre, T. Torres, *Chem. Commun.* **2010**, *46*, 7090–7108.

[13] A. Yella, H.-W. Lee, H. N. Tsao, C. Yi, A. K. Chandiran, M. K. Nazeeruddin, E. W.-G. Diau, C.-Y. Yeh, S. M. Zakeeruddin, M. Grätzel, *Science* **2011**, *334*, 629–634.
[14] B. E. Hardin, H. J. Snaith, M. D. McGehee, *Nature Photon.* **2012**, *6*, 162–169.
[15] S. Mathew, A. Yella, P. Gao, R. Humphry-Baker, B. F. E. Curchod, N. Ashari-Astani, I. Tavernelli, U. Rothlisberger, M. K. Nazeeruddin, M. Grätzel, *Nature Chem.* **2014**, *6*, 242–247.
[16] H. L. Anderson, *Chem. Commun.* **1999**, 2323–2330.
[17] D. Holten, D. F. Bocian, J. S. Lindsey, *Acc. Chem. Res.* **2002**, *35*, 57–69.
[18] A. Tsuda, A. Osuka, *Science* **2001**, *293*, 79–82.
[19] V. S.-Y. Lin, S. G. DiMagno, M. J. Therien, *Science* **1994**, *264*, 1105–1111.
[20] A. Osuka, S. Nakajima, K. Maruyama, N. Mataga, T. Asahi, I. Yamazaki, Y. Nishimura, T. Ohno, K. Nozaki, *J. Am. Chem. Soc.* **1993**, *115*, 4577–4589.
[21] S. Anderson, H. L. Anderson, J. K. M. Sanders, *J. Chem. Soc., Perkin Trans. 1* **1995**, 2255–2267.
[22] C. Maeda, T. Taniguchi, K. Ogawa, T. Ema, *Angew. Chem. Int. Ed.* **2015**, *54*, 134–138.
[23] M. Pawlicki, M. Morisue, N. K. S. Davis, D. G. McLean, J. E. Haley, E. Beuerman, M. Drobizhev, A. Rebane, A. L. Thompson, S. I. Pascu, G. Accorsi, N. Armaroli, H. L. Anderson, *Chem. Sci.* **2012**, *3*, 1541–1547.
[24] L. R. Milgrom, *The Colours of Life: An Introduction to the Chemistry of Porphyrins and Related Compounds*, OUP, Oxford, **1997**.
[25] M. Gouterman, *J. Mol. Spectrosc.* **1961**, *6*, 138–163.
[26] D. Kondratiuk, *Synthesis and Properties of Giant Porphyrin Nanorings*, D.Phil. thesis, University of Oxford, Oxford, 2013.
[27] M. U. Winters, J. Kärnbratt, M. Eng, C. J. Wilson, H. L. Anderson, B. Albinsson, *J. Phys. Chem. C* **2007**, *111*, 7192–7199.
[28] M. U. Winters, E. Dahlstedt, H. E. Blades, C. J. Wilson, M. J. Frampton, H. L. Anderson, B. Albinsson, *J. Am. Chem. Soc.* **2007**, *129*, 4291–4297.
[29] C. Glaser, *Ber. Dtsch. Chem. Ges.* **1869**, *2*, 422–424.
[30] D. P. Arnold, A. W. Johnson, M. Mahendran, *J. Chem. Soc., Perkin Trans. 1* **1978**, 366–370.
[31] M. Kawao, H. Ozawa, H. Tanaka, T. Ogawa, *Thin Solid Films*, **2006**, *499*, 23–28.
[32] H. L. Anderson, *Inorg. Chem.* **1994**, *33*, 972–981.
[33] P. N. Taylor, H. L. Anderson, *J. Am. Chem. Soc.* **1999**, *121,* 11538–11545.
[34] M. Drobizhev, Y. Stepanenko, A. Rebane, C. J. Wilson, T. E. O. Screen, H. L. Anderson, *J. Am. Chem. Soc.* **2006**, *128*, 12432–12433.
[35] F. C. Grozema, C. Houarner-Rassin, P. Prins, L. D. A. Siebbeles, H. L. Anderson, *J. Am. Chem. Soc.* **2007**, *129*, 13370–13371.
[36] C. E. Tait, P. Neuhaus, M. D. Peeks, H. L. Anderson, C. R. Timmel, *J. Am. Chem. Soc.* **2015**, *137*, 8284–8293.
[37] J. K. Laha, S. Dhanalekshmi, M. Taniguchi, A. Ambroise, J. S. Lindsey, *Org. Process Res. Dev.* **2003**, *7*, 799−812.
[38] J. D. Megiatto, Jr., D. I. Schuster, S. Abwandner, G. de Miguel, D. M. Guldi, *J. Am. Chem. Soc.* **2010**, *132*, 3847–3861.
[39] N. Aratani, A. Takagi, Y. Yanagawa, T. Matsumoto, T. Kawai, Z. S. Yoon, D. Kim, A. Osuka, *Chem. Eur. J.* **2005**, *11*, 3389–3404.

[40] J. S. Lindsey, *Acc. Chem. Res.* **2010**, *43*, 300–311.
[41] L. R. Nudy, H. G. Hutchinson, C. Schieber, F. R. Longo, *Tetrahedron* **1984**, *40*, 2359–2363.
[42] J. A. Marsden, J. J. Miller, M. M. Haley, *Angew. Chem. Int. Ed.* **2004**, *43*, 1694–1697.
[43] J. K. Sprafke, D. V. Kondratuk, M. Wykes, A. L. Thompson, M. Hoffmann, R. Drevinskas, W.-H. Chen, C. K. Yong, J. Kärnbratt, J. E. Bullock, M. Malfois, M. R. Wasielewski, B. Albinsson, L. M. Herz, D. Zigmantas, D. Beljonne, H. L. Anderson, *J. Am. Chem. Soc.* **2011**, *133*, 17262–17273.
[44] P. Parkinson, D. V. Kondratuk, C. Menelaou, J. Q. Gong, H. L. Anderson, L. M. Herz, *J. Phys. Chem. Lett.* **2014**, *5*, 4356−4361.
[45] J. Q. Gong, P. Parkinson, D. V. Kondratuk, G. Gil-Ramírez, H. L. Anderson, L. M. Herz, *J. Phys. Chem. C* **2015**, *119*, 6414−6420.
[46] P. Parkinson, C. E. I. Knappke, N. Kamonsutthipaijit, K. Sirithip, J. D. Matichak, H. L. Anderson, L. M. Herz, *J. Am. Chem. Soc.* **2014**, *136*, 8217−8220.
[47] S. Anderson, H. L. Anderson, J. K. M. Sanders, *Acc. Chem. Res.* **1993**, *26*, 469−475.
[48] M. Hoffmann, C. J. Wilson, B. Odell, H. L. Anderson, *Angew. Chem. Int. Ed.* **2007**, *46*, 3122–3125.
[49] M. Hoffmann, J. Kärnbratt, M.-H. Chang, L. M. Herz, B. Albinsson, H. L. Anderson, *Angew. Chem. Int. Ed.* **2008**, *47*, 4993–4996.
[50] M. C. O'Sullivan, J. K. Sprafke, D. V. Kondratuk, C. Rinfray, T. D. W. Claridge, A. Saywell, M. O. Blunt, J. N. O'Shea, P. H. Beton, M. Malfois, H. L. Anderson, *Nature* **2011**, *469*, 72–75.
[51] D. V. Kondratuk, J. K. Sprafke, M. C. O'Sullivan, L. M. A. Perdigao, A. Saywell, M. Malfois, J. N. O'Shea, P. H. Beton, A. L. Thompson, H. L. Anderson, *Chem. Eur. J.* **2014**, *20*, 12826–12834.
[52] D. V. Kondratuk, L. M. A. Perdigao, M. C. O'Sullivan, S. Svatek, G. Smith, J. N. O'Shea, P. H. Beton, H. L. Anderson, *Angew. Chem. Int. Ed.* **2012**, *51*, 6696–6699.
[53] D. V. Kondratuk, L. M. A. Perdigao, A. M. S. Esmail, J. N. O'Shea, P. H. Beton, H. L. Anderson, *Nature Chem.* **2015**, *7*, 317–322.
[54] P. Neuhaus, A. Cnossen, J. Q. Gong, L. M. Herz, H. L. Anderson, *Angew. Chem. Int. Ed.* **2015**, *54*, 7344–7348.
[55] J. S. Lindsey, *New J. Chem.* **1991**, *15*, 153–180.
[56] T. R. Kelly, R. L. Xie, C. K. Weinreb, T. Bregant, *Tetrahedron Lett.* **1998**, *39*, 3675–3678.
[57] C. A. Hunter, S. Tomas, *J. Am. Chem. Soc.* **2006**, *128*, 8975–8979.
[58] M. F. Perutz, *Q. Rev. Biophys.* **1989**, *22*, 139–236.
[59] C. A. Hunter, H. L. Anderson, *Angew. Chem. Int. Ed.* **2009**, *48*, 7488–7499.
[60] G. Ercolani, L. Schiaffino, *Angew. Chem. Int. Ed.* **2011**, *50*, 1762–1768.
[61] J. Monod, J. Wyman, J. P. Changeux, *J. Mol. Biol.* **1965**, *12*, 88–118.
[62] E. Terzi, G. Hölzemann, J. Seelig, *J. Mol. Biol.* **1995**, *252*, 633–642.
[63] D. Zhao, J. S. Moore, *Org. Biomol. Chem.* **2003**, *1*, 3471–3491.
[64] N. Fatin-Rouge, S. Blanc, A. Pfeil, A. Rigault, A.-M. Albrecht-Gary, J.-M. Lehn, *Helv. Chim. Acta* **2001**, *84*, 1694–1711.
[65] D. H. Williams, A. J. Maguire, W. Tsuzuki, M. S. Westwell, *Science* **1998**, *280*, 711–714.
[66] H. J. Hogben, J. K. Sprafke, M. Hoffmann, M. Pawlicki, H. L. Anderson, *J. Am. Chem. Soc.* **2011**, *133*, 20962–20969.

[67] C. A. Hunter, M. C. Misuraca, S. M. Turega, *Chem. Sci.* **2012**, *3*, 589–601.
[68] A. Fersht, *Enzyme Structure and Mechanism: A Guide to Enzyme Catalysis and Protein Folding*, W. H. Freeman and Company, 1999, New York, pp. 66–67.
[69] K. Hirose, *J. Incl. Phenom. Macro.* **2001**, *39*, 193–209.
[70] G. Crini, *Chem. Rev.* **2014**, *114*, 10940−10975.
[71] K. Uekama, F. Hirayama, T. Irie, *Chem. Rev.* **1998**, *98*, 2045−2076.
[72] A. Harada, J. Li, M. Kamachi, *Nature* **1992**, *356*, 325−327.
[73] G. Wenz, *Angew. Chem. Int. Ed. Engl.* **1994**, *33*, 803–822.
[74] S. A. Nepogodiev, J. F. Stoddart, *Chem. Rev.* **1998**, *98*, 1959−1976.
[75] A. Harada, *Acc. Chem. Res.* **2001**, *34*, 456−464.
[76] F. Cacialli, J. S. Wilson, J. J. Michels, C. Daniel, C. Silva, R. H. Friend, N. Severin, P. Samorì, J. P. Rabe, M. J. O'Connell, P. N. Taylor, H. L. Anderson, *Nature Mater.* **2002**, *1*, 160–164.
[77] A. R. Khan, P. Forgo, K. J. Stine, V. T. D'Souza, *Chem. Rev.* **1998**, *98*, 1977−1996.
[78] W. Saenger, M. Noltemeyer, P. C. Manor, B. Hingerty, B. Klar, *Bioorg. Chem.* **1976**, *5*, 187−195.
[79] A. Hybl, R. E. Rundle, D. E. Williams, *J. Am. Chem. Soc.* **1965**, *87*, 2779–2788.
[80] P. R. Ashton, E. Y. Hartwell, D. Philp, N. Spencer, J. F. Stoddart, *J. Chem. Soc., Perkin Trans. 2* **1995**, 1263–1277.
[81] K. Takeo, K. Ueraura, H. Mitoh, *J. Carbohydr. Chem.* **1988**, *7*, 293–308.
[82] F. Cramer, G. Mackensen, K. Sensse, *Chem. Ber.* **1969**, *102*, 494–508.
[83] T. J. Kealy, P. L. Pauson, *Nature* **1951**, *168*, 1039–1040.
[84] A. Stark, B. L. MacLean, R. D. Singer, *J. Chem. Soc., Dalton Trans.* **1999**, 63–66.
[85] I. R. Butler, W. R. Cullen, J. Ni, S. J. Rettig, *Organometallics* **1985**, *4*, 2196–2201.
[86] F. Rebiere, O. Samuel, H. B. Kagan, *Tetrahedron Lett.* **1990**, *31*, 3121–3124.
[87] L.-X. Dai, T. Tu, S.-L. You, W.-P. Deng, X.-L. Hou, *Acc. Chem. Res.* **2003**, *36*, 659–667.
[88] R. G. Arrayás, J. Adrio, J. C. Carretero, *Angew. Chem. Int. Ed.* **2006**, *45*, 7674–7715.
[89] N. Kataoka, Q. Shelby, J. P. Stambuli, J. F. Hartwig, *J. Org. Chem.* **2002**, *67*, 5553–5566.
[90] O. Oms, T. Jarrosson, L. H. Tong, A. Vaccaro, G. Bernardinelli, A. F. Williams, *Chem. Eur. J.* **2009**, *15*, 5012–5022.
[91] I. R. Butler, *Inorg. Chem. Commun.* **2008**, *11*, 15–19.
[92] I. R. Butler, *Inorg. Chem. Commun.* **2008**, *11*, 484–486.
[93] K. Sünkel, S. Bernhartzeder, *J. Organomet. Chem.* **2011**, *696*, 1536–1540.

Chapter 2

Cyclodextrin-Templated Porphyrin Nanorings

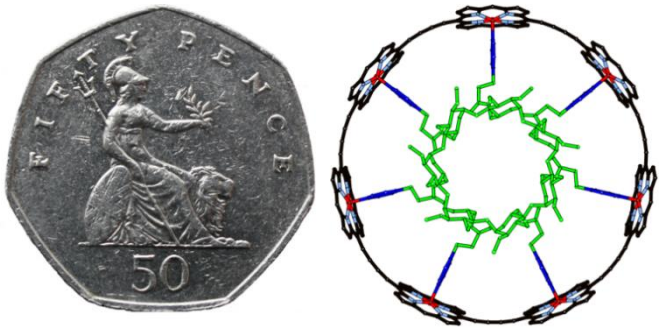

This chapter describes the chemistry towards cyclodextrin-based templates for porphyrin nanoring synthesis. The related chirality and cooperativity of the supramolecular complexes are investigated in detail. The study proves that flexible templates are effective for porphyrin nanoring synthesis; meanwhile, the influences of the flexibility towards the supramolecular system are revealed by the effective molarities of the corresponding complexes.

Parts of the results in this chapter have been published in the following article:

Cyclodextrin-Templated Porphyrin Nanorings

P. Liu, P. Neuhaus, D. V. Kondratuk, T. S. Balaban, H. L. Anderson, *Angew. Chem. Int. Ed.* **2014**, *53*, 7770–7773.

2.1 Background Information

In the series of porphyrin nanoring chemistry, the rigid template **T6**, as is shown in **Chapter 1** (**Scheme 1.5**, **Figures 1.8** and **1.9**), is a star molecule as it had been (and is still) producing a good number of beautiful porphyrin nanorings. As **T6** is a hexaphenylbenzene-based rigid template, a question is raised: Could the template be flexible but at the same time function similarly to the rigid one? To answer this question, the cyclodextrin-based porphyrin nanoring chemistry is performed, as is shown in the following sections.

2.2 Molecular Design

Our design set to link the cyclodextrin core to the pyridyl ligand through the 6-OH position of the sugar units. Esterification of the hydroxyl was selected as the functionalization method. The linkers between the ester carbonyl and the pyridyl can be varied to adjust the size and flexibility of the templates.

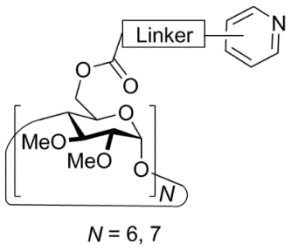

Figure 2.1 Rationale in the design of the cyclodextrin-based templates for porphyrin nanorings.

We performed molecular mechanics calculations for three cyclodextrin derivatives chelated to porphyrin nanorings: two α-CD derivatives (**T6*** and ***meta*-T6***) and one β-CD derivative (**T7***). In **T6***, the ester carbonyl is directly linked to the *para*-pyridyl group; in *meta*-**T6***, the ester carbonyl is directly linked to the *meta*-pyridyl group; in ***c*-P7·T7***, the ester carbonyl is linked to a *para*-pyridyl through two sp^3 carbons.

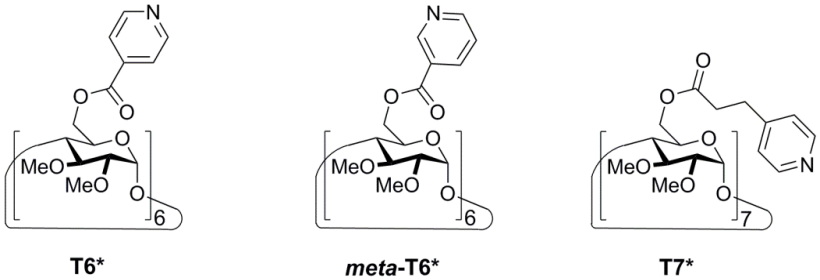

Figure 2.2 The molecular structures of the designed cyclodextrin-based templates.

In the molecular mechanics models, ***c*-P6·T6*** and ***c*-P7·T7*** both gave nice ring-template structures with their intrinsic 6-fold or 7-fold symmetries; the ring structures were slightly distorted, which makes the two faces of the ring-template complexes different. In contrast, ***c*-P6·*meta*-T6*** was hugely distorted, and the intrinsic 6-fold symmetries of the template as well as the ring were lost. We attempted porphyrin nanoring synthesis using ***meta*-T6*** as the template to explore whether the flexibility of the cyclodextrin template could overcome the distortion inside the molecular system.

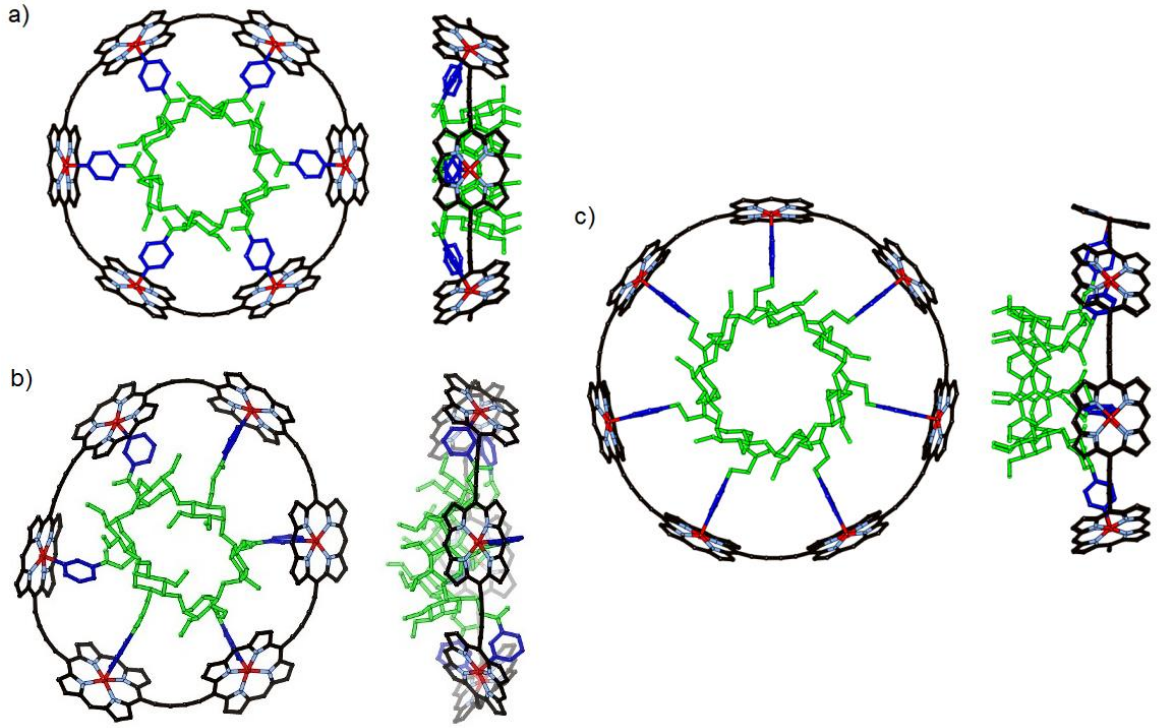

Figure 2.3 The structures of a) ***c*-P6·T6***, b) ***c*-P6·*meta*-T6*** and c) ***c*-P7·T7*** from molecular mechanics calculation. MM+ forcefield, orthogonal views, *meso*-aryl groups and hydrogen atoms are omitted for clarity.

2.3 Cyclodextrin Templates and Porphyrin Nanoring Chemistry

2.3.1 Syntheses of Cyclodextrin Templates

The method to prepare cyclodextrin templates is to perform esterification on the 6-OH site of per-2,3-di-*O*-methylcyclodextrins, which can be prepared as introduced in **Scheme 1.7**, **Chapter 1**. The corresponding carboxylic acids were transformed into their pentafluorophenyl esters in advance to maximize their reactivity.[1]

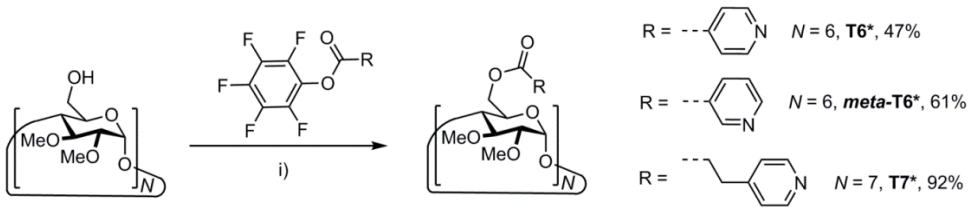

Scheme 2.1 The preparation of cyclodextrin-based templates. i) DMAP, pyridine, 90 ºC.

2.3.2 Syntheses of Cyclodextrin-Templated Porphyrin Nanorings

T6* and **T7*** were used as templates for the syntheses of 6- and 7-porphyrin nanorings from porphyrin monomers/dimers. The oxidative coupling reactions were performed in chloroform at room temperature and monitored by UV-vis and MALDI-MS spectra.

The efficiency of flexible **T6*** was very similar to rigid **T6** in synthesizing 6-porphyrin nanorings: coupling ***l*-P2$_{t\text{-Bu}}$(H,H)** in the presence of **T6*** gave ***c*-P6$_{t\text{-Bu}}$·T6*** in 59% yield under the Pd/Cu co-catalyst reaction conditions.[2] Under the same conditions, coupling ***l*-P2$_{t\text{-Bu}}$(H,H)** in the presence of **T6** gave ***c*-P6$_{t\text{-Bu}}$·T6** in 62% yield. Coupling ***l*-P1$_{t\text{-Bu}}$(H,H)** in the presence of **T6*** gave ***c*-P6$_{t\text{-Bu}}$·T6*** in 22% yield and ***c*-P12$_{t\text{-Bu}}$·(T6*)$_2$** in 1.4% yield. In comparison, coupling ***l*-P1$_{t\text{-Bu}}$(H,H)** in the presence of **T6** gives ***c*-P6$_{t\text{-Bu}}$·T6** in 21% yield and ***c*-P12$_{t\text{-Bu}}$·(T6)$_2$** in 4% yield.[3] A prime-numbered porphyrin nanoring ***c*-P7$_{t\text{-Bu}}$·T7*** was prepared by coupling ***l*-P1$_{t\text{-Bu}}$** in the presence of **T7*** in 4.7% yield.

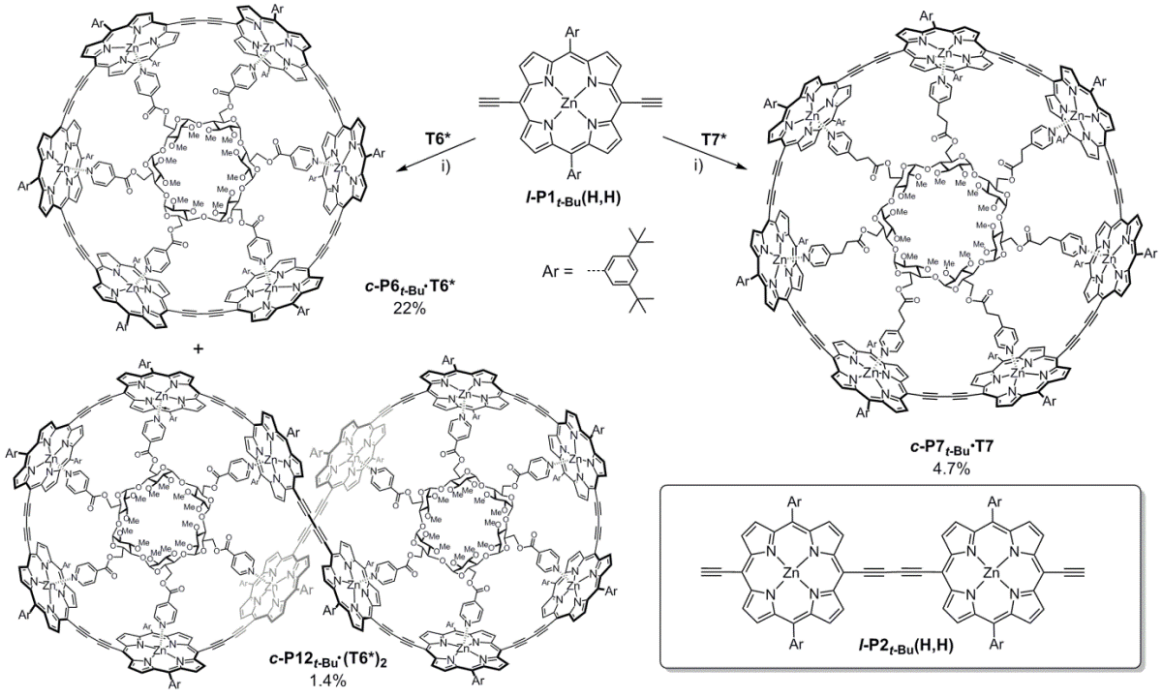

Scheme 2.2 Syntheses of ***c*-P6$_{t\text{-Bu}}$·T6***, ***c*-P12$_{t\text{-Bu}}$·(T6*)$_2$** and ***c*-P7$_{t\text{-Bu}}$·T7***. Inset: the structure of ***l*-P2$_{t\text{-Bu}}$(H,H)**, which was also a precursor to ***c*-P6$_{t\text{-Bu}}$·T6***. i) 1,4-benzoquinone, Pd(PPh$_3$)$_2$Cl$_2$, CuI, *i*-Pr$_2$NH.

Template-free nanorings ***c*-P6$_{t\text{-Bu}}$**, ***c*-P12$_{t\text{-Bu}}$** and ***c*-P7$_{t\text{-Bu}}$** could be isolated in virtually quantitative yield by adding excess pyridine into ***c*-P6$_{t\text{-Bu}}$·T6***, ***c*-P12$_{t\text{-Bu}}$·(T6*)$_2$** and ***c*-P7$_{t\text{-Bu}}$·T7***, respectively. In all cases, adding templates back into the template-free nanorings immediately regenerates the template-nanoring complexes. As template-free nanorings are easier to purify in gel-permeation chromatography (GPC), the displacement-regeneration method is usually adopted in the purification process of template-nanoring complexes.

Unfortunately, coupling either ***l*-P1$_{t\text{-Bu}}$(H,H)** or ***l*-P2$_{t\text{-Bu}}$(H,H)** in the presence of ***meta*-T6*** did not give any traces of cyclic porphyrin oligomer, which was proven in the analytical results in gel-permeation chromatography and MS spectra; only linear porphyrin polymers were found.

2.4 Structural Details

As is shown in **Figure 2.4** (example from ***c*-P6$_{t\text{-Bu}}$·T6***), the protons in the templates are influenced by the typical shielding effects from porphyrin ring structure. The change of chemical shifts Δδ is subject to the distances between the protons and the porphyrin units.

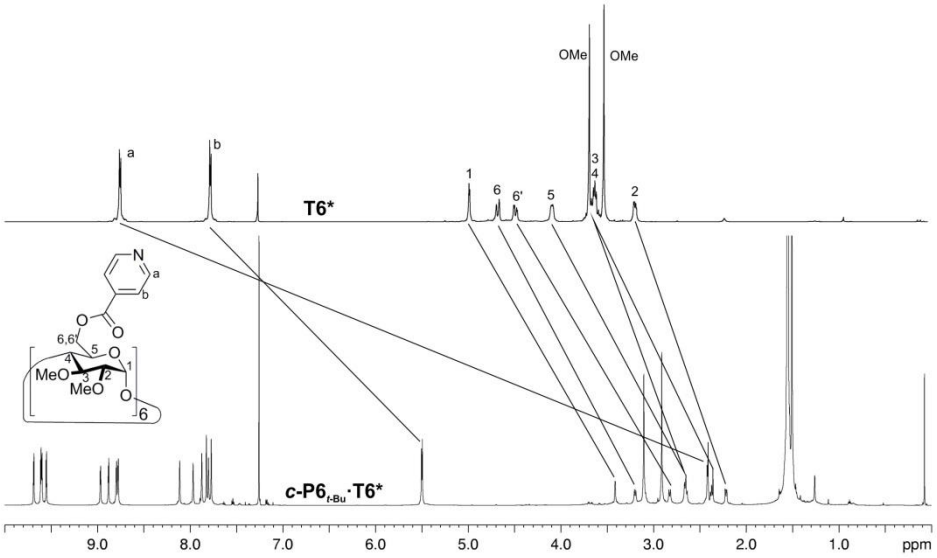

Figure 2.4 The ^{1}H NMR spectra of **T6*** (top, $CDCl_3$, 400 MHz, 298 K) and ***c*-P6$_{t\text{-Bu}}$·T6*** (bottom, $CDCl_3$, 700 MHz, 298 K).

D_{6h} symmetric **T6** does not induce distortion to the 6-porphyrin nanoring; so the eight β-protons in each porphyrin unit of ***c*-P6$_{t\text{-Bu}}$·T6** give two doublet signals. In contrast, the CD templates impose chirality on the ring structure and in the same time gives a conical shape to the nanoring (top-bottom difference, see molecular models in **Figure 2.3**), making all eight β-protons

inequivalent in the ^{1}H NMR spectra of ***c*-P6$_{t\text{-Bu}}$·T6*** and ***c*-P7$_{t\text{-Bu}}$·T7***. The splitting of the peaks is more obvious in ***c*-P6$_{t\text{-Bu}}$·T6*** compared to ***c*-P7$_{t\text{-Bu}}$·T7***, which means the distortion of the nanoring structure induced by the cyclodextrin template in ***c*-P6$_{t\text{-Bu}}$·T6*** is stronger.

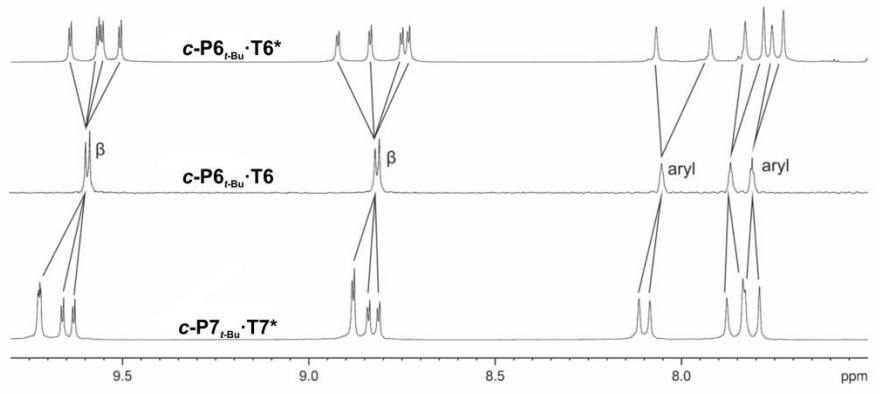

Figure 2.5 Partial ^{1}H NMR spectra of ***c*-P6$_{t\text{-Bu}}$·T6***, ***c*-P6$_{t\text{-Bu}}$·T6** and ***c*-P7$_{t\text{-Bu}}$·T7*** ($CDCl_3$, 700 MHz, 298 K).

The chirality of the template-nanoring complexes were further investigated by circular dichroism. ***c*-P6$_{t\text{-Bu}}$·T6***, ***c*-P7$_{t\text{-Bu}}$·T7*** and ***c*-P12$_{t\text{-Bu}}$·(T6*)$_2$** all have Cotton effects in the circular dichroism spectra. The cyclodextrin templates do not have absorption in the visible region of the spectra; but the chiral signals are present in this region. Hence the chirality of the template is transferred from the template to the porphyrin nanoring. ***c*-P6$_{t\text{-Bu}}$·T6*** and ***c*-P7$_{t\text{-Bu}}$·T7*** have similar intensities; whereas ***c*-P12$_{t\text{-Bu}}$·(T6*)$_2$** has about 20 times stronger intensity in the Q band region compared to ***c*-P6$_{t\text{-Bu}}$·T6***.

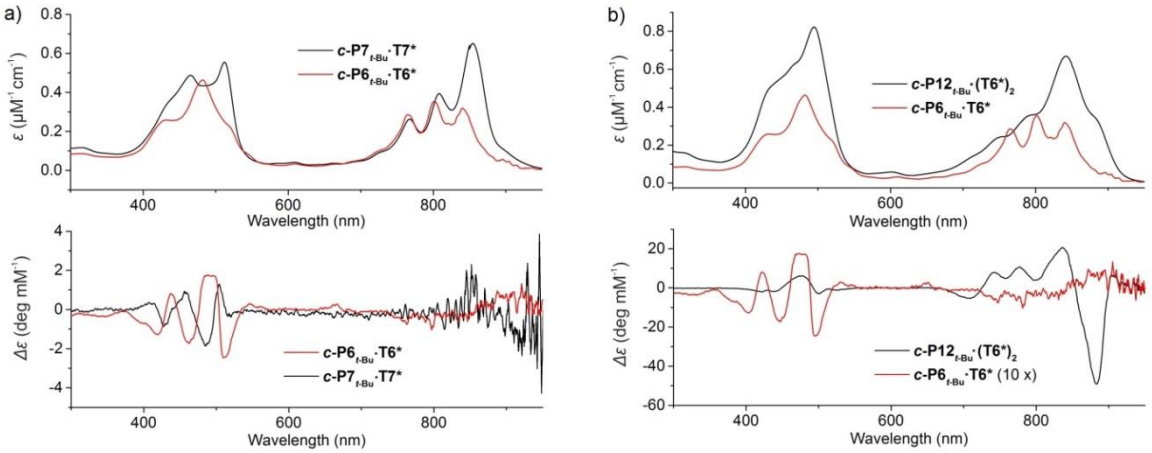

Figure 2.6 Extinction coefficient (ε) and circular dichroism ($\Delta\varepsilon$) spectra comparison between a) ***c*-P6$_{t\text{-Bu}}$·T6*** and ***c*-P7$_{t\text{-Bu}}$·T7***; b) ***c*-P6$_{t\text{-Bu}}$·T6*** ($\Delta\varepsilon$ multiplied by a factor of 10 for clarity) and ***c*-P12$_{t\text{-Bu}}$·(T6*)$_2$** in toluene, 298 K. Measurement performed by Prof. T. Silviu Balaban, Aix Marseille Univeristé.

A plausible explanation for the strong Cotton effect of ***c*-P12$_{t\text{-Bu}}$·(T6*)$_2$** is the combination of the chirality of the template and the figure-of-eight structure. Our group has previously reported

the racemic figure-of-eight crystal structure of ***c*-P12$_{t\text{-Bu}}$·(T6)$_2$**.[3] ***c*-P12$_{t\text{-Bu}}$·(T6)$_2$** did not give chiral signals from circular dichroism spectra and attempts to separate the enantiomers of the figure-of-eight structures all failed. So presumably, there are four diastereomers of ***c*-P12$_{t\text{-Bu}}$·(T6*)$_2$**, each with two **T6*** binding to the narrow primary rings both pointing to the same direction or in the opposite way. The mixture is likely to favor one (or a pair with the same rotary polarization properties) of the four diastereomers over the others, which would result in strong Cotton effects.

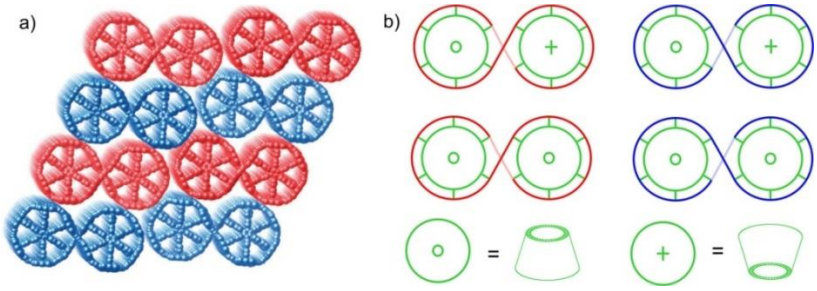

Figure 2.7 a) Crystal packing diagram of ***c*-P12$_{t\text{-Bu}}$·(T6)$_2$** showing two enantiomers in two different colors. Reprinted with permission from ref. 3, Copyright 2015 John Wiley and Sons. b) Proposed four diastereomers of ***c*-P12$_{t\text{-Bu}}$·(T6*)$_2$**, the red/blue circles represent for two different conformations of the figure-of-eight structure; the green circles represent different pointing directions of the cyclodextrin template **T6***.

2.5 Cooperativity Study

As was shown in **Chapter 1**, the key factor determining the stability of a chelate supramolecular system is effective molarity.[4] For a ring-template complex with *n* sites of binding, there are (*n* - 1) effective molarities involved. The geometric mean effective molarity for an *n*-site binding template-nanoring complex can be calculated using the equation below:

$$\overline{EM} = \sqrt[n-1]{\frac{K_{\mathrm{f}}}{K_{\sigma}K_1^n}} \tag{2.1}$$

where K_{f} is the formation constant of the template-nanoring complex; K_{σ} is the statistical factor; K_1 is the statistically-corrected single-site association constant between a porphyrin unit and the monodentate ligand for the corresponding template-nanoring complex (**L1** for ***c*-P6$_{t\text{-Bu}}$·T6**, **L2** for ***c*-P6$_{t\text{-Bu}}$·T6***, **L3** for ***c*-P7$_{t\text{-Bu}}$·T7***); *n* is the number of binding sites (6 for ***c*-P6$_{t\text{-Bu}}$·T6** and ***c*-P6$_{t\text{-Bu}}$·T6***, 7 for ***c*-P7$_{t\text{-Bu}}$·T7***).

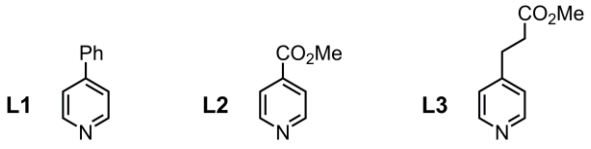

Figure 2.8 The binding ligands for ***c*-P6$_{t\text{-Bu}}$·T6**, ***c*-P6$_{t\text{-Bu}}$·T6*** and ***c*-P7$_{t\text{-Bu}}$·T7*** for measuring K_1.

The statistical factor K_σ reflects the symmetry change between the starting host/guest component state and the ending host-guest complex state: the calculation method of K_σ is based on the symmetry numbers of corresponding species; and the details of the method will be shown in **Section S.1** in the Appendix.[5] The statistically corrected formation constant K_f/K_σ reflects the formation constants at microscopic level and can be used for the calculation of EMs.

K_1 can be measured directly between a specific ligand and the corresponding template-free nanoring since there is no cooperativity between the porphyrin units in a butadiyne-linked porphyrin oligomer system.[6] In a 6- or 7-site chelate binding system, K_f is very high and cannot be directly measured. Indirect measurement can be made through a denaturation cycle shown in **Figure 2.9**.

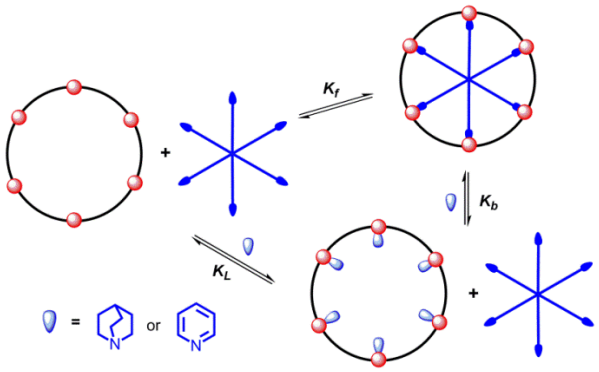

Figure 2.9 Denaturation cycle used to determine K_f of template-nanoring complexes (n = 6 in this figure).

The denaturation cycle gives the equation to calculate K_f, which is shown below:

$$K_f = \frac{K_L^n}{K_b} \tag{2.2}$$

where K_b is the denaturation constant for a specific ligand with the template-nanoring; K_L is the association constant for a specific monodentate ligand with the template-free nanoring. The commonly used ligands are pyridine and quinuclidine. For ***c*-P6$_{t\text{-Bu}}$·T6**, the binding between ***c*-P6$_{t\text{-Bu}}$** and **T6** is extremely strong: **T6** cannot be replaced even by neat pyridine solvent; only quinuclidine can perform effective denaturation titration for the complex. For ***c*-P6$_{t\text{-Bu}}$·T6*** and ***c*-P7$_{t\text{-Bu}}$·T7***, the bindings between templates and nanorings are moderate and both pyridine and quinuclidine can be used for the denaturation titrations.

The association constant for a monodentate ligand with a porphyrin unit (either a porphyrin monomer or a porphyrin unit inside linear/cyclic porphyrin oligomer), K_L, is related to the corresponding statistically-corrected single-site association constant K_1 through the statistical

factor K_σ, i.e. $K_L = K_\sigma K_1$. **Figure 2.10** gives an example of calculating the K_σ of a specific process.

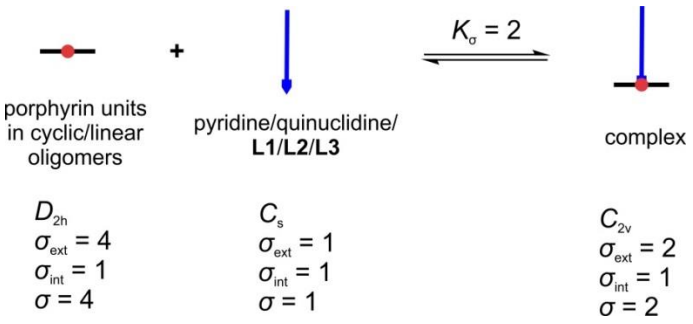

Figure 2.10 The statistical factors involved in a monodentate ligand binding to a porphyrin unit.

As a result, two types of titrations are needed for the EM calculation.

*A. Monodentate ligand binding between pyridine/quinuclidine/**L1**/**L2**/**L3** and template-free **c-P6**$_{t\text{-}Bu}$/**c-P7**$_{t\text{-}Bu}$.* The titrations involving pyridine/quinuclidine are used for the calculation of K_L, which leads to the K_f calculation; the titrations involving **L1**/**L2**/**L3** are used for the calculation of K_1, which are used for calculating EM.

*B. Denaturation of template-nanoring complexes **c-P6**$_{t\text{-}Bu}$**·T6**, **c-P6**$_{t\text{-}Bu}$**·T6*** and **c-P7**$_{t\text{-}Bu}$**·T7*** by pyridine/quinuclidine*. The titrations are all used to calculate K_b, which leads to the K_f calculation.

The detailed experimental and data processing procedure are shown as follows.

2.5.1 Titrations of Monodentate Ligands with Nanorings *c*-P6$_{t\text{-Bu}}$ and *c*-P7$_{t\text{-Bu}}$

***c*-P6**$_{t\text{-Bu}}$ was titrated with the ligands shown in **Figure 2.11** (quinuclidine, pyridine, **L1** and **L2**) to measure their association constants K_L.

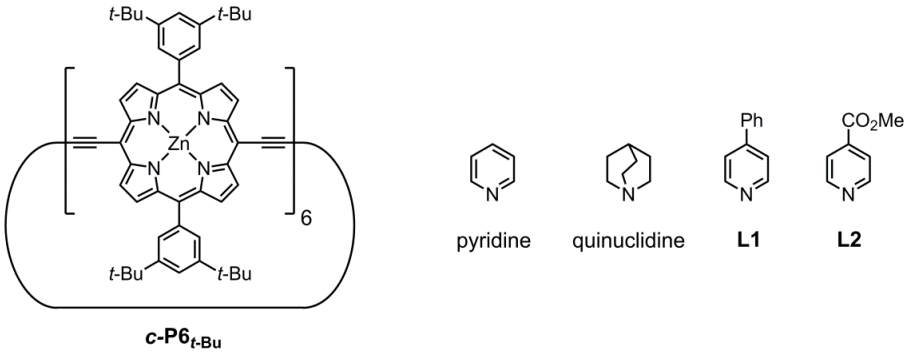

Figure 2.11 The ligands used for measuring the reference association constants with ***c*-P6**$_{t\text{-Bu}}$.

Titration curves were fitted to a 1:1 binding isotherm using the equation (2.3). The detailed derivation of the equation is shown in **Section S.2** in the Appendix.

$$\frac{A - A_{initial}}{A_{\infty} - A_{initial}} = \left(\frac{(K_{\mathrm{L}}([\mathrm{L}]_0 + [\mathrm{P}]_0) + 1) - \sqrt{(K_{\mathrm{L}}([\mathrm{L}]_0 + [\mathrm{P}]_0) + 1)^2 - 4K_{\mathrm{L}}^2[\mathrm{P}]_0[\mathrm{L}]_0}}{2K_{\mathrm{L}}[\mathrm{P}]_0} \right) \quad (2.3)$$

where A is the observed absorption at a specific wavelength or difference of absorption at two wavelengths; $A_{initial}$ is the starting absorption at this wavelength or difference of absorption in these two wavelengths; A_{∞} is the asymptotic final absorption at this wavelength or difference of absorption in these two wavelengths; K_{L} is the association constant between ligand and porphyrin host; $[\mathrm{L}]_0$ is the total (free and bound) concentration of ligand; $[\mathrm{P}]_0$ is the total concentration of porphyrin host.

It should be noted that $[\mathrm{P}]_0$ is a 6-fold multiply for the concentration of ***c*-P6$_{t\text{-Bu}}$** since each 6-porphyrin nanoring contains 6 porphyrin units, as we assume that all six zinc-porphyrin sites bind to the ligand independently and there is essentially no allosteric cooperativity.[6]

For a specific porphyrin oligomer host, the titration spectra with different ligands are similar in that the ligands do not absorb light in the wavelength range of the titrations. For a set of titrations with the same porphyrin oligomer, only one titration spectrum and fitting curve will be presented for the brevity of the contents. In the spectra, the bold black lines represent starting points and the red lines represent terminal points. Full results and sample spectra-fitting curve are shown below.

Table 2.1 The association constants (K_{L}) of ***c*-P6$_{t\text{-Bu}}$** and ligands (1:1 association constants in M^{-1}).

Ligand	Run 1	Run 2	Average
quinuclidine	$(3.2 \pm 0.1) \times 10^5$	$(2.8 \pm 0.1) \times 10^5$	$(3.0 \pm 0.2) \times 10^5$
pyridine	$(1.1 \pm 0.1) \times 10^4$	$(8.0 \pm 0.3) \times 10^3$	$(9.5 \pm 1.5) \times 10^3$
L1	$(8.4 \pm 0.3) \times 10^3$	$(8.4 \pm 0.3) \times 10^3$	$(8.4 \pm 0.3) \times 10^3$
L2	$(1.4 \pm 0.1) \times 10^3$	$(1.2 \pm 0.1) \times 10^3$	$(1.3 \pm 0.1) \times 10^3$

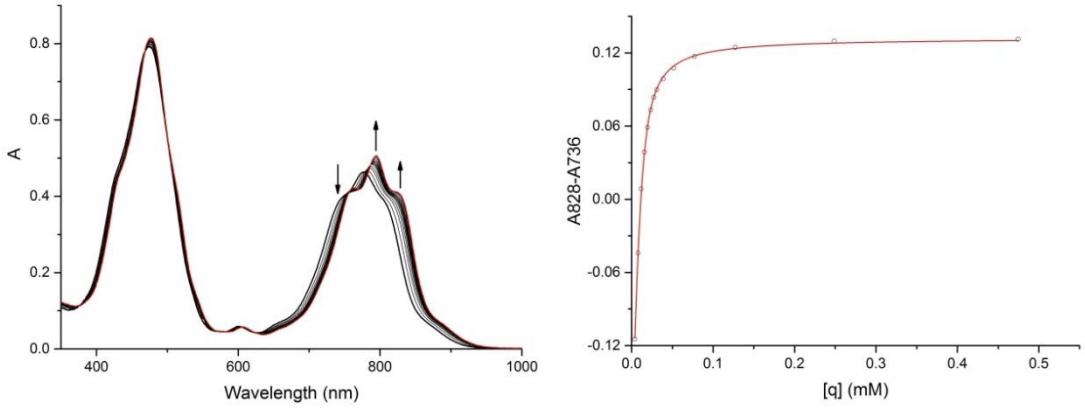

Figure 2.12 UV-vis titration of quinuclidine and ***c*-P6$_{t\text{-Bu}}$**, $K_{\mathrm{L}} = (3.2 \pm 0.1) \times 10^5$ M^{-1}, $R^2 = 0.999$. (Run 1, $CHCl_3$, 298 K, [***c*-P6$_{t\text{-Bu}}$**] = 1.8 μM)

***c*-P7$_{t\text{-Bu}}$** was titrated with the ligands shown in **Figure 2.13** (quinuclidine, pyridine and **L3**) to measure their association constants.

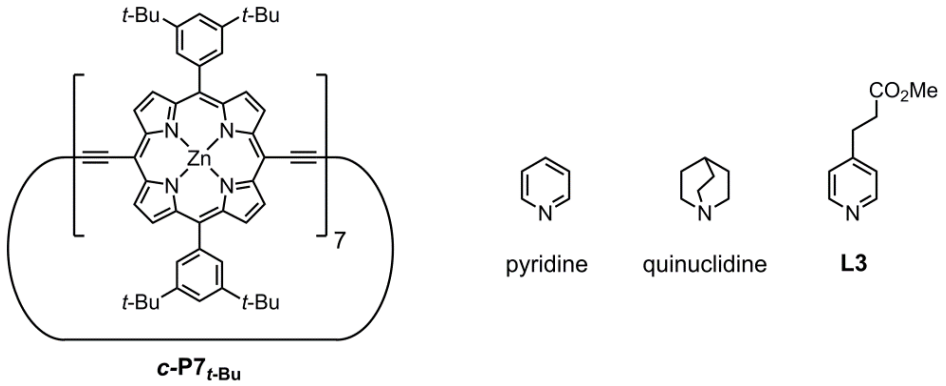

Figure 2.13 The ligands used for measuring the reference association constants with ***c*-P7$_{t\text{-Bu}}$**.

Titration curves were fitted to equation (2.3), the 1:1 binding isotherm. It should be noted that $[P]_0$ is a 7-fold multiply for the concentration of ***c*-P7$_{t\text{-Bu}}$** since each 7-porphyrin nanoring contains 7 porphyrin units. The sample spectra-fitting curve and full results are shown below.

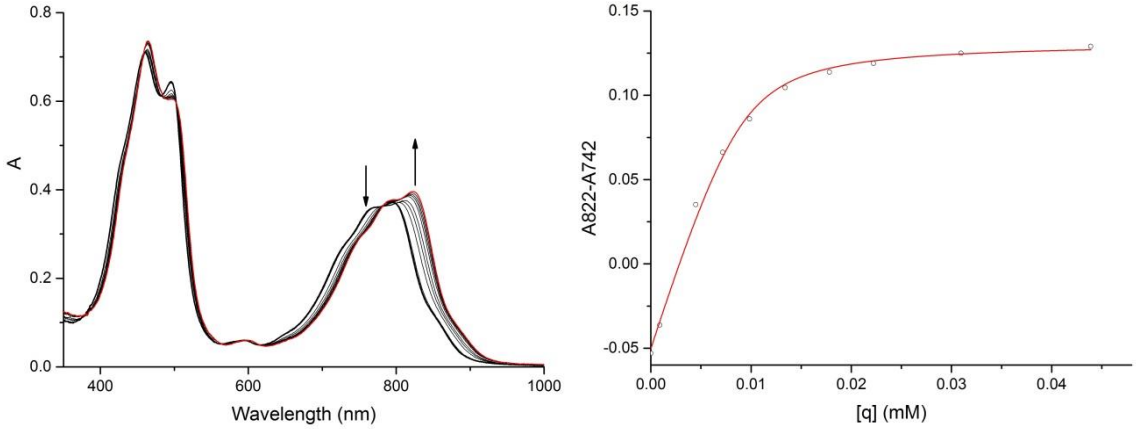

Figure 2.14 UV-vis titration of quinuclidine and ***c*-P7$_{t\text{-Bu}}$**, $K_L = (1.2 \pm 0.2) \times 10^6$ M^{-1}, $R^2 = 0.996$. (Run 1, $CHCl_3$, 298 K, [***c*-P7$_{t\text{-Bu}}$**] = 1.3 μM)

Table 2.2 The association constants (K_L) of ***c*-P7$_{t\text{-Bu}}$** and ligands (1:1 association constants in M^{-1}).

Ligand	Run 1	Run 2	Average
quinuclidine	$(1.2 \pm 0.2) \times 10^6$	$(1.0 \pm 0.4) \times 10^6$	$(1.1 \pm 0.3) \times 10^6$
pyridine	$(2.3 \pm 0.1) \times 10^4$	$(1.9 \pm 0.1) \times 10^4$	$(2.1 \pm 0.2) \times 10^4$
L3	$(3.8 \pm 0.1) \times 10^4$	$(3.2 \pm 0.1) \times 10^4$	$(3.5 \pm 0.3) \times 10^4$

2.5.2 Denaturation Titrations

c*-P6$_{t\text{-Bu}}$·T6** was titrated with quinuclidine only, because quinuclidine is the only known ligand which displaces the template from ***c*-P6$_{t\text{-Bu}}$·T6**. The corresponding denaturation constant is labeled as K_{qp6t6}. ***c*-P6$_{t\text{-Bu}}$·T6 and ***c*-P7$_{t\text{-Bu}}$·T7*** were titrated both with quinuclidine and pyridine. The corresponding denaturation constants are labeled as $K_{\text{qp6t6*}}$, $K_{\text{pyp6t6*}}$, $K_{\text{qp7t7*}}$ and $K_{\text{pyp7t7*}}$, respectively.

All the data were fitted to equation (2.4), the *n*-dentate denaturation isotherm. The detailed derivation of the equation is shown in **Section S.3** in the Appendix.

$$\frac{A - A_{initial}}{A_{\infty} - A_{initial}} = \left(\frac{-K_{\text{b}}[\text{L}]_0{}^{n} + \sqrt{K_{\text{b}}^2[\text{L}]_0{}^{2n} + 4K_{\text{b}}[\text{L}]_0{}^{n}[\text{P}]_0}}{2[\text{P}]_0} \right) \tag{2.4}$$

where A is the observed absorption at a specific wavelength or difference of absorption in two wavelengths; $A_{initial}$ is the starting absorption at a specific wavelength or difference of absorption in two wavelengths; A_{∞} is the terminal absorption at a specific wavelength or difference of absorption in two wavelengths; K_{b} is the denaturation (breaking-up) constant between ligand and porphyrin nanoring complex; $[\text{L}]_0$ is the total concentration of ligand; $[\text{P}]_0$ is the total concentration of porphyrin nanoring complex and template-free porphyrin nanorings; n is the number of binding sites of nanoring complexes. For ***c*-P6$_{t\text{-Bu}}$·T6** and ***c*-P6$_{t\text{-Bu}}$·T6***, n = 6; for ***c*-P7$_{t\text{-Bu}}$·T7***, n = 7.

The full results and sample spectra-fitting curves are shown below. In the spectra, the bold black lines represent starting points and the red lines represent terminal points.

Table 2.3 Denaturation constants of nanoring-template complexes with quinuclidine and pyridine.

Ligand, complex	Equilibrium constant	Run 1	Run 2	Average
quinuclidine, ***c*-P6$_{t\text{-Bu}}$·T6**	K_{qp6t6} (M^{-5})	$(1.0 \pm 0.1) \times 10^{-3}$	$(8.4 \pm 0.4) \times 10^{-4}$	$(9.2 \pm 0.8) \times 10^{-4}$
quinuclidine, ***c*-P6$_{t\text{-Bu}}$·T6***	$K_{\text{qp6t6*}}$ (M^{-5})	$(7.6 \pm 0.6) \times 10^{3}$	$(8.3 \pm 0.7) \times 10^{3}$	$(8.0 \pm 0.7) \times 10^{3}$
pyridine, ***c*-P6$_{t\text{-Bu}}$·T6***	$K_{\text{pyp6t6*}}$ (M^{-5})	$(3.9 \pm 0.4) \times 10^{-6}$	$(4.7 \pm 0.4) \times 10^{-6}$	$(4.3 \pm 0.4) \times 10^{-6}$
quinuclidine, ***c*-P7$_{t\text{-Bu}}$·T7***	$K_{\text{qp7t7*}}$(M^{-6})	$(1.6 \pm 0.1) \times 10^{10}$	$(2.3 \pm 0.2) \times 10^{10}$	$(2.0 \pm 0.3) \times 10^{10}$
pyridine, ***c*-P7$_{t\text{-Bu}}$·T7***	$K_{\text{pyp7t7*}}$(M^{-6})	$(1.9 \pm 0.1) \times 10^{-2}$	$(2.4 \pm 0.1) \times 10^{-2}$	$(2.2 \pm 0.3) \times 10^{-2}$

From the titration results, it can be seen that for the same concentrations of the complexes at 0.34 μM, the system requires around 0.5 M, 40 mM and 8 mM of quinuclidine to completely break up ***c*-P6$_{t\text{-Bu}}$·T6**, ***c*-P6$_{t\text{-Bu}}$·T6*** and ***c*-P7$_{t\text{-Bu}}$·T7*** respectively. ***c*-P6$_{t\text{-Bu}}$·T6** has the strongest binding between the template and the nanoring; ***c*-P6$_{t\text{-Bu}}$·T6*** has relatively weaker binding and ***c*-P7$_{t\text{-Bu}}$·T7*** has the weakest binding among the three complexes.

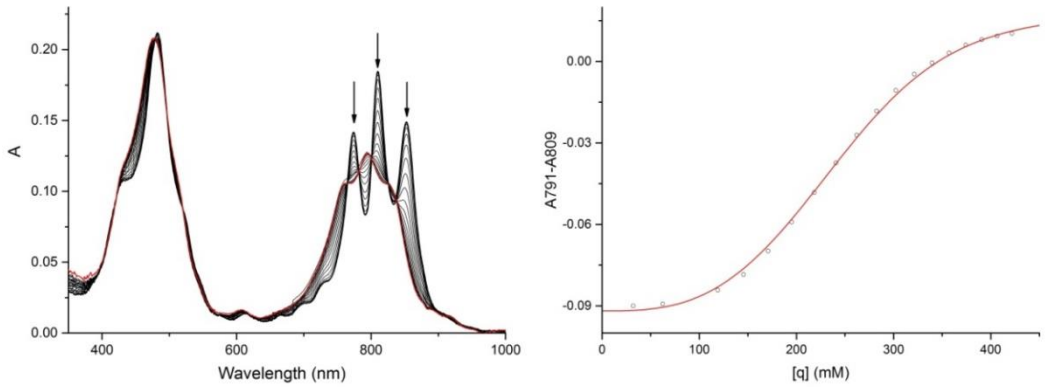

Figure 2.15 UV-vis titration of quinuclidine and ***c*-P6$_{t\text{-Bu}}$·T6**, K_{qp6t6} = (1.0 ± 0.1) × 10^{-3} M^{-5}, R^2 = 0.999. (Run 1, $CHCl_3$, 297 K, [***c*-P6$_{t\text{-Bu}}$·T6**] = 0.34 μM)

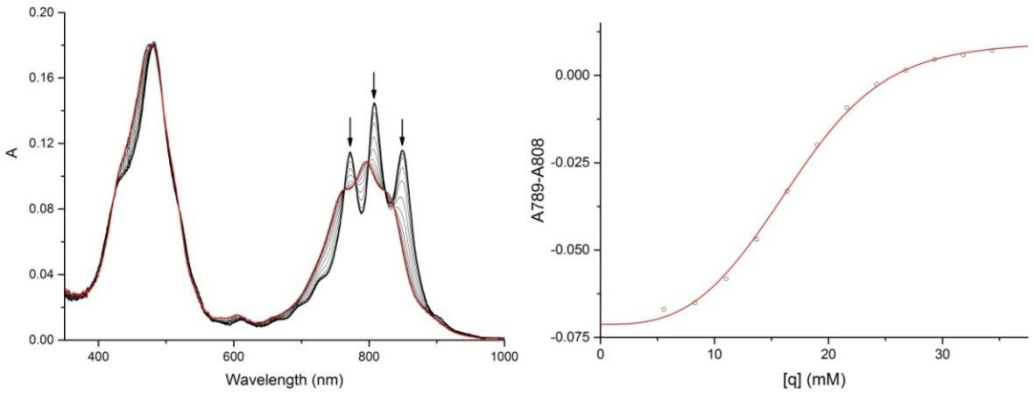

Figure 2.16 UV-vis titration of quinuclidine and ***c*-P6$_{t\text{-Bu}}$·T6***, K_{qp6t6*} = (7.6 ± 0.6) × 10^{3} M^{-5}, R^2 = 0.998. (Run 1, $CHCl_3$, 298 K, [***c*-P6$_{t\text{-Bu}}$·T6***] = 0.34 μM)

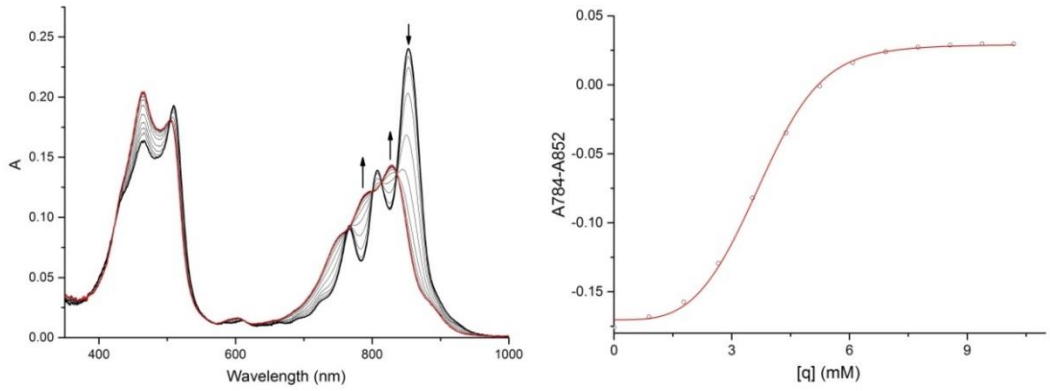

Figure 2.17 UV-vis titration of quinuclidine and ***c*-P7$_{t\text{-Bu}}$·T7***, K_{qp7t7*} = (1.6 ± 0.1) × 10^{10} M^{-6}, R^2 = 0.999. (Run 1, $CHCl_3$, 298 K, [***c*-P7$_{t\text{-Bu}}$·T7***] = 0.34 μM)

2.5.3 Calculation of Effective Molarities

The formation constants K_f of nanoring-template complexes were calculated from equation (2.5), which is derived from equation (2.2):

$$\log K_f = \log \frac{{K_L}^n}{K_{b,L}} = n\log K_L - \log K_{b,L} \quad (2.5)$$

where K_L is the association constants of the template-free ring ***c*-P*n*** with ligand L; $K_{b,L}$ is the denaturation constants of the nanoring-template complex with this ligand; n is the chelation number of nanoring-template complexes. For ***c*-P6$_{t\text{-Bu}}$·T6** and ***c*-P6$_{t\text{-Bu}}$·T6***, n = 6; for ***c*-P7$_{t\text{-Bu}}$·T7***, n = 7.

The logK_f values calculated from different ligand denaturation cycles are shown in **Table 2.4**.

Table 2.4 The formation constants of nanoring-template complexes.

Complex	logK_f (from quinuclidine denaturation)	logK_f (from pyridine denaturation)
***c*-P6$_{t\text{-Bu}}$·T6**	35.9 ± 0.2	—
c*-P6$_{t\text{-Bu}}$·T6	29.0 ± 0.2	29.2 ± 0.4
c*-P7$_{t\text{-Bu}}$·T7	32.0 ± 0.8	31.9 ±0.3

The geometric average effective molarities ($\overline{EM}$) of the nanoring-template complexes were calculated from equation (2.6), which is derived from equation (2.1):

$$\log\overline{EM} = \log \sqrt[n-1]{\frac{K_{chem,n}}{K_1^n}} = \log \sqrt[n-1]{\frac{K_f}{K_\sigma K_1^n}} = \frac{(\log K_f - \log K_\sigma - n\log K_1)}{(n-1)} \quad (2.6)$$

where $K_{chem,n}$ is the statistically corrected value of K_f (K_f/K_σ). As is shown in **Figure 2.18**, for ***c*-P6$_{t\text{-Bu}}$·T6** and ***c*-P6$_{t\text{-Bu}}$·T6***, K_σ = 768; for ***c*-P7$_{t\text{-Bu}}$·T7***, K_σ = 1792. K_1 is the reference ligand-ring single-site association constants statistically corrected from the association constants (K_L) measured in **Section 2.5.1**. The corresponding ligand for a specific template-nanoring complex has been shown in **Figure 2.8**.

The geometric average effective molarities of the nanoring complexes are shown in **Table 2.5**.

Table 2.5 The geometric average effective molarities of nanoring-template complexes.

Complex	K_1 (M^{-1})	K_σ	log$\overline{EM}$ (quinuclidine data)	log$\overline{EM}$ (pyridine data)	$\overline{EM}$(M)
***c*-P6$_{t\text{-Bu}}$·T6**	$(4.2 \pm 0.2) \times 10^3$	768	2.25 ± 0.05	—	180 ± 20
c*-P6$_{t\text{-Bu}}$·T6	$(6.5 \pm 0.5) \times 10^2$	768	1.85 ± 0.06	1.89 ± 0.09	74 ± 20
c*-P7$_{t\text{-Bu}}$·T7	$(1.8 \pm 0.1) \times 10^4$	1792	–0.16 ± 0.14	–0.17 ± 0.07	0.7 ± 0.1

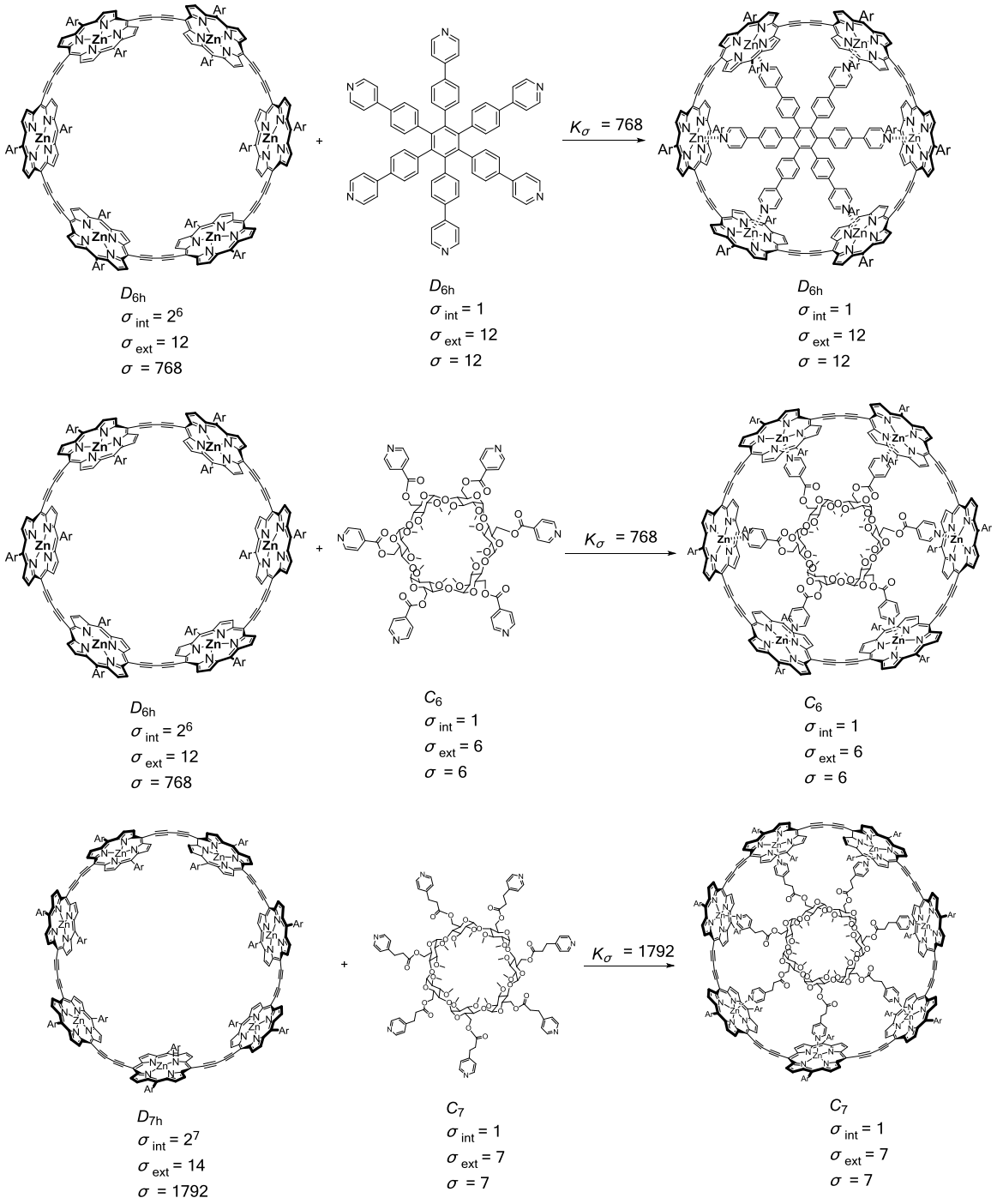

Figure 2.18 Statistical factors of ***c*-P6$_{t\text{-Bu}}$·T6**, ***c*-P6$_{t\text{-Bu}}$·T6*** and ***c*-P7$_{t\text{-Bu}}$·T7***.

2.5.4 Interpretation of Results

As is shown in **Table 2.5**, the difference between the log$\overline{EM}$ of ***c*-P6$_{t\text{-Bu}}$·T6** and ***c*-P6$_{t\text{-Bu}}$·T6*** is around 0.4; whereas 1/6 (geometric average distributed to each binding site) of the difference between the logK_f of ***c*-P6$_{t\text{-Bu}}$·T6** and ***c*-P6$_{t\text{-Bu}}$·T6*** is around 1.0, as is shown in **Table 2.4**. It can be seen that the $\overline{EM}$ values of two complexes are very similar; but their binding affinities have higher

differences. The explanation for the phenomenon comes from the microscopic single-site binding, i.e. the differences in K_1 of the two complexes (note the comparison of K_1 in **Table 2.5**). The electron-withdrawing COOMe group in **L2** gives a lower association constant compared to **L1**.

To verify this assumption, a set of reference titrations were performed between a porphyrin monomer ***l*-P1$_{t\text{-Bu}}$(THS,THS)** and the monodentate ligands: pyridine, **L1**, **L2** and **L3**. The titrations were performed to investigate the relationship between the *para*-substituents of pyridine and the association constants.

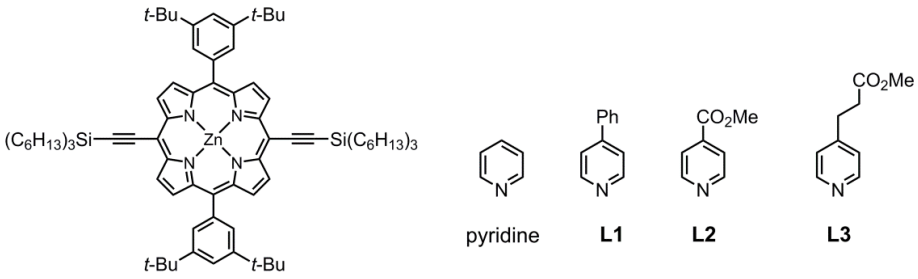

Figure 2.19 Structures of monodentate ligands and reference porphyrin monomer.

Titration curves were fitted to a 1:1 binding isotherm using equation (2.3). The sample spectra-fitting curve and full results are shown below.

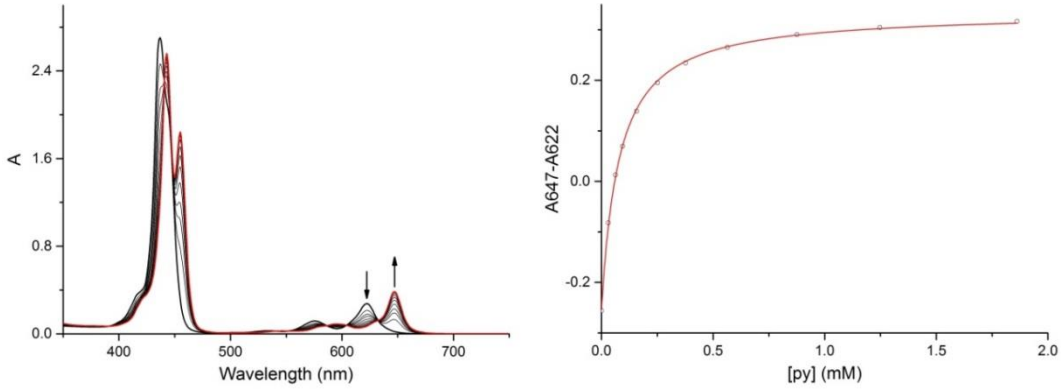

Figure 2.20 UV-vis titration of pyridine and ***l*-P1$_{t\text{-Bu}}$(THS,THS)**, K_L = (1.3 ± 0.1) × 10^4 M^{-1}, R^2 = 0.999. (Run 1, $CHCl_3$, 298 K, [***l*-P1$_{t\text{-Bu}}$(THS,THS)**] = 8.3 μM)

Table 2.6 The association constants of ***l*-P1$_{t\text{-Bu}}$(THS,THS)** and ligands (1:1 association constants in M^{-1})

Ligand	Run 1	Run 2	Average
pyridine	(1.3 ± 0.1) × 10^4	(1.2 ± 0.1) × 10^4	(1.2 ± 0.1) × 10^4
L1	(7.8 ± 0.2) × 10^3	(8.5 ± 0.1) × 10^3	(8.1 ± 0.4) × 10^3
L2	(2.8 ± 0.1) × 10^3	(2.5 ± 0.1) × 10^3	(2.6 ± 0.2) × 10^3
L3	(1.2 ± 0.1) × 10^4	(1.4 ± 0.1) × 10^4	(1.3 ± 0.1) × 10^4

As is shown in **Table 2.6**, the ligand with electron-withdrawing COOMe group, **L2**, has a significantly lower K_L than the other ligands, which proves the previous assumption.

2.5.5 EM Comparison – Flexibility and Cooperativity

Flexible constituents in supramolecular systems change the preorganization status in the interactions and give entropy increase to the system, which is reflected in the value of EM. Previous investigations revealed that in a cyclic cooperative system of a completely flexible chain, the EM is proportional to $i^{-1.5}$, where i is the number of segments in the chain.[7] Hunter reported that in a supramolecular system, the cost of freezing a rotor is in general 5 kJ mol^{-1}.[8]

As is shown in **Figure 2.21**, the preorganization statuses of templates for porphyrin nanoring syntheses have distinctive differences. All the bond rotations in **T6** do not change the ligand orientation; thus **T6** has no rotors inside to be frozen in the complex. The free rotation of ester bond also does not alter the orientation in the cyclodextrin templates. **T6*** has two rotors in 5- and 6-C of the CD core, which have already been partially hindered (frozen) by the bulky CD core. In addition to the rotors in **T6***, **T7*** has two more rotors from –$(CH_2)_2$– in the bridge between the pyridyl and the ester bond; all the aromatic bonds in the pyridyl ligand of ***meta*-T6*** are free rotors.

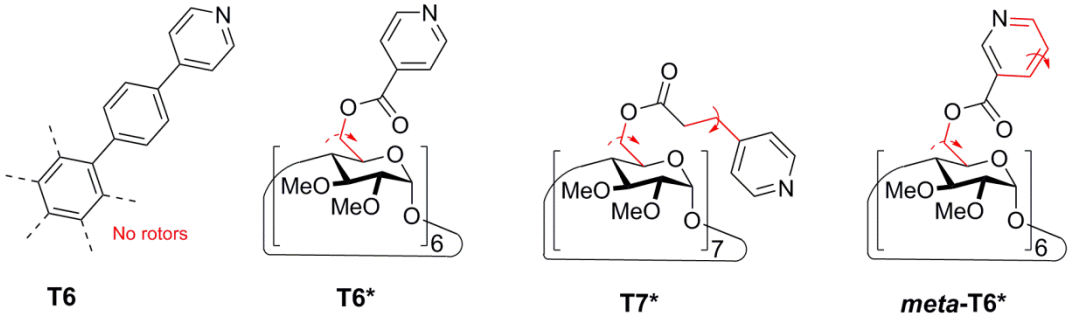

Figure 2.21 The free rotors inside the templates to be frozen in the template-nanoring complex.

As we have subtracted the electrostatic effects in the calculation of $\overline{EM}$, the free energy differences averaged to each binding site of ***c*-P6·T6**, ***c*-P6·T6***, and ***c*-P7·T7*** i.e. the costs of freezing the rotors in each ligand in **T6*** and **T7*** can be calculated using the derivation of equation (1.3).

$$\Delta\Delta G_{\mathbf{T6}*} = \Delta G_{\boldsymbol{c}\mathbf{-P6\cdot T6}} - \Delta G_{\boldsymbol{c}\mathbf{-P6\cdot T6}*} = -(RTln\overline{EM_{\boldsymbol{c}\mathbf{-P6\cdot T6}}} - RTln\overline{EM_{\boldsymbol{c}\mathbf{-P6\cdot T6}*}}) \qquad (2.7)$$

$$\Delta\Delta G_{\mathbf{T7}*} = \Delta G_{\boldsymbol{c}\mathbf{-P6\cdot T6}} - \Delta G_{\boldsymbol{c}\mathbf{-P7\cdot T7}*} = -(RTln\overline{EM_{\boldsymbol{c}\mathbf{-P6\cdot T6}}} - RTln\overline{EM_{\boldsymbol{c}\mathbf{-P7\cdot T7}*}}) \qquad (2.8)$$

The costs of freezing the rotors in each ligand is 2.2 kJ mol^{-1} for **T6*** and 13.7 kJ mol^{-1} for **T7***.

If we assume the freezing energy of one rotor is 5.0 kJ mol^{-1},[8] there is 0.44 rotor in each ligand of **T6***. The number of the rotor is not integral, which reflects the hindering effects of the CD core. There are 2.74 rotors in in each ligand of **T7***, which is more than the expected 2.44 rotors based on the comparison of **T6***. The reason for this phenomenon is that ***c*-P7** is a larger and more flexible ring compared to ***c*-P6**; and the flexibility of the ring is taken into equation (2.8), which gives an increase of the free energy cost.

The EM has a close relationship with the efficiency in the syntheses. For rigid **T6** and **T6*** (only with a fraction of flexibility), the yield of ***c*-P6** is above 20% from porphyrin monomer; for flexible **T7***, the yield of ***c*-P7** is below 5% from porphyrin monomer; for ***meta*-T6*** with even more flexibility, the template fails to direct the synthesis of porphyrin nanorings.

2.6 Summary

To summarize, three chiral templates based on cyclodextrin structures have been synthesized and two of them have been successfully applied in the syntheses porphyrin nanorings. A molecular template does not need to be totally rigid to direct the syntheses of porphyrin nanorings. The cooperativity of the nanoring-template systems has been investigated in detail, revealing that flexibility causes free energy cost in the system. Flexible components should be restricted to a certain limit, so that the chelation inside the system outcompetes the free energy cost and the target molecule can be achieved.

T7* is the first prime-numbered template for porphyrin nanoring synthesis. This opens up many possibilities in the Vernier-templating synthesis, which will be shown in the next chapter.

2.7 References

[1] G. Sforazzini, *Supramolecular Engineering of Threaded Molecular Wires*, D.Phil. thesis, University of Oxford, Oxford, 2010.

[2] J. K. Sprafke, D. V. Kondratuk, M. Wykes, A. L. Thompson, M. Hoffmann, R. Drevinskas, W.-H. Chen, C. K. Yong, J. Kärnbratt, J. E. Bullock, M. Malfois, M. R. Wasielewski, B. Albinsson, L. M. Herz, D. Zigmantas, D. Beljonne, H. L. Anderson, *J. Am. Chem. Soc.* **2011**, *133*, 17262–17273.

[3] D. V. Kondratuk, J. K. Sprafke, M. C. O'Sullivan, L. M. A. Perdigao, A. Saywell, M. Malfois, J. N. O'Shea, P. H. Beton, A. L. Thompson, H. L. Anderson, *Chem. Eur. J.* **2014**, *20*, 12826–12834.

[4] H. J. Hogben, J. K. Sprafke, M. Hoffmann, M. Pawlicki, H. L. Anderson, *J. Am. Chem. Soc.* **2011**, *133*, 20962–20969.

[5] C. A. Hunter, H. L. Anderson, *Angew. Chem. Int. Ed.* **2009**, *48*, 7488–7499.

[6] P. N. Taylor, H. L. Anderson, *J. Am. Chem. Soc.* **1999**, *121,* 11538–11545.

[7] M. C. Misuraca, T. Grecu, Z. Freixa, V. Garavini, C. A. Hunter, P. W. N. M. van Leeuwen, M. D. Segarra-Maset, S. M. Turega, *J. Org. Chem.* **2011**, *76*, 2723–2732.

[8] H. Adams, E. Chekmeneva, C. A. Hunter, M. C. Misuraca, C. Navarro, S. M. Turega, *J. Am. Chem. Soc.* **2013**, *135*, 1853−1863.

Chapter 3

Vernier-Templating Behavior of the Flexible 7-Dentate Template

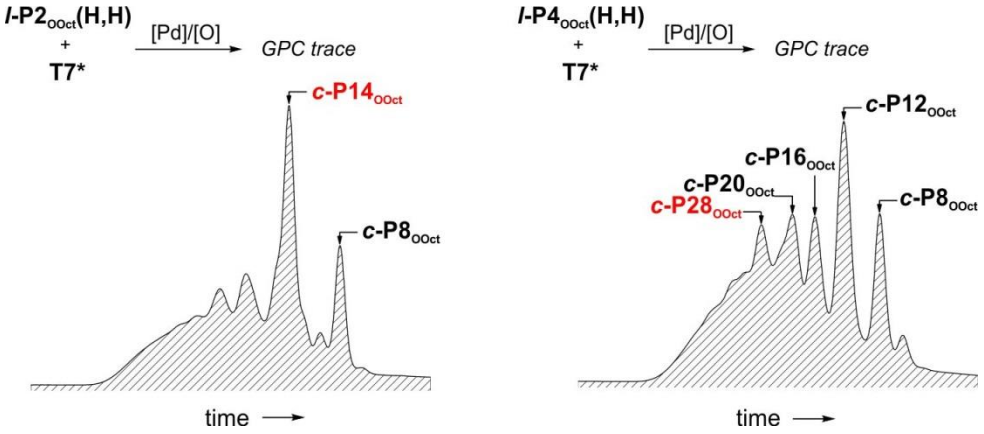

*This chapter describes the Vernier-templating synthetic attempts using linear porphyrin oligomers and **T7*** to prepare larger porphyrin nanorings. The investigations were focused on the optimization of reaction conditions for higher yields of porphyrin nanorings. The behavior of flexible templates in the Vernier-templating syntheses gives more insights to the role of rigidity/flexibility in supramolecular systems.*

3.1 Background Information

As was shown in **Chapter 1**, previous investigations in Anderson's group on the Vernier-templating syntheses were focused on the rigid templates **T6** and **T8** (**Scheme 1.5**, **Figure 1.8**). As we have obtained a prime-numbered flexible template **T7*** which was shown in **Chapter 2**, coupling linear porphyrin oligomers ***l*-P*N*(H,H)** in the presence of **T7*** should give a Vernier-templating product as ***c*-P(7*N*)**, provided $N \neq 7$.

In this chapter, we attempt to add new porphyrin nanorings with different number of units to the nanoring library by Vernier-templating synthesis; at the same time, the role of flexibility in supramolecular systems will be investigated in more detail from the synthetic results.

Linear porphyrin oligomers ***l*-P*N*** (N = 1, 2, 4, 8) were prepared using the half-deprotection/ coupling strategy introduced in **Scheme 1.2** of **Chapter 1**. The aryl side groups on the porphyrins were chosen as octyloxy groups since this side group endows sufficient solubility to larger porphyrin nanorings and systematic calibration data of the analytical GPC traces of ***c*-P*N*$_{\mathbf{OOct}}$** are available so that the identification of the signals in GPC trace will be easier.[1,2]

3.2 Reaction Conditions for Vernier-Templating Synthesis

Vernier-templating reactions are very demanding in terms of reaction conditions since many factors can affect the pre-reaction binding between porphyrin oligomers and the template. These factors include competing ligands, the template-oligomer ratio, and even the nature of solvents. Non-optimal reaction conditions normally lead to the formation of linear polymers of porphyrins, indicating that the choice of the solvent is wrong; or there might be pyridine (or other molecules with affinities to porphyrin) impurities in the solvent; or the template/oligomer ratio is not ideal.

Previous experience in Vernier-templating synthesis gave a general idea of the choice of reaction conditions.

Solvents. Toluene and chloroform are most frequently chosen as they are usually very stable for oxidation reactions and can dissolve both template and porphyrin oligomers. Chloroform can dissolve a wider range of compounds; but its solvent quality is variable since chloroform can generate traces of acid in the presence of oxygen and the trace of acid would affect the binding

between template and porphyrin oligomers.[3] Also, ethanol is often used as the stabilizer of chloroform and it has weak binding to the porphyrin sites. Toluene has better stability, giving a slightly better binding between porphyrin oligomers and the template; but it has a smaller range of dissolvable compounds. The choice of solvents needs to be determined by trial experiments.

Concentration of porphyrin oligomers. Porphyrin oligomers are the molecules with highest molecular weight in the reaction system and are often considered as the basis for the concentration of the reaction. An ordinary concentration for the reaction is: 1 mg of porphyrin oligomer dissolved in 1 – 1.5 mL of the solvent. More dilute conditions usually reduce the interactions between molecule clusters, giving less polymeric porphyrin side-products and also elevating the yields of small porphyrin nanorings; more concentrated conditions usually increase the interactions between molecule clusters, thereby elevating the yield of larger porphyrin nanorings but in the same time generating more polymeric porphyrin side-products.

Template/oligomer molar ratios. There is a theoretical stoichiometry between the two components according to their number of binding sites; however, the experimental results usually indicated that a slight excess of one reactant gives better yield of the desired Vernier product. The detailed mechanism involved in the reaction process is complicated and is not fully understood yet. A tentative description of two possible mechanisms of the Vernier-templating reaction (the figures use **T7*** and ***l*-P2(H,H)** system as example) process is shown.

As is shown in **Figure 3.1**, the Vernier complex **(*l*-P2(H,H))$_7$·(T7*)$_2$** is the precursor to the desired product. There is a competitive equilibrium between the Vernier complex and the mixture of ***l*-P2(H,H)** and **(*l*-P2(H,H))$_3$·T7***, which is the precursor of linear oligomers. Excess ***l*-P2(H,H)** pushes the equilibrium towards the Vernier complex side, giving a better yield to the reaction.

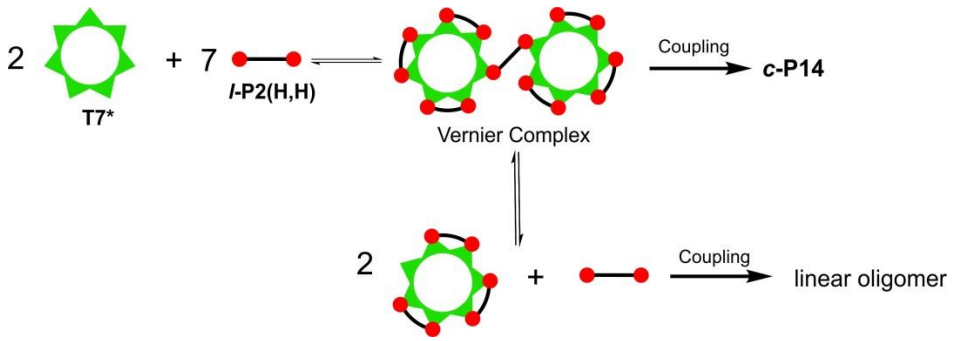

Figure 3.1 Proposed mechanism in Vernier-templating synthesis – Vernier complex pre-formation.

As is shown in **Figure 3.2**, the system first forms a linear intermediate ***l*-P14(H,H)** from

coupling of 7 porphyrin dimers. The subsequent binding between ***l*-P14(H,H)** and two **T7*** templates results in the formation of closed nanoring form and the chain elongation stops. Excess **T7*** terminates the chain elongation in time, giving a better yield to the reaction by reducing the formation of longer linear/cyclic porphyrin oligomers.

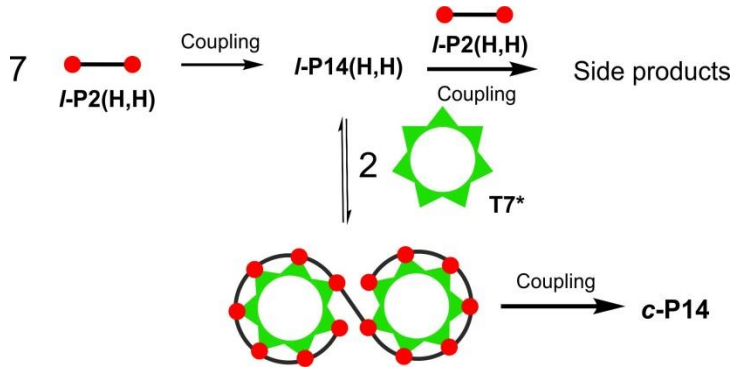

Figure 3.2 Proposed mechanism in Vernier-templating synthesis – linear oligomer pre-formation.

The two mechanisms shown above are two extremes and the real situation might be a combination of them (chain elongation accompanied by template binding). We can never precisely predict which intermediate complex in the mechanisms is more favored; since we are still accumulating experiences in the area of Vernier-templating synthesis. So a sensible strategy is to perform trial reactions in different ratios and to obtain information from the ratio-yield relationship.

Temperature. The temperature and catalyst/oxidant systems were optimized for the synthesis of ***c*-P6·T6** and the conditions were adopted in the Vernier-templating synthesis.[4] The reactions were performed at room temperature to give a better binding between template and porphyrin oligomers.[5]

Catalyst/oxidant system. Pd/Cu co-catalyst system was used with 1,4-benzoquinone oxidant to give a good oxidative catalytic cycle.[6] The nature and concentration of the catalyst/oxidant system influence the coupling efficiency of the reaction; but we do not currently know the exact relationship between the product distribution and coupling efficiency.

Reaction time. The synthesis of ***c*-P6·T6** from ***l*-P1(H,H)** requires about 5 h to complete. As large porphyrin nanorings are no longer active for coupling reactions, we elongate the reaction time to overnight to maximize the chain growth of the linear polymer by-product, thereby facilitating the separation process.

3.3 Experimental Results

3.3.1 Synthesis of *c*-P14 from Porphyrin Dimer and T7*

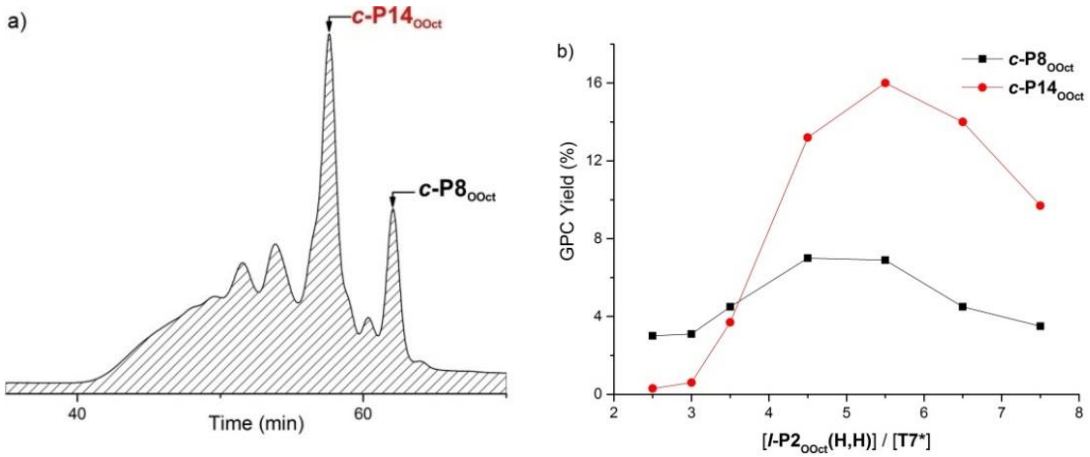

Figure 3.3 a) Analytical GPC trace of the reaction mixture of Vernier-templating synthesis between ***l*-P2$_{OOct}$(H,H)** and **T7***, [***l*-P2$_{OOct}$(H,H)**] / [**T7***] = 5.5. b) GPC yields of ***c*-P8$_{OOct}$** and ***c*-P14$_{OOct}$** in different template-oligomer molar ratios. Reaction conditions: 1.0 mL $CHCl_3$ per milligram of ***l*-P2$_{OOct}$(H,H)** (1 equiv.), $Pd(PPh_3)_2Cl_2$ (0.5 equiv.), CuI (5 equiv.), 1,4-benzoquinone (10 equiv.), r.t., overnight. Trial reaction scale: ***l*-P2$_{OOct}$(H,H)** (5.0 mg).

l*-P2$_{OOct}$(H,H)** underwent Pd/Cu co-catalyzed oxidative coupling in the presence of **T7 to give the Vernier product as ***c*-P14$_{OOct}$**. Different template/oligomer molar ratios were performed in trial reactions to generate the maximum yield of ***c*-P14$_{OOct}$**. The analytical results gave the highest GPC yield of 16% when the template-oligomer molar ratio is: [***l*-P2$_{OOct}$(H,H)**] / [**T7***] = 5.5. Under this condition, ***c*-P14$_{OOct}$** was isolated in 6.4% yield. ***c*-P8$_{OOct}$** is a significant byproduct of the reactions. Note that the stoichiometry of the Vernier complex is: [***l*-P2$_{OOct}$(H,H)**] / [**T7***] = 3.5.

3.3.2 Synthesis of *c*-P28 from Porphyrin Tetramer and T7*

l*-P4$_{OOct}$(H,H)** underwent Pd/Cu co-catalyzed oxidative coupling in the presence of **T7 to give the Vernier product as ***c*-P28$_{OOct}$**. Unfortunately, the major product of the reactions was not ***c*-P28$_{OOct}$**.

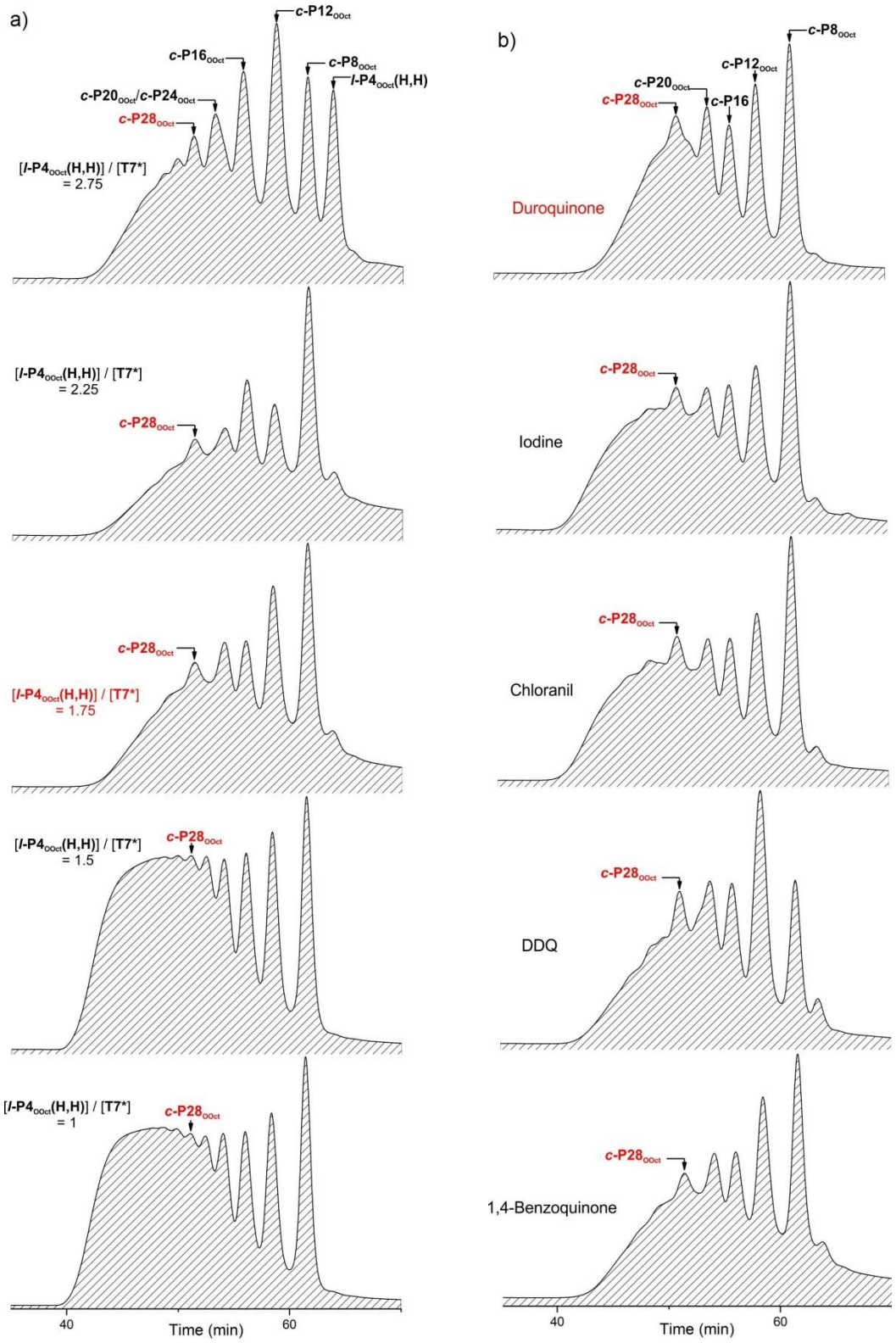

Figure 3.4 Analytical GPC traces of the reaction mixture of Vernier-templating synthesis between **T7*** and ***l*-P4$_{OOct}$(H,H)**. Reaction conditions: 1.5 mL $CHCl_3$ per milligram of ***l*-P4$_{OOct}$(H,H)** (1 equiv.), $Pd(PPh_3)_2Cl_2$ (0.5 equiv.), CuI (5 equiv.), oxidants (10 equiv.), r.t., overnight. Trial reaction scale: ***l*-P4$_{OOct}$(H,H)** (4.0 mg). a) Oxidant: 1,4-benzoquinone, variable: template/oligomer molar ratio; b) [***l*-P4$_{OOct}$(H,H)**] / [**T7***] = 1.75, variable: oxidants. DDQ: 2,3-dichloro-5,6-dicyano-*para*-benzoquinone.

As is shown in **Figure 3.4**, we tried adjusting reaction conditions such as template/oligomer molar ratio and the nature of the oxidant to improve the yield of Vernier product; but the improvement was very limited: either ***c*-P8$_{OOct}$** or ***c*-P12$_{OOct}$** was the main product; and the ideal reaction conditions still resulted in many porphyrin nanorings that were smaller than expected. Nevertheless, although ***c*-P28$_{OOct}$** was not the main product, its formation was favored compared to the porphyrin nanorings with similar sizes (***c*-P24$_{OOct}$** and ***c*-P32$_{OOct}$**), which proved that the template had influences on the product distribution.

For template/oligomer molar ratio, the yield of desired product ***c*-P28$_{OOct}$** did not vary much when ***l*-P4$_{OOct}$(H,H)** was in excess ([***l*-P4$_{OOct}$(H,H)**] / [**T7***] > 1.75); except that the amount of unreacted ***l*-P4$_{OOct}$(H,H)** increased in the reaction mixture as more linear porphyrin oligomer was in excess. The result of the reaction was not ideal when **T7*** was in excess ([***l*-P4$_{OOct}$(H,H)**] / [**T7***] < 1.75), indicating that the mechanism of the Vernier-templating reaction probably follows the proposal shown in **Figure 3.1**: a Vernier complex between template and linear porphyrin oligomer. When **T7*** was in excess, the Vernier complex was disrupted to give precursors for linear porphyrin polymers. So the recommended reaction molar ratio is the stoichiometry; however, as there might be possible mechanical errors in the weighting process, a slight excess of linear porphyrin oligomer might be a safer bet.

For oxidants, the results also did not vary much for oxidants with different reactivity. Duroquinone gave a slightly better result; the reason for this phenomenon is probably that duroquinone forms a more thermodynamically stable hydroquinone product, which does not lead to other side reactions. Thus the oxidation procedure proceeded in a cleaner way.

***c*-P28$_{OOct}$** did not dominate the relative concentration in the mixture due to the inefficiency of the reaction, which made the isolation of Vernier product ***c*-P28$_{OOct}$** tedious. We did not successfully isolate the Vernier product in high purity.

3.3.3 Synthesis of *c*-P56 from Porphyrin Octamer and T7*

As is shown in **Figure 3.5**, the synthesis of ***c*-P56** from ***l*-P8$_{OOct}$(H,H)** and **T7*** was investigated in comparison with the template-directed syntheses using **T7*** and ***l*-P*N*$_{OOct}$(H,H)** (*N* = 1, 2, 4) in identical reaction conditions. The reason is that the other reactions provided references to judge the qualities of the reaction conditions. ***c*-P7$_{OOct}$**, ***c*-P14$_{OOct}$** and ***c*-P28$_{OOct}$** were prepared successfully

in respective reactions, proving that the quality of the solvent and oxidants along with other reaction conditions was acceptable for the set of experiments.

It can be seen that in the Vernier-templating synthesis between ***l*-P8$_{OOct}$(H,H)** and **T7***, the desired product is virtually not formed. This can be explained from the fact that the synthesis of ***c*-P28$_{OOct}$** is not ideal using the method: the Vernier complex for a 28-porphyrin nanoring is already not favored enough in the reactions, let alone a nanoring that is twice as big. In all, the flexible **T7*** is not potent enough to hold up Vernier complexes higher than 14 porphyrin units in the reactions.

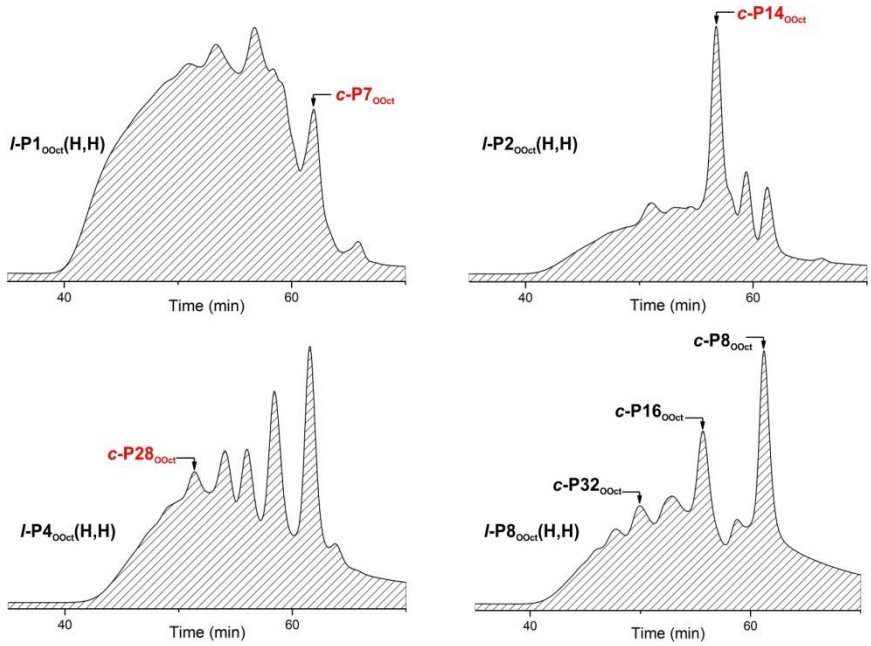

Figure 3.5 Analytical GPC traces of the reaction mixture of Vernier-templating synthesis between **T7*** and ***l*-P*N*$_{OOct}$(H,H)** (*N* = 1, 2, 4, 8). Reaction conditions: 1.4 mL $CHCl_3$ per milligram of ***l*-P*N*$_{OOct}$(H,H)** (1 equiv.), [porphyrin units] / [**T7***] = 8.0, $Pd(PPh_3)_2Cl_2$ (0.5 equiv.), CuI (5 equiv.), duroquinone (10 equiv.), r.t., overnight. Trial reaction scale: ***l*-P*N*$_{OOct}$(H,H)** (5.0 mg).

3.3.4 Product Characterization

As is shown in **Figure 3.6**, ***c*-P14$_{OOct}$** was characterized by ^{1}H NMR and mass spectra. The molecular weights (in logarithm form) of other porphyrin nanoring products were plotted against their corresponding retention time to prove their identity.[2]

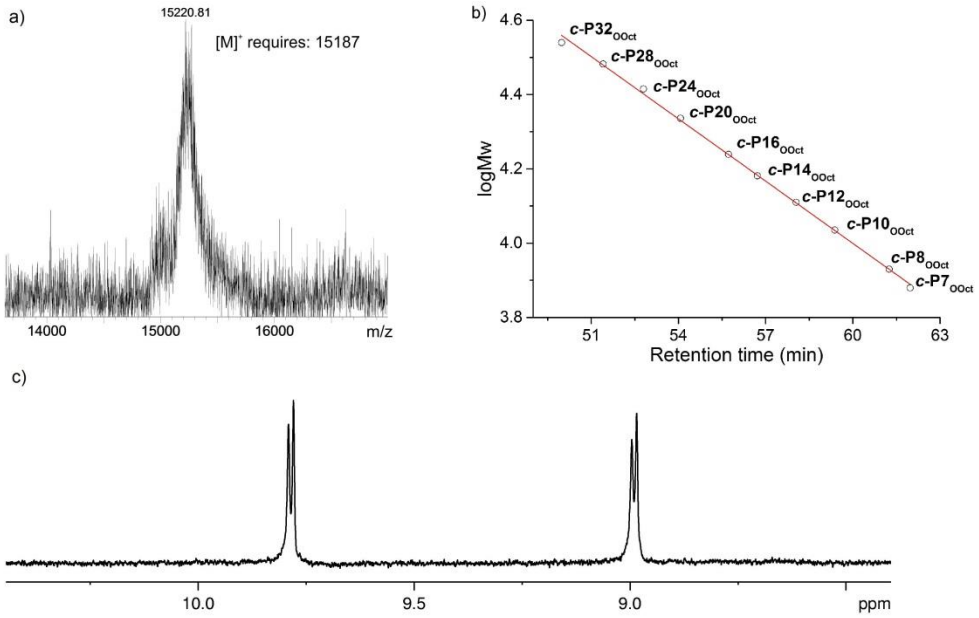

Figure 3.6 a) MALDI-MS spectrum of ***c*-P14$_{OOct}$** (flight mode: linear; matrix: DCTB); b) Calibration of porphyrin nanorings synthesized in the reactions reported in this chapter. logMw = 7.3524 – 0.0559t. GPC columns: line of JAIGEL 3H (20 × 600 mm) and JAIGEL 4H (20 × 600 mm) columns; eluent: toluene/pyridine (100/1, *v*/*v*); flow rate: 3.5 mL/min; c) β-proton region in the ^{1}H NMR spectra of ***c*-P14$_{OOct}$**. ($CDCl_3$, 400 MHz, 298 K)

3.4 Discussion and Summary

As is shown in **Figure 3.7**, the rigid template **T6** had better efficiencies than the flexible template **T7*** in synthesizing porphyrin nanorings with similar sizes, especially with regard to bigger porphyrin nanorings. The results indicate that the Vernier complex is a balance between rigidity and flexibility: **T6** is rigid enough to guarantee the stability of a Vernier complex bearing up to 30 porphyrin units with flexible butadiyne linkers; whereas with flexible **T7*** as the template, the similar-sized Vernier complex bearing 28 porphyrin units is not stable enough to be the major product of the reaction. For ***c*-P30·(T6)$_5$**, the balance between rigidity and flexibility still retains; whereas for ***c*-P28·(T7*)$_4$**, too much flexibility disrupts the balance and the yield of desired product is not ideal.

On the other hand, in the Vernier-templating syntheses using **T7*** as the template, the reaction mixture always gave a wider distribution of the products: ***c*-P8**, ***c*-P9**, ***c*-P10** and other products were obtained along with ***c*-P7** in the coupling of ***l*-P1(H,H)** with **T7***; this phenomenon applies for coupling of other oligomers with **T7*** as well.

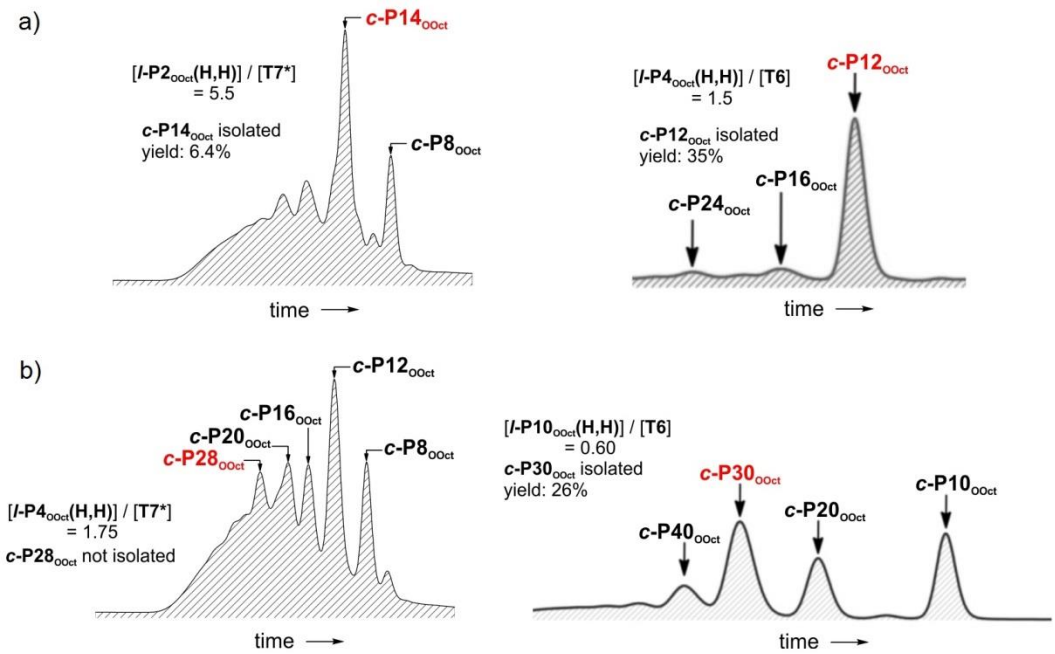

Figure 3.7 Comparison of the performances of **T7*** and **T6** in Vernier-templating reactions to synthesize porphyrin nanorings with similar sizes. a) ***c*-P14** (from **T7***) vs ***c*-P12** (from **T6**); b) ***c*-P28** (from **T7***) vs ***c*-P30** (from **T6**). GPC traces of **T6** Vernier-templating reaction mixtures were adapted from ref. 1 with permission. The time scales are not presented as they adopt different GPC separation conditions.

So what is the role of rigidity and flexibility in the supramolecular system?

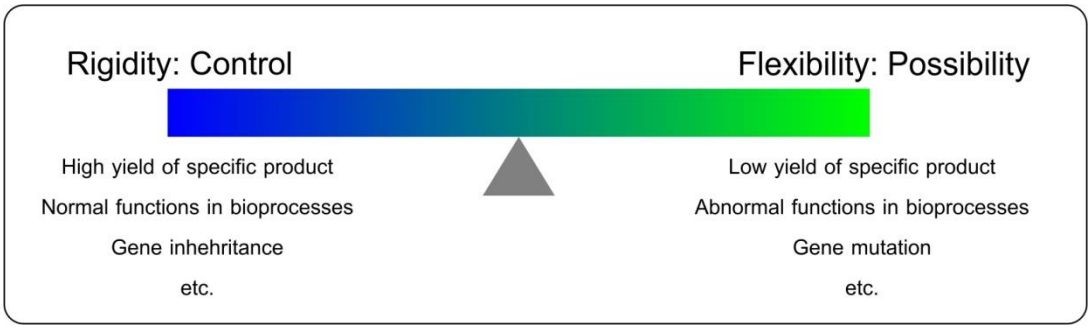

Figure 3.8 Balance between rigidity and flexibility in supramolecular systems.

Rigidity symbolizes control in supramolecular systems. If the geometry is right, it will guarantee the high yield of desired product in the syntheses by increasing the stability of the corresponding complexes.[7,8] Looking into an even bigger supramolecular system – life, the rigidity controls normal (expected) functioning in bioprocesses, such as gene inheritance and normal functioning of enzymes. It should be noted that rigidity in biomolecules is often generated by steric hinderance, H-bonds, π-π stacking and other delicate interactions for secondary structures and above; whereas in our Vernier-templating synthetic systems, the rigidity of the template is

generated by aromatic planar structures.

Flexibility is just on the other side, symbolizing possibility in supramolecular systems. Flexibility gives a lot of undesired product; but what is undesired in this specific reaction might be interesting for other experiments. In biochemistry, flexibility symbolizes abnormal (unexpected) functioning in bioprocesses, such as gene mutation and abnormal pathways that the enzymes take. Most of the time, flexibility is undesired; but it is necessary since the biosystem keeps changing and life needs new possibilities to adapt. Flexibility is also necessary for the Vernier-templating synthesis of porphyrin nanorings: if the butadiyne linker were not flexible at all, we would not obtain any ring structures with curved linkers, let alone Vernier products.

In summary, Vernier template-directed synthesis, just like life, is a magic balance between the interplay of rigidity and flexibility. We have investigated the performances of a flexible template **T7*** and have drawn more insights of the role of rigidity and flexibility in supramolecular systems, despite the fact that our desired 28- and 56-porphyrin nanorings were not efficiently synthesized.

3.5 References

[1] D. Kondratiuk, *Synthesis and Properties of Giant Porphyrin Nanorings*, D.Phil. thesis, University of Oxford, Oxford, 2013.

[2] D. V. Kondratuk, L. M. A. Perdigao, A. M. S. Esmail, J. N. O'Shea, P. H. Beton, H. L. Anderson, *Nature Chem.* **2015**, *7*, 317–322.

[3] E. Turk, *C&EN* **1998**, *76*, 6.

[4] J. K. Sprafke, D. V. Kondratuk, M. Wykes, A. L. Thompson, M. Hoffmann, R. Drevinskas, W.-H. Chen, C. K. Yong, J. Kärnbratt, J. E. Bullock, M. Malfois, M. R. Wasielewski, B. Albinsson, L. M. Herz, D. Zigmantas, D. Beljonne, H. L. Anderson, *J. Am. Chem. Soc.* **2011**, *133*, 17262–17273.

[5] D. W. McCallien, J. K. M. Sanders, *J. Am. Chem. Soc.* **1995**, *117*, 6611–6612.

[6] V. E. Williams, T. M. Swager, *J. Polym. Sci., Part A: Polym. Chem.* **2000**, *38*, 4669–4676.

[7] A. Camara-Campos, C. A. Hunter, S. Tomas, *Proc. Natl. Acad. Sci. U.S.A.* **2006**, *103*, 3034–3038.

[8] H. J. Hogben, J. K. Sprafke, M. Hoffmann, M. Pawlicki, H. L. Anderson, *J. Am. Chem. Soc.* **2011**, *133*, 20962–20969.

Chapter 4

Five-Porphyrin Nanorings

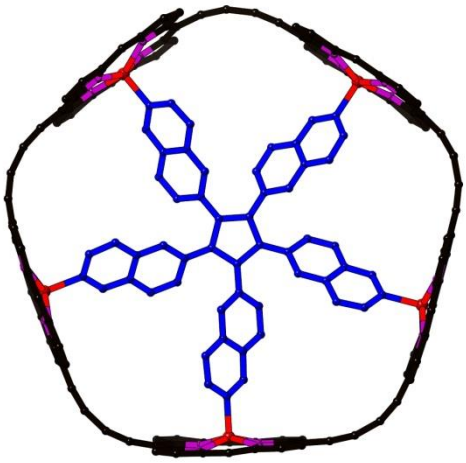

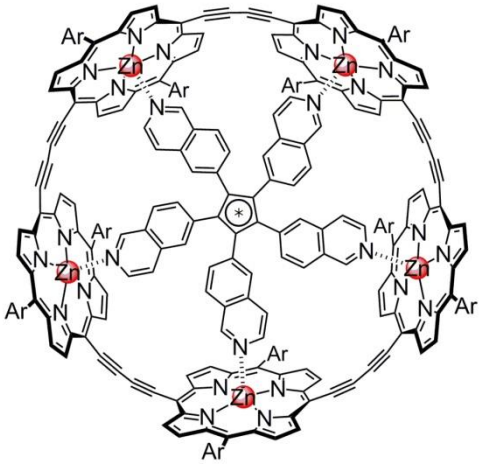

This chapter describes the molecular design and synthesis of 5-porphyrin nanorings using a ferrocene-based template. The corresponding cooperativity was investigated by measuring the geometric average of the effective molarity of the template-nanoring complex. The strain in the 5-porphyrin nanoring structure accounts for the instability of the 5-porphyrin nanoring.

4.1 Background Information

Currently, the smallest porphyrin nanoring based on butadiyne linkers is ***c*-P6**, which has high yield in template-directed syntheses and good stability. The idea behind this chapter is fairly simple: based on butadiyne linkers, how small can a porphyrin nanoring be? Can a 5-porphyrin nanoring be made and what specific properties will be interesting for this porphyrin nanoring?

4.2 Molecular Design

The 5-fold symmetric structure based on a cyclopentadienyl unit was adopted for the modelling of the templates. As the template for a five-porphyrin nanoring has never been made, we only considered rigid structures in the design to maximize the chances of success. 6-Isoquinolinyl and 4-pyridylethynyl were chosen as the functional groups on the Cp ring. The calculation results and chemical structure are shown in **Figure 4.1**.

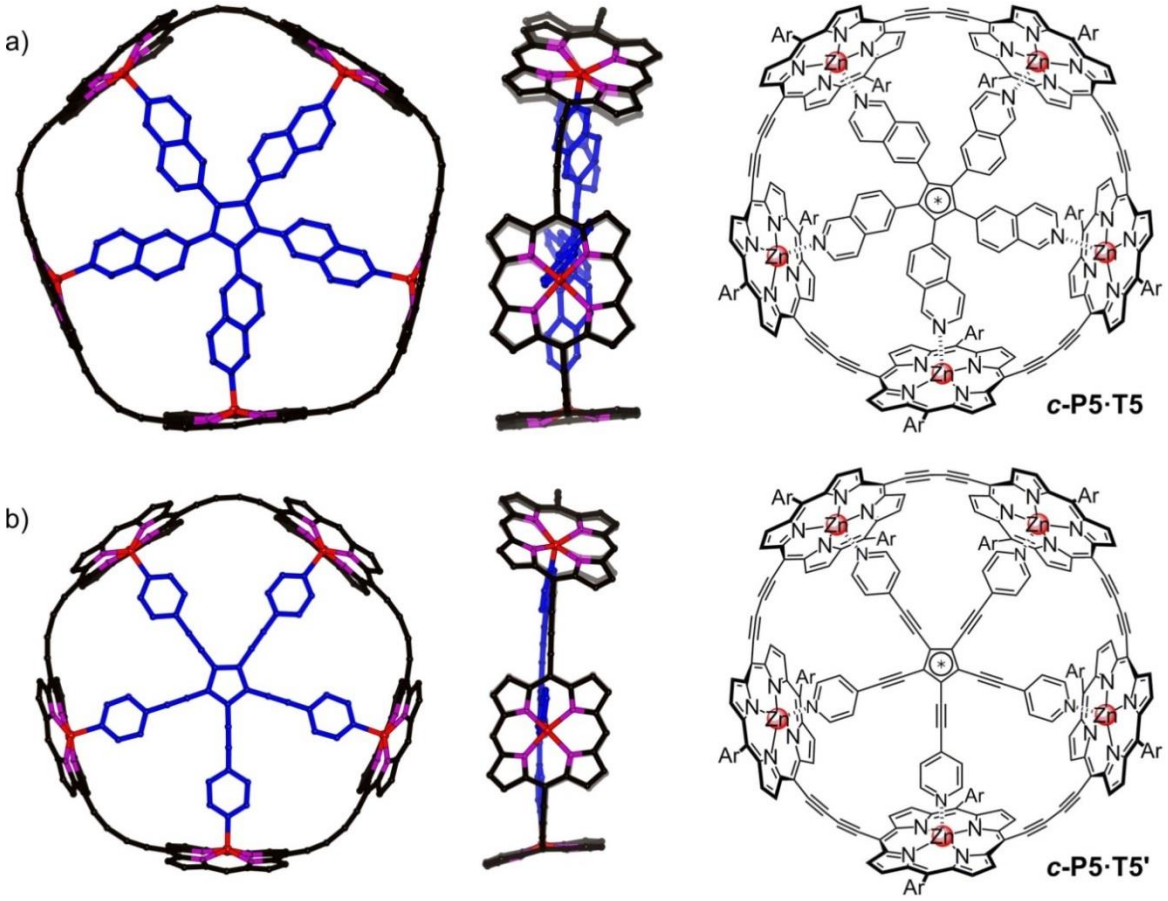

Figure 4.1 Molecular mechanics calculation (orthogonal views) and chemical structure of a) ***c*-P5·T5** and b) ***c*-P5·T5'**. *meso*-Aryl groups, hydrogen atoms and one of the Cp groups in the template are omitted for clarity. See ref. 1 for detailed parameters for the modeling of butadiyne-linked porphyrin oligomers.

For rigid templates, we can compare their geometry to that of template-free 5-porphyrin nanoring to predict how well the template and nanoring fit with each other. We assume the template-free porphyrin nanorings as perfect circles for the templates to fit in. Then the ring size can be determined by the circumference of the perfect circle. Our group has previously reported the crystal structure of ***l*-P2$_{t\text{-Bu}}$(THS,THS)**, which we can be used as the basis for the calculation of the circumference.[2] As is shown in **Figure 4.2**, the zinc atom is slightly out of the porphyrin plane. Two artificial atoms are added to the crystal structure by calculation of the centroid of N_4Zn units in each porphyrin unit. The distance between the two centroids is 13.51 Å.

Figure 4.2 The distance between two centroids of the N_4Zn units in the porphyrin unit in ***l*-P2$_{t\text{-Bu}}$(THS,THS)** crystal structure. H atoms, *meso*-substituents and coordinating pyridines are omitted for clarity. Crystal structure obtained from ref. 2, CCDC 182/798.

Theoretically, the circumference of an *n*-porphyrin nanoring with butadiyne linkers will be the *n*-fold of 13.51 Å, if we assume the template-free nanorings are perfect circles. The radius of a perfectly circular template-free 5-porphyrin nanoring is calculated as 10.75 Å.

When coordinated to ligands, zinc atom is slightly out of the porphyrin plane (which can be seen in **Figure 4.1** and **Figure 4.2**). We adopt the distance between the zinc atom and porphyrin plane in the reported crystal structure of ***c*-P6$_{t\text{-Bu}}$·T6** as 0.24 Å.[3] We adopt the distance between nitrogen and zinc atom in coordination from the same crystal structure of ***c*-P6$_{t\text{-Bu}}$·T6** as 2.16 Å.[3] Using this assumption, the ideal size for a rigid template **T5** to fit into ***c*-P5** should be 10.75 – 2.16 – 0.24 = 8.35 Å for the *N*-centroid distance.

For **T5**, its *N*-centroid distance from molecular mechanics calculation is 7.34 Å, which means **T5** is 1.01 Å smaller than the ideal size. For **T5'**, its *N*-centroid distance from molecular mechanics calculation is 7.65 Å, which means **T5'** is 0.70 Å smaller than the ideal size.

4.3 Template and Porphyrin Nanoring Chemistry

4.3.1 Synthesis of Pentadentate Templates

T5 was prepared using the intramolecular phosphine ligand-assisted palladium-catalyzed coupling method reported by Hartwig and Williams, which has been introduced in **Section 1.4.2**.[4,5] The reason for oxidizing the phosphine in pre-**T5** is that unoxidized phosphine is easy to oxidize under air and the lone pair on the phosphorous atom makes itself possible to coordinate with porphyrin units.[5] Oxidizing pre-**T5** with *N*-methylmorpholine *N*-oxide (NMO) gives **T5**, which was used in the porphyrin nanoring synthesis.

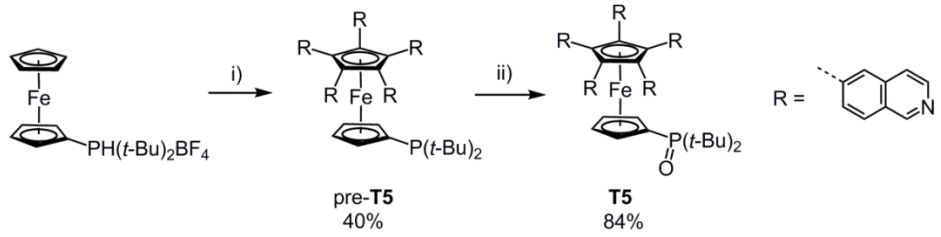

Scheme 4.1 The synthesis of **T5**. i) 6-Bromoisoquinoline, $Pd(OAc)_2$, PPh_3, *t*-BuOK, 107 °C, 2 d; ii) NMO.

It should be noted that the palladium-catalyzed coupling reaction is a delicate step and the amount of strong base (*t*-BuOK) has an important influence on the yield of desired product. The reaction uses rigorous conditions (strong base, temperature higher than 100 °C) to activate the C–H bonds on the Cp ring. Under rigorous conditions, the isoquinoline structure is susceptible to nucleophilic attack.[6] Although the side reaction is not favored compared to the Pd-catalyzed coupling reactions, the reaction virtually failed if the amount of *t*-BuOK exceeded the amount of 6-bromoisoquinoline in the reaction.

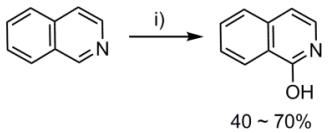

Scheme 4.2 Experimental evidence of a possible side reaction in pre-**T5** synthesis. i) KOH, 220 °C, 5 h.

In practice, the amount of *t*-BuOK was 8 equiv. (stoichiometry: 6 equiv.) and the amount of 6-bromoisoquinoline was 12 equiv. (stoichiometry: 5 equiv.) compared to the substrate ferrocene phosphine (1 equiv.). The reason for adding a large excess of 6-bromoisoquinoline was that the reagent can undergo self-coupling in the presence of phosphine ligands.

We attempted to synthesize **T5a** (**T5** without the phosphine ligand) and **T5'** from 1,2,3,4,5-pentabromoferrocene (1,2,3,4,5-$FcBr_5$), which has been introduced in **Section 1.4.2**. 1,2,3,4,5-$FcBr_5$ underwent Suzuki and Sonogashira coupling conditions in the presence of corresponding reagents. Unfortunately, both attempts failed to give the desired product. For the Suzuki coupling, most of the starting material was not consumed after 2 days of reaction probably because the ferrocene bromide is not reactive enough. For the Sonogashira reaction, the signal of desired compound was detected by MALDI-MS, but the reaction mixture gave many new signals from MALDI-MS that could not be explained, which probably indicates the instability of the compound.

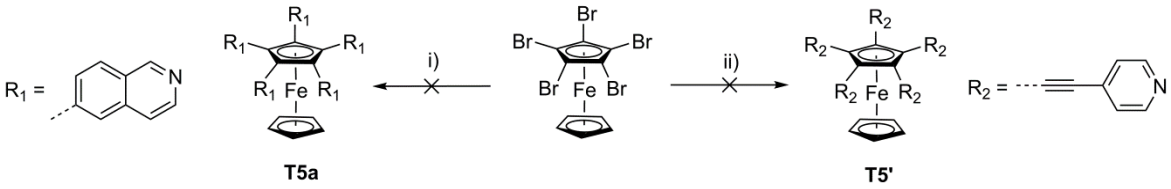

Scheme 4.3 Synthetic attempt towards **T5a** and **T5'** through Suzuki and Sonogashira coupling. i) 6-(Bpin)isoquinoline, SPhos, $Pd(OAc)_2$, K_3PO_4; ii) 4-ethynylpyridine, $Pd_2(dba)_3$, CuI, *i*-Pr_2NH.

We continued synthetic attempts of 5-porphyrin nanorings with **T5**.

4.3.2 Syntheses of Five-Porphyrin Nanorings

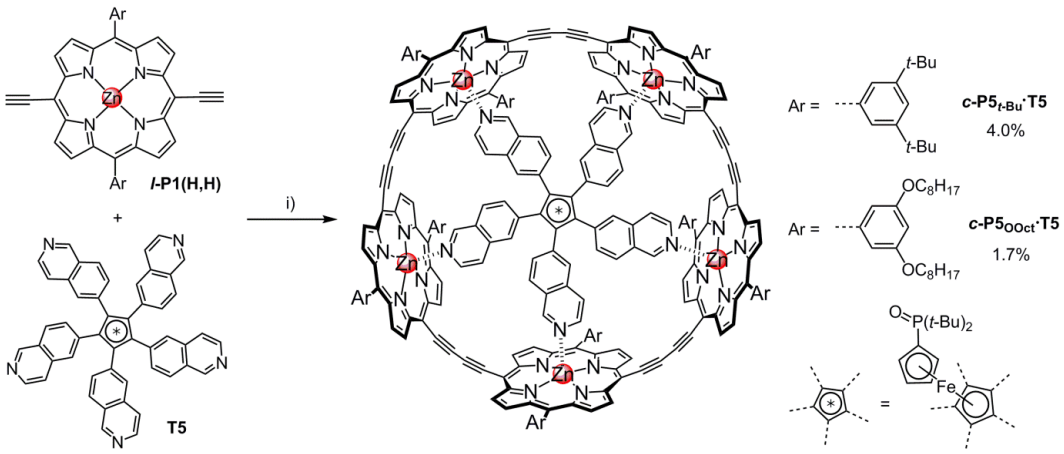

Scheme 4.4 The syntheses of ***c*-P5$_{t\text{-Bu}}$·T5** and ***c*-P5$_{OOct}$·T5**.

c*-P5·T5** was successfully prepared by coupling ***l*-P1(H,H)** in the presence of **T5**. The yields of the reaction were 4.0% for ***c*-P5$_{t\text{-Bu}}$·T5** and 1.7% for ***c*-P5$_{OOct}$·T5**. Similar to ***c*-P6·T6 and ***c*-P7·T7***, addition of excess pyridine quantitatively displaces the template from the complex and forms template-free 5-porphyrin nanorings. The ring-template complex can be immediately regenerated by adding **T5** into the template-free ring.

4.3.3 Detailed Structural Study by NMR Analysis

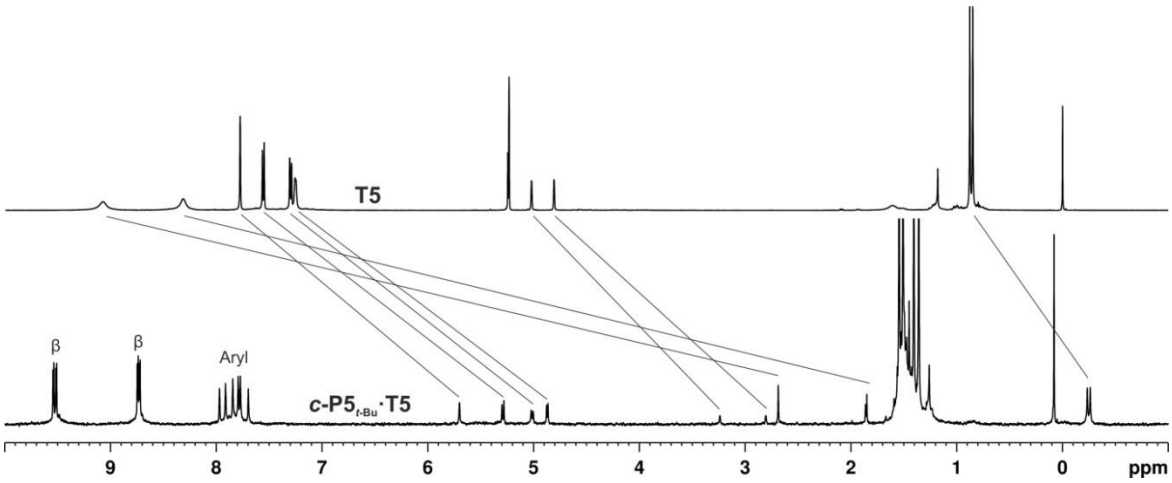

Figure 4.3 Full ^{1}H NMR spectra of **T5** and ***c*-P5$_{t\text{-Bu}}$·T5** (DOSY-edited ^{1}H NMR spectrum for ***c*-P5$_{t\text{-Bu}}$·T5**, CD_2Cl_2, 298 K, 500 MHz).

In the ^{1}H NMR spectra of ***c*-P5·T5**, the protons on the template are significantly shifted upfield by the shielding effects of the porphyrins. The upfield shift is dependent on the distances between the template and the ring structure. The D_{5h} symmetry of the ring-template complex is retained; and the ferrocene unit causes the two faces of the complex to be unequal; so the β-protons give four doublets. The six aryl protons on each porphyrin have both inside-outside-ring differences as well as top-down-face differences; so the aryl protons give six separate signals in the spectrum. The spectra of ***c*-P5$_{t\text{-Bu}}$·T5** are used as examples in this section.

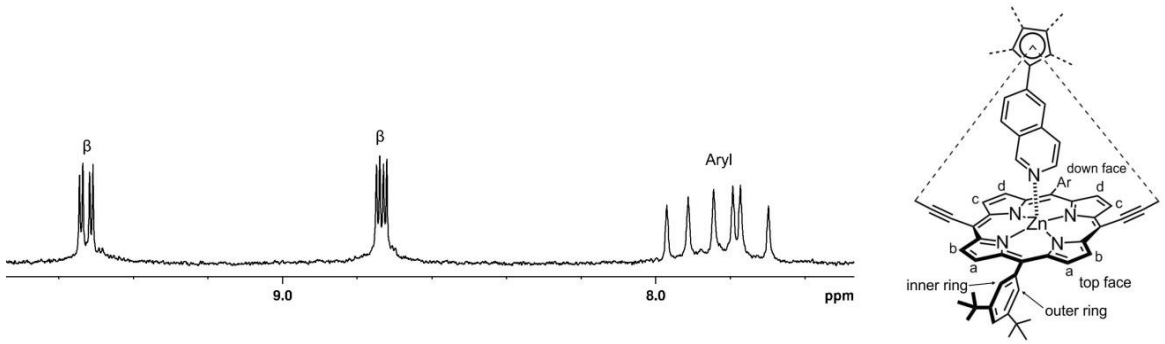

Figure 4.4 The inside-outside-ring and top-down-face differences of six inequivalent aryl protons and four inequivalent β-protons on one porphyrin unit of ***c*-P5$_{t\text{-Bu}}$·T5**.

The chemical shifts of the protons on porphyrin structure ***c*-P5·T5** are similar to those reported for ***c*-P6·T6**.[7] 2D spectra were used to assign the protons on the isoquinoline and Cp units of **T5**. The protons on the isoquinoline and Cp units of **T5** are designated as below.

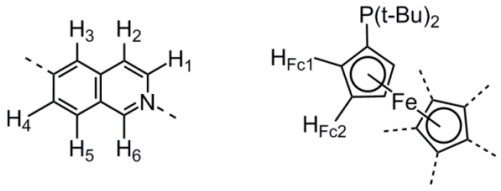

Figure 4.5 Designation of the protons in **T5**.

As is shown in **Figure 4.6**, the assignment starts from the HSQC spectrum. The correlation signals of the 6 protons on the isoquinoline structure are in the range between 120 ppm and 145 ppm, which is the range of aromatic carbons. All the peaks in the ^{1}H NMR of this region are labelled as the result of final assignment, which is a summary of the following correlation spectra.

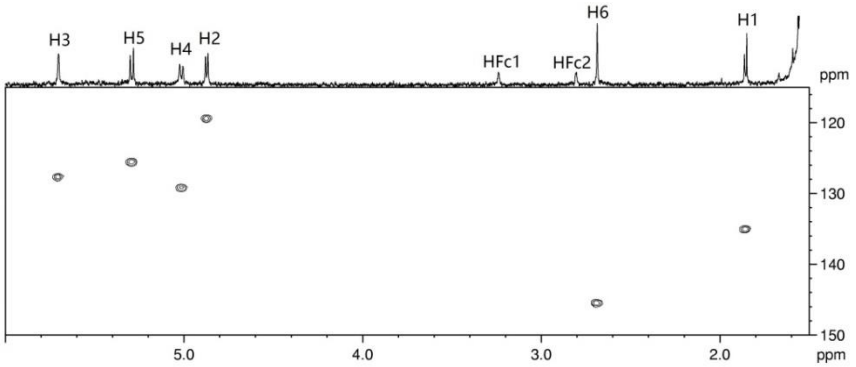

Figure 4.6 Assignment of six isoquinoline protons from ^{1}H-^{13}C HSQC spectrum (DOSY edited ^{1}H spectrum projection of ***c*-P5$_{t\text{-Bu}}$·T5**, CD_2Cl_2, 500 MHz, 298 K).

As is shown in **Figure 4.7** and **Figure 4.8**, the isoquinoline protons H_1 – H_6 are assigned by COSY and NOESY spectra.

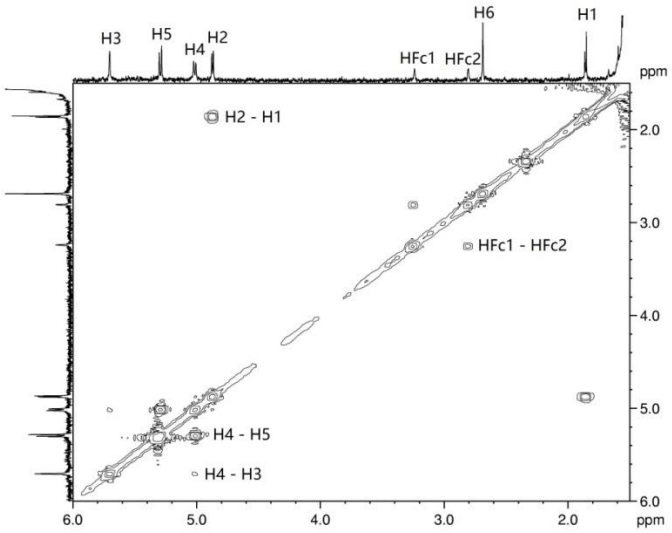

Figure 4.7 Assignment of six isoquinoline protons from ^{1}H-^{1}H COSY spectrum (DOSY edited ^{1}H spectrum projection of ***c*-P5$_{t\text{-Bu}}$·T5**, CD_2Cl_2, 500 MHz, 298 K).

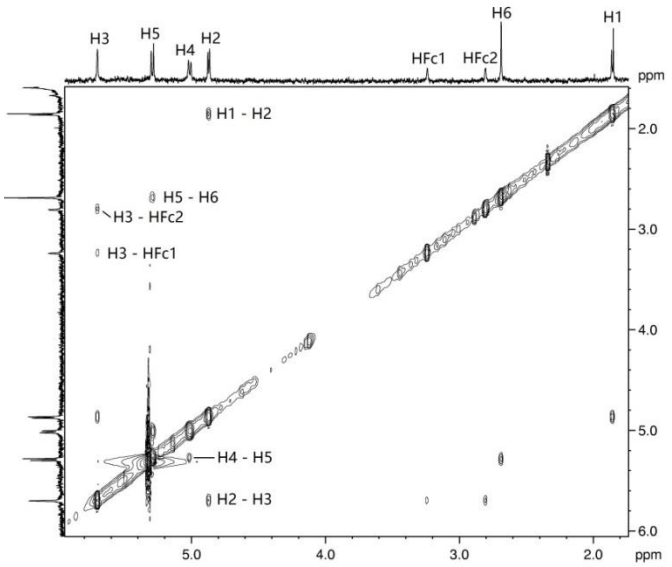

Figure 4.8 Assignment of six isoquinoline protons from ^{1}H-^{1}H COSY spectrum (DOSY edited ^{1}H spectrum projection of ***c*-P5$_{t\text{-Bu}}$·T5**, CD_2Cl_2, 500 MHz, 298 K).

As is shown in **Figure 4.9**, The peaks at 3.24 ppm and 2.80 ppm belong to ferrocene protons, which have various NOE signals with isoquinoline protons. The *tert*-butyl protons (-0.25 ppm) on the ferrocene phosphine structure have NOE signals with H_{Fc1} (3.24 ppm); yet they don't have NOE signals with H_{Fc2} (2.80 ppm), which has longer distance in between. Both H_{Fc1} and H_{Fc2} have NOE signals to H_3 and H_4, which are the isoquinoline protons close to the ferrocene core.

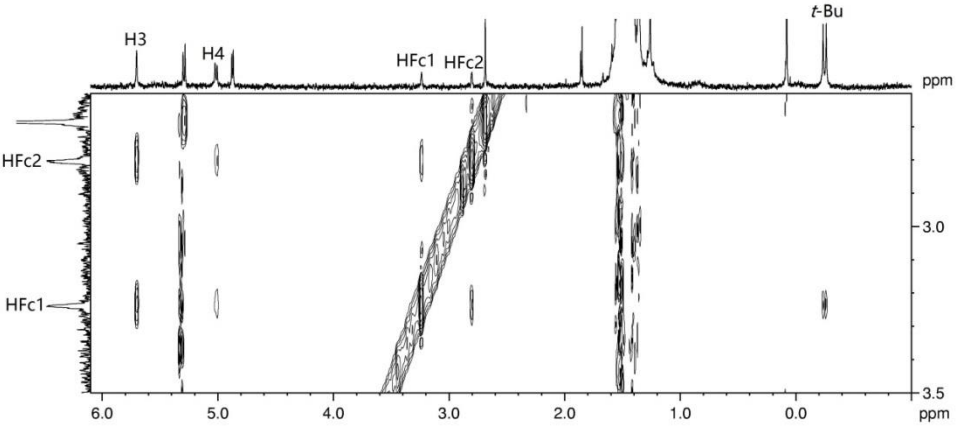

Figure 4.9 The correlation signals of H_{Fc1} - H_3, H_{Fc1} - H_4, H_{Fc1} - $H_{t\text{-Bu}}$, H_{Fc2} - H_3, H_{Fc2} - H_4 and H_{Fc1} - H_{Fc2} in ^{1}H-^{1}H NOESY spectrum (DOSY edited ^{1}H spectrum projection of ***c*-P5$_{t\text{-Bu}}$·T5**, CD_2Cl_2, 500 MHz, 298 K).

As is shown in **Figure 4.10**, the summary of shielding effect of the porphyrin nanoring can be described by the change of chemical shifts ($\Delta\delta$) of **T5** protons between the free form and the bound form (to the nanorings). The chemical shift of the phosphorus atom has also similar shielding effects from ^{31}P NMR spectra.

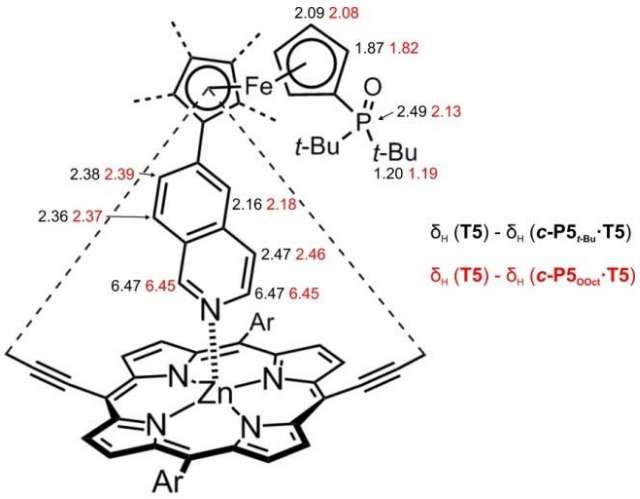

Figure 4.10 The chemical shift changes ($\Delta\delta$) induced by the shielding effects of porphyrin nanorings. Black: ***c*-P5$_{t\text{-Bu}}$·T5**; red: ***c*-P5$_{OOct}$·T5**.

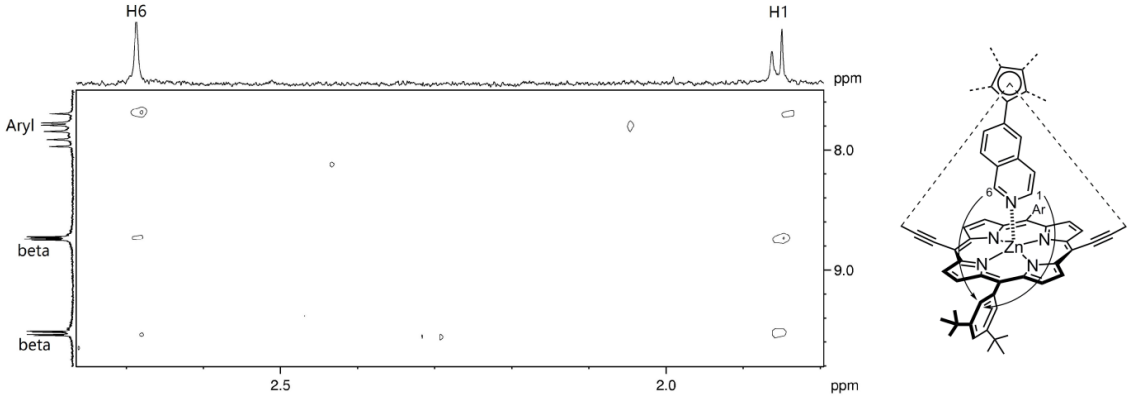

Figure 4.11 The correlation signals of H_1 and H_6 with the aryl and only one of the six beta-protons in ^{1}H-^{1}H NOESY spectrum (DOSY edited ^{1}H spectrum projection of ***c*-P5$_{t\text{-Bu}}$·T5**, CD_2Cl_2, 500 MHz, 298 K).

As is shown in **Figure 4.11**, H_1 and H_6, which are the closest protons (in the template) to the porphyrins, has NOE signals with the beta- and only one (the one facing towards the inner side of the porphyrin ring structure) of the six aryl protons in the porphyrin.

4.3.4 UV-vis Absorption and Photoluminescence Spectra of Five-Porphyrin Nanorings

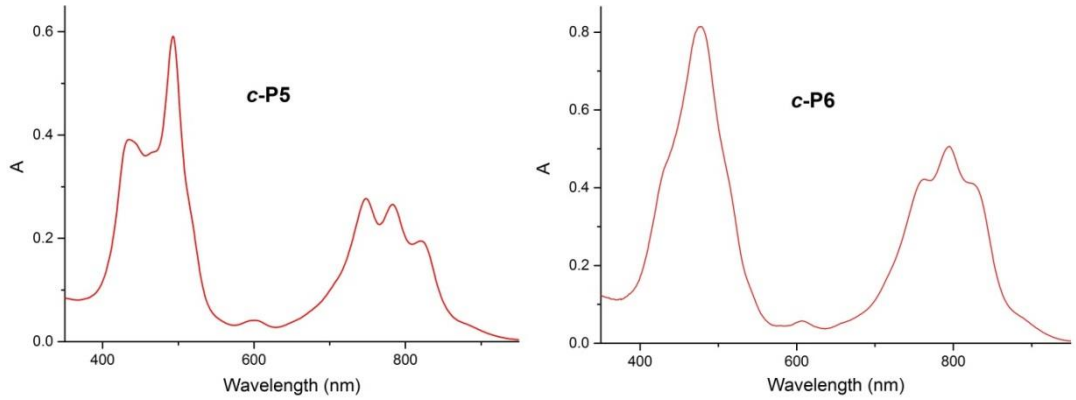

Figure 4.12 Comparison of the UV-vis absorption spectra of template-free ***c*-P5**$_{t\text{-Bu}}$ (left, toluene, 298 K) and ***c*-P6**$_{t\text{-Bu}}$ (right, chloroform, 298 K). The porphyrin nanorings are fully-bound to pyridine ligand to eliminate the aggregation effects to the spectra.

The UV-vis absorption spectra of template-free ***c*-P5** and ***c*-P6** are compared in **Figure 4.12**: ***c*-P5** has three well-resolved peaks whereas the peaks for ***c*-P6** are broader in the Q band region. This is caused by the spatial confinement in ***c*-P5** and the porphyrin units have fewer chances to rotate alongside the axis of the nanoring structure. The structure of ***c*-P5** is more rigid as the ring structure is smaller.

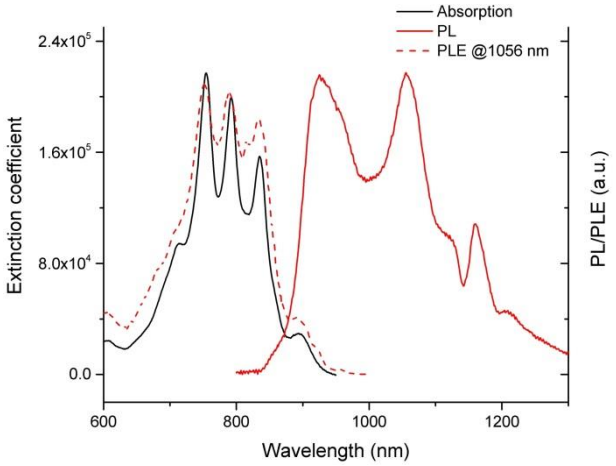

Figure 4.13 The photoluminescence (excited at 430 nm) in comparison to photoluminescence excitation at 1056 nm and the Q absorption band of ***c*-P5**$_{t\text{-Bu}}$**·T5** in toluene at 298 K. Measurement performed by Juliane Gong, Laura M. Herz group (Oxford physics).

Figure 4.13 shows the spectra of the photoluminescence (PL, red), photoluminescence excitation (PLE, red dashed) at 1056 nm and absorption spectra (Q band, black) of ***c*-P5**$_{t\text{-Bu}}$**·T5**. The Q band of ***c*-P5**$_{t\text{-Bu}}$**·T5** gives fluorescence at infrared region, which is similar to ***c*-P6**$_{t\text{-Bu}}$**·T6**.[3]

4.3.5 Stability of Five-Porphyrin Nanorings

It was difficult to get a good ^{1}H NMR spectrum of ***c*-P5$_{t\text{-Bu}}$·T5** because of the poor stability of the ring-template complex. It was found that ***c*-P5$_{t\text{-Bu}}$·T5** gave obvious degradation signals if the compound was left in the solvent-free states as a dry solid. Template-free ***c*-P5$_{t\text{-Bu}}$** has better stability compared to ***c*-P5$_{t\text{-Bu}}$·T5**; but obvious degradation signals are also observed if the compound is dried under high vacuum for 30 min.

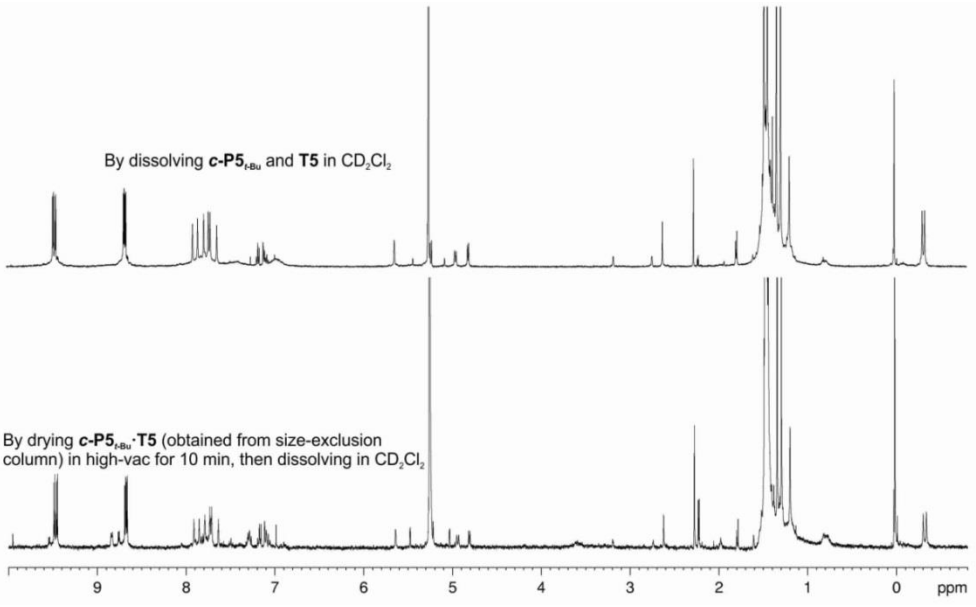

Figure 4.14 Spectra comparison showing the difference of the ^{1}H-NMR spectra of ***c*-P5$_{t\text{-Bu}}$·T5** using different preparation methods. Top: CD_2Cl_2 500 MHz, 298 K; Bottom: CD_2Cl_2 400 MHz, 298 K.

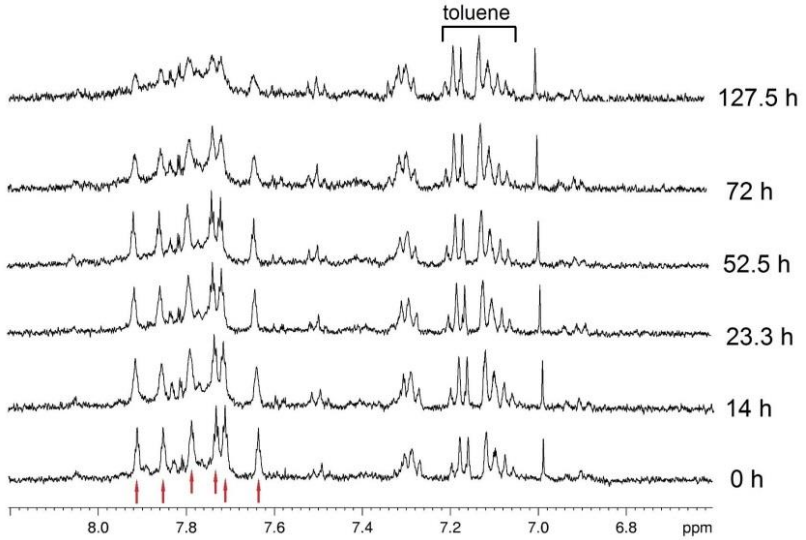

Figure 4.15 Degradation process over 6 days in the original ^{1}H-NMR spectra of ***c*-P5$_{t\text{-Bu}}$·T5** (CD_2Cl_2, 400 MHz, 298 K). The red-arrowed peaks are six aryl peaks of ***c*-P5$_{t\text{-Bu}}$·T5**; the peaks between 7.0 – 7.3 ppm come from toluene residues (used as a comparison to the peaks from ***c*-P5$_{t\text{-Bu}}$·T5**) and impurities.

As is shown in **Figure 4.14**, the top spectrum is recorded from the sample prepared by weighing out stoichiometric dry ***c*-P5$_{t\text{-Bu}}$** and **T5** and mixing them with CD_2Cl_2; the spectrum is also the origin of the DOSY-edited spectrum in the previous section and in corresponding 2D spectra projections. The bottom spectrum is recorded from the sample prepared by drying ***c*-P5$_{t\text{-Bu}}$·T5** (freshly obtained from size-exclusion column of the reaction mixture) in high vacuum for 10 min; the spectrum is also the starting spectrum (0 h) for the spectra set tracing the degradation process of ***c*-P5$_{t\text{-Bu}}$·T5** shown in **Figure 4.15** which indicates that ***c*-P5$_{t\text{-Bu}}$·T5** can slowly degrade over days in solution.

As the aryl peaks are mingled with impurities, the concentration of the sample and impurities could not be quantitatively analyzed from **Figure 4.15**. Analysis of the β-proton peaks with the nearby impurity peak can generate a first-order decay fitting of the signals, if we assume the concentration of the impurities stays constant. The apparent rate constant of the decay process is calculated as 0.029 h^{-1}. The fitting indicates that the decay might stop at a certain extent, when the concentration of ***c*-P5$_{t\text{-Bu}}$·T5** is low enough.

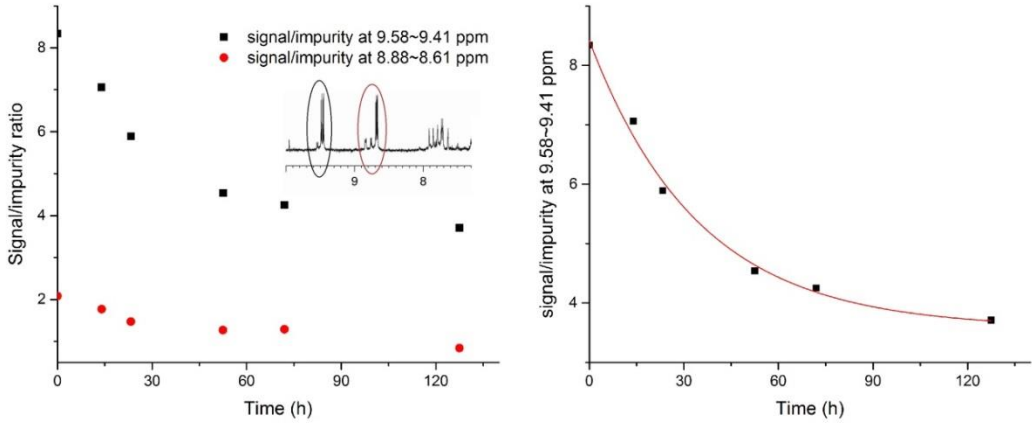

Figure 4.16 a) The signal/impurity ratio in the β-proton region in ^{1}H NMR spectra of ***c*-P5$_{t\text{-Bu}}$·T5**. b) First-order decay fitting of the signal/impurity ratio at 9.58 – 9.41 ppm: $y = 3.58 + 4.84e^{-0.029t}$.

Compared to ***c*-P5$_{t\text{-Bu}}$·T5**, ***c*-P5$_{\text{OOct}}$·T5** is more stable as all the NMR spectra were obtained by ordinary procedure: drying ***c*-P5$_{\text{OOct}}$·T5** under high vacuum for 30 min and dissolving the sample in CD_2Cl_2. We did find insoluble residues when we dissolved the solid sample of ***c*-P5$_{\text{OOct}}$·T5** after crystallization attempts, which indicates that ***c*-P5$_{\text{OOct}}$·T5** does degrade, but much slower compared to ***c*-P5$_{t\text{-Bu}}$·T5**. **Figure 4.17** shows the full spectrum of ***c*-P5$_{\text{OOct}}$·T5**. In the spectrum, the proton designations are identical to those of ***c*-P5$_{t\text{-Bu}}$·T5**.

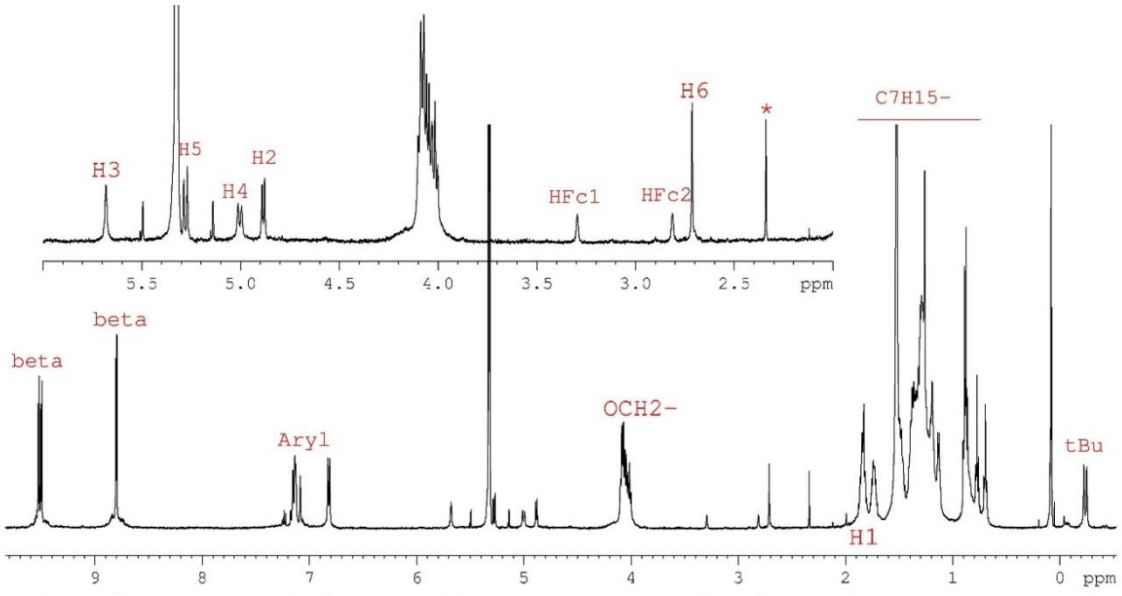

Figure 4.17 ^{1}H NMR spectrum of ***c*-P5$_{OOct}$·T5** (CD_2Cl_2, 500 MHz, 298 K, * represents toluene impurity).

From the evidences shown above, we can see that the instability of ***c*-P5$_{t\text{-}Bu}$·T5** might be caused by the high bending strain of the butadiyne chains: assuming there is no strain in porphyrin units, each butadiyne linker shares 72 degrees of curvature; the template is 1.01 Å smaller than the expected ideal size (**T5** *N*-centroid distance: 7.34 Å; ideal: 8.35 Å. See **Section 4.2**), which might force the nanoring to "squeeze" itself to bind the template and give even more strain to the whole system. Template-free ***c*-P5$_{t\text{-}Bu}$** is slightly more stable than the ring-template complex, probably because no extra curvature is given to the system in the absence of **T5** and the ring structure is less strained.

The long alkyl chains of octyloxy groups might provide protection to the butadiyne linkers and give them less chances to interact with each other, which probably explains the phenomenon that ***c*-P5$_{OOct}$·T5** is more stable than ***c*-P5$_{t\text{-}Bu}$·T5**.

4.3.6 Product Distribution in the Syntheses of *c*-P5·T5

The separation process of porphyrin nanorings with octyloxy side chains is usually more tedious than that of porphyrin nanorings with *tert*-butyl side chains. The reason is that linear/cyclic porphyrin oligomers with *tert*-butyl side chains are less soluble in pure toluene/chloroform compared to those with octyloxy side chains, so that most of the impurities can be removed by a basic alumina plug.

***c*-P5·T5** follows the same trend: ***c*-P5$_{t\text{-Bu}}$·T5** can be purified only by ordinary size-exclusion column chromatography; whereas ***c*-P5$_{OOct}$·T5** needs recycling GPC separation method, in which the sample cannot be fully separated at one run and is re-injected into the instrument after the sample comes out of the GPC column.

Before GPC separation, the reaction mixture was passed through basic alumina to remove catalysts, oxidants and porphyrin polymers; the sample was afterwards passed through a size-exclusion column with toluene (1% pyridine, *v*/*v*) to remove **T5** which chelated to linear/cyclic porphyrin oligomers (**T5** stays in ***c*-P5·T5** when the amount of pyridine is 1%, as will be shown in the following cooperativity study section). The resulting mixture was injected into GPC instrument and the recycling GPC trace of ***c*-P5$_{OOct}$·T5** gives us the product distribution in the synthesis of ***c*-P5·T5**, which is shown in **Figure 4.18**.

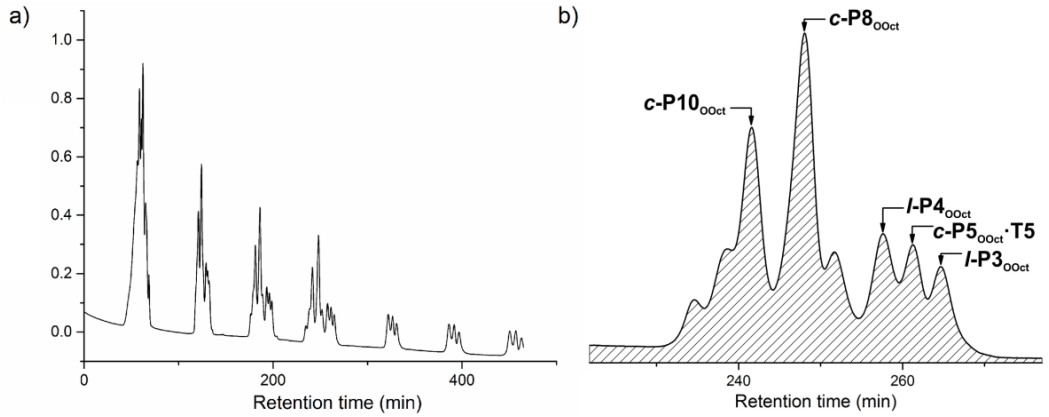

Figure 4.18 a) Full GPC trace of ***c*-P5$_{OOct}$·T5** purification process; the impurities were removed in 4th cycle and the product was collected in 7th cycle. b) 4th cycle of the full trace and the designation of the compounds to corresponding peaks, the designation method is the relationship between retention time and molecular weight introduced in **Section 3.3.4**.[8] GPC conditions: line of JAIGEL 3H (20 × 600 mm) and JAIGEL 4H (20 × 600 mm) columns; eluent: toluene/pyridine (100/1, *v*/*v*); flow rate: 3.5 mL/min.

From the GPC traces of ***c*-P5$_{OOct}$·T5** purification, we can see that the major product of the nanoring synthesis is ***c*-P8** (which is also proved by MALDI-MS analysis). This is probably because the curvature of the ligands in **T5** causes a non-Vernier templating synthesis, which is similar to the behavior of **T4** in ref. 9. The less strained ***c*-P8** is more favored compared to ***c*-P5** in the **T5**-directed synthesis, which indicates that the free energy cost from the strain has outcompeted coordination to a certain extent inside the supramolecular system.

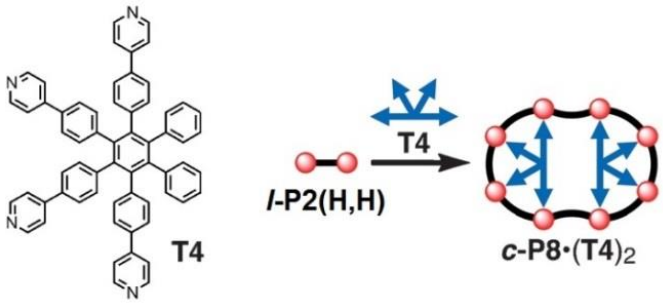

Figure 4.19 The non-Vernier templating synthesis of ***c*-P8**. ***c*-P8** might also form a similar complex with **T5**, which gives the explanation of the product distribution in **Figure 4.18**. Adapted with permission from ref. 9, Copyright 2015 John Wiley and Sons.

4.4 Cooperativity Study

The measurement of EM for ***c*-P5·T5** systems follows the method shown in **Chapter 2**. Similar to ***c*-P6·T6*** and ***c*-P7·T7***, the formation constant K_f of the template-nanoring complex ***c*-P5·T5** was measured by the denaturation cycle shown in **Figure 2.9**; and both quinuclidine and pyridine were used in the experiments to determine the K_f of ***c*-P5·T5**. The reference titration was performed by measuring the association constant (K_L) between isoquinoline and template-free ***c*-P5**. Porphyrin nanorings with *tert*-butyl side groups (***c*-P5$_{t\text{-Bu}}$·T5** and ***c*-P5$_{t\text{-Bu}}$**) were used in the titrations and toluene was used as the solvent, as the reactions to prepare 5-porphyrin nanorings were performed in toluene solvent.

4.4.1 Reference Titrations

***c*-P5$_{t\text{-Bu}}$** was titrated with monodentate ligands (quinuclidine, pyridine and isoquinoline) to measure their association constants.

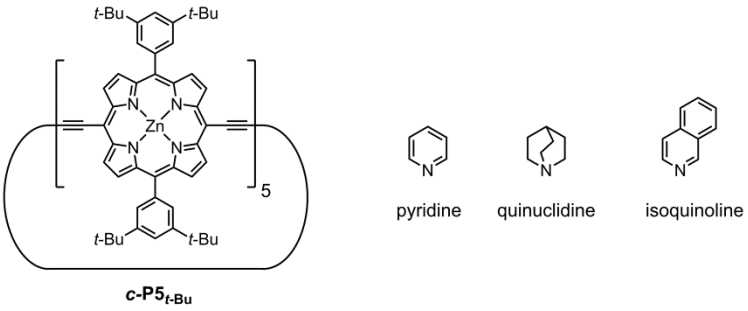

Figure 4.20 Ligands used for measurements of reference association constants of ***c*-P5$_{t\text{-Bu}}$**.

All the titrations were performed in toluene at 298 K and the concentrations of porphyrin

nanorings were 1.5 μM. All titrations were carried out at constant porphyrin concentration by adding porphyrin to the ligand stock solution before titrations started. Titration curves were fitted to a 1:1 binding isotherm using equation (2.3):

$$\frac{A - A_{initial}}{A_{\infty} - A_{initial}} = \left(\frac{(K_{\mathrm{L}}([\mathrm{L}]_0 + [\mathrm{P}]_0) + 1) - \sqrt{(K_{\mathrm{L}}([\mathrm{L}]_0 + [\mathrm{P}]_0) + 1)^2 - 4K_{\mathrm{L}}^2[\mathrm{P}]_0[\mathrm{L}]_0}}{2K_{\mathrm{L}}[\mathrm{P}]_0} \right) \quad (2.3)$$

where A is the observed absorption at a specific wavelength or difference of absorption at two wavelengths; $A_{initial}$ is the starting absorption at this wavelength or difference of absorption in these two wavelengths; A_{∞} is the asymptotic final absorption at this wavelength or difference of absorption in these two wavelengths; K_{L} is the association constant of the template-free ring ***c*-P5** with ligand L; $[\mathrm{L}]_0$ is the total (free and bound) concentration of ligand; $[\mathrm{P}]_0$ is a 5-fold multiply for the concentration of ***c*-P5** as it has five porphyrin units inside the molecule.

As in **Chapter 2**, only one titration spectrum and fitting curve will be presented for a specific set of titrations with the same porphyrin oligomer. In the spectra, the bold black lines represent starting points and the red lines represent terminal points. The sample spectra-fitting curve and full results are shown below.

Table 4.1 The association constants (K_{L}) of ***c*-P5$_{t\text{-Bu}}$** and ligands (1:1 association constants in M^{-1}).

Ligand	Run 1	Run 2	Average
Quinuclidine	$(8.8 \pm 0.6) \times 10^5$	$(7.4 \pm 0.8) \times 10^5$	$(8.1 \pm 0.8) \times 10^5$
Pyridine	$(1.9 \pm 0.1) \times 10^4$	$(1.7 \pm 0.1) \times 10^4$	$(1.8 \pm 0.1) \times 10^4$
Isoquinoline	$(2.4 \pm 0.3) \times 10^4$	$(2.2 \pm 0.2) \times 10^4$	$(2.3 \pm 0.3) \times 10^4$

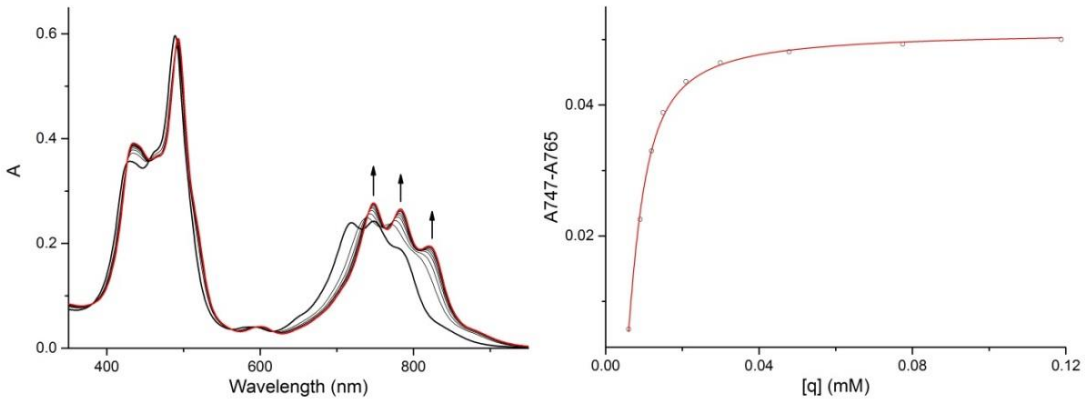

Figure 4.21 UV/Vis titration results of quinuclidine and ***c*-P5$_{t\text{-Bu}}$**, $K_{\mathrm{L}} = (8.8 \pm 0.6) \times 10^5$ M^{-1}, $R^2 = 0.998$. (Run 1, toluene, 298 K, [***c*-P5$_{t\text{-Bu}}$**] = 1.5 μM)

4.4.2 Denaturation Titrations

***c*-P5$_{t\text{-Bu}}$·T5** was titrated both with quinuclidine and pyridine. The corresponding denaturation constants are labeled as K_{dq} and K_{dpy} respectively.

All the titrations were performed in toluene at 298 K. All titrations were carried out at constant porphyrin nanoring concentration (0.35 μM) by adding porphyrin to the ligand stock solution before titrations started. All the data were fitted to the breaking-up isotherm derived from equation (2.4):

$$\frac{A - A_{initial}}{A_{\infty} - A_{initial}} = \left(\frac{-K_b[L]_0{}^5 + \sqrt{K_b^2[L]_0{}^{10} + 4K_b[L]_0{}^5[P]_0}}{2[P]_0} \right) \quad (4.1)$$

where A is the observed absorption at a specific wavelength or difference of absorption in two wavelengths; $A_{initial}$ is the starting absorption at a specific wavelength or difference of absorption in two wavelengths; A_{∞} is the terminal absorption at a specific wavelength or difference of absorption in two wavelengths; K_b is the dissociation (breaking-up) constant between ligand and porphyrin nanoring complex; $[L]_0$ is the total concentration of ligand; $[P]_0$ is the concentration of porphyrin nanoring complex.

The titration results are listed in the tables and figures below. In the spectra, the bold black lines represent starting points and the red lines represent terminal points.

Table 4.2 Dissociation constants of ***c*-P5$_{t\text{-Bu}}$·T5** with quinuclidine and pyridine.

Ligand	Dissociation constant	Run 1	Run 2	Average
quinuclidine	K_{dq} (M^{-4})	(1.5 ± 0.1)	(1.6 ± 0.1)	(1.6 ± 0.1)
pyridine	K_{dpy} (M^{-4})	(1.7 ± 0.1) × 10^{-8}	(1.6 ± 0.2) × 10^{-8}	(1.6 ± 0.2) × 10^{-8}

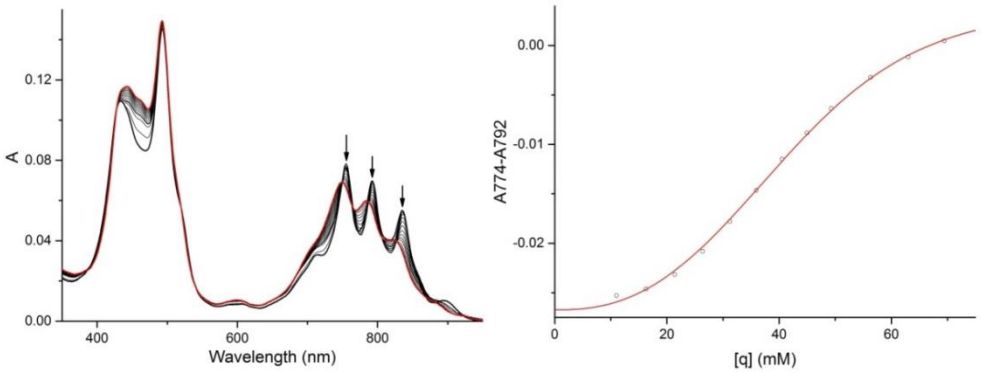

Figure 4.22 UV-vis titration results of quinuclidine and ***c*-P5$_{t\text{-Bu}}$·T5**, K_{dq} = (1.5 ± 0.1) M^{-4}, R^2 = 0.999. (Run 1, toluene, 298 K, [***c*-P5$_{t\text{-Bu}}$·T5**] = 0.35 μM)

4.4.3 Calculation of Effective Molarities

The formation constants K_f of nanoring-template complexes were calculated from the equation derived from equation (2.5):

$$\log K_f = \log \frac{{K_L}^5}{K_{b,L}} = 5\log K_L - \log K_{b,L} \tag{4.2}$$

where K_L is the association constant of the template-free ring ***c*-P5** with ligand L; $K_{b,L}$ is the denaturation constant of the nanoring-template complex with this ligand.

The geometric average effective molarities ($\overline{EM}$) of the nanoring complexes were calculated from the equation derived from equation (2.6):

$$\log\overline{EM} = \log \sqrt[4]{\frac{K_{chem,5}}{K_1^n}} = \log \sqrt[4]{\frac{K_f}{K_\sigma K_1^5}} = \frac{(\log K_f - \log K_\sigma - 5\log K_1)}{4} \tag{4.3}$$

where $K_{chem,5}$ is the statistically corrected value of K_f. As is shown in **Figure 4.23**, for ***c*-P5·T5**, K_σ = 320. K_1 is the reference ligand-ring (***c*-P5$_{t\text{-Bu}}$·**isoquinoline) single-site association constants statistically corrected from K_L; in this case, $K_1 = 0.5K_{L(isoquinoline)} = (1.2 \pm 0.2) \times 10^4$ M^{-1}.

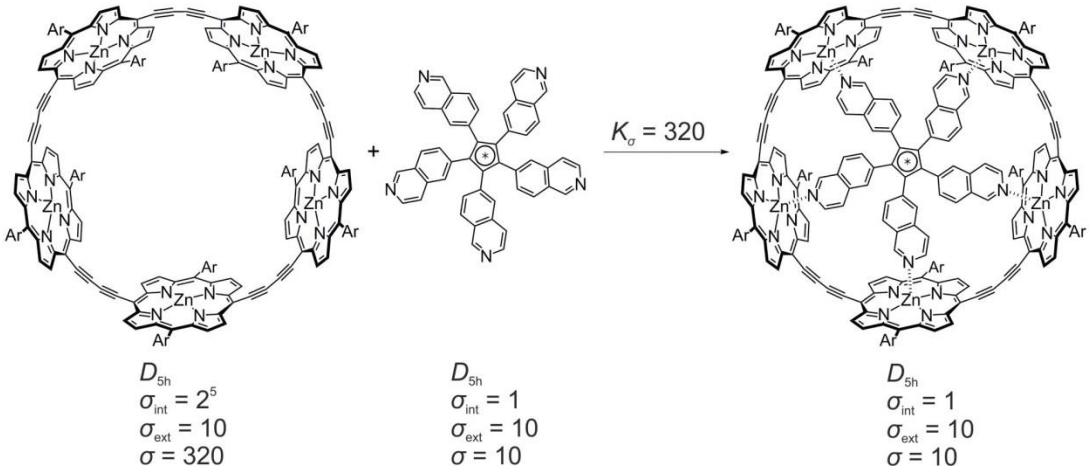

Figure 4.23 Statistical factor of ***c*-P5·T5**.

The calculation results of K_f and $\overline{EM}$ are shown in **Table 4.3**:

Table 4.3 The K_f and $\overline{EM}$ of ***c*-P5$_{t\text{-Bu}}$·T5** calculated from different denaturation cycles.

Denaturation ligand	logK_f	log$\overline{EM}$	$\overline{EM}$ (M)
quinuclidine	29.3 ± 0.2	1.62 ± 0.09	41 ± 9
pyridine	29.1 ± 0.1	1.57 ± 0.07	

4.4.4 Interpretation of EM Results

The geometric average effective molarities of ***c*-P5·T5**, ***c*-P6·T6**, ***c*-P6·T6*** and ***c*-P8·T8** are listed in **Table 4.4** for comparison.

Table 4.4 Comparison of the EMs of different template-nanoring systems.

Complexes	***c*-P5·T5**	***c*-P6·T6** (**Scheme 1.5**)[3,10]	***c*-P6·T6***	***c*-P8·T8** (**Scheme 1.4**)[11]
$\overline{EM}$ (M)	41 ± 9	180 ± 20	74 ± 20	4 ± 1
Ideal template *N*-centroid distance	8.35 Å	10.50 Å	Flexible, not discussed	14.8 Å
Template *N*-centroid distance	7.34 Å	10.03 Å		14.8 Å

Both ***c*-P5·T5** and ***c*-P6·T6** are porphyrin nanorings with rigid templates. ***c*-P5** has a smaller size and thus has less flexibility in the butadiyne linkers of the nanoring structure, as can be seen in **Figure 4.12**. However, the $\overline{EM}$ of ***c*-P5·T5** is smaller than that of ***c*-P6·T6** (and also ***c*-P6·T6***, with a flexible template). The reason for this phenomenon is that the geometry fit of ***c*-P5·T5** is not as good as ***c*-P6·T6** and the ring structure needs to "squeeze" itself to bind the template, which generates a free energy cost either from the weaker binding in each site or from higher strain of the nanoring-template structure.

From this phenomenon, it can be seen that a rigid supramolecular structure gives a higher possible effective molarity; but this is based on the prerequisite of accuracy in the design. The smaller ***c*-P5** has less flexibility compared to ***c*-P6**; thus ***c*-P5·T5** has the possibility to give a higher $\overline{EM}$ than ***c*-P6·T6**, only if the geometry of **T5** is very accurate for ***c*-P5**. In our case, the template-nanoring geometry match is not so ideal; and this causes a decrease in the $\overline{EM}$.

The $\overline{EM}$ of ***c*-P5·T5** is still slightly higher compared to ***c*-P8·T8**, a much larger system with rigid template. This is because the flexibility increases as the size of molecule grows, especially with regard to the increase of flexible butadiyne linkers. Also, the template is bigger for **T8**, a template based on free-base porphyrin structure: this gives the template more flexibility compared to **T5** and **T6**. As a result, the $\overline{EM}$ of ***c*-P8·T8** drops substantially, even though the fit of the template to the porphyrin nanoring is almost perfect.

4.5 Summary

To summarize, ***c*-P5**, the smallest porphyrin nanoring with butadiyne linkers to date, has been synthesized and characterized. The intramolecular strain of the template-nanoring complex reduces the stability of ***c*-P5$_{t\text{-Bu}}$·T5**. ***c*-P5$_{\text{OOct}}$·T5** is stable enough to be handled by ordinary separation procedures, which is probably due to the protection of long alkyl chains on the porphyrin side groups. The slight geometry mismatch between the template and the nanoring has given a decrease in the effective molarity of the complex. The rigid supramolecular system requires more accuracy in the molecular design to achieve a higher positive cooperativity as it confines the possibility of the host-guest interactions in a narrower space.

4.6 References

[1] P. Neuhaus, A. Cnossen, J. Q. Gong, L. M. Herz, H. L. Anderson, *Angew. Chem. Int. Ed.* **2015**, *54*, 7344–7348.

[2] P. N. Taylor, J. Huuskonen, G. Rumbles, R. T. Aplin, E. Williams, H. L. Anderson, *Chem. Commun.* **1998**, 909–910.

[3] J. K. Sprafke, D. V. Kondratuk, M. Wykes, A. L. Thompson, M. Hoffmann, R. Drevinskas, W.-H. Chen, C. K. Yong, J. Kärnbratt, J. E. Bullock, M. Malfois, M. R. Wasielewski, B. Albinsson, L. M. Herz, D. Zigmantas, D. Beljonne, H. L. Anderson, *J. Am. Chem. Soc.* **2011**, *133*, 17262–17273.

[4] N. Kataoka, Q. Shelby, J. P. Stambuli, J. F. Hartwig, *J. Org. Chem.* **2002**, *67*, 5553–5566.

[5] O. Oms, T. Jarrosson, L. H. Tong, A. Vaccaro, G. Bernardinelli, A. F. Williams, *Chem. Eur. J.* **2009**, *15*, 5012–5022.

[6] A. E. Tschitschibabin, A. I. Kurssanow, *Chem. Zentralbl.* **1931**, *102*, 86.

[7] M. Hoffmann, J. Kärnbratt, M.-H. Chang, L. M. Herz, B. Albinsson, H. L. Anderson, *Angew. Chem. Int. Ed.* **2008**, *47*, 4993–4996.

[8] D. V. Kondratuk, L. M. A. Perdigao, A. M. S. Esmail, J. N. O'Shea, P. H. Beton, H. L. Anderson, *Nature Chem.* **2015**, *7*, 317–322.

[9] S. Liu, D. V. Kondratuk, S. A. L. Rousseaux, G. Gil-Ramírez, M. C. O'Sullivan, J. Cremers, T. D. W. Claridge, H. L. Anderson, *Angew .Chem. Int. Ed.* **2015**, *54*, 5355–5359.

[10] H. J. Hogben, J. K. Sprafke, M. Hoffmann, M. Pawlicki, H. L. Anderson, *J. Am. Chem. Soc.* **2011**, *133*, 20962–20969.

[11] M. Hoffmann, C. J. Wilson, B. Odell, H. L. Anderson, *Angew. Chem. Int. Ed.* **2007**, *46*, 3122–3125.

Chapter 5

Cooperativity in T5/Linear Porphyrin Oligomer Systems

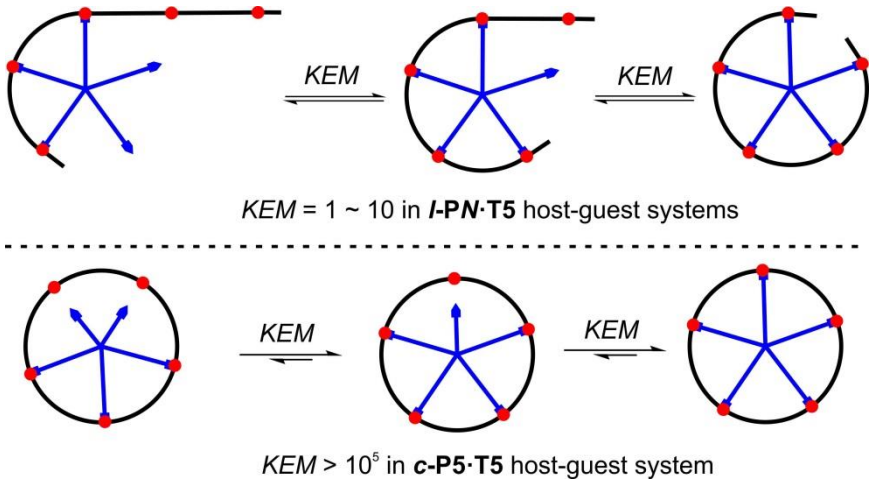

*This chapter investigates the cooperativity in the complexes formed by **T5** and linear porphyrin oligomers. It was found that the geometry of the template has endowed sufficient strain to the complex so that the equilibrium between fully-bound and partially-bound states of the complexes was observed by UV-vis-NIR titrations. The association constants of the complexes were measured and the contributions of all the binding states to the observation results were analyzed in detail.*

5.1 Background Information

5.1.1 Motivation of the Work

To further investigate the binding effects induced by the geometry of **T5**, we aim to measure the strain energy in the **T5**-bound porphyrin oligomers. In previous investigations of linear/cyclic porphyrin oligomer-template systems by the Anderson group, one strategy can be applied to measure the strain energy, which is shown in **Figure 5.1**.

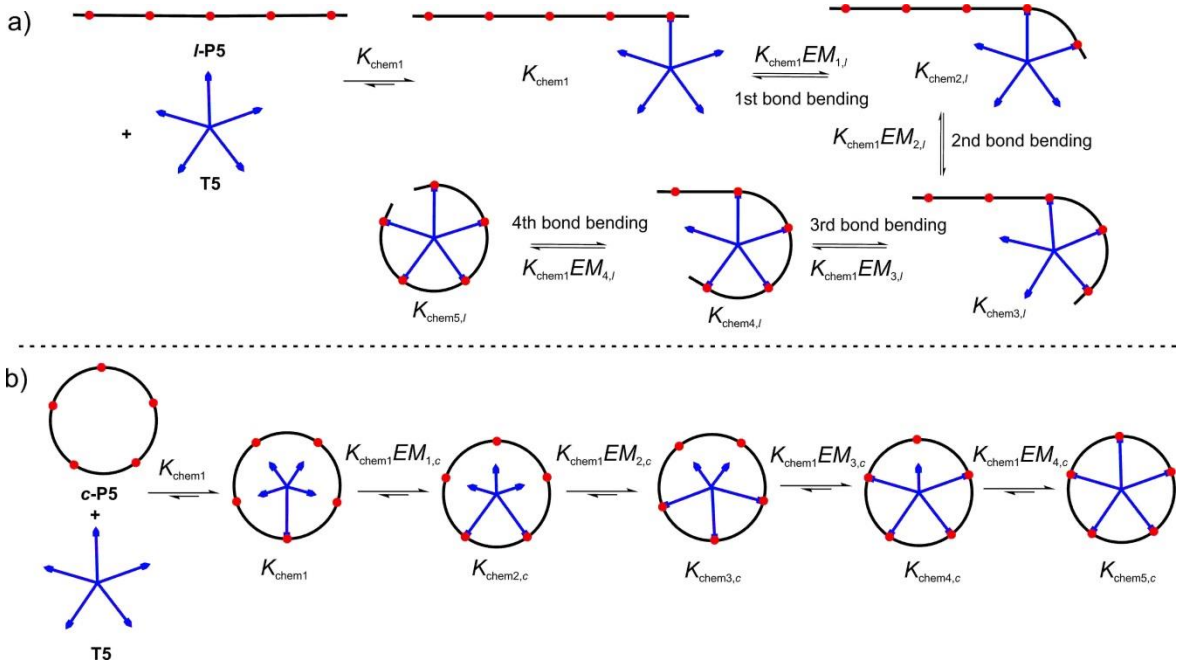

Figure 5.1 Stepwise binding between **T5** and linear (a)/cyclic (b) porphyrin oligomers, the statistical factors are excluded.

If we assume that **T5** is a perfect size and shape for ***c*-P5**, then in ***c*-P5·T5**, the porphyrin units are pre-organized: the binding between the porphyrin oligomer and template is not affected by the strain. In ***l*-P5·T5**, the same binding is affected by the strain and the energy cost is revealed by the decrease of the stability of the host-guest complex.[1,2]

The Gibbs free energy of the formation of a specific complex with N sites of binding can be calculated as:

$$\Delta G = -RTlnK_{\mathrm{chem}N} \tag{5.1}$$

where $K_{\mathrm{chem}N}$ is the statistically corrected association constant of the corresponding complex with N sites of binding (N = 1 – 5).

We assume that the butadiyne linkers in ***c*-P5·T5** have the same geometry as in ***l*-P5·T5**, as the binding template is the same for linear/cyclic porphyrin oligomers. The average strain energy in each butadiyne linker (*ΔΔG*) of the curved porphyrin oligomer can be calculated using the equation below.

$$\Delta\Delta G = \frac{1}{N-1}(\Delta G_l - \Delta G_c) = \frac{-RT}{N-1}(lnK_{\mathrm{chem}N,l} - lnK_{\mathrm{chem}N,c}) \tag{5.2}$$

where ΔG_l and ΔG_c are the Gibbs free energy of the formation of **T5**-linear/cyclic porphyrin oligomer complexes with *N* sites of binding (*N* = 2 – 5).

$K_{\mathrm{chem}N}$ can be expressed by the statistically corrected association constant for single-site binding (K_{chem1}):

$$K_{\mathrm{chem}N,l} = (\overline{EM})_l^{\,N-1} K_{\mathrm{chem1}}^{N} \tag{5.3}$$

$$K_{\mathrm{chem}N,c} = (\overline{EM})_c^{\,N-1} K_{\mathrm{chem1}}^{N} \tag{5.4}$$

where $(\overline{EM})_l$ is the geometric average of the (*N* - 1) *EM* values of ***l*-P*N*·T5** complex with *N* sites of binding; $(\overline{EM})_c$ is the geometric average of the (*N* - 1) *EM* values of ***c*-P5·T5** complex with *N* sites of binding. As the linear/cyclic porphyrin oligomers are bound with the same template, the statistically corrected association constants for single-site binding (K_{chem1}) are identical in equations (5.3) and (5.4).

Substituting equations (5.3) and (5.4) into equation (5.2) gives:

$$\Delta\Delta G = -RT(ln(\overline{EM})_l - ln(\overline{EM})_c) \tag{5.5}$$

From the equation above, it can be seen that *ΔΔG* is directly revealed by the difference between the effective molarities of template-linear/cyclic porphyrin oligomer host-guest systems.

It should be noted that in equation (5.5), we only use the value of $(\overline{EM})_c$ generated from $K_{\mathrm{chem5},c}$ to calculate the strain energy in a curved butadiyne linker. The reason is that ***c*-P5·T5** is a highly positive cooperative host-guest system and the values of $K_{\mathrm{chem}N,c}$ cannot be measured unless templates **T*N*** (similar templates with the same geometry but only *N* neighboring ligands on the molecules, *N* = 2 – 4, see **Figure 5.1b**) can be synthesized to titrate with ***c*-P5**, which is chemically challenging. Also, similar work has been reported for ***c*-P6·T6**-related host-guest systems in ref. 2: as the template is slightly smaller than the ideal size, the steric effects from other unbound porphyrin units inside the porphyrin nanoring makes the bindings not perfectly pre-organized. As a result, the measured values of $EM_{(N\text{-}1),c}$ are more fluctuating than that of $EM_{(N\text{-}1),l}$ (see **Table 1** from

ref. 2). So it is a better idea to use the value of $(\overline{EM})_c$ from just $K_{\text{chem5},c}$ (template-porphyrin nanoring complex with all the porphyrin units bound to the template) to estimate the strain energy in a curved butadiyne linker since ***c*-P5·T5** is the complex closest to perfect preorganization compared to ***c*-P5·T*N*** (N = 2 – 4).

The measurement of $(\overline{EM})_c$ of ***c*-P5·T5** has been described in **Section 4.4.3**. The aim in this chapter is to measure the value of $(\overline{EM})_l$ in **T5**-linear porphyrin oligomer systems. The values of effective molarities can be calculated from relationship between $K_{\text{chem}N}$ and $K_{\text{chem}(N\text{-}1)}$ (see also **Figure 5.1**):[2]

$$K_{\text{chem}N} = EM_{(N-1)}K_{\text{chem}(N-1)}K_{\text{chem}1} \quad (N = 2-5) \tag{5.6}$$

Then the work in this chapter is to measure the values of $K_{\text{chem}N}$ of ***l*-P*N*·T5** (N = 2 – 5) host-guest systems, which can be performed by the titration experiments between ***l*-P*N*** and **T5**.[2] As can be seen later in **Section 5.3**, the measurement is complicated due to the existence of partially-bound complexes.[3]

5.1.2 Partially-Bound Complexes – Introduction and Method of Analysis

Partially-bound complexes widely exist in biochemical processes. Although most of the multi-site chelated supramolecules in biochemistry bear strong positive cooperativity and the supramolecular systems are often either fully-bound or fully-unbound in the processes, there are several processes involving partially-bound complexes that are important to be studied. These processes include the loosening of the DNA double helix in replication/transcription[4] and the folding of proteins.[5,6] As the processes are dynamic, the partially-bound biomolecules are usually in intermediate states and are not easy to isolate. This can make it difficult to study their thermodynamic stability.

Model compounds, however, can be built to investigate the partially-bound states in equilibria. Hunter first proposed the existence of partially-bound states in model supramolecular systems in 2003.[7] In the report, they argued that the partially-bound states of a chelate system are favored (compared to the rigid complex) by the enthalpy-entropy compensation effects from the flexible rotors in the molecules. As is shown in **Figure 5.2**, the supramolecular system with rigid linkers (also well pre-organized) has stronger binding compared to the one with flexible linkers.

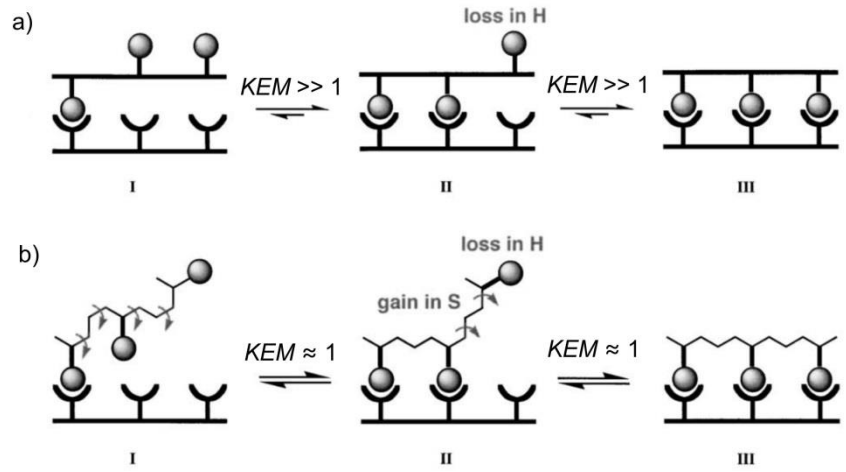

Figure 5.2 Illustration of partially bound states in a) a rigid complex and b) a flexible complex. The associated gain in conformational entropy leads to an increase in the population of partially bound states in flexible systems. Adapted with permission from ref. 7, Copyright 2015 Elsevier.

In 2008, Hunter reported a detailed analysis of partially-bound states in a model system built by zinc porphyrin host and pyridine derivatives.[3] As is shown in **Figure 5.3**, the host-guest systems has Zn-N interactions along with the H-bonds on the *meso*-substituents. However, the stability of the H-bonds varies in different solvents and the population of partially-bound states will change with the choice of solvents.

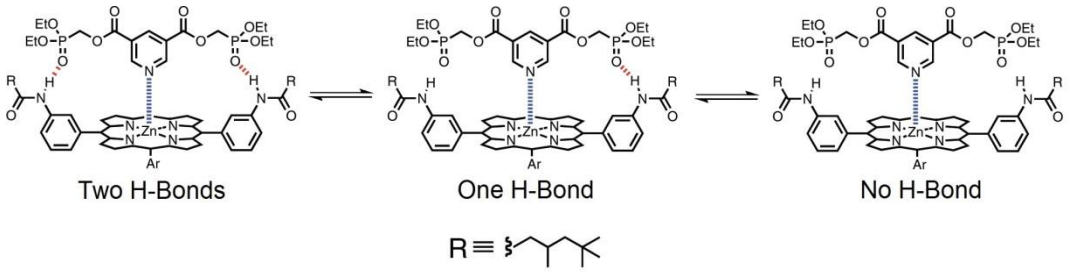

Figure 5.3 Equilibria of partially-bound states and fully bound states between a zinc porphyrin host and pyridine derivative. Adapted with permission from ref. 3, Copyright 2015 American Chemical Society.

The method to analyze the population of each binding state in the equilibria is to build sub-structures of the complex, i.e. a complex with only Zn-N binding and a complex with Zn-N binding and only one possible H-bond. The illustration is shown in **Figure 5.4**.

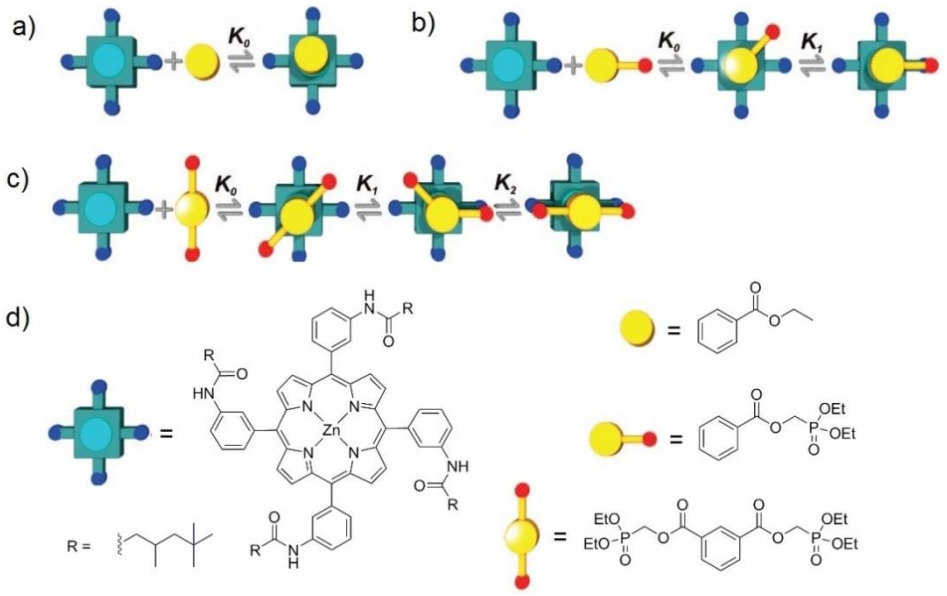

Figure 5.4 a) Complex with only Zn-N binding, b) complex with Zn-N binding and only one possible H-bond and c) complex with Zn-N binding and two possible H-bonds in the analysis of partially-bound states in Hunter's report. The chemical structures of the models are shown in d). Adapted with permission from ref. 3, Copyright 2015 American Chemical Society.

As can be seen in the figure, the stability of each interaction (metal-ligand interaction, H-bonds) is assumed as invariable in different complexes. The complexes consisting more than one binding are considered to be built up by the sub-structures, in which the contribution of the partially-bound states to the observed binding constant can be deduced from the analyses of the reference sub-structures. Also, the population of all the binding states can be analyzed in detail.[3] The host-guest system in **Figure 5.4b** uses the one in **Figure 5.4a** as the reference system; and the host-guest system in **Figure 5.4c** uses the one in **Figure 5.4b** as the reference system.

This analytical method was also used in many other reports involving similar structures in Hunter's group, where the contributions from the partially-bound states of the complexes were all considered.[8-11] We adopt this method to analyze the contributions of the partially-bound states of the ***l*-P*N*·T5** system by using the data from sub-structure complexes as the reference systems.

5.2 Rationale

5.2.1 Compounds and Cartoons in the Titration Experiments

As is shown in **Figure 5.5**, ***l*-PN_{THS}(THS,THS)** (N = 1 – 5) were used as porphyrin hosts in the

titrations; for brevity, their names are simplified as **P*N***. Isoquinoline was titrated with **P1** to determine the statistically corrected association constant for 1-site binding (K_{chem1}); **T5** was used to titrate with **P*N*** to determine the statistically corrected association constants for *N*-site binding (K_{chemN}, N = 2 – 5). K_{chemN} can be used to calculate the Gibbs free energy (ΔG_l) in the formation of the *N*-site binding complexes ***l*-P*N*·T5** shown in **Figure 5.1**.

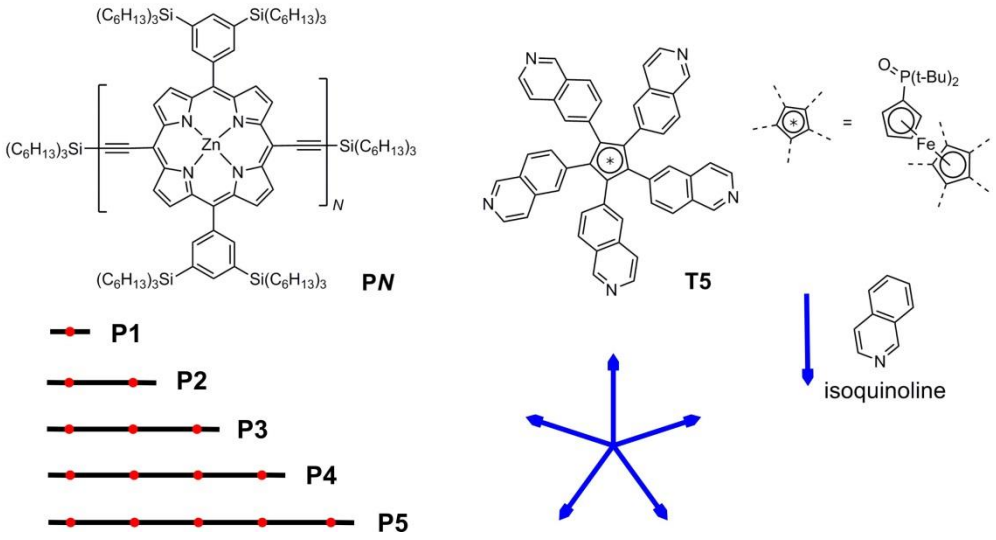

Figure 5.5 The compounds and cartoons used in the UV-vis-NIR titration experiments in this chapter.

5.2.2 Association Constants Involved in the Calculations

Statistically corrected association constant K_{chem} and formation constant K_f (for a single complex). The statistically corrected association constant K_{chem} for a specific complex (complex *i* in the following sections) is determined by the nature of the binding sites at the microscopic scale. It is related to the formation constant K_f (at macroscopic level) through the statistical factor K_σ, as have been introduced in **Chapter 2**, **Section 2.5**.

$$K_{f(\text{complex } i)} = (K_\sigma K_{chem})_{\text{complex } i} = \frac{[\text{Complex } i\,]}{[\text{Host}][\text{Guest}]^n} \tag{5.7}$$

Note that in the equation above, the host-guest systems built by **P*N*** and **T5** could give 1:1, 1:2 and 1:3 complexes, as can be seen in the following analyses. Thus *n* could equal to 1, 2 and 3 in equation (5.7) for the host-guest systems built by **P*N*** host and **T5** guest.

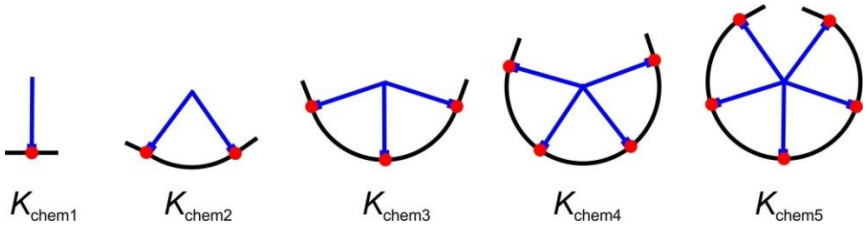

Figure 5.6 The binding modes and statistically corrected formation constants for *N*-site bindings ($N = 1 – 5$).

For K_{chem}, the term "chem" symbolizes the chemical nature of the binding. K_{chemN} ($N = 1 – 5$) is assumed as constant for the same binding mode in the complexes formed between **T5** and different porphyrin oligomers, as is shown in **Figure 5.6**. This is because **T5** is effectively a D_{5h} symmetric template (see **Section S.4** in the Appendix for the symmetry approximation of **T5**, which is an assumption to simplify the calculations); the porphyrin sites are essentially identical with each other in **P*N***; and there is no significant allosteric cooperativity between two separate porphyrin-ligand bindings in butadiyne-linked porphyrin oligomers.[2,12]

For K_f, the term "f" symbolizes the formation of a complex. The formation constant K_f of a specific complex is a constant at the macroscopic scale which determines the stability of the complex with respect to its individual components and thus its population in the mixture.

Observed association constants from UV-vis-NIR titrations K_{obs} (for host-guest systems with regard to stoichiometry).[3] In UV-vis-NIR titrations, the experimental data give the spectral change of the titration system at different ratios of host and guest molecules. The experimental data can be fitted to binding models with different stoichiometry of host-guest complexes to give the observed association constants (K_{obs}) for the host-guest systems with respect to stoichiometry;[13] but they may not directly reflect the distribution of the complexes in the system. Thus complexes with the same stoichiometry but different binding modes from each other may be indistinguishable.

An example of the titration between **P3** and **T5** is given to illustrate the relationships between all the association constants involved in the analyses. As will be shown later in the experimental results in **Section 5.3**, there are two host-guest systems formed in **P3**/**T5** titration: 1:1 complexes **P3·T5** and 1:2 complexes **P3·(T5)$_2$**. The experimental data can be fitted to a combination of 1:1 and 1:2 binding models to give the K_{obs} of the **P3·T5** and **P3·(T5)$_2$** host-guest systems, which is shown in **Figure 5.7**.[13]

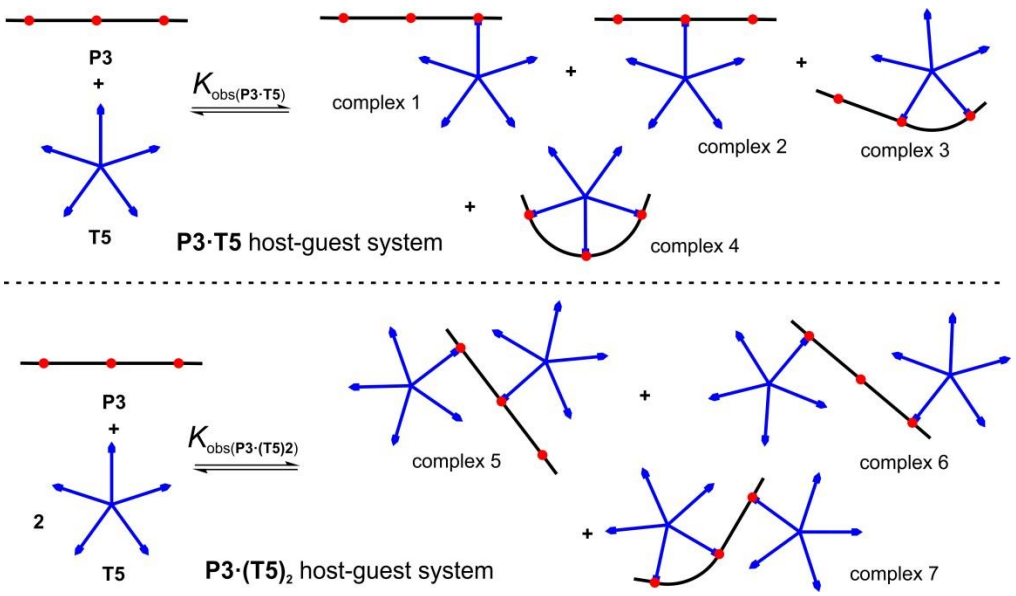

Figure 5.7 The binding modes and related association constants in the titration between **P3** and **T5**.

However, the experiment cannot directly reveal the detailed distribution of all the complexes in different binding modes (four 1:1 complexes for **P3·T5** and three 1:2 complexes for **P3·(T5)$_2$**). There are equilibria between all the complexes as well; but we use "+" instead of double-sided arrow to simplify the figures). Each complex in the host-guest system has a formation constant K_f which can be calculated from statistically corrected association constants K_{chem} and statistical factor K_σ; and they contribute to the observed association constant determined by the titration experiments.[3,8-11]

$$K_{obs(\mathbf{P3\cdot T5})} = \sum_{i=1}^{4} K_{f(complex\ i)} = \sum_{i=1}^{4} (K_\sigma K_{chem})_{complex\ i} \quad (5.8)$$

$$K_{obs(\mathbf{P3\cdot(T5)_2})} = \sum_{i=5}^{7} K_{f(complex\ i)} = \sum_{i=5}^{7} (K_\sigma K_{chem})_{complex\ i} \quad (5.9)$$

This relationship enables us to analyze the distribution of each complex in the titration systems. In **Chapter 2** and **Chapter 4**, the template-nanoring systems all had high positive chelate cooperativity[14] (i.e. $KEM >> 1$) and the influences of the partially-bound complexes can be ignored. Thus the observed association constants can be directly regarded as the formation constants of the fully-bound complexes, i.e. $K_{obs} = K_\sigma K_{chem}$.

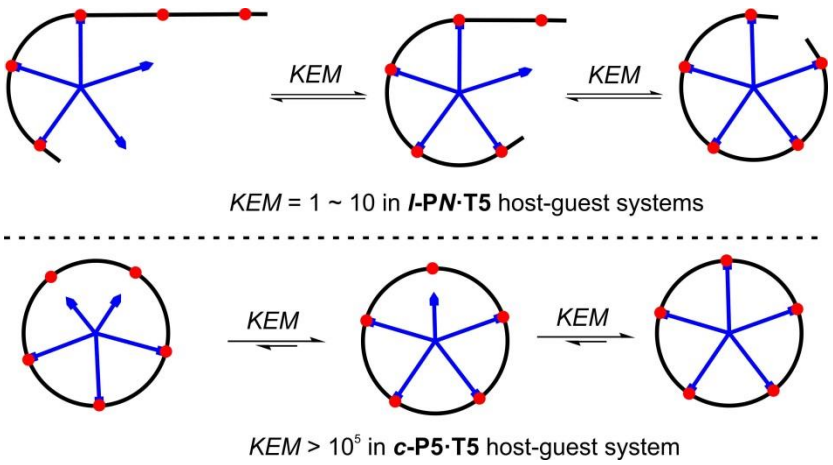

Figure 5.8 Comparison of the *KEM* values in ***l*-P*N*·T5** and ***c*-P5·T5** systems (*N* = 5 in this figure, the 1- and 2-site binding modes are not shown).

5.2.3 Assumptions and Simplifications

We assume that there are no higher-ordered complexes (i.e. one **T5** guest binding to more than one **P*N*** host, thus making **P*N*** and **T5** available to polymerize) formed in the host-guest systems, as this would make the analyses much more complicated. The experimental basis of this assumption comes from the titration between **T5** and **P2**, in which bound **T5** has most free binding sites to bind to other porphyrin oligomers, but formation of $\mathbf{(P2)_2{\cdot}T5}$ was not observed from the detailed analysis of experimental data in **Section 5.3.3**.

There is the possibility for **P2** to bind to two **T5** molecules to form $\mathbf{P2{\cdot}(T5)_2}$. This also means that the complexes $\mathbf{P3{\cdot}(T5)_3}$, $\mathbf{P4{\cdot}(T5)_3}$, $\mathbf{P4{\cdot}(T5)_4}$, $\mathbf{P5{\cdot}(T5)_4}$ and $\mathbf{P5{\cdot}(T5)_5}$ can be formed in their respective systems, which would make the analyses more complicated. However, the maximum concentration of **T5** added in the titration experiments is around 1/10 of the value of the corresponding effective molarity (in **Section 5.4.2**, EM_1 = 320 μM; in **Section 5.3.3**, the maximum concentration of **T5** in **P2/T5** titrations is around 20 μM), which is the concentration required to give equal concentrations of **P2·T5** and $\mathbf{P2{\cdot}(T5)_2}$.[14] Another evidence to support the simplification is the concentration of $\mathbf{P3{\cdot}(T5)_3}$ in **P3/T5** titrations (see simulation results in **Section 5.3.5**), in which the distribution of $\mathbf{P3{\cdot}(T5)_3}$ can be ignored. Thus the simplification takes away $\mathbf{P2{\cdot}(T5)_2}$ and $\mathbf{P3{\cdot}(T5)_3}$, as well as $\mathbf{P4{\cdot}(T5)_3}$, $\mathbf{P4{\cdot}(T5)_4}$, $\mathbf{P5{\cdot}(T5)_4}$ and $\mathbf{P5{\cdot}(T5)_5}$ from the analyses.

5.3 Experimental and Data Analyses

5.3.1 General Remarks

All titrations were performed in toluene at 298 K. All titrations were carried out at constant porphyrin concentration and by stepwise addition of the ligand (**T5** or isoquinoline) solutions into the solution of porphyrin oligomers.

In the spectra, the bold black lines represent initial states; the bold blue lines represent important intermediate (approximately 1:1 complex) states; and the red lines represent terminal states of the titrations.

In the cases where a set of titration data was fitted to the 1:1 binding model only, the data processing method was identical to the one determining the reference association constants, as described in **Chapter 2** and **Chapter 4**. The isotherm used in the fitting procedure is shown in **Section S.2** in the Appendix and Origin™ software was used to perform the fitting procedure.

When a set of titration data was fitted to a combination of two (1:1 and 1:2) or three (1:1, 1:2 and 1:3) binding models, a combination of models was needed to fit the titration data. The data processing was performed in Specfit™ software, which is designed by currently TgK Scientific Limited specifically for processing the UV-vis-NIR data using a single binding model or a combination of multiple binding models to fit the titration data. Thus more than one association constant can be retrieved from the fitting procedure.

The analysis of the series of titration experiments involves a build-up process, which means K_{chem1} (determined by **P1**/isoquinoline titrations) is used in **P2/T5** titrations to calculate K_{chem2}; both K_{chem1} and K_{chem2} are used in **P3/T5** titrations to calculate K_{chem3}. The same situation applies for **P4/T5** and **P5/T5** titrations. Thus the propagation/accummulation of the errors in the calculation process needs to be considered. We assume that the values in the calculations are all independent from each other, then the standard deviation for a function $f = f(x, y, z...)$ can be calculated using the equation below:

$$s_f = \sqrt{(\frac{\partial f}{\partial x})^2 s_x^2 + (\frac{\partial f}{\partial y})^2 s_y^2 + (\frac{\partial f}{\partial z})^2 s_z^2 + \cdots} \tag{5.10}$$

where s_f is the standard deviation of the function f, s_x is the standard deviation of x, s_y is the

standard deviation of *y*, and so forth. In this chapter, *f* stands for the target values to be calculated; *x*, *y*, *z* and so forth stand for the values that have been determined by previous calculations or by fitting of the experimental (titration) results.

5.3.2 P1/Isoquinoline Titrations

Porphyrin monomer **P1** was titrated with isoquinoline to determine the statistically corrected association constant for 1-site binding (K_{chem1}). The titration results were fitted to the 1:1 binding isotherm (equation (2.3)). The average of two titration results gives the observed association constant as $K_{obs(\mathbf{P1}\cdot isoquinoline)} = (2.0 \pm 0.1) \times 10^4\ M^{-1}$. Only the spectra from one of the two runs are shown for brevity; this also applies for the following titration systems.

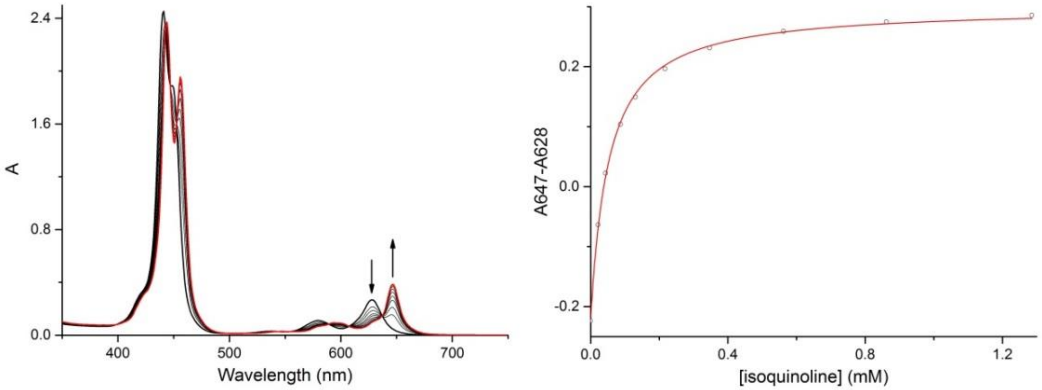

Figure 5.9 UV-vis titration results of isoquinoline and **P1**, $K_{obs(\mathbf{P1}\cdot isoquinoline)} = (2.0 \pm 0.1) \times 10^4\ M^{-1}$, $R^2 = 0.999$. (Run 1, toluene, 298 K, [**P1**] = 6.4 μM)

As is shown in **Figure 5.10**, the statistical factor for the binding $K_\sigma = 2$, which can be understood as a reflection of the fact that the porphyrin has two faces.

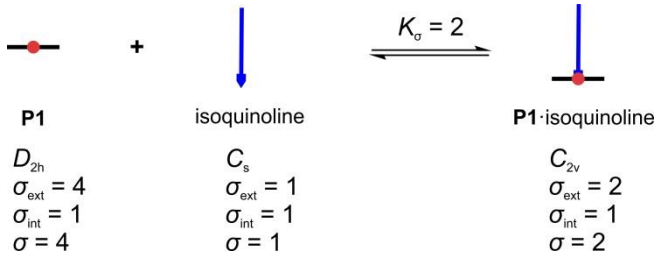

Figure 5.10 The statistical factors involved in single-site reference binding.

For 1-site binding:

$$K_{obs(\mathbf{P1}\cdot isoquinoline)} = K_{f(\mathbf{P1}\cdot isoquinoline)} = K_\sigma K_{chem1} \tag{5.11}$$

Thus $K_{chem1} = (1.0 \pm 0.1) \times 10^4\ M^{-1}$.

5.3.3 P2/T5 Titrations

Porphyrin dimer **P2** was titrated with **T5** to determine the statistically corrected association constant for 2-site binding (K_{chem2}). Similar to **P1**/isoquinoline system, the titration results were also fitted to the 1:1 binding isotherm. The average of two titration results gives the observed association constant as $K_{obs(\mathbf{P2}\cdot\mathbf{T5})} = (1.5 \pm 0.1) \times 10^6\ M^{-1}$.

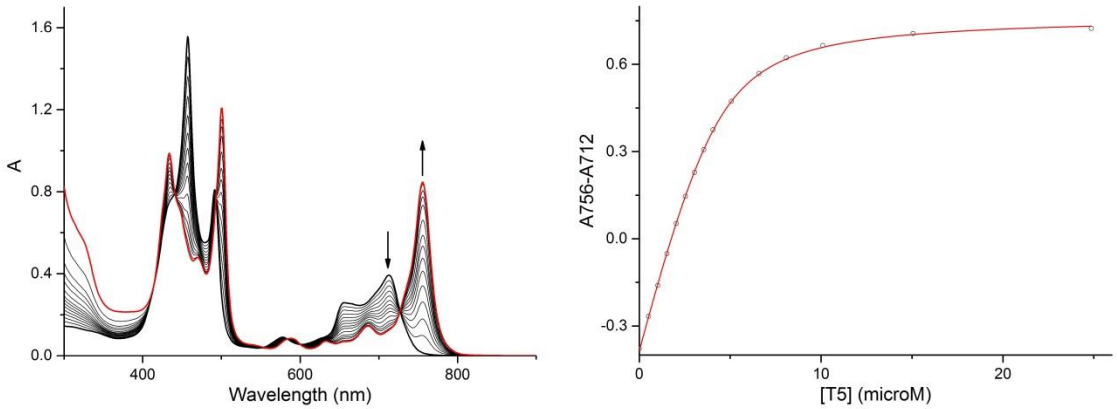

Figure 5.11 UV-vis-NIR titration results of **T5** and **P2**, $K_{obs(\mathbf{P2}\cdot\mathbf{T5})} = (1.6 \pm 0.1) \times 10^6\ M^{-1}$, $R^2 = 0.999$. (Run 1, toluene, 298 K, [**P2**] = 4.3 μM)

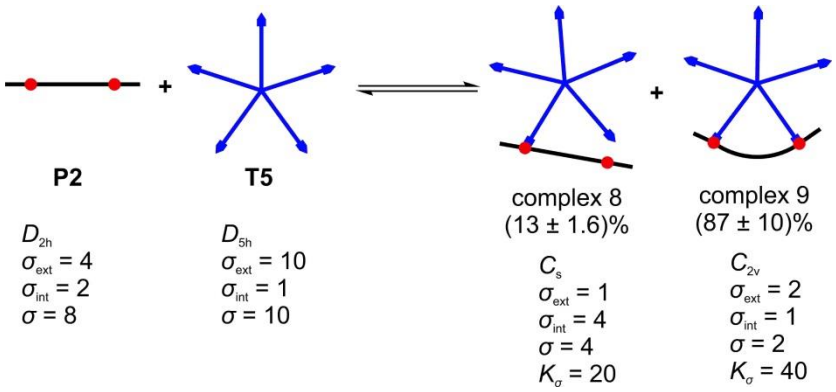

Figure 5.12 Statistical factors and distribution of the complexes in **P2·T5** host-guest system.

The formation constants of complex 8 and complex 9 are:

$$K_{f(\text{complex 8})} = K_\sigma K_{chem1} = 20K_{chem1} \tag{5.12}$$

$$K_{f(\text{complex 9})} = K_\sigma K_{chem2} = 40K_{chem2} \tag{5.13}$$

The observed association constant $K_{obs(\mathbf{P2}\cdot\mathbf{T5})}$ is the sum of the formation constants of complex 8 and complex 9:

$$K_{obs(\mathbf{P2}\cdot\mathbf{T5})} = K_{f(\text{complex 8})} + K_{f(\text{complex 9})} = 20K_{chem1} + 40K_{chem2} \tag{5.14}$$

As K_{chem1} and $K_{obs(\mathbf{P2}\cdot\mathbf{T5})}$ are known values in the equation above, K_{chem2} can be generated from

solving equation (5.14): the calculation gives the result as $K_{chem2} = (3.2 \pm 0.3) \times 10^4\ M^{-1}$.

The proportion of the partially-bound complex (complex 8) in the mixture of **P2·T5** host-guest system is:

$$\frac{K_{f(\text{complex 8})}}{K_{obs(\mathbf{P2}\cdot\mathbf{T5})}} = (13 \pm 2)\% \qquad (5.15)$$

For the titration between **P2** and **T5**, there is a possibility for the system to form **$(P2)_2$·T5**, as was discussed in **Section 5.2.3**. If the titration experiment is interpreted by the formation of **P2·T5** and **$(P2)_2$·T5** host-guest systems, as is shown in **Figure 5.13a**, the two bindings on the same template could be regarded as completely independent from each other. Similar to the formation of **P2·T5**, each **P2** host is bound to one **T5** guest in the formation of **$(P2)_2$·T5**. Thus the fitting model of **$(P2)_2$·T5** host-guest system is the same (1:1 binding mode) as **P2·T5** host-guest system, except for that the concentration of the guest ligand should be the concentration of **T5** multiplied by a factor of two, as each **T5** guest can bind to two **P2** hosts (i.e. **T5** presents two independent binding regions).

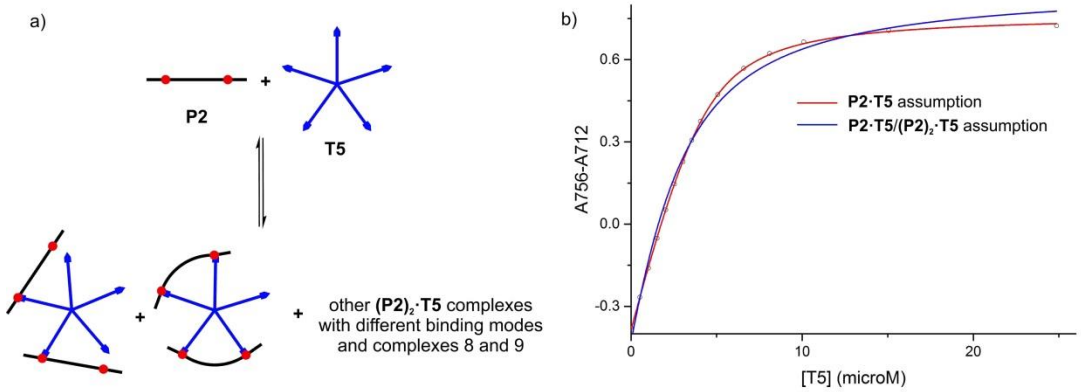

Figure 5.13 a) Assumption of the formation of: **P2·T5**/**$(P2)_2$·T5** host-guest system in the titrations and b) contrast of fitting results based on two assumptions. Red: **P2·T5** assumption, $R^2 = 0.999$ (also seen in **Figure 5.11**); blue: **P2·T5**/**$(P2)_2$·T5** assumption (the data was also fitted to equation (2.3), except for that the concentration of **T5** was multiplied by a factor of 2 in the equation), $R^2 = 0.991$.

Figure 5.13b shows the comparison of the fitting results of two assumptions. Although the fitting result is also reasonable for the assumption of **P2·T5**/**$(P2)_2$·T5** host-guest systems, it is not as good as the fitting for the assumption that only **P2·T5** is formed. This gives the evidence for that **$(P2)_2$·T5** was not formed in the titrations.

A possible explanation for the observation that **$(P2)_2$·T5** was not formed is that the terminal THS protecting groups on **P2** have strong steric hindrance for two **P2** to bind to one **T5**. The strong

steric hindrance of terminal THS groups on the porphyrin oligomers also influences the formation of fully-bound **P5·T5**, as will be discussed in **Section 5.3.7**.

Further evidence for the simple formation of **P2·T5** (rather than a mixture of **P2·T5** and **$(P2)_2$·T5**) comes from the sharp isosbestic point in the UV-vis-NIR titration results in **Figure 5.11**: if the **$(P2)_2$·T5** complex were formed, the interactions of the porphyrin units from two different porphyrin oligomers would possibly give the spectra a slight red shift, which can be seen from the titration spectra between monodentate ligands and template-free ***c*-P6** (**Figure 2.12**) or ***c*-P7** (**Figure 2.14**).

5.3.4 P3/T5 Titrations

Porphyrin trimer **P3** was titrated with **T5** to determine the statistically corrected association constant for 3-site binding (K_{chem3}). For the **P3**/**T5** system (and also the **P4**/**T5** and **P5**/**T5** systems), titration spectra had two stages of changes. Before **T5** reached 1:1 stoichiometry, the spectral change indicated the formation of 1:1 complexes (**P3·T5**); when **T5** exceeded 1:1 stoichiometry, the spectral change followed a totally different style, indicating that excess **T5** came to bind **P3·T5** and 1:2 complexes (**P3·$(T5)_2$**) were formed.

Preliminary analyses. The titration data fitted to a combination of 1:1 and 1:2 binding models using Specfit to generate the observed association constants shown in **Table 5.1**. In the calculations, both $K_{obs(\mathbf{P3\cdot T5})}$ and $K_{obs(\mathbf{P3\cdot (T5)2})}$ were set as unknown values: their values were generated by the fitting procedure of Specfit program.

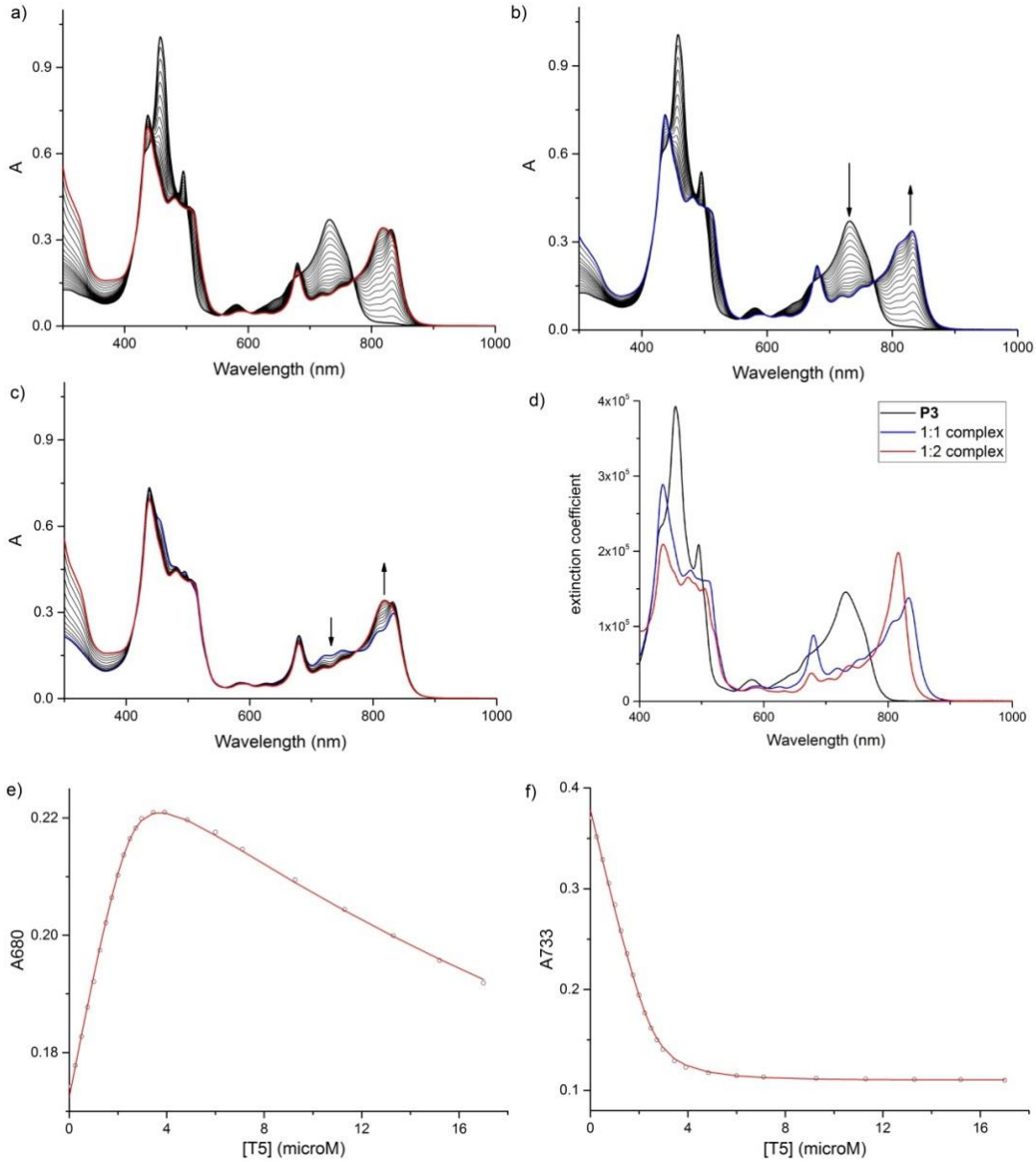

Figure 5.14 UV-vis-NIR titration spectra of **T5** and **P3** (Run 1, toluene, 298 K, [**P3**] = 2.6 μM): a) full spectra; b) formation of 1:1 complexes ([**P3**]/[**T5**] > 1:1); c) formation of 1:2 complexes ([**P3**]/[**T5**] < 1:1); d) calculated extinction coefficient spectra ($cm^{-1} \cdot M^{-1}$) of the host-guest systems involving all complexes of the same stoichiometry; fitting of the experimental data by Specfit at e) 680 nm and f) 733 nm.

Table 5.1 The observed association constants of **P3·T5** and **P3·(T5)$_2$**.

	$K_{obs(\mathbf{P3 \cdot T5})}$ (M^{-1})	$K_{obs(\mathbf{P3 \cdot (T5)2})}$ (M^{-2})
Run 1	$(8.9 \pm 0.8) \times 10^6$	$(2.7 \pm 1.3) \times 10^{11}$
Run 2	$(9.0 \pm 0.9) \times 10^6$	$(5.2 \pm 2.1) \times 10^{11}$

Generating $K_{obs(\mathbf{P3 \cdot (T5)2})}$ from K_{chem}. The value of the observed association constant for 1:2 complexes $K_{obs(\mathbf{P3 \cdot (T5)2})}$, which is directly generated by Specfit, has a relatively high error range for

$K_{obs(\mathbf{P3\cdot(T5)2})}$ (see **Table 5.1**); also, the observed association constant for 1:1 complexes ($K_{obs(\mathbf{P3\cdot T5})}$) nearly reaches the limit of reliable association constant range by direct measurement since the fraction bound at 1:1 stoichiometry is around 90%.[15] We need to verify the reliability of the data using a different method.

For butadiyne-linked porphyrin oligomers, there is essentially no allosteric cooperativity between two separate porphyrin-ligand bindings,[2,12] i.e. the binding of one **T5** doesn't change the K_{chem} of the binding between **P3** and the other **T5**. Then the K_{chem} of 1:2 complexes is the multiple of the K_{chem} from two separate bindings in the complex. Using this strategy, we can calculate $K_{obs(\mathbf{P3\cdot(T5)2})}$ from statistically corrected association constants K_{chem1} and K_{chem2}. As is shown in **Figure 5.15**, there are three different binding modes of **P3·(T5)$_2$** in the equilibria (the binding modes can also be seen in **Figure 5.7**).

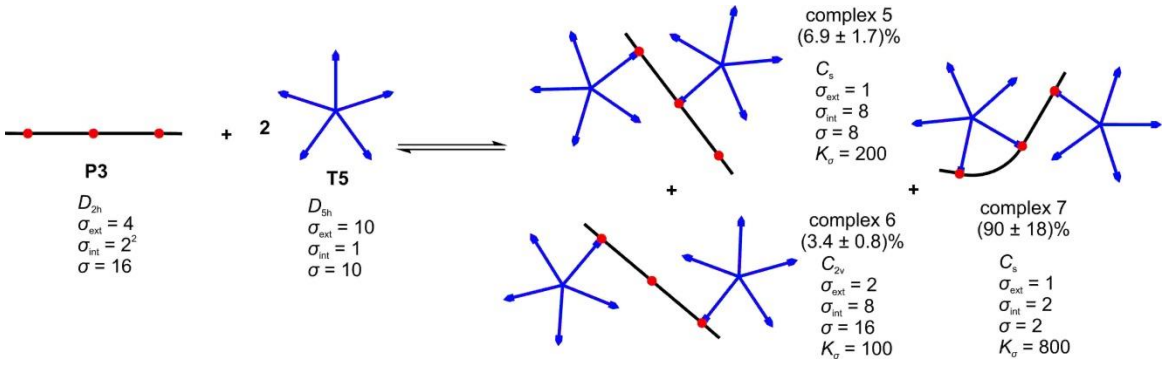

Figure 5.15 Statistical factors and distribution of the complexes in **P3·(T5)$_2$** host-guest system. Note that the free rotations in the butadiyne linkers and metal-ligand bonds in complex 6 give two vertical reflection planes, making the structure effectively C_{2v} symmetry.

The K_f of complexes 5, 6 and 7 can all be calculated by K_{chem}:

$$K_{f(\text{complex 5})} = K_\sigma K_{chem} = 200K_{chem1}^2 \quad (5.16)$$

$$K_{f(\text{complex 6})} = K_\sigma K_{chem} = 100K_{chem1}^2 \quad (5.17)$$

$$K_{f(\text{complex 7})} = K_\sigma K_{chem} = 800K_{chem1}K_{chem2} \quad (5.18)$$

The observed association constant for the **P3·(T5)$_2$** is the sum of the three formation constants, which was shown as equation (5.9). The calculation gives $K_{obs(\mathbf{P3\cdot(T5)2})} = (2.9 \pm 0.4) \times 10^{11}$ M^{-2}. The calculated result is 7% higher than the fitting result of Run 1 and 46% lower than the fitting result of Run 2. Comparing the results of the Specfit data processing method, this approach has less error.

The proportion of the partially-bound complexes (complexes 5 and 6) in the mixture of **P3·(T5)$_2$** host-guest system is:

$$\frac{K_{\mathrm{f(complex\ 5)}} + K_{\mathrm{f(complex\ 6)}}}{\sum_{i=5}^{7} K_{\mathrm{f(complex}\ i\mathrm{)}}} = \frac{200K_{\mathrm{chem1}}^2 + 100K_{\mathrm{chem1}}^2}{200K_{\mathrm{chem1}}^2 + 100K_{\mathrm{chem1}}^2 + 800K_{\mathrm{chem1}}K_{\mathrm{chem2}}} \quad (5.19)$$

$$= (10 \pm 3)\%$$

Determination of $K_{\mathrm{obs(P3{\cdot}T5)}}$. We believe that using the K_{chem} to calculate the K_{obs} for higher-ordered host-guest systems (1:2 and 1:3 complexes) is a more reliable method than using Specfit to generate their values. Meanwhile, the K_{obs} for higher-ordered host-guest systems can be set as fixed values in Specfit to generate the values of K_{obs} for 1:1 host-guest systems. The calculation method will make the results more reliable.

The titration data such as those in **Figure 5.14** were re-analyzed by Specfit using the combination of 1:1 and 1:2 binding models with $K_{\mathrm{obs(P3{\cdot}(T5)2)}}$ set as fixed value (2.9×10^{11} M^{-2}). The results gave $K_{\mathrm{obs(P3{\cdot}T5)}}$ as $(9.2 \pm 0.7) \times 10^6$ M^{-1} (Run 1) and $(8.5 \pm 0.8) \times 10^6$ M^{-1} (Run 2). The average of the two values ($K_{\mathrm{obs(P3{\cdot}T5)}} = (8.8 \pm 1.1) \times 10^6$ M^{-1}) was used in the calculation of K_{chem3}.

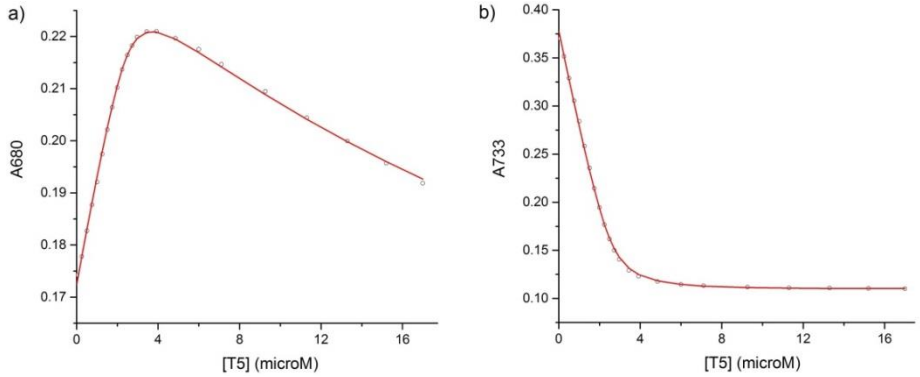

Figure 5.16 Fitting results of the experimental data by Specfit with $K_{\mathrm{obs(P3{\cdot}(T5)2)}}$ set as fixed value (2.9×10^{11} M^{-2}) at selected wavelengths: a) 680 nm, b) 733 nm (Run 1, toluene, 298 K, [**P3**] = 2.6 μM).

Determination of K_{chem3}. Similar to **P2·T5**, the **P3·T5** host-guest system has the equilibria between the complexes of different binding modes (the binding modes can also be seen in **Figure 5.7**). The complexes and their statistical factors are shown in **Figure 5.17**.

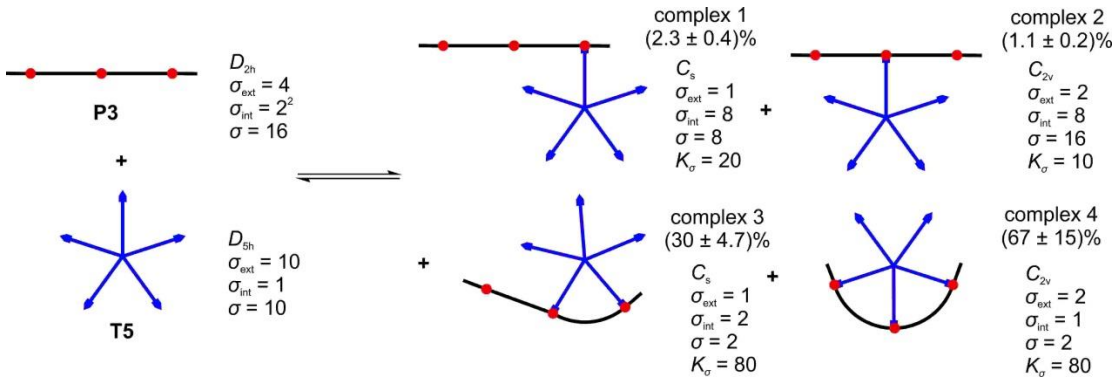

Figure 5.17 Statistical factors and distribution of the complexes in **P3·T5** host-guest system.

As before, the K_f of each complex can be calculated and the values are shown in **Table 5.2**.

Table 5.2 The K_f of the complexes in the mixture of **P3·T5** host-guest system.

	K_f
complex 1	$20K_{chem1}$
complex 2	$10K_{chem1}$
complex 3	$80K_{chem2}$
complex 4	$80K_{chem3}$

$K_{obs(\mathbf{P3\cdot T5})}$ is related to K_{chemN} (N = 1 – 3) by equation (5.8): in the equation, $K_{obs(\mathbf{P3\cdot T5})}$ = (8.8 ± 1.1) × 10^6 M^{-1}; only the value of K_{chem3} is unknown. Solving equation gives the result as K_{chem3} = (7.4 ± 1.4) × 10^4 M^{-1}.

The proportion of the partially-bound complexes (complexes 1 – 3) in the mixture of **P3·T5** host-guest system is:

$$\frac{\sum_{i=1}^{3} K_{f(\text{complex } i)}}{\sum_{i=1}^{4} K_{f(\text{complex } i)}} = \frac{20K_{chem1} + 10K_{chem1} + 80K_{chem2}}{20K_{chem1} + 10K_{chem1} + 80K_{chem2} + 80K_{chem3}} = (33 \pm 5)\% \qquad (5.20)$$

5.3.5 Distribution of P3·(T5)$_3$ – Evidence to Ignore the 1:3 Complex

In **P3/T5** titrations, there is the possibility for another **T5** to bind to complex 5 or complex 6, forming **P3·(T5)$_3$**. As the formation of **P3·(T5)$_2$** only gives a very small spectral change (see **Figure 5.14c**), the formation of **P3·(T5)$_3$** might not be distinguishable from the spectral change. Then the titration data can be analyzed by the formation of **P3·T5**, **P3·(T5)$_2$** and **P3·(T5)$_3$** host-guest systems.

Generating $K_{obs(\mathbf{P3\cdot(T5)3})}$ from K_{chem}. There is only one binding model for the 1:3 complex, as is shown in **Figure 5.18**. Thus $K_{obs(\mathbf{P3\cdot(T5)3})} = 1000K_{chem1}^{\ 3}$ = (1.0 ± 0.1) × 10^{15} M^{-3}.

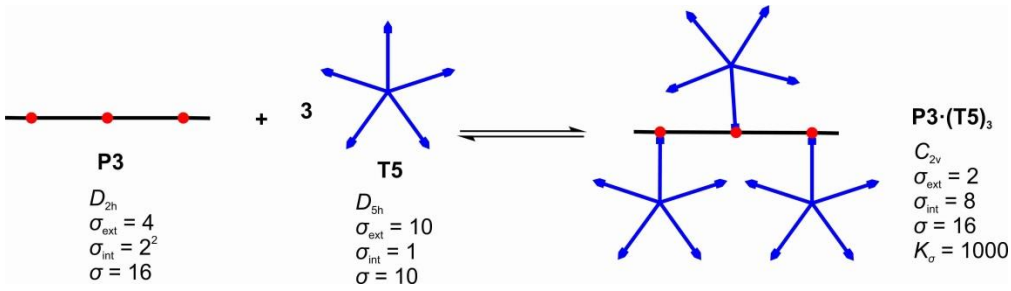

Figure 5.18 The statistical factor of **P3·(T5)$_3$** complex.

Result of Specfit simulation and distribution of P3·(T5)$_3$. Now that we have known all the values of $K_{obs(\mathbf{P3\cdot T5})}$, $K_{obs(\mathbf{P3\cdot(T5)2})}$ and $K_{obs(\mathbf{P3\cdot(T5)3})}$, the titration data of **P3/T5** titrations in previous

section can be simulated by Specfit using the combination of 1:1, 1:2 and 1:3 binding models with all of $K_{obs(\mathbf{P3\cdot T5})}$, $K_{obs(\mathbf{P3\cdot (T5)2})}$ and $K_{obs(\mathbf{P3\cdot (T5)3})}$ set as fixed value ($K_{obs(\mathbf{P3\cdot T5})} = 8.8 \times 10^6$ M^{-1}, $K_{obs(\mathbf{P3\cdot (T5)2})} = 2.9 \times 10^{11}$ M^{-2}, $K_{obs(\mathbf{P3\cdot (T5)3})} = 1.0 \times 10^{15}$ M^{-3}). The concentrations of the complexes are shown in **Figure 5.19**. It can be seen that the distribution of **P3·(T5)$_3$** complexes is less than 1% at the endpoint of the titrations.

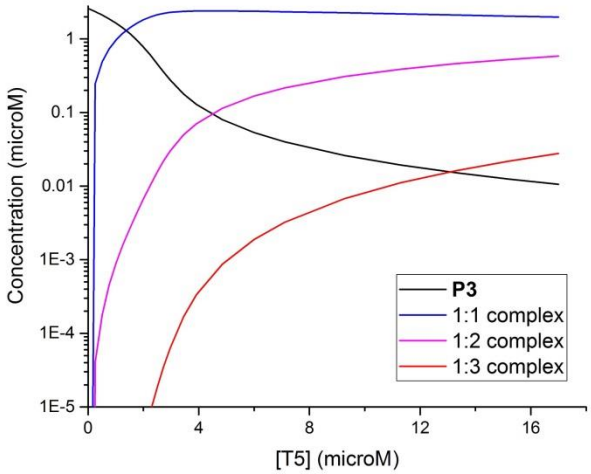

Figure 5.19 Concentrations (of the complexes of the same stoichiometry) of the host-guest systems from the Specfit results in **P3/T5** titrations with $K_{obs(\mathbf{P3\cdot T5})}$, $K_{obs(\mathbf{P3\cdot (T5)2})}$ and $K_{obs(\mathbf{P3\cdot (T5)3})}$ set as fixed values. (Run 1, toluene, 298 K, [**P3**] = 2.6 μM)

Thus the formation of **P3·(T5)$_3$** can be ignored in the analyses and the data generated in this section is not used for the determination of K_{chem3}. For the same reason, **P4·(T5)$_3$**, **P4·(T5)$_4$**, **P5·(T5)$_4$** and **P5·(T5)$_5$** host-guest systems are ignored in the following sections when analyzing **P4/T5** and **P5/T5** titrations.

5.3.6 P4/T5 Titrations

Porphyrin tetramer **P4** was titrated with **T5** to determine the statistically corrected association constant for 4-site binding (K_{chem4}). Similar to **P3/T5** system, the titration also had two stages of spectral change, which indicates the formation of **P4·T5** complexes (at [**P4**]/[**T5**] > 1:1) followed by the formation of **P4·(T5)$_2$** complexes (at [**P4**]/[**T5**] < 1:1).

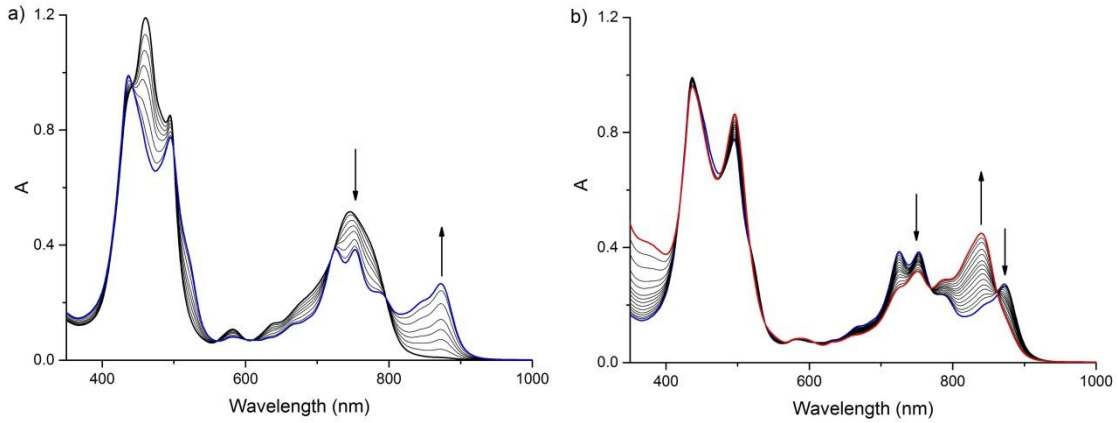

Figure 5.20 UV-vis-NIR titration spectra of **T5** and **P4** (Run 1, toluene, 298 K, [**P4**] = 2.8 μM): a) formation of 1:1 complexes ([**P4**]/[**T5**] > 1:1); b) formation of 1:2 complexes ([**P4**]/[**T5**] < 1:1).

Generating $K_{obs(P4\cdot(T5)2)}$ from K_{chem}. Similar to **P3/T5** titrations, $K_{obs(P4\cdot(T5)2)}$ can be generated from the statistically corrected association constants K_{chem}. $K_{obs(P4\cdot(T5)2)}$, being generated from K_{chem}, has higher reliability compared to the Specfit approach which generates the values of $K_{obs(P4\cdot T5)}$ and $K_{obs(P4\cdot(T5)2)}$ all at once. The K_f of each complex in **P4·(T5)$_2$** host-guest system is shown in **Table 5.3** and their statistical factors are shown in **Figure 5.21**.

Table 5.3 The K_f of the complexes in the mixture of **P4·(T5)$_2$** host-guest system.

	K_f		K_f
complex 10	$100K_{chem1}^2$	complex 14	$800K_{chem1}K_{chem2}$
complex 11	$200K_{chem1}^2$	complex 15	$800K_{chem1}K_{chem2}$
complex 12	$200K_{chem1}^2$	complex 16	$800K_{chem1}K_{chem2}$
complex 13	$100K_{chem1}^2$	complex 17	$1600K_{chem2}^2$
		complex 18	$1600K_{chem1}K_{chem3}$

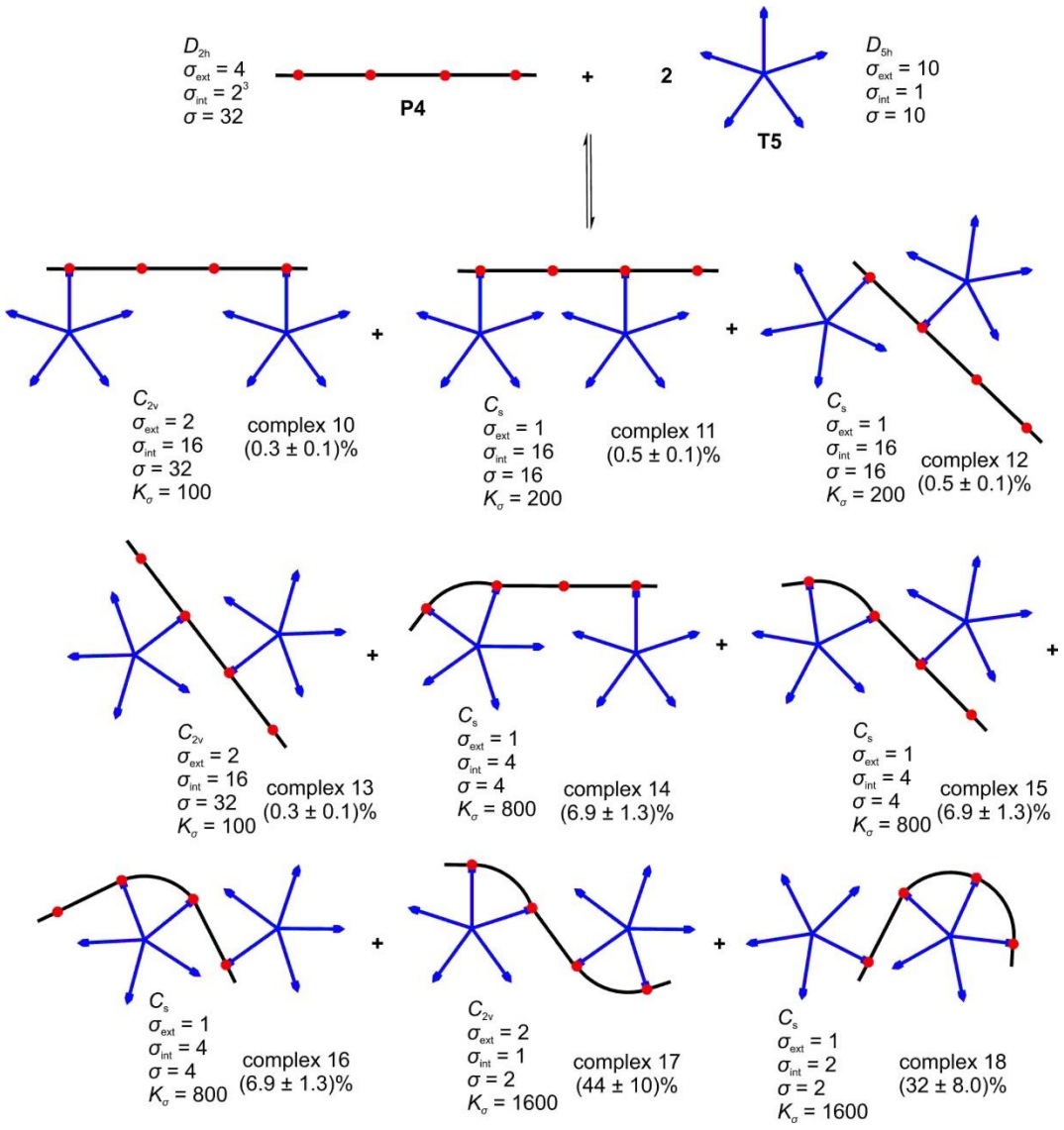

Figure 5.21 Statistical factors and distribution of the complexes in **P4·(T5)$_2$** host-guest system.

The calculation gave the result as $K_{\text{obs(P4·(T5)2)}} = (3.7 \pm 0.5) \times 10^{12}$ M^{-2}. The proportion of the partially-bound complexes (complexes 10 – 16) in the mixture of **P4·(T5)$_2$** host-guest system is (22 ± 4)%.

Determination of $K_{\text{obs(P4·T5)}}$. The titration data were analyzed by Specfit using the combination of 1:1 and 1:2 binding models with $K_{\text{obs(P4·(T5)2)}}$ set as fixed value (3.7×10^{12} M^{-2}). The results gave $K_{\text{obs(P4·T5)}}$ as $(6.2 \pm 0.4) \times 10^{7}$ M^{-1} (Run 1) and $(6.3 \pm 0.7) \times 10^{7}$ M^{-1} (Run 2). The average of the two values ($(6.2 \pm 0.8) \times 10^{7}$ M^{-1}) was used to calculate K_{chem4}.

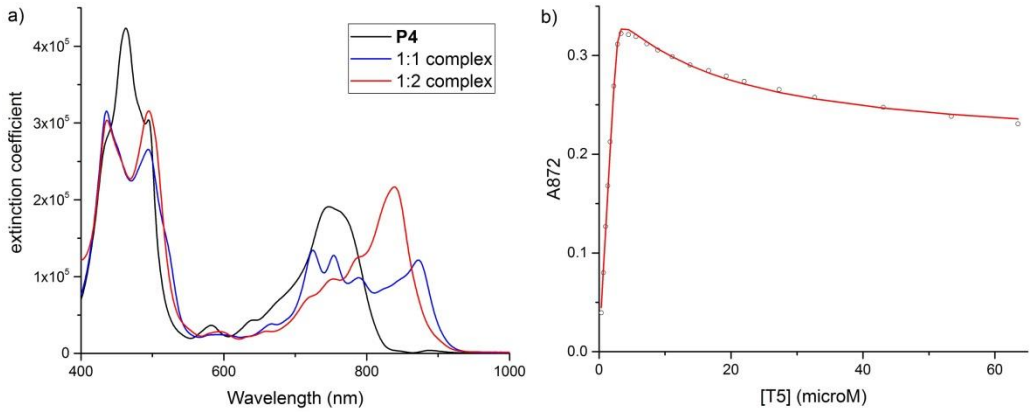

Figure 5.22 a) Calculated extinction coefficient spectra ($cm^{-1}·M^{-1}$) of the host-guest systems involving all complexes of the same stoichiometry; b) fitting results of experimental data at 872 nm. (Run 1, toluene, 298 K, [**P4**] = 2.8 μM, calculation by Specfit with $K_{obs(\mathbf{P4}\cdot(\mathbf{T5})2)}$ set as fixed value (3.7×10^{12} M^{-2}))

Determination of K_{chem4}. The K_f of the complexes in **P4·T5** host-guest system are shown in **Table 5.4** and their statistical factors are shown in **Figure 5.23**. The sum of the K_f of complexes 19 – 24 is the value of $K_{obs(\mathbf{P4}\cdot\mathbf{T5})}$, which equals to $(6.2 \pm 0.8) \times 10^7$ M^{-1} in the calculation.

Table 5.4 The K_f of the complexes in **P4·T5** host-guest system.

	K_f		K_f
complex 19	$20K_{chem1}$	complex 22	$80K_{chem2}$
complex 20	$20K_{chem1}$	complex 23	$160K_{chem3}$
complex 21	$40K_{chem2}$	complex 24	$160K_{chem4}$

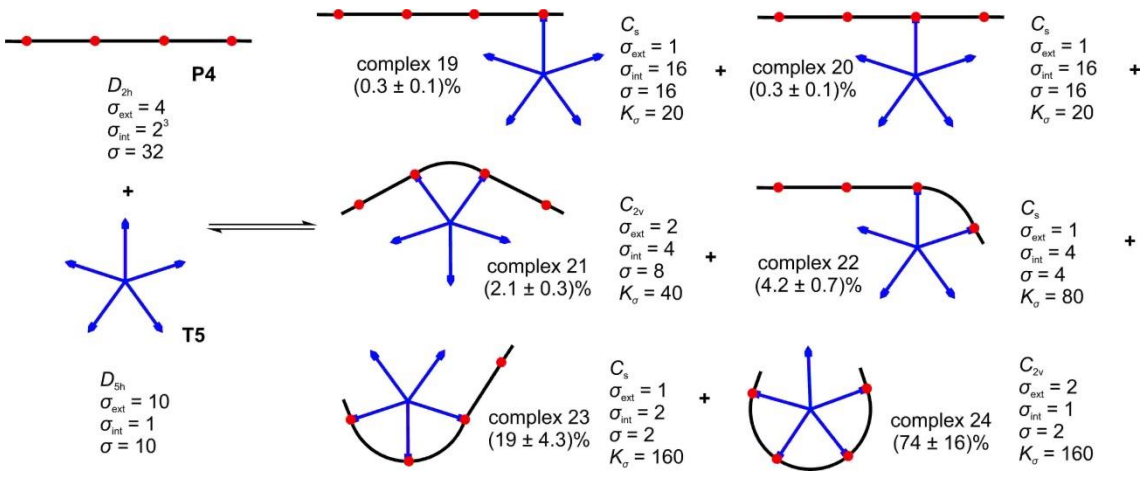

Figure 5.23 Statistical factors and distribution of the complexes in **P4·T5** host-guest system.

The calculation gives the result as $K_{chem4} = (2.9 \pm 0.5) \times 10^5$ M^{-1}. The proportion of the partially-bound complexes (complexes19 – 23) in the mixture of **P4·T5** host-guest system is (26 ± 5)%.

5.3.7 P5/T5 Titrations

Porphyrin pentamer **P5** was titrated with **T5** to determine the statistically corrected association constant for 5-site binding (K_{chem5}). Similar to **P3/T5** and **P4/T5** titrations, **P5/T5** titration also had two stages of spectral change.

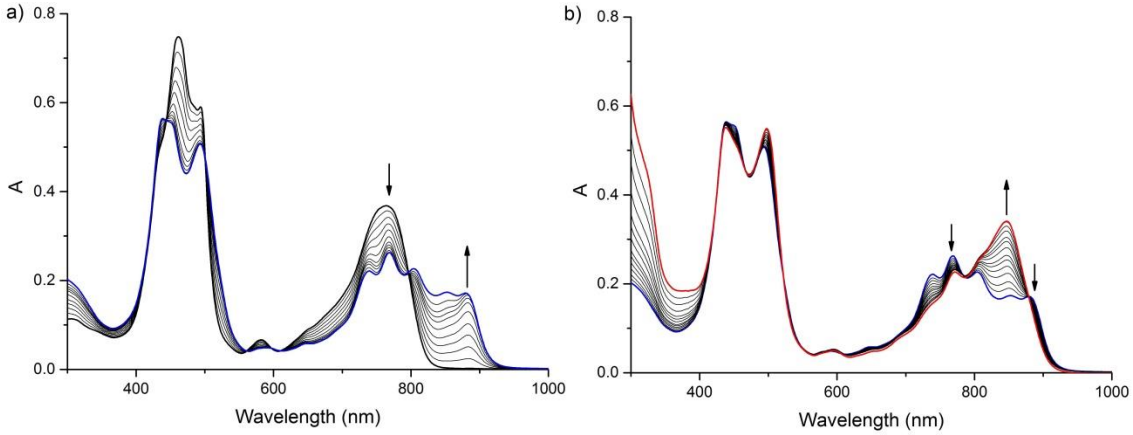

Figure 5.24 UV-vis-NIR titration spectra of **T5** and **P5**: a) spectral change at [**P5**]/[**T5**] > 1:1; b) spectral change at [**P5**]/[**T5**] < 1:1. (Run 1, toluene, 298 K, [**P5**] = 1.4 μM)

But unlike **P3/T5** and **P4/T5** systems, in which the highest ordered complex in the calculation is 1:2 complex, we need to take **P5·(T5)$_3$** along with **P5·T5** and **P5·(T5)$_2$** into the calculation procedure. **Figure 5.25** shows the logic: since excess **T5** can knock out one binding site in **P3·T5** to give **P3·(T5)$_2$**, **T5** should also knock out one binding site in **P5·(T5)$_2$** to give **P5·(T5)$_3$**. In both cases, there is the equilibrium between a 3-site binding and the (1-site + 2-site) bindings. **P5·(T5)$_3$** should be taken into the analyses, since **P3·(T5)$_2$** was taken into the analyses.

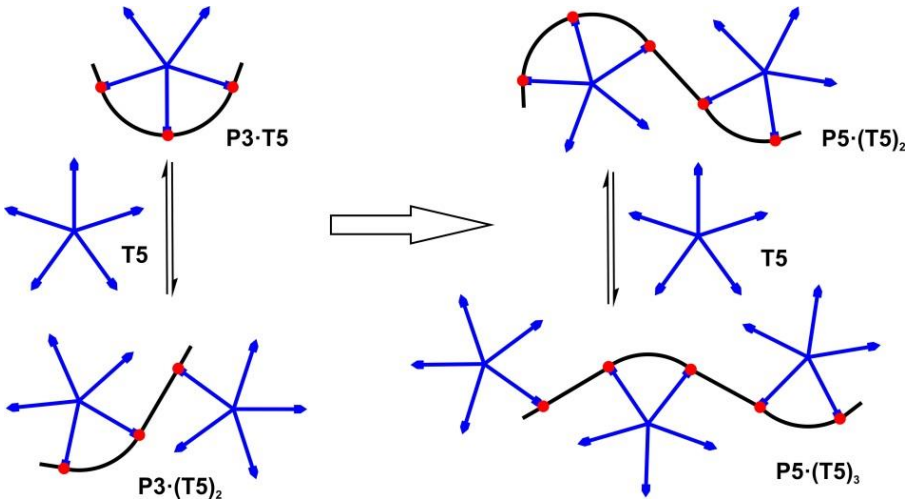

Figure 5.25 The formation of **P5·(T5)$_3$**.

Now the titration system involves three observed association constants: $K_{obs(\mathbf{P5\cdot T5})}$, $K_{obs(\mathbf{P5\cdot (T5)2})}$ and $K_{obs(\mathbf{P5\cdot (T5)3})}$. If we use Specfit to process the titration data and generate the three association constants all at once, the result will be less reliable: all the three unknown values give the program a large space to fit the data in a perfect way and the error might be big. Similar to previous sections, $K_{obs(\mathbf{P5\cdot (T5)2})}$, $K_{obs(\mathbf{P5\cdot (T5)3})}$ can be calculated from K_{chem}. The values of $K_{obs(\mathbf{P5\cdot (T5)2})}$ and $K_{obs(\mathbf{P5\cdot (T5)3})}$ are set as fixed values in the Specfit program to generate the value of $K_{obs(\mathbf{P5\cdot T5})}$.

Generating $K_{obs(\mathbf{P5\cdot (T5)2})}$ and $K_{obs(\mathbf{P5\cdot (T5)3})}$ from K_{chem}. There are totally 19 complexes in the **P5·(T5)$_2$** host-guest system and 16 complexes in the **P5·(T5)$_3$** host-guest system: the detailed K_f of the complexes in **P5·(T5)$_2$** and **P5·(T5)$_3$** host-guest systems are shown in the figures and tables below. The calculated results are: $K_{obs(\mathbf{P5\cdot (T5)2})}$ = (3.4 ± 0.5) × 10^{13} M^{-2}, the proportion of the partially-bound complexes (complexes 25 – 41) in the mixture of **P5·(T5)$_2$** host-guest system is (28 ± 6)%; $K_{obs(\mathbf{P5\cdot (T5)3})}$ = (8.3 ± 1.6) × 10^{17} M^{-3}, the proportion of the partially-bound complexes (complexes 44 – 55) in the mixture of **P5·(T5)$_3$** host-guest system is (19 ± 6)%.

Table 5.5 The K_f of the complexes in **P5·(T5)$_2$** host-guest system.

	K_f		K_f
complex 25	$200K_{chem1}^2$	complex 35	$800K_{chem1}K_{chem2}$
complex 26	$200K_{chem1}^2$	complex 36	$800K_{chem1}K_{chem2}$
complex 27	$200K_{chem1}^2$	complex 37	$1600K_{chem1}K_{chem3}$
complex 28	$100K_{chem1}^2$	complex 38	$1600K_{chem1}K_{chem3}$
complex 29	$200K_{chem1}^2$	complex 39	$1600K_{chem1}K_{chem3}$
complex 30	$100K_{chem1}^2$	complex 40	$1600K_{chem2}^2$
complex 31	$800K_{chem1}K_{chem2}$	complex 41	$3200K_{chem2}^2$
complex 32	$800K_{chem1}K_{chem2}$	complex 42	$3200K_{chem1}K_{chem4}$
complex 33	$800K_{chem1}K_{chem2}$	complex 43	$6400K_{chem2}K_{chem3}$
complex 34	$800K_{chem1}K_{chem2}$		

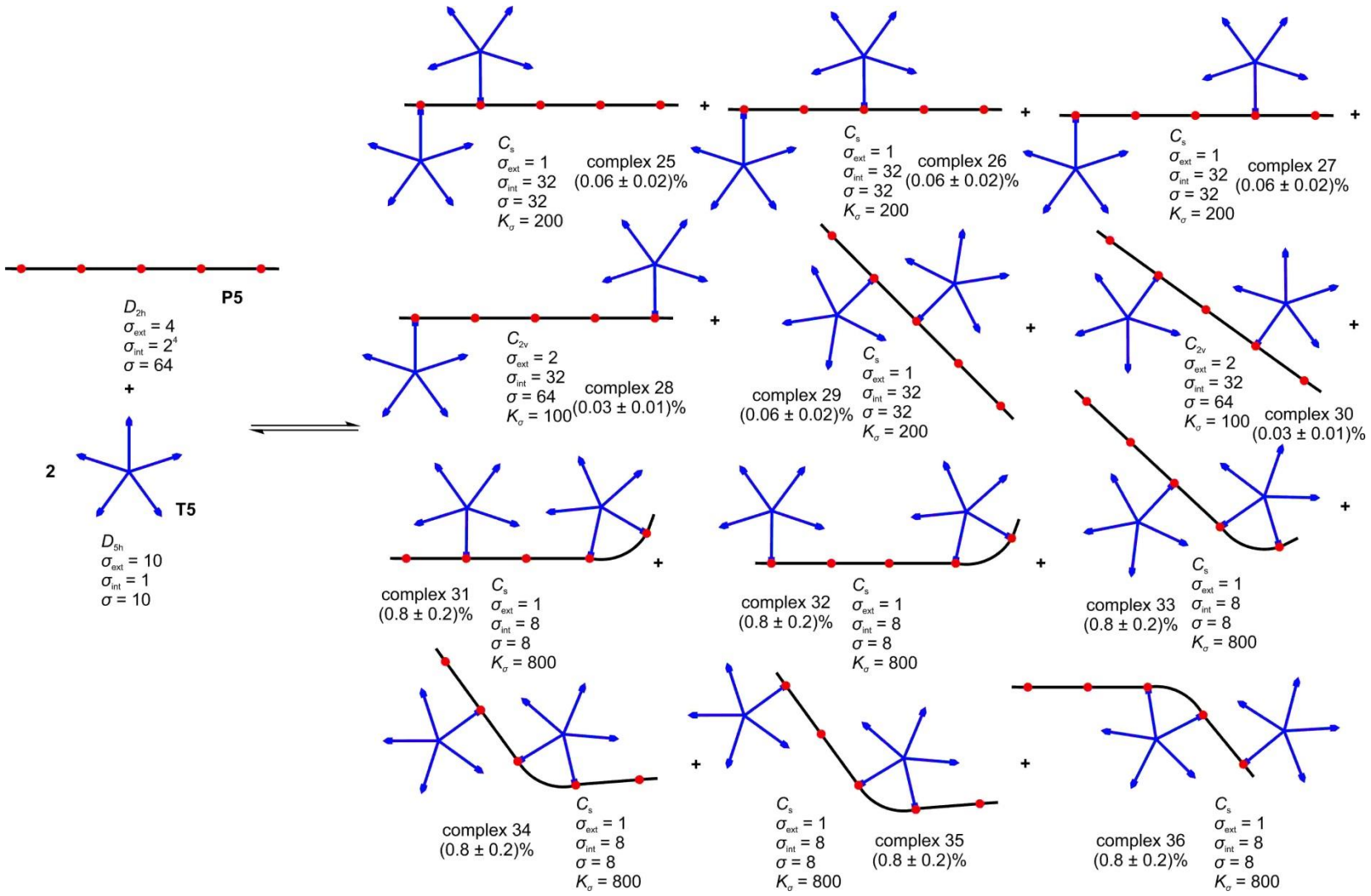

Figure 5.26 Statistical factors and distribution of the complexes in **P5·(T5)$_2$** host-guest system (part 1).

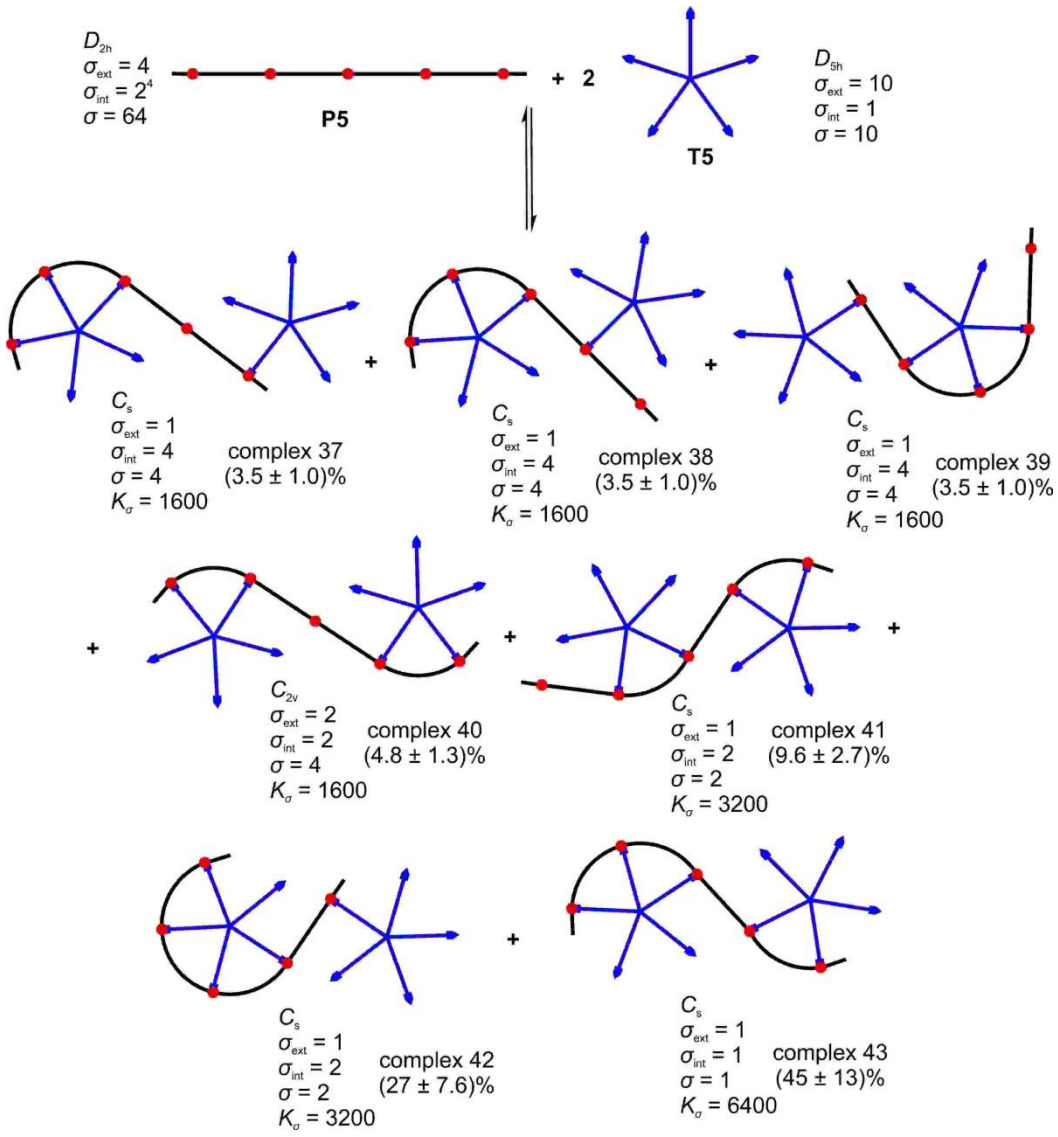

Figure 5.27 Statistical factors and distribution of the complexes in **P5·(T5)$_2$** host-guest system (part 2).

Table 5.6 The K_f of the complexes in **P5·(T5)$_3$** host-guest system.

	K_f		K_f
complex 44	$2000K_{chem1}^3$	complex 52	$8000K_{chem1}^2K_{chem2}$
complex 45	$2000K_{chem1}^3$	complex 53	$8000K_{chem1}^2K_{chem2}$
complex 46	$2000K_{chem1}^3$	complex 54	$8000K_{chem1}^2K_{chem2}$
complex 47	$1000K_{chem1}^3$	complex 55	$8000K_{chem1}^2K_{chem2}$
complex 48	$2000K_{chem1}^3$	complex 56	$8000K_{chem1}^2K_{chem3}$
complex 49	$1000K_{chem1}^3$	complex 57	$16000K_{chem1}^2K_{chem3}$
complex 50	$8000K_{chem1}^2K_{chem2}$	complex 58	$16000K_{chem1}K_{chem2}^2$
complex 51	$8000K_{chem1}^2K_{chem2}$	complex 59	$32000K_{chem1}K_{chem2}^2$

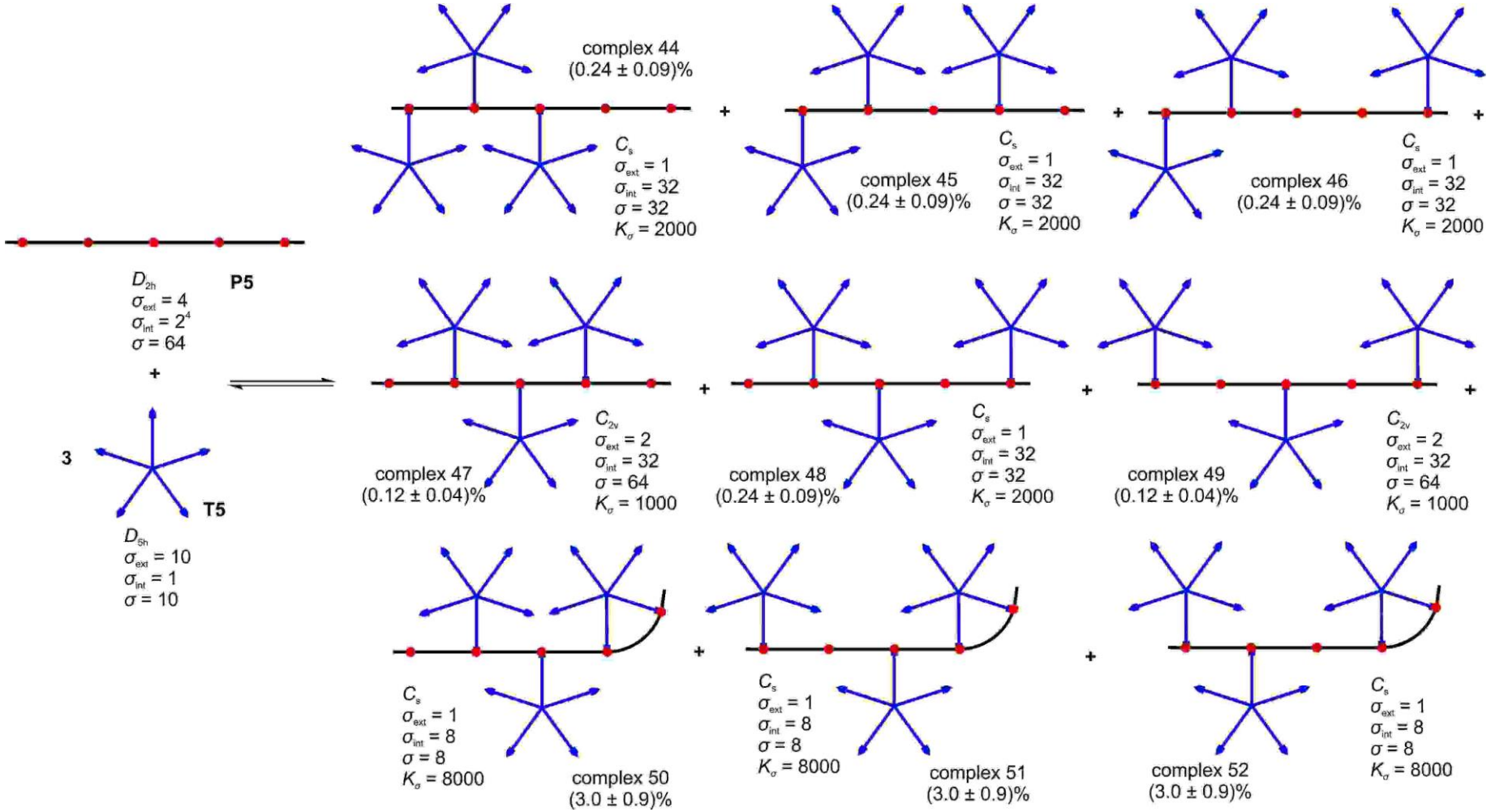

Figure 5.28 Statistical factors and distribution of the complexes in **P5·(T5)$_3$** host-guest system (part 1).

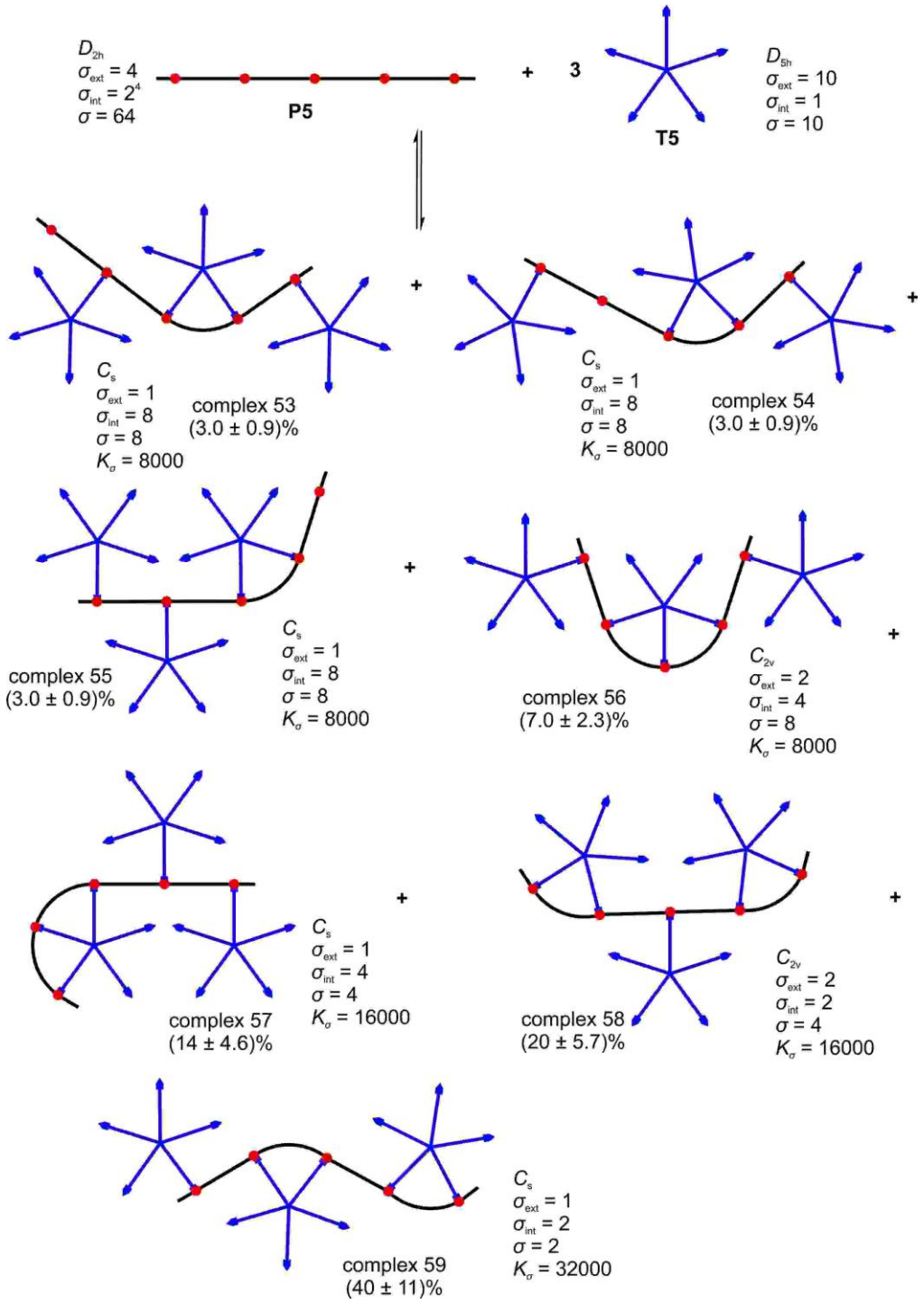

Figure 5.29 Statistical factors and distribution of the complexes in **P5·(T5)$_3$** host-guest system (part 2).

Determination of $K_{obs(P5·T5)}$. As is shown in **Figure 5.30**, the titration data were analyzed by Specfit using the combination of 1:1, 1:2 and 1:3 binding models with $K_{obs(P5·(T5)2)}$ (3.4×10^{13} M^{-2}) and $K_{obs(P5·(T5)3)}$ (8.3×10^{17} M^{-3}) set as fixed values. The results gave $K_{obs(P5·T5)}$ as $(1.1 \pm 0.1) \times 10^8$ M^{-1} (Run 1) and $(1.0 \pm 0.1) \times 10^8$ M^{-1} (Run 2). The average of the two values ($K_{obs(P5·T5)}$ = $(1.0 \pm 0.2) \times 10^8$ M^{-1}) was used to calculate K_{chem5}.

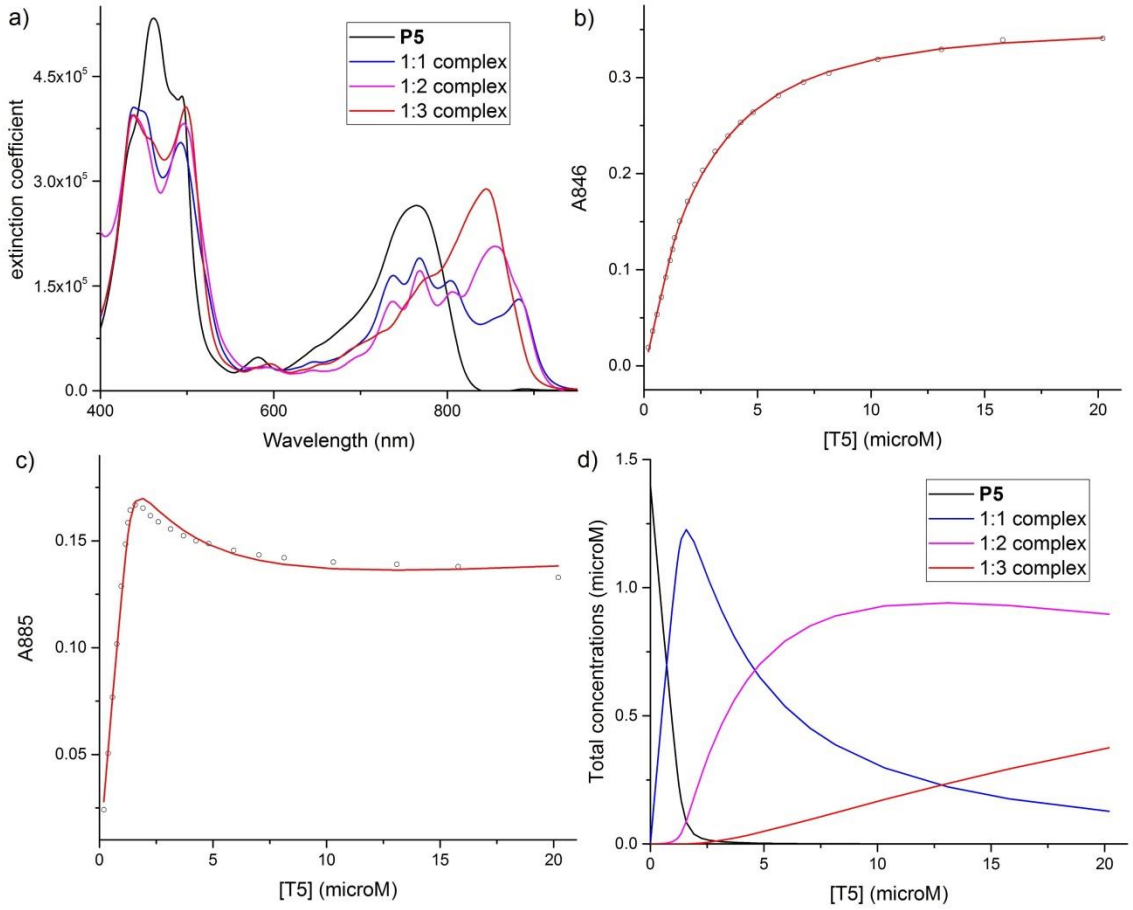

Figure 5.30 a) Calculated extinction coefficient spectra ($cm^{-1}\cdot M^{-1}$) of the host-guest systems involving all complexes of the same stoichiometry; fitting results of experimental data at b) 846 nm and c) 885 nm; d) total concentrations (of the complexes of the same stoichiometry) of the host-guest systems. (Run 1, toluene, 298 K, [**P5**] = 1.4 μM, calculation by Specfit with $K_{obs(\mathbf{P5\cdot(T5)2})}$ (3.4×10^{13} M^{-2}) and $K_{obs(\mathbf{P5\cdot(T5)3})}$ (8.3×10^{17} M^{-3}) set as fixed values)

Determination of K_{chem5}. The calculation method is the same as for the previous 1:1 host-guest systems. The K_f of the complexes in **P5·T5** host-guest system are shown **Table 5.7** and their statistical factors are shown in **Figure 5.31**. The calculation gives the result as K_{chem5} = (-5.1 ± 8.1) × 10^4 M^{-1}.

Table 5.7 The K_f of the complexes in the mixture of **P5·T5** complex.

	K_f		K_f
complex 60	$20K_{chem1}$	complex 65	$160K_{chem3}$
complex 61	$10K_{chem1}$	complex 66	$80K_{chem3}$
complex 62	$20K_{chem1}$	complex 67	$320K_{chem4}$
complex 63	$80K_{chem2}$	complex 68	$320K_{chem5}$
complex 64	$80K_{chem2}$		

As an association constant cannot be negative, this means that K_{chem5} is smaller than 3.0×10^4 M^{-1}. We can even argue that $K_{f(complex\ 68)} = 0$ and the K_f of partially-bound complexes (complexes 60 – 67) contributes to $K_{obs(\mathbf{P5 \cdot T5})}$. Steric repulsion of the terminal THS groups in complex 68 may contribute to the low stability of this complex. The steric hindrance of the terminal THS groups can also be seen in the binding between **T5** and **P2**, where only 1:1 complexes can be formed in the titration (**Figure 5.13**).

As a result, K_{chem5} is too small to be measured accurately: complex 68 is either a very unstable complex ($K_{chem5} \leq 3.0 \times 10^4$ M^{-1}) or is not formed at all.

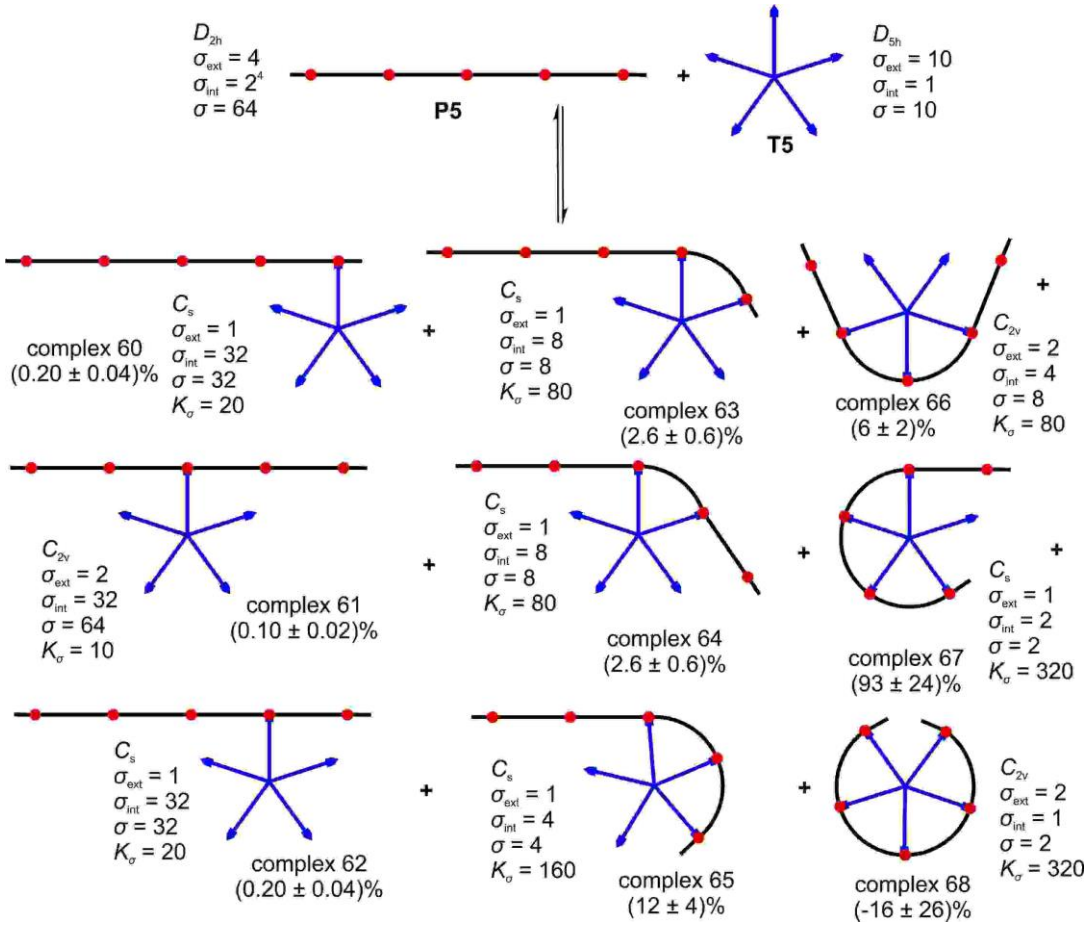

Figure 5.31 Statistical factors and distribution of the complexes in **P5·T5** host-guest system.

5.3.8 $P5_H$/T5 Titrations

To further explore the linear porphyrin oligomer/**T5** titrations and to obtain a value of K_{chem5} with better reliability, we used a different porphyrin pentamer with terminal groups as protons (**$P5_H$**) to titrate with **T5**. The intention is to avoid the influences of THS terminal groups in the binding of fully-bound complex. Similar to **P5/T5** titrations, the titrations also had two stages of spectral change.

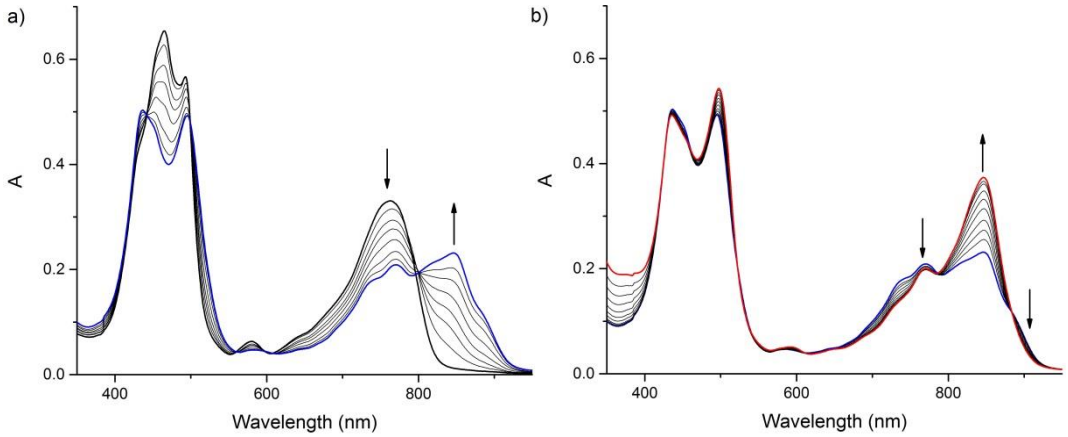

Figure 5.32 UV-vis-NIR titration spectra of **T5** and **$P5_H$**: a) spectral change at [**$P5_H$**]/[**T5**] > 1:1; b) spectral change at [**$P5_H$**]/[**T5**] < 1:1. (Run 1, toluene, 298 K, [**$P5_H$**] = 1.3 μM).

We assume that the 1:2 and 1:3 complexes formed by **T5** and **$P5_H$** are exactly the same as the host-guest systems formed by **T5** and **P5**, since there is not any complex in the host-guest system with the situation of steric repulsion of the terminal THS groups. Thus $K_{obs(\mathbf{P5H\cdot(T5)2})} = K_{obs(\mathbf{P5\cdot(T5)2})} = (3.4 \pm 0.5) \times 10^{13}$ M^{-2}, $K_{obs(\mathbf{P5H\cdot(T5)3})} = K_{obs(\mathbf{P5\cdot(T5)3})} = (8.3 \pm 1.6) \times 10^{17}$ M^{-3}.

The titration data were analyzed by Specfit using the combination of 1:1, 1:2 and 1:3 binding models with $K_{obs(\mathbf{P5H\cdot(T5)2})}$ (3.4×10^{13} M^{-2}) and $K_{obs(\mathbf{P5H\cdot(T5)3})}$ (8.3×10^{17} M^{-3}) set as fixed values. The results gave $K_{obs(\mathbf{P5H\cdot T5})}$ as $(1.2 \pm 0.3) \times 10^{8}$ M^{-1} (Run 1) and $(1.2 \pm 0.3) \times 10^{8}$ M^{-1} (Run 2). The average of the two values ($K_{obs(\mathbf{P5\cdot T5})} = (1.2 \pm 0.3) \times 10^{8}$ M^{-1}) was used to calculate K_{chem5}.

The value of $K_{obs(\mathbf{P5H\cdot T5})}$ was used to calculate K_{chem5}, giving the result as $K_{chem5} = (1.2 \pm 10) \times 10^{4}$ M^{-1}. The detailed distribution of the complexes in **$P5_H$·T5** host-guest system are shown in **Figure 5.34**.

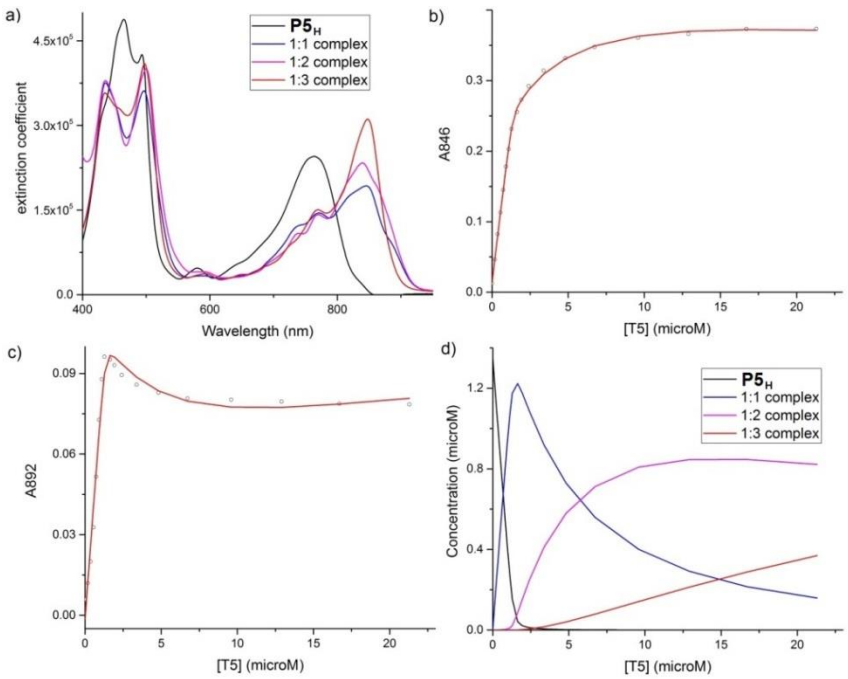

Figure 5.33 a) Calculated extinction coefficient spectra ($cm^{-1}\cdot M^{-1}$) of the host-guest systems involving all complexes of the same stoichiometry; fitting results of experimental data at b) 846 nm and c) 892 nm; d) total concentrations (of the complexes of the same stoichiometry) of the host-guest systems. (Run 1, toluene, 298 K, [**P5$_H$**] = 1.3 μM, calculation by Specfit with $K_{obs(\mathbf{P5H\cdot(T5)2})}$ (3.4×10^{13} M^{-2}) and $K_{obs(\mathbf{P5H\cdot(T5)3})}$ (8.3×10^{17} M^{-3}) set as fixed values). $K_{obs(\mathbf{P5H\cdot T5})} = (1.2 \pm 0.3) \times 10^8$ M^{-1}.

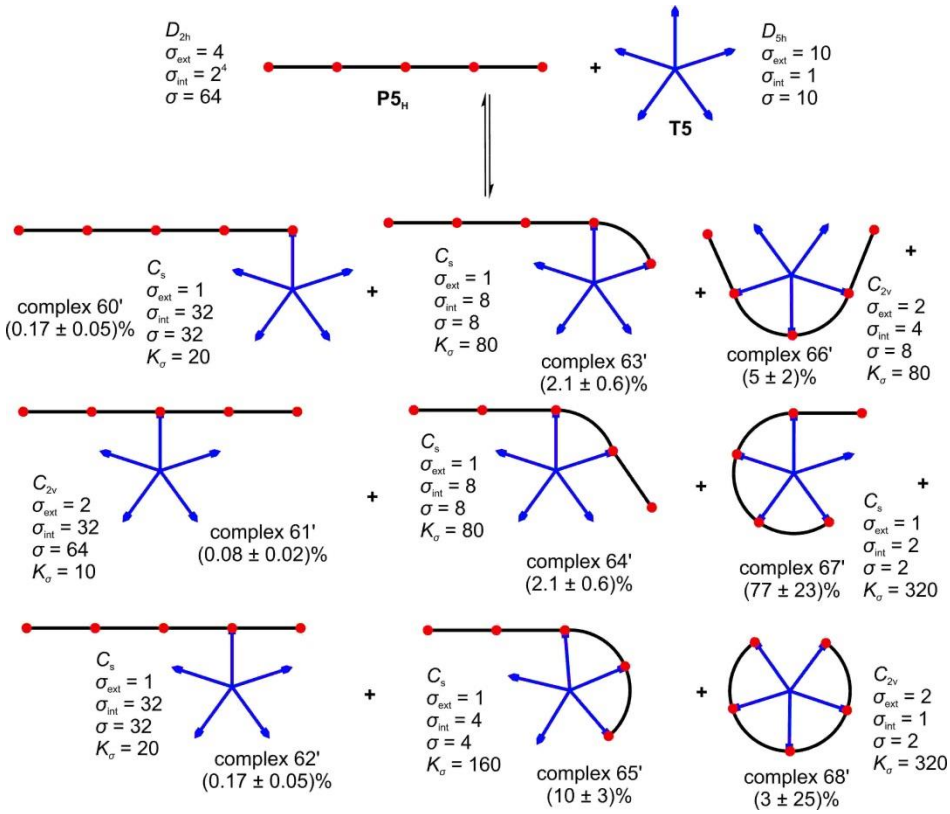

Figure 5.34 Statistical factors and distribution of the complexes in **P5$_H$·T5** host-guest system.

It can be seen that the highest possible distributions of fully-bound complex (complex 68'/68) are 10% and 28% for **P5·T5** host-guest system and **$P5_H$·T5** host-guest system, respectively. The result gives a rough idea of the steric repulsion effects of the bulky terminal THS groups in the porphyrin oligomers.

The distribution of the complexes in **$P5_H$·T5** host-guest system can be used as the model to interpret the product distribution in the syntheses of porphyrin nanorings from ***l*-$P1_{OOct}$(H,H)** and **T5**, which is illustrated in **Figure 4.18b**. ***c*-P8** is generated from the 4-site binding precursor, and the ***c*-P8** product dominates in the mixture of porphyrin nanorings. From **Figure 5.34**, it can be seen that the distribution of complex 67' in **$P5_H$·T5** host-guest system is the highest, which can explain the result from synthesis. The fully-bound precursor gives the ***c*-P5** product; and the distribution of complex 68' in **$P5_H$·T5** host-guest system should be in the range of 0% − 25%, as we know for sure that the fully bound complex do exist in the **$P5_H$·T5** host-guest system.

Thus the value of K_{chem5} obtained from **$P5_H$/T5** titrations is a more reliable value in the dataset to calculate $(\overline{EM})_l$. The value of K_{chem5} used to calculate $(\overline{EM})_l$ is $K_{chem5} \leq 1.1 \times 10^5$ M^{-1}.

5.4 Results and Discussion

5.4.1 Summary of Titration Results

The summary of the observed association constants and proportions from partially-bound complexes is shown in **Table 5.8**.

Table 5.8 Summary of the observed association constants and proportions of partially-bound complexes.

Complexes	K_{obs}	Proportion of partially-bound complexes
P1·isoquinoline	$(2.0 \pm 0.1) \times 10^4$ M^{-1}	0%
P2·T5	$(1.5 \pm 0.1) \times 10^6$ M^{-1}	(13 ± 2)%
P3·T5	$(8.8 \pm 1.1) \times 10^6$ M^{-1}	(33 ± 5)%
P4·T5	$(6.2 \pm 0.8) \times 10^7$ M^{-1}	(26 ± 5)%
P5·T5	$(1.0 \pm 0.2) \times 10^8$ M^{-1}	ca. 100%
$P5_H$·T5	$(1.2 \pm 0.3) \times 10^8$ M^{-1}	(97 ± 27)%
P3·$(T5)_2$	$(2.9 \pm 0.4) \times 10^{11}$ M^{-2}	(10 ± 3)%
P4·$(T5)_2$	$(3.7 \pm 0.5) \times 10^{12}$ M^{-2}	(22 ± 4)%
P5·$(T5)_2$	$(3.5 \pm 0.7) \times 10^{13}$ M^{-2}	(28 ± 6)%
P5·$(T5)_3$	$(8.4 \pm 1.6) \times 10^{17}$ M^{-3}	(19 ± 6)%

We can see that as the porphyrin oligomer elongates, the partially-bound complexes generally have higher proportions in the equilibria of corresponding complexes (exception occurs between the results of **P3·T5** and **P4·T5** host-guest systems; but the tendency might still apply due to the range of errors). This is because longer porphyrin oligomers need to bend more to be fully-bound to the template and this causes free energy cost. As a result, the proportion of partially-bound complexes rises.

5.4.2 Calculation of Effective Molarities

The method to calculate effective molarities in **P*N*·T5** (N = 2 – 5) systems has been shown in equation (5.6). The calculation results are shown in **Table 5.9**.

Table 5.9 Calculation results of $K_{\text{chem}N}$ and corresponding effective molarities (logarithms are decadic).

N sites of binding	$K_{\text{chem}N}$ (M^{-1})	log$EM_{(N\text{-}1)}$ (M)	log$(\overline{EM})_l$ (M)
1	$(1.0 \pm 0.1) \times 10^4$	-	-
2	$(3.2 \pm 0.3) \times 10^4$	-3.5 ± 0.1	-3.5 ± 0.1
3	$(7.4 \pm 1.4) \times 10^4$	-3.6 ± 0.1	-3.6 ± 0.1
4	$(2.9 \pm 0.5) \times 10^5$	-3.4 ± 0.1	-3.5 ± 0.1
5	$\leq 1.1 \times 10^5$	≤ -4.4	≤ -3.7

In the previously reported host-guest systems relating **T6** and linear porphyrin oligomers, the logEM of each additional binding in **T6**/linear porphyrin oligomer is between -1.2 and -1.6.[2] The much lower EM values found with **T5** can be explained by the fact that the geometry change imposed by **T6** to a butadiyne linker (60º) is smaller than that from **T5** (72º). The butadiyne-linked porphyrin oligomer is not easy to bend, as can be seen from the EM values of the host-guest systems.

5.4.3 Estimation of Strain in T5-Bound Porphyrin Oligomers

The geometric average of the effective molarities in ***c*-P5·T5** has been introduced in **Section 4.4.3**: $(\overline{EM})_c$ = (41 ± 9) M.

Using $(\overline{EM})_l$ and $(\overline{EM})_c$, the strain energy in the curved porphyrin oligomers can be calculated from equation (5.5).

Table 5.10 Strain energy distributed to each butadiyne linker ($\Delta\Delta G$) of **T5**-bound porphyrin oligomers.

Data source	$\Delta\Delta G$ (kJ mol^{-1})	Average value (kJ mol^{-1})
P2/T5 titrations (K_{chem2})	29.1 ± 1.1	≥ 29.5
P3/T5 titrations (K_{chem3})	29.7 ± 1.1	
P4/T5 titrations (K_{chem4})	29.1 ± 1.1	
P5$_H$/T5 titrations (K_{chem5})	≥ 30.3	

It costs at least 29.5 kJ mol^{-1} to bend a linear butadiyne bond by 72º. In comparison, the energy cost to bend a linear butadiyne bond is 19.4 kJ mol^{-1} for 60º curvature (**T6**-linear/cyclic porphyrin oligomer host-guest systems;[2] in ref. 16, the value is 20.2 kJ mol^{-1}) and 7.1 kJ mol^{-1} for 45º curvature (**T8**-linear/cyclic porphyrin oligomer host-guest systems).[1] At 298 K, the Boltzmann distributions of a butadiyne-linked linear porphyrin oligomer curved by different degrees are:

$$F(45° \text{ curvature}) = e^{-\frac{\Delta\Delta G(45°)}{RT}} = 0.057 \quad (5.21)$$

$$F(60° \text{ curvature}) = e^{-\frac{\Delta\Delta G(60°)}{RT}} = 4.0 \times 10^{-4} \quad (5.22)$$

$$F(72° \text{ curvature}) = e^{-\frac{\Delta\Delta G(72°)}{RT}} = 6.8 \times 10^{-6} \quad (5.23)$$

This indicates that the butadiyne-linked linear porphyrin oligomer is shape-persistent.

In 5-porphyrin nanoring which consists of five curved butadiyne bonds, the total strain energy is around 146 kJ mol^{-1}. This can be compared to the 6- and 8-porphyrin nanorings, in which the strain energies are 116 kJ mol^{-1} and 56.5 kJ mol^{-1} respectively. This probably explains the phenomenon that ***c*-P5** is less stable than ***c*-P6**.

In comparison with cyclic supramolecules with similar sizes (diameter of ***c*-P5**: 2.15 nm, see **Section 4.2**), DFT calculation results gives the strain as 164 kJ mol^{-1} for [15]cycloparaphenylene (diameter: 2.06 nm) and 149 kJ mol^{-1} for [16]cycloparaphenylene (diameter: 2.21 nm).[17] The experimental results in this chapter indicate that the situation of strain in butadiyne-linked porphyrin nanorings is very similar to that of cycloparaphenylenes, although the series of cycloparaphenylene compounds has a much wider range of strain energy (theoretical calculation of [5]cycloparaphenylene gives the strain energy as 498 kJ mol^{-1}, diameter from X-ray diffraction: 0.67 nm).[18]

5.5 Summary

We have investigated the cooperativity in a group of strained supramolecular complexes formed by **T5** and linear porphyrin oligomers. The geometry (preorganization) of the chelation induced intramolecular strain and the partially-bound complexes could not be neglected in the equilibria. The distribution of partially-bound complexes was studied by analyzing sub-structures of ***l*-P*N*·T5** (N = 2 – 5). The effective molarities of the chelation steps between **T5** and linear porphyrin oligomers have been studied and the strain energy inside curved porphyrin oligomers has been properly estimated.

5.6 References

[1] M. Hoffmann, C. J. Wilson, B. Odell, H. L. Anderson, *Angew. Chem. Int. Ed.* **2007**, *46*, 3122–3125.

[2] H. J. Hogben, J. K. Sprafke, M. Hoffmann, M. Pawlicki, H. L. Anderson, *J. Am. Chem. Soc.* **2011**, *133*, 20962–20969.

[3] E. Chekmeneva, C. A. Hunter, M. J. Packer, S. M. Turega, *J. Am. Chem. Soc.* **2008**, *130*, 17718–17725.

[4] M. Dellarole, I. E. Sánchez, G. de Prat Gay, *Biochemistry* **2010**, *49*, 10277–10286.

[5] E. Freire, D. T. Haynie, D. Xie, *Proteins* **1993**, *17*, 111–123.

[6] J.-C. Horng, V. Moroz, D. P. Raleigh, *J. Mol. Biol.* **2003**, *326*, 1261–1270.

[7] C. A. Hunter, S. Tomas, *Chem. Biol.* **2003**, *10*, 1023–1032.

[8] C. A. Hunter, M. C. Misuraca, S. M. Turega, *J. Am. Chem. Soc.* **2011**, *133*, 20416–20425.

[9] C. A. Hunter, M. C. Misuraca, S. M. Turega, *Chem. Sci.* **2012**, *3*, 2462–2469.

[10] H. Adams, E. Chekmeneva, C. A. Hunter, M. C. Misuraca, C. Navarro, S. M. Turega, *J. Am. Chem. Soc.* **2013**, *135*, 1853−1863.

[11] H. Sun, C. A. Hunter, C. Navarro, S. Turega, *J. Am. Chem. Soc.* **2013**, *135*, 13129−13141.

[12] P. N. Taylor, H. L. Anderson, *J. Am. Chem. Soc.* **1999**, *121*, 11538–11545.

[13] P. Thordarson, *Chem. Soc. Rev.* **2011**, *40*, 1305–1323.

[14] C. A. Hunter, H. L. Anderson, *Angew. Chem. Int. Ed.* **2009**, *48*, 7488–7499.

[15] K. Hirose, *J. Incl. Phenom. Macro.* **2001**, *39*, 193–209.

[16] M. Hoffmann, J. Kärnbratt, M.-H. Chang, L. M. Herz, B. Albinsson, H. L. Anderson, *Angew. Chem. Int. Ed.* **2008**, *47*, 4993–4996.

[17] Y. Segawa, H. Omachi, K. Itami, *Org. Lett.* **2012**, *12*, 2262–2265.

[18] P. J. Evans, E. R. Darzi, R. Jasti, *Nature Chem.* **2014**, *6*, 404–408.

Chapter 6

Experimental Procedures

This chapter describes the experimental details and characterization data for the known and novel compounds synthesized in the course of completing this thesis.

6.1 General Procedures

All manipulations of air- or water-sensitive compounds were performed using standard high-vacuum techniques. When required, solvents were freeze-pump-thaw degassing cycle with backfilling of argon. The cycle was further repeated twice. Dry toluene and THF were obtained by passing the solvents through columns of alumina, under nitrogen. Diisopropylamine (DIPA) was distilled from CaH_2 and kept over activated molecular sieves (3Å, 8–12 mesh). Unless specified otherwise, all other solvents were used as commercially supplied.

l*-P2$_{t\text{-Bu}}$(THS,THS)** (the precursor of ***l*-P2$_{t\text{-Bu}}$(H,H)**) was prepared by Dr. Qianfu Luo; part of the ***l*-P1$_{t\text{-Bu}}$(H,H)** was prepared by Dr. Cécile Roche; ***l*-P1$_{\text{OOct}}$(H,H)** was prepared by Dr. Dmitry Kondratuk and Nuntaporn Kamonsutthipaijit; ***l*-P1$_{\text{THS}}$(THS,THS)** (**P1** in **Chapter 5**) was prepared by Martin Peeks; ***l*-P*N*$_{\text{THS}}$(THS,THS)** (**P*N in **Chapter 5**, $N = 2 – 4$) was prepared by Dr. Patrik Neuhaus; ***l*-P5$_{\text{THS}}$(THS,THS)** (**P5** in **Chapter 5**) was prepared by Dr. Patrik Neuhaus and Dr. Ibrahim Bulut.

Flash chromatography was carried out on silica gel 60 under positive pressure. Analytical thin-layer chromatography was carried out on aluminum-backed silica gel 60 F254 plates. Visualization was achieved using UV light, iodine dip or $KMnO_4$ dip when necessary. Size exclusion chromatography (SEC) was performed using Bio-Beads S-X1, 40–80 μm bead size (Bio Rad) and Bio-Beads S-X3, 40–80 μm bead size (Bio Rad). Semi-preparative/analytical gel-permeation chromatography (GPC) was performed on a line of JAIGEL 3H (20 × 600 mm) and JAIGEL 4H (20 × 600 mm) columns in the solvent of toluene/pyridine (100/1, *v*/*v*) and the flow rate of 3.5 mL/min. Preparative GPC was performed on a line of PLgel 10 μm 500 Å columns (25 × (600 + 300) mm) and PLgel 10 μm 1000 Å column with the flow rate of 8.5 mL/min.

All UV-vis spectra were recorded in solution using a Perkin-Lambda 20 spectrometer (1 cm path length quartz cell). All UV-vis titrations were performed in chloroform (passed through short basic alumina column to remove stabilizers) for cyclodextrin-templated porphyrin nanoring systems; all UV-vis titrations were performed in dry toluene for ferrocene-templated porphyrin nanoring systems.

Unless stated otherwise, $^{1}H/^{13}C$ NMR spectra were recorded at 298 K using Bruker AV200 (200/50 MHz), Bruker AV400 (400/100 MHz), Bruker AV500 (500/125 MHz) and Bruker AV700

(700/175 MHz) instruments. ^{1}H, ^{13}C, ^{19}F, and ^{31}P NMR spectra are reported in ppm; coupling constants are given in Hertz, to the nearest 0.1 Hz. ^{1}H and ^{13}C NMR spectra are referenced by solvent peaks; ^{31}P NMR spectra are referenced by proton NMR decoupling.

ESI mass spectra were carried out either using Fisons Platform or Micromass LCT spectrometer. MALDI-TOF mass spectra were carried out using Waters MALDI Micro MX spectrometer. The matrices for MALDI-TOF mass spectra were dithranol (1,8-dihydroxy-9,10-dihydroanthracen-9-one) or DCTB (*trans*-2-[3-(4-*tert*-butylphenyl)-2-methyl-2-propenylidene] malononitrile).

Electronic circular dichroism spectra were recorded by Prof. T. Silvu Balaban on a JASCO 815 instrument from 950 to 250/280 nm, and were measured in a quartz cuvette from Hellma with 1 mm pathlength. The spectra of the samples were recorded in toluene solution after subtraction from the baseline and were an average of two or four scans.

Molecular mechanics modelling was carried out using MM2POR parameter set optimized for porphyrins to work with MM+ (molecular mechanics) forcefields (see the Supporting Information of ref. 1 for the details of the method) in Hyperchem^{TM} 8.0.10 (Hypercube Inc.) package.

6.2 Synthetic Procedures for Known Compounds

Ethynyltrihexylsilane[2]

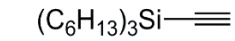

Chlorotrihexylsilane (15.2 mL, 41.6 mmol) was added by syringe under N_2 protection to a stirred solution of ethynylmagnesium bromide (0.5 M in THF, 100 mL, 50 mmol). The reaction mixture was heated at reflux for 1 h before HCl (aq) (10%, 80 mL) was added. The organic layer was washed with water (80 mL) and dried over $MgSO_4$ to give the product as yellow oil (11.65 g, 90.3%).

^{1}H NMR (400 MHz, $CDCl_3$): δ = 2.35 (s, 1H), 1.38 – 1.26 (m, 24H), 0.88 (m, 9H), 0.61 (m, 6H).

2,2'-Dipyrromethane[3]

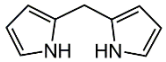

Aqueous formaldehyde (5.4 mL, 33% *w*/*w*, 60 mmol) was added into pyrrole (100 mL, 1440 mmol) and the mixture was degassed. Trifluoroacetic acid (TFA, 0.54 mL, 3.09 mmol) was added into the solution and the mixture was stirred vigorously for 5 min. DCM (100 mL) was added into the mixture and saturated Na_2CO_3 (aq, 100 mL) was immediately added to stop the reaction. The organic layer was washed with saturated Na_2CO_3 (aq, 2 × 100 mL) and water. The DCM solvent and excess pyrrole were removed under vacuum and distillation of the residue using Kugelrohr apparatus yielded the product as light yellow solid (3.42 g, 39.6%).

^{1}H NMR (400 MHz, $CDCl_3$): δ = 7.76 (br, s, 2H), 6.67 – 6.62 (m, 2H), 6.17 – 6.15 (m, 2H), 6.10 – 6.02 (m, 2H), 3.96 (s, 1H).

Zinc (II) 5,15-bis-(3,5-bis-*tert*-butylphenyl)porphyrin P1$_{Zn,t\text{-}Bu}$[4]

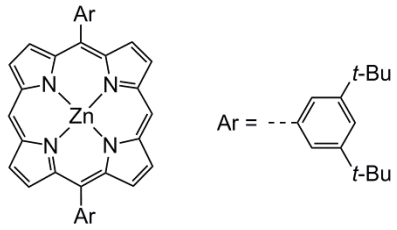

3,5-Bis(*tert*-butyl) benzaldehyde[5] (2.00 g, 9.13 mmol) and 2,2'-dipyrromethane (1.34 g, 9.13 mmol) were placed in a dry flask under N_2 and dissolved in fresh Winchester of CH_2Cl_2 (1.8 L). The solution was degassed three times by repeated evacuation and stirring under nitrogen. Trifluoroacetic acid (0.44 mL, 5.7 mmol) was added and the reaction mixture stirred in the dark for 3 h. 2,3-Dichloro-5,6-dicyano-1,4-benzoquinone (DDQ, 2.65 g, 11.8 mmol) was added and stirring continued for 0.5 h. Triethylamine (8.9 mL) was added to quench the acid formed and the DCM solvent was removed under vacuum. The residue was passed through a short silica plug using DCM and the obtained solution was again dried under vacuum and dissolved in chloroform (220 mL). $ZnCl_2 \cdot 2H_2O$ (2.26 g, 10.3 mmol) was dissolved in methanol (22 mL) and added into the chloroform solution. The mixture was stirred for 1 h and the solvents were removed under vacuum. The residue was recrystallized using DCM/MeOH to give the product as dark reddish powder (1.6 g, 48%).

^{1}H NMR (400 MHz, $CDCl_3$): δ = 10.34 (s, 2H), 9.47 (d, *J* = 4.5 Hz, 4H), 9.23 (d, *J* = 4.5 Hz, 4H), 8.18 (d, *J* = 1.8 Hz, 2H), 7.87 (t, *J* = 1.8 Hz, 2H), 1.60 (s, 36H).

Zinc(II) 5,15-bis-(3,5-bis-*tert*-butylphenyl)-10,20-dibromoporphyrin P1$_{t\text{-Bu}}$(Br,Br)[6]

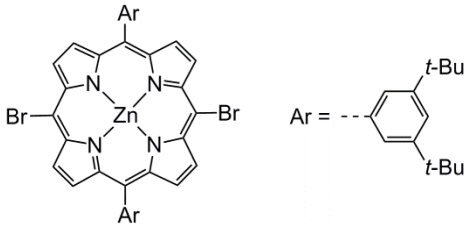

P1$_{Zn,t\text{-Bu}}$ (1.2 g, 1.6 mmol) was dissolved in chloroform (190 mL). Pyridine (0.8 mL) was added and the solution was stirred in dark at room temperature. *N*-bromosuccinimide (NBS, 0.57 g, 3.2 mmol) was dissolved in chloroform (50 mL) and added into the mixture by syringe. The reaction mixture was stirred at dark for 15 min. Acetone (1 mL) was added to stop reaction and solvents were removed under vacuum. Recrystallization of the residue using DCM/MeOH gave the product as dark reddish powder (1.1 g, 75%).

^{1}H NMR (400 MHz, $CDCl_3$/1% pyridine-d_5): δ = 9.58 (d, *J* = 4.7 Hz, 4H), 8.83 (d, *J* = 4.7 Hz, 4H), 7.90 (d, *J* = 1.8 Hz, 4H), 7.72 (t, *J* = 1.8 Hz, 2H), 1.45 (s, 36H).

Zinc (II) 5,15-bis-(3,5-bis-*tert*-butylphenyl)-10,20-bis-trihexylsilanylethynyl porphyrin *l*-P1$_{t\text{-Bu}}$(THS,THS)[7]

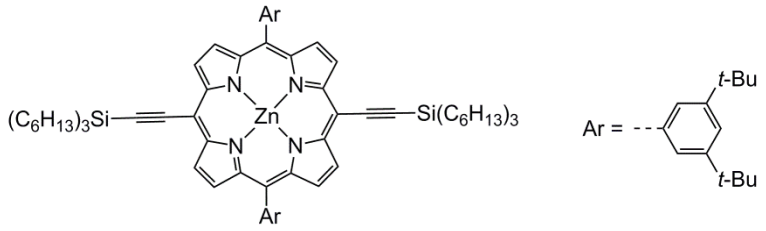

P1$_{t\text{-Bu}}$(Br,Br) (0.32 g, 0.35 mmol), tris-(dibenzylideneacetone)di-palladium(0) (32 mg, 0.035 mmol), CuI (14 mg, 0.07 mmol) and triphenylphosphine (18 mg, 0.07 mmol) were added to a dried flask under N_2 protection. Anhydrous toluene (23 mL), diisopropylamine (DIPA, 12 mL) and pyridine (0.65 mL) were added into the flask under N_2 protection and the reaction mixture was deoxygenated. Ethynyltrihexylsilane (0.38 mL, 0.99 mmol) was added into the mixture and the reaction proceeded at 50°C for 3 h and TLC analysis (petroleum ether/DCM, 2/1, *v*/*v*) showed that reaction was incomplete and ethynyltrihexylsilane (0.11 mL, 0.28 mmol) was added into the

mixture to resume the reaction. The reaction continued for another 50 min and TLC analysis showed the reaction went complete. The solvents of the reaction mixture were evaporated and the residue went through a silica plug using DCM. The solvent was evaporated and the residue was recrystallized using DCM/MeOH to give the product as spongy purple solid (0.48 g, 99%).

^{1}H NMR (400 MHz, $CDCl_3$): δ = 9.72 (d, *J* = 4.6 Hz, 4H), 8.96 (d, *J* = 4.6 Hz, 4H), 8.05 (d, *J* = 1.8 Hz, 4H), 7.82 (t, *J* = 1.8 Hz, 2H), 1.81 – 1.71 (m, 12H), 1.55 (s, 36H), 1.37 – 1.31 (m, 32H), 1.03 – 0.99 (m, 12H), 0.92 – 0.87 (m, 24H).

Zinc (II) 5,15-bis-(3,5-bis-*tert*-butylphenyl)-10,20-bis-ethynylporphyrin *l*-P1$_{t\text{-Bu}}$(H,H)[8]

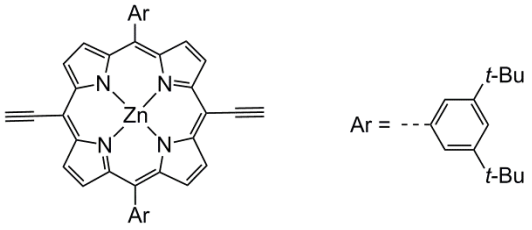

***l*-P1$_{t\text{-Bu}}$(THS,THS)** (250 mg, 0.183 mmol) was dissolved in DCM (25 mL) and Tetra-*n*-butylammonium fluoride (TBAF, 1.75 mL, 1.0 M in THF, 1.75 mmol) was added. The reaction proceeded for 15 min and TLC analysis showed that the reaction went to completion. The reaction mixture was passed immediately through a short silica plug using chloroform (1% pyridine, *v*/*v*). The obtained solution was evaporated and the residue was recrystallized using DCM/MeOH to give the product as purple powder (106 mg, 72.2%).

^{1}H NMR (400 MHz, $CDCl_3$): δ = 9.64 (d, *J* = 4.6 Hz, 4H), 8.87 (d, *J* = 4.6 Hz, 4H), 7.96 (d, *J* = 1.8 Hz, 4H), 7.75 (t, *J* = 1.8 Hz, 2H), 4.11 (s, 2H), 1.49 (s, 36H).

Zinc (II) 5,15-bis-(3,5-bis-*tert*-butylphenyl)-10,20-bis-ethynylporphyrin dimer *l*-P2$_{t\text{-Bu}}$(H,H)[8]

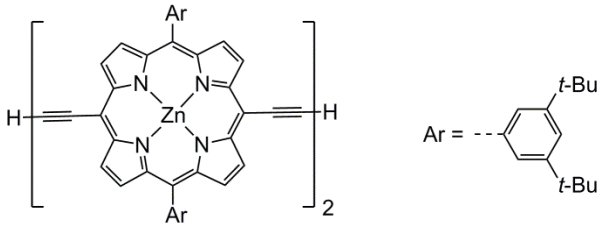

***l*-P2$_{t\text{-Bu}}$(THS,THS)** (100 mg, 0.046 mmol) was dissolved in DCM (25 mL) and TBAF (0.5 mL, 1 M in THF, 0.5 mmol) was added. The reaction proceeded for 15 min and TLC analysis showed that the reaction went to completion. The reaction mixture was passed immediately through a short

silica plug using chloroform (1% pyridine, *v*/*v*). The obtained solution was evaporated and the residue was recrystallized using DCM/MeOH to give the product as purple powder (75 mg, 98%).

^{1}H NMR (200 MHz, $CDCl_3$): δ = 9.84 (d, *J* = 4.6 Hz, 4H), 9.60 (d, *J* = 4.6 Hz, 4H), 8.92 (d, *J* = 4.6 Hz, 4H), 8.84 (d, *J* = 4.6 Hz, 4H), 7.96 (d, *J* = 1.8 Hz, 8H), 7.73 (t, *J* = 1.7 Hz, 4H), 4.11 (s, 2H), 1.46 (s, 72H).

Zinc(II) 5,15-bis-(3,5-bis-octyloxy-phenyl)-porphyrin P1$_{Zn,OOct}$[4]

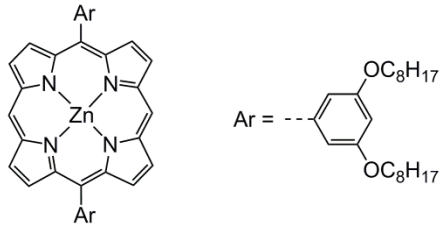

2,2'-Dipyrromethane (2.00 g, 13.7 mmol) and 3,5-bis(octyloxy)benzaldehyde[9,10] (5.00 g, 13.7 mmol) were dissolved in DCM (2.20 L, from unopened winchesters). The system was degassed under vacuum and saturated with N_2 and the degas-saturation procedure was repeated for 3 times. Trifluoroacetic acid (TFA, 0.66 mL) was added and the system was stirred under dark at room temperature for 3 h. DDQ (4.4 g, 19 mmol) was added and the mixture was stirred under dark at room temperature for 40 min. Triethylamine (TEA, 10 mL) was added to stop the oxidation and the mixture was stirred for another 20 min. The solvent was evaporated and the residue was passed through a short silica column using CH_2Cl_2. The resulting mixture was dried and dissolved in a mixed solvent of DCM (400 mL) and methanol (50 mL) containing $Zn(OAc)_2 \cdot 2H_2O$ (2.5 g, 18 mmol). The mixture was stirred for 1 h and the solvent was evaporated. The mixture was passed through silica plug with DCM as the eluent to give the product as red oily solid (3.4 g, 48%).

^{1}H NMR (400 MHz, $CDCl_3$): δ = 10.33 (s, 2H), 9.44 (d, 4H, *J* = 4.4 Hz), 9.27 (d, 4H, *J* = 4.4 Hz), 7.44 (d, 4H, *J* = 2.4 Hz), 6.93 (t, 2H, *J* = 2.4 Hz), 4.16 (t, 8H, *J* = 6.5 Hz), 1.92 – 1.86 (m, 8H), 1.55 – 1.32 (m, 40H), 0.87 (t, 12H, *J* = 6.5 Hz).

Zinc(II) 5,15-bis-(3,5-bis-octyloxy-phenyl)-10,20-dibromoporphyrin $P1_{OOct}$(Br,Br)[6]

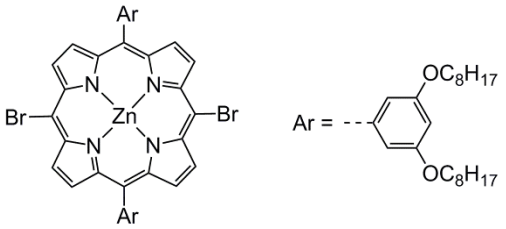

$P1_{Zn,OOct}$ (3.38 g, 3.25 mmol) was dissolved in chloroform (180 mL). Pyridine (1.5 mL) was added and the mixture was stirred under dark. NBS (1.16 g, 6.51 mmol) was dissolved in chloroform (100 mL) and added into the solution. The mixture was stirred under dark at room temperature for 15 min. Acetone (1 mL) was added to stop the reaction. The solvent was evaporated and the residue was precipitated using chloroform/methanol to give the product as red solid (3.84 g, 98%).

^{1}H NMR (400 MHz, $CDCl_3$): δ = 9.65 (d, 4H, *J* = 4.4 Hz), 8.99 (d, 4H, *J* = 4.4 Hz), 7.31 (d, 4H, *J* = 2.1 Hz), 6.89 (t, 2H, *J* = 2.1 Hz), 4.14 (t, 8H, *J* = 6.5 Hz), 1.92 – 1.86 (m, 8H), 1.55 – 1.29 (m, 40H), 0.89 (t, 12H, *J* = 6.6 Hz).

Zinc(II) 5,15-bis-(3,5-bis-octyloxy-phenyl)-10,20-bis-trihexylsilylethynylporphyrin *l*-$P1_{OOct}$(THS,THS)[7]

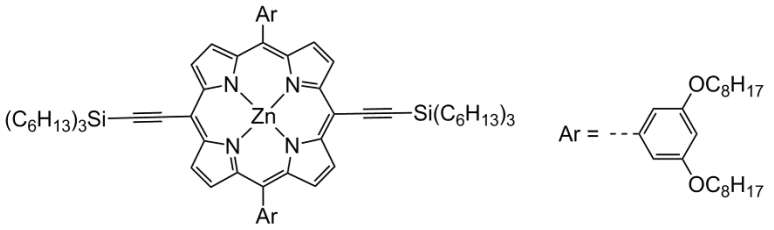

$P1_{OOct}$(Br,Br) (1.9 g, 1.6 mmol), tris-(dibenzylidene-acetone) di-palladium(0) (145 mg, 0.16 mmol), CuI (61 mg, 0.32 mmol), triphenylphosphine (84 mg, 0.32 mmol) were added to a dried flask under N_2 protection. Anhydrous toluene (80 mL) and DIPA (40 mL) were added into the flask under N_2 protection and the reaction mixture was deoxygenated using freeze-pump-thaw method. Ethynyltrihexylsilane (1.80 mL, 4.64 mmol) was added into the mixture and the reaction proceeded at 50°C for 2.5 h and TLC analysis (petroleum ether/EtOAc/pyridine, 10/1/1, *v*/*v*/*v*) showed that reaction went complete. The solvents of the reaction mixture were removed under vacuum and the residue went through a short silica plug using DCM. The obtained solution was evaporated and the residue was precipitated using DCM/MeOH to give the product as purple solid (2.60 g, 99%).

^{1}H NMR (400 MHz, $CDCl_3$): δ = 9.63 (d, 4H, *J* = 4.4 Hz), 8.96 (d, 4H, *J* = 4.4 Hz), 7.34 (d, 4H, *J* = 2.1 Hz), 6.89 (t, 2H, *J* = 2.1 Hz), 4.14 (t, 8H, *J* = 6.6 Hz), 1.92 – 1.73 (m, 20H), 1.58 – 1.28 (m, 78H), 1.04 – 0.86 (m, 40H).

Zinc(II) 5,15-bis-(3,5-bis-octyloxy-phenyl)-10-ethynyl-20-trihexylsilylethynylporphyrin *l*-P1$_{OOct}$(THS,H)[11]

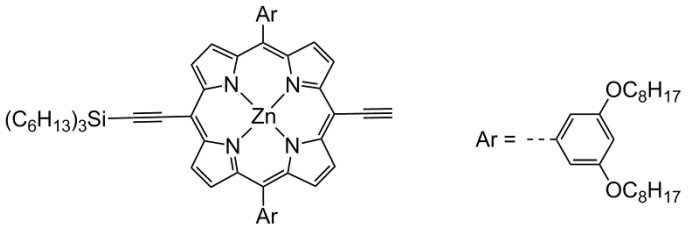

***l*-P1$_{OOct}$(THS,THS)** (1.65 g, 0.10 mmol) was dissolved in a mixed solvent of chloroform (35 mL) and DCM (35 mL). TBAF (1.0 M in THF, 0.75 mL, 0.75 mmol) was added and the mixture was stirred at room temperature. The reaction was monitored by TLC analysis (petroleum ether/EtOAc/pyridine, 10/1/1, *v*/*v*/*v*). At the time when the densities of ***l*-P1$_{OOct}$(THS,H)** and ***l*-P1$_{OOct}$(THS,THS)** reached approximately the same, the reaction was terminated by plugging the mixture through a short silica plug with DCM. The solvent was evaporated and the mixture was separated by column chromatography (silica, petroleum ether/EtOAc/pyridine, 100/10/5, *v*/*v*/*v*) to give the recovered starting material (658 mg, 40%) and ***l*-P1$_{OOct}$(THS,H)** as purple solid (413 mg, 34%).

^{1}H NMR (400 MHz, $CDCl_3$): δ = 9.64 – 9.63 (m, 4H), 8.98 – 8.95 (m, 4H), 7.33 (d, 4H, *J* = 2.2 Hz), 6.89 (t, 2H, *J* = 2.2 Hz), 4.14 (s, 1H), 4.14 (t, 8H, *J* = 6.5 Hz), 1.92 – 1.73 (m, 14H), 1.58 – 1.25 (m, 58H), 1.04 – 0.86 (m, 27H).

Zinc(II) 5,15-bis-(3,5-bis-octyloxy-phenyl)-10,20-bis-trihexylsilylethynylporphyrin dimer *l*-P2$_{OOct}$(THS,THS)[12]

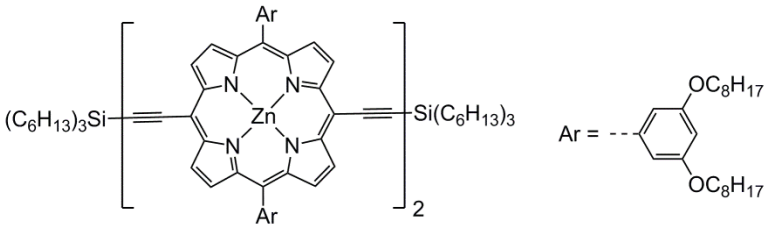

***l*-P1$_{OOct}$(THS,H)** (413 mg, 0.30 mmol), $Pd(PPh_3)_2Cl_2$ (15 mg, 0.021 mmol), CuI (29 mg, 0.15 mmol) and 1,4-benzoquinone (65 mg, 0.60 mmol) was added to a dried flask and dissolved with dry toluene (21 mL) and DIPA (5.5 mL). The mixture was stirred at room temperature under air overnight. The mixture was plugged through a short silica column using DCM and the solvent was evaporated. The residue was separated by size-exclusion column (Biobeads SX-1) using toluene as eluent to give the product as dark purple solid (351 mg, 85%).

^{1}H NMR (200 MHz, $CDCl_3$): δ = 9.97 (d, 4H, *J* = 4.4 Hz), 9.72 (d, 4H, *J* = 4.4 Hz), 9.17 (d, 4H, *J* = 4.4 Hz), 9.05 (d, 4H, *J* = 4.4 Hz), 7.38 (d, 8H, *J* = 2.1 Hz), 6.90 (t, 4H, *J* = 2.1 Hz), 4.15 (t, 16H, *J* = 6.4 Hz), 1.96 – 1.72 (m, 28H), 1.56 – 1.28 (m, 116H), 1.08 – 0.84 (m, 54H).

Zinc(II) 5,15-bis-(3,5-bis-octyloxy-phenyl)-10-ethynyl-20-trihexylsilylethynylporphyrin dimer *l*-P2$_{OOct}$(THS,H)[11]

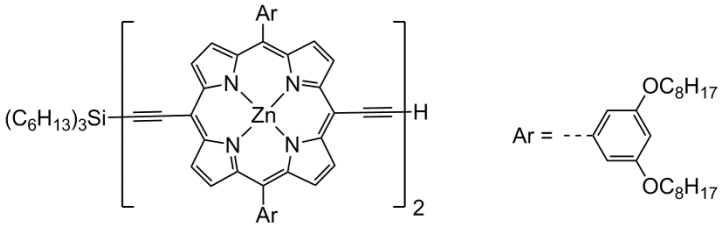

***l*-P2$_{OOct}$(THS,THS)** (0.77 g, 0.28 mmol) was dissolved in DCM (30 mL) and chloroform (30 mL). TBAF (1.0 M in THF, 0.30 mL, 0.30 mmol) was added and the mixture was stirred at room temperature. The reaction was carefully monitored by TLC analysis (petroleum ether/EtOAc/pyridine, 10/1/1, *v*/*v*/*v*). The reaction was terminated by passing the mixture through a short silica plug (chloroform/pyridine, 100/1, *v*/*v*) when TLC analysis showed the existence of double-deprotected product ***l*-P2$_{OOct}$(H,H)**. The solvent was evaporated and the mixture was separated by column chromatography (silica, petroleum ether/EtOAc/pyridine, 15/1/1 gradually

increasing the polarity to 10/1/1, *v*/*v*/*v*) to give the recovered starting material (0.46 g, 60%) and ***l*-P2$_{OOct}$(THS,H)** as brown solid (0.25 g, 33%).

^{1}H NMR (400 MHz, $CDCl_3$): δ = 9.88 – 9.86 (m, 4H), 9.66 – 9.63 (m, 4H), 9.08 – 9.06 (m, 4H), 9.00 – 8.96 (m, 4H), 7.37 (d, 8H, *J* = 2.5 Hz), 6.90 (s, 4H), 4.17 – 4.14 (m, 17H), 1.92 – 0.85 (m, 159H).

Zinc(II) 5,15-bis-(3,5-bis-octyloxy-phenyl)-10,20-bis-ethynylporphyrin dimer

***l*-P2$_{OOct}$(H,H)**[8]

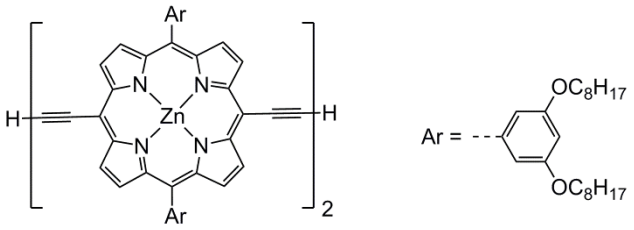

***l*-P2$_{OOct}$(THS,THS)** (110 mg, 0.040 mmol) was dissolved in DCM (30 mL). TBAF (1.0 M in THF, 0.40 mL, 0.40 mmol) was added and the mixture was stirred at room temperature for over 15 min. TLC analysis (petroleum ether/EtOAc/pyridine, 10/1/1, *v*/*v*/*v*) showed the reaction to be complete. The mixture was passed through a short silica plug (chloroform/pyridine, 10/1, *v*/*v*) and the solvent was evaporated. The residue was precipitated using DCM/methanol to give the product as dark purple solid (72 mg, 83%).

^{1}H NMR (400 MHz, $CDCl_3$): δ = 9.89 (d, 4H, *J* = 4.4 Hz), 9.66 (d, 4H, *J* = 4.4 Hz), 9.07 (d, 4H, *J* = 4.4 Hz), 8.99 (d, 4H, *J* = 4.4 Hz), 7.37 (d, 8H, *J* = 2.1 Hz), 6.91 (t, 4H, *J* = 2.1 Hz), 4.18 (s, 2H), 4.17 (t, 16H, *J* = 6.5 Hz), 1.93 – 1.86 (m, 16H), 1.43 – 1.29 (m, 80H), 0.91 – 0.85 (m, 24H).

Zinc(II) 5,15-bis-(3,5-bis-octyloxy-phenyl)-10,20-bis-trihexylsilylethynylporphyrin tetramer

***l*-P4$_{OOct}$(THS,THS)**[12]

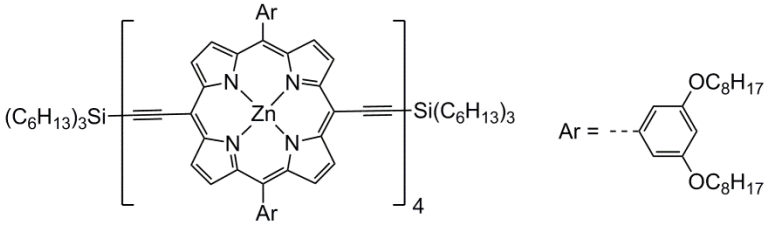

***l*-P2$_{OOct}$(THS,H)** (0.34 g, 0.14 mmol) was dissolved in chloroform (30 mL), pyridine (1 mL) and DIPA (5 mL). $Pd(PPh_3)_2Cl_2$ (60 mg, 0.084 mmol), CuI (90 mg, 0.61 mmol) and 1,4-benzoquinone

(96 mg, 0.90 mmol) were added into the mixture and the reaction was stirred at room temperature at dark under air overnight. The mixture was plugged through a short silica column (chloroform/ pyridine, 100/1, *v*/*v*) and the solvent was evaporated. The residue was separated by size-exclusion column (Biobeads SX-1) using toluene as eluent to give the product as dark brown solid (0.29 mg, 88%).

^{1}H NMR (400 MHz, $CDCl_3$): δ = 9.90 – 9.88 (m, 12H), 9.65 (d, 4H, *J* = 4.5 Hz), 9.09 – 9.07 (m, 12H), 8.97 (d, 4H, *J* = 4.5 Hz), 7.42 (d, 8H, *J* = 2.5 Hz), 7.38 (d, 8H, *J* = 2.5 Hz), 6.93 – 6.91 (m, 8H), 4.21 – 4.15 (m, 32H), 1.93 – 1.00 (m, 318H); MALDI-TOF MS+: m/z 4891 ($[M]^+$, $C_{308}H_{406}N_{16}O_{16}Zn_4Si_2$ requires: 4906).

Zinc(II) 5,15-bis-(3,5-bis-octyloxy-phenyl)-10-ethynyl-20-trihexylsilylethynylporphyrin tetramer

***l*-P4$_{OOct}$(THS,H)**[11]

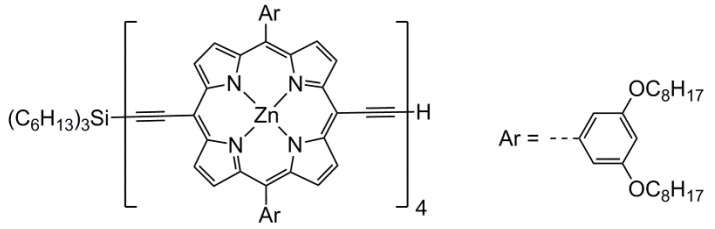

***l*-P4$_{OOct}$(THS,THS)** (0.29 g, 0.059 mmol) was dissolved in a mixture of DCM (10 mL), chloroform (10 mL) and pyridine (0.5 mL). TBAF (1.0 M in THF, 0.10 mL, 0.10 mmol) was added and the mixture was stirred at room temperature. The reaction was monitored by TLC analysis (petroleum ether/pyridine/DCM, 85/15/2, *v*/*v*/*v*). The reaction was terminated by passing the mixture through a short silica plug (chloroform/pyridine, 100/1, *v*/*v*) when TLC analysis showed the existence of double-deprotected ***l*-P4$_{OOct}$(H,H)**. The solvent was evaporated and the mixture was separated by column chromatography (silica, petroleum ether/EtOAc/pyridine, 25/1/1 gradually increasing the polarity to 15/1/1, *v*/*v*/*v*) to give the recovered starting material (0.17 g, 59%) and ***l*-P4$_{OOct}$(THS,H)** as dark brown solid (95 mg, 34%).

^{1}H NMR (400 MHz, $CDCl_3$): δ = 9.88 – 9.86 (m, 12H), 9.68 – 9.64 (m, 4H), 9.09 – 9.07 (m, 12H), 9.00 – 8.96 (m, 4H), 7.42 (d, 4H, *J* = 4.5 Hz), 7.38 (d, 4H, *J* = 4.5 Hz), 6.93 – 6.91 (m, 8H), 4.21 – 4.15 (m, 32H), 1.93 – 0.85 (m, 279H); MALDI-TOF MS+: m/z 4620 ($[M]^+$, $C_{290}H_{368}N_{16}O_{16}Zn_4Si$ requires: 4624).

Zinc(II) 5,15-bis-(3,5-bis-octyloxy-phenyl)-10,20-bis-ethynylporphyrin tetramer *l*-P4$_{OOct}$(H,H)[8]

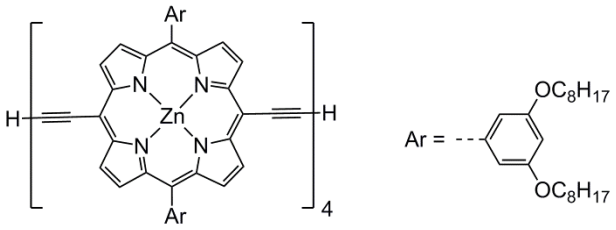

***l*-P4$_{OOct}$(THS,THS)** (60 mg, 0.012 mmol) was dissolved DCM (10 mL) and pyridine (0.5 mL). TBAF (1.0 M in THF, 0.20 mL, 0.20 mmol) was added and the mixture was stirred at room temperature for 15 min. TLC analysis (petroleum ether/pyridine/DCM, 85/15/2, *v*/*v*/*v*) indicated the completion of the reaction and the mixture was passed through a short silica plug (chloroform/pyridine, 100/1, *v*/*v*). The solvent was evaporated and the residue was precipitated using DCM/methanol as the solvent. ***l*-P4$_{OOct}$(H,H)** was obtained as black powder (49 mg, 93%).

^{1}H NMR (400 MHz, $CDCl_3$): δ = 9.90 – 9.88 (m, 12H), 9.66 (d, 4H, *J* = 4.5 Hz), 9.09 – 9.07 (m, 12H), 9.00 (d, 4H, *J* = 4.5 Hz), 7.42 – 7.37 (m, 16H), 6.93 – 6.91 (m, 8H), 4.21 – 4.15 (m, 34H), 1.92 – 0.87 (m, 240H); MALDI-TOF MS+: m/z 4338 ($[M]^+$, $C_{272}H_{330}N_{16}O_{16}Zn_4$ requires: 4342).

Zinc(II) 5,15-bis-(3,5-bis-octyloxy-phenyl)-10,20-bis-trihexylsilylethynylporphyrin octamer *l*-P8$_{OOct}$(THS,THS)[12]

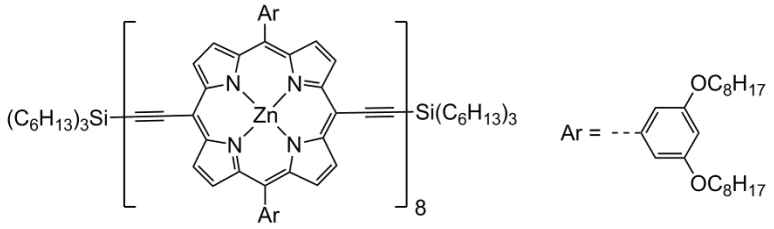

***l*-P4$_{OOct}$(THS,H)** (95 mg, 0.020 mmol) was dissolved in a mixture of chloroform (15 mL), pyridine (1 mL) and DIPA (3 mL). $Pd(PPh_3)_2Cl_2$ (10 mg, 0.014 mmol), CuI (15 mg, 0.10 mmol) and 1,4-benzoquinone (16 mg, 0.15 mmol) were added into the mixture and the reaction was stirred at room temperature at dark under air overnight. The mixture was plugged through a short silica column (chloroform/pyridine, 100/1, *v*/*v*) and the solvent was evaporated. The mixture was separated using preparative GPC (toluene/pyridine, 9/1, *v*/*v*) to give ***l*-P8$_{OOct}$(THS,THS)** as dark brown solid (88 mg, 93%).

^{1}H NMR (400 MHz, $CDCl_3$): δ = 9.90 – 9.87 (m, 28H), 9.65 – 9.64 (m, 4H), 9.10 – 9.07 (m, 28H), 8.97 – 8.96 (m, 4H), 7.43 – 7.38 (m, 32H), 6.94 – 6.91 (m, 16H), 4.20 (s, 64H), 1.44 – 0.86 (m, 558H); MALDI-TOF MS+: m/z 9237 ($[M]^+$, $C_{580}H_{734}N_{32}O_{32}Si_2Zn_8$ requires: 9246).

Zinc(II) 5,15-bis-(3,5-bis-octyloxy-phenyl)-10,20-bis-ethynylporphyrin octamer *l*-P8$_{OOct}$(H,H)[8]

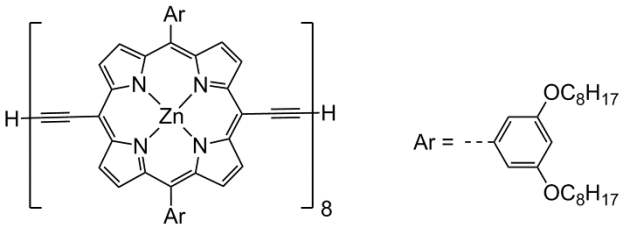

***l*-P8$_{OOct}$(THS,THS)** (32 mg, 3.5 µmol) was dissolved in a mixture of DCM (5.0 mL) and pyridine (0.050 mL). TBAF (1.0 M in THF, 0.050 mL, 50 µmol) was added and the mixture was stirred at room temperature for 15 min. Methanol (5.0 mL) was added to quench the reaction and the product precipitated after stirring for another 5 min. The product was filtered and washed with methanol. ***l*-P8$_{OOct}$(H,H)** was obtained as black powder (23 mg, 77%).

^{1}H NMR (400 MHz, $CDCl_3$): δ = 9.90 – 9.88 (m, 28H), 9.66 (d, 4H, *J* = 4.5 Hz), 9.09 – 9.07 (m, 28H), 8.99 (d, 4H, *J* = 4.5 Hz), 7.43 – 7.38 (m, 32H), 6.94 – 6.91 (m, 16H), 4.21 – 4.15 (m, 66H), 1.94 – 0.86 (m, 480H); MALDI-TOF MS+: m/z 8674 ($[M]^+$, $C_{544}H_{658}N_{32}O_{32}Zn_8$ requires: 8680).

Hexakis(6-*O*-*tert*-butyldimethylsilyl)-α-cyclodextrin[13]

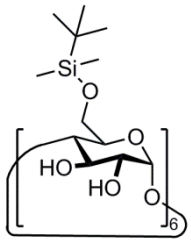

α-Cyclodextrin (5.0 g, 5.15 mmol) was dried in a flask under vacuum at 100°C for over 2 h. The flask was cooled to room temperature and put under N_2 protection. Imidazole (4.55 g, 68 mmol) was added into the flask under N_2 protection. 130 mL anhydrous *N*,*N*-dimethylformamide (DMF) was added by syringe. *tert*-Butyldimethylsilyl chloride (5.2 g, 33.8 mmol) was dissolved in anhydrous DMF (25 mL) and was added by syringe. The reaction proceeded for 2.5 h and the mixture was poured into ice-water (1.5 L). The precipitate was filtered and washed with water. The

filter cake was dissolved in dichloromethane (DCM) and washed successively with water, cold HCl (aq, 500 mL, 0.4% *w*/*w*), $NaHCO_3$ (aq) and water. The solvent was removed and the residue was dried under vacuum at 60°C for 1 h, titurated with hexane (30 mL) to remove impurities and redissolved in DCM. Final evaporation of the solvents gave the product as white solid (6.35 g, 74%).

^{1}H NMR (400 MHz, $CDCl_3$): δ = 6.52 (s, 1H), 5.26 (s, 1H), 4.88 (d, *J* = 3.1 Hz, 1H), 4.01 (t, *J* = 9.0 Hz, 1H), 3.92 (dd, *J* = 11.3 Hz, 3.4 Hz, 1H), 3.86 (d, *J* = 9.9 Hz, 1H), 3.75 (d, *J* = 10.6 Hz, 1H), 3.65 (dd, *J* = 9.6 Hz, 3.2 Hz, 1H), 3.57 (t, *J* = 9.0 Hz, 1H), 0.88 (s, 9H), 0.04 (d, *J* = 2.7 Hz, 6H); ^{13}C NMR (100 MHz, $CDCl_3$): δ = 101.27, 81.28, 74.34, 72.92, 72.07, 61.84, 25.87, 18.32, -5.29.

Hexakis(6-*O*-*tert*-butyldimethylsilyl-2,3-di-*O*-methyl)-α-cyclodextrin[13]

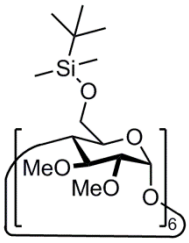

Hexakis(6-*O*-*tert*-butyldimethylsilyl)-α-cyclodextrin (3.11 g, 1.87 mmol) was dried in a flask under vacuum at 50°C for over 1 h. The flask was cooled to room temperature and was put under N_2 protection. Sodium hydride (60% in oil, 3.24 g, 80.4 mmol) was added and the flask was evacuated to vacuum and saturated with N_2. The flask was put under ice-water bath and 90 mL anhydrous DMF was added by syringe. The mixture was stirred at 0°C for 1 h. Methyl iodide (5.6 mL, 91.8 mmol) was added by syringe and the mixture was stirred at 0°C for 1 h, allowed to attain room temperature, and stirred at room temperature overnight. The mixture was cooled to 0°C and methanol (5 mL) was added to quench the excess sodium hydride. The mixture was concentrated and partitioned by DCM and water. The organic phase was washed successively with water, sodium thiosulfate (aq), water, and was dried and concentrated. Column chromatography (DCM/MeOH, 5/1, *v*/*v*) of the residue gave the product as transparent solid (2.73 g, 79.9%).

^{1}H NMR (400 MHz, $CDCl_3$): δ = 5.04 (d, *J* = 3.1 Hz, 1H), 4.08 (d, *J* = 9.0 Hz, 1H), 3.73 – 3.67 (m, 2H), 3.66 (s, 3H), 3.63 – 3.55 (m, 2H), 3.50 (s, 3H), 3.06 (dd, *J* = 9.8 Hz, 3.1 Hz, 1H), 0.87 (s, 9H), 0.03 (d, *J* = 3.9 Hz, 6H); ^{13}C NMR (100 MHz, $CDCl_3$): δ = 99.39, 82.32, 81.34, 81.07, 72.48, 62.22, 61.74, 57.87, 25.86, 18.19, -4.96, -5.19; MALDI-TOF MS+: m/z 1848.42 ($[M+Na]^+$,

$C_{84}H_{168}O_{30}Si_6Na$ requires: 1849.02).

Per-2,3-di-*O*-methyl-α-cyclodextrin[14]

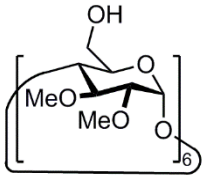

Hexakis(6-*O*-*tert*-butyldimethylsilyl-2,3-di-*O*-methyl)-α-cyclodextrin (4.2 g, 2.30 mmol) was dried in a flask under vacuum at 50°C for over 1 h. The flask was cooled to room temperature and put under N_2 protection. Anhydrous THF (110 mL) was added by syringe. TBAF (15 mL, 1.0 M in THF, 15 mmol) was added by syringe and the reaction mixture was stirred at room temperature under N_2 protection overnight. The reaction mixture was concentrated and dissolved in 200 mL water. Hexane (80 mL × 2) was used to wash the water solution. The aqueous solution of the mixture was separated using Amberjet 1200(H) cation exchange resin and was collected over potassium carbonate (360 mg). The water was removed from the solution and the residue was redissolved in DCM. The solution was filtered by cotton, concentrated and dried under vacuum to give the product as light yellowish solid (2.06 g, 80.0%).

^{1}H NMR (400 MHz, D_2O): δ = 5.08 (d, *J* = 3.4 Hz, 1H), 3.83 – 3.60 (m, 3H), 3.56 – 3.49 (m, 2H), 3.46 (s, 3H), 3.34 (s, 3H), 3.17 (dd, *J* = 9.6 Hz, 3.5 Hz, 1H); ^{13}C NMR (100 MHz, D_2O): δ = 100.27, 83.38, 82.55, 81.68, 74.40, 63.20, 62.55, 60.21; MALDI-TOF MS+: m/z 1180.29 ($[M+K]^+$, $C_{48}H_{84}O_{30}K$ requires: 1180.48).

Heptakis(6-*O*-*tert*-butyldimethylsilyl)-β-cyclodextrin[13]

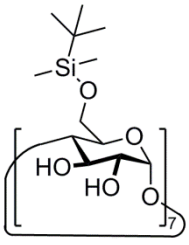

β-Cyclodextrin (3.0 g, 2.64 mmol) was dried in a flask under vacuum at 100°C for over 2 h. The flask was cooled to room temperature and put under N_2 protection. Imidazole (2.73 g, 40.2 mmol) was added into the flask under N_2 protection. Anhydrous DMF (75 mL) was added by syringe. *tert*-

Butyldimethylsilyl chloride (3.03 g, 20.1 mmol) was dissolved in anhydrous DMF (20 mL) and was added by syringe. The reaction proceeded for 130 min and the mixture was poured into ice-water (1 L). The precipitate was filtered and washed with water. The filter cake was dissolved in DCM and washed successively with water, cold HCl (aq, 300 mL, 0.4% *w*/*w*), $NaHCO_3$ (aq) and water. The solvent was removed and the residue was dried under vacuum overnight to give the product as white solid (4.6 g, 89%).

^{1}H NMR (400 MHz, $CDCl_3$): δ = 6.73 (s, 7H), 5.28 (s, 7H), 4.89 (d, *J* = 3.4 Hz, 7H), 4.04 (t, *J* = 9.1 Hz, 7H), 3.90 (dd, *J* = 11.2, 2.8 Hz, 7H), 3.76 – 3.50 (m, 28H), 0.87 (s, 63H), 0.04 (d, *J* = 4.2 Hz, 42H); ^{13}C NMR (100 MHz, $CDCl_3$): δ = 101.99, 81.73, 73.57, 73.38, 72.50, 25.88, 18.25, -5.09, -5.21.

Heptakis(6-*O*-*tert*-butyldimethylsilyl-2,3-di-*O*-methyl)-β-cyclodextrin[13]

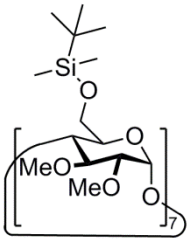

Heptakis(6-*O*-*tert*-butyldimethylsilyl)-β-cyclodextrin (4.6 g, 2.4 mmol) was dried in a flask under vacuum at 80°C for over 3 h. The flask was cooled to room temperature and put under N_2 protection. Sodium hydride (60% in oil, 4.7 g, 0.12 mol) was added and the flask was evacuated to vacuum and saturated with N_2. The flask was put under ice-water bath and anhydrous DMF (135 mL) was added by syringe. The mixture was stirred at 0°C for 1 h. Methyl iodide (8.1 mL, 0.13 mol) was added by syringe and the mixture was stirred at 0°C for 1 h, allowed to attain room temperature, and stirred at room temperature for another 2 h. The mixture was cooled to 0°C and methanol (5 mL) was added to quench the excess sodium hydride. The mixture was concentrated and partitioned by DCM and water. The organic phase was washed with water and dried. Column chromatography (DCM/MeOH, 5/1, *v*/*v*) of the residue gave the product as transparent solid (4.0 g, 78%).

^{1}H NMR (400 MHz, $CDCl_3$): δ = 5.20 (d, *J* = 3.5 Hz, 7H), 4.12 (dd, *J* = 11.5, 2.4 Hz, 7H), 3.68 (s, 21H), 3.52 (s, 21H), 3.73 – 3.54 (m, 28H), 3.07 (dd, *J* = 9.8, 3.5 Hz, 7H), 0.90 (s, 63H), 0.02 (s, 42H); ^{13}C NMR (100 MHz, $CDCl_3$): δ = 98.05, 82.14, 81.98, 78.63, 72.12, 62.27, 61.51, 58.62,

25.89, 18.28, -4.87, -5.22; MALDI-TOF MS+: m/z 2153.09 ($[M+Na]^+$, $C_{98}H_{196}O_{35}Si_7Na$ requires: 2153.19).

Per-2,3-di-*O*-methyl-β-cyclodextrin[14]

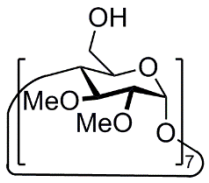

Heptakis(6-*O*-*tert*-butyldimethylsilyl-2,3-di-*O*-methyl)-β-cyclodextrin (3.9 g, 1.8 mmol) was dried in a flask under vacuum at 80°C for over 2 h. The flask was cooled to room temperature and put under N_2 protection. Anhydrous THF (100 mL) was added by syringe. TBAF (22 mL, 1 M in THF, 22 mmol) was added by syringe and the reaction mixture was stirred at room temperature under N_2 protection overnight. The reaction mixture was concentrated and dissolved in water (150 mL). Hexane (80 mL × 3) was used to wash the water solution. The aqueous solution of the mixture was separated using Amberjet 1200(H) cation exchange resin and was collected over potassium carbonate (620 mg). The water was removed from the solution and the residue was redissolved in DCM. The solution was filtered by cotton, concentrated and dried under vacuum to give the product as light yellowish solid (2.24 g, 92%).

^{1}H NMR (400 MHz, D_2O): δ = 5.19 (d, *J* = 3.6 Hz, 7H), 3.82 – 3.72 (m, 21H), 3.66 – 3.57 (m, 14H), 3.50 (s, 21H), 3.41 (s, 21H), 3.27 (dd, *J* = 9.3, 3.5 Hz, 7H); ^{13}C NMR (100 MHz, D_2O): δ = 97.42, 81.26, 80.33, 77.30, 71.91, 60.82, 60.08, 58.38; MALDI-TOF MS+: m/z 1369.72 ($[M+K]^+$, $C_{56}H_{98}O_{35}K$ requires: 1369.55), 1355.72 ($[M+Na]^+$, $C_{56}H_{98}O_{35}Na$ requires: 1353.59).

***trans*-3-(4-Pyridyl) acrylic acid**[15]

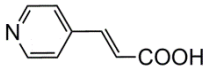

Malonic acid (10.4 g, 100 mmol) and 4-pyridyl aldehyde (9.4 mL, 100 mmol) were added into 100 mL flask. Pyridine (8.5 mL) and piperidine (0.2 mL) were added and the mixture was placed under oil bath at 100°C for 2 h. The mixture was cooled and water was added to dissolve impurities. The mixture was filtered and washed with water (1 L). The solid was dried under vacuum to give the product as pale white solid (9.4 g, 63%).

^{1}H NMR (400 MHz, DMSO-d_6) δ = 12.74 (s, 1H), 8.62 (d, *J* = 4.0 Hz, 2H), 7.67 (d, *J* = 4.0 Hz, 2H), 7.57 (d, *J* = 16 Hz, 1H), 6.79 (d, *J* = 16 Hz, 1H).

4-Pyridyl propanic acid

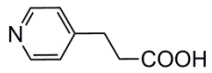

trans-3-(4-Pyridyl) acrylic acid (6.0 g, 40 mmol) and palladium on activated charcoal (0.5 g, 10% *w*/*w* Pd) were mixed in a round bottom flask (3 L) with THF (400 mL) and methanol (360 mL). The mixture was degassed under vacuum and saturated with nitrogen. The degas procedure was repeated twice and the mixture under vacuum was finally saturated with hydrogen contained in a balloon. The mixture was stirred vigorously under hydrogen for 3 h and the atmosphere of the system was substituted with nitrogen. The mixture was filtered with celite and the solvent was evaporated to give the product as white solid (3.7 g, 60%).

^{1}H NMR (400 MHz, DMSO-d_6) δ = 8.47 (d, *J* = 12 Hz, 2H), 7.28 (d, *J* = 12 Hz, 2H), 2.85 (t, *J* = 15 Hz, 2H), 2.60 (t, *J* = 15 Hz, 2H).

Isonicotinic acid pentafluorophenyl ester[16]

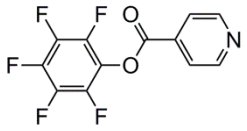

Isonicotinic acid (1.2 g, 10 mmol) and pentafluorophenol (2.0 g, 11 mmol) were dissolved in dioxane (30 mL). 1,3-Dicyclohexylcarbodiimide (DCC) (2.3 g, 11 mmol) was added to start the reaction. The mixture was stirred for 1 h at room temperature. The dicyclohexylurea formed was filtered and the solvent was evaporated under vacuum. The residue was purified by crystallisation from hexane to give the product as white solid (1.8 g, 61%).

^{1}H NMR (400 MHz, $CDCl_3$): δ = 8.92 (dd, *J* = 4.4 Hz, 1.6 Hz, 2H), 8.02 (dd, *J* = 4.4 Hz, 1.6 Hz, 2H); ^{19}F NMR (377 MHz, $CDCl_3$): δ = -152.14 (d, *J* = 17.1 Hz, 2F), -156.50 (t, *J* = 21.8 Hz, 1F), -161.43 (t, 17.1 Hz, 2F).

Nicotinic acid pentafluorophenyl ester[16]

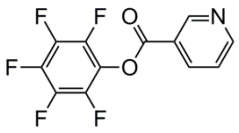

Nicotinic acid (1.2 g, 10 mmol) and pentafluorophenol (2.0 g, 11 mmol) were dissolved in dioxane (30 mL). DCC (2.3 g, 11 mmol) was added to start the reaction. The mixture was stirred for 1 h at room temperature. The dicyclohexylurea formed was filtered and the solvent was evaporated under vacuum. The residue was purified by crystallisation from hexane to give the product as white solid (1.5 g, 53%).

^{1}H NMR (400 MHz, $CDCl_3$): δ = 9.41 (d, *J* = 1.6 Hz, 1H), 8.93 (dd, *J* = 4.9 Hz, 1.7 Hz, 1H), 8.46 (dt, *J* = 8.0 Hz, 2.0 Hz, 1H), 7.52 (ddd, *J* = 8.0 Hz, 4.9 Hz, 0.7 Hz, 1H); ^{19}F NMR (377 MHz, $CDCl_3$): δ = -152.22 (d, *J* = 18.5 Hz, 2F), -156.99 (t, *J* = 21.8 Hz, 1F), -161.74 (t, *J* = 18.5 Hz, 2F).

Isonicotinic acid methyl ester

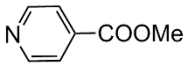

Thionyl chloride (6.3 mL, 87 mmol) was placed in a 50 mL flask under ice-water bath and isonicotinic acid (2.5 g, 20 mmol) was added. The ice-water bath was removed and the mixture was stirred at room temperature for 10 min. Excess thionyl chloride was removed by vacuum and the flask was placed back in ice-water bath. MeOH (7.0 mL, 17 mmol) was added and the mixture was stirred under ice-water bath and left until the bath reached room temperature. The mixture was stirred for another 10 min and the excess MeOH was removed by vacuum. The residue was dissolved in water and $NaHCO_3$ was added to neutralize the solution until pH reached 6. The product was extracted with ethyl acetate and the solvent was removed by vacuum. The product was obtained as transparent oil (1.3 g, 47%).

^{1}H NMR (200 MHz, $CDCl_3$): δ = 8.75 (dd, *J* = 4.3 Hz, 1.6 Hz, 2H), 7.81 (dd, *J* = 4.3 Hz, 1.6 Hz, 2H), 3.93 (s, 3H); ESI MS+: m/z 138.1 ($[M+H]^+$, $C_7H_8NO_2$ requires: 138.1).

4-Pyridyl propanic acid methyl ester

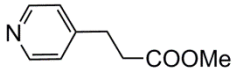

Thionyl chloride (0.63 mL, 8.7 mmol) was placed in a 10 mL flask under ice-water bath and 4-pyridyl propanic acid (0.26 g, 1.7 mmol) was added. The ice-water bath was removed and the mixture was stirred at room temperature for 10 min. Excess thionyl chloride was removed by vacuum and the flask was placed back in ice-water bath. MeOH (0.7 mL, 1.7 mmol) was added and the mixture was stirred under ice-water bath and left until the bath reached room temperature. The mixture was stirred for another 10 min and the excess MeOH was removed by vacuum. The residue was dissolved in water and $NaHCO_3$ was added to neutralize the solution until pH reached 6. The product was extracted with ethyl acetate and the solvent was removed by vacuum. The product was obtained as transparent oil (0.18 g, 63%).

^{1}H NMR (200 MHz, $CDCl_3$): δ = 8.52 (dd, *J* = 4.3 Hz, 1.6 Hz, 2H), 7.14 (dd, *J* = 4.3 Hz, 1.6 Hz, 2H), 3.68 (s, 3H), 2.96 (t, *J* = 7.5 Hz, 2H), 2.66 (t, *J* = 7.5 Hz, 2H); ESI MS+: m/z 166.1 ($[M+H]^+$, $C_9H_{12}NO_2$ requires: 166.1).

6-Isoquinoline[17]

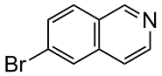

4-Bromobenzaldehyde (16 g, 84 mmol) and aminoacetaldehyde diethylacetal (12 mL, 85 mmol) were dissolved in toluene (100 mL). The mixture was refluxed in a Dean Stark apparatus for 3 h. The solvent was evaporated under vacuum and the residue was dissolved in chlorobenzene (200 mL). The solution was placed in ice water bath and ethyl chloroformate (8.2 mL, 85 mmol) was added under N_2 protection. The mixture was stirred for 30 min under ice water bath and N_2 protection. Trimethylphosphite (12 mL, 0.10 mol) was added; the mixture was warmed to room temperature and stirred under N_2 protection for 48 h. The mixture was placed in ice water bath. $TiCl_4$ (54 mL, 0.29 mol) was slowly added and the mixture was stirred at 100°C under N_2 for 24 h. The mixture was cooled to room temperature and diluted with ethyl acetate and basified by NaOH (5 M in water) under ice water bath. Ethyl acetate and hexane (0.5 L/1 L) was added into the mixture and TiO_2 was filtered, leaving the product in the organic phase. The organic phase was extracted by 1 M aqueous HCl solution. The aqueous solution of the product was basified by

NaOH (5 M in water) to pH > 10, extracted by DCM and dried by Na_2SO_4. The solvent was evaporated and the crude product was distilled using Kugelrohr distillation apparatus (140°C, 1.5 mbar) to give the product as white crystal (2.7 g, 15%).

^{1}H NMR (400 MHz, $CDCl_3$): δ = 9.25 (s, 1H), 8.57 (d, *J* = 5.8 Hz, 1H), 8.02 (s, 1H), 7.86 (d, *J* = 8.7 Hz, 1H), 7.70 (dd, *J* = 8.7 Hz, *J* = 1.7 Hz, 1H), 7.58 (d, *J* = 5.8 Hz, 1H); ^{13}C NMR (100 MHz, $CDCl_3$) δ = 152.4, 144.1, 136.8, 130.9, 129.3, 128.8, 127.0, 125.2, 119.4.

6-(4,4,5,5-Tetramethyl[1,3,2]dioxaborolan-2-yl)isoquinoline, 6-(Bpin)isoquinoline[18]

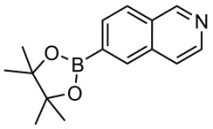

6-Bromoisoquinoline (3.2 g, 15 mmol), $PdCl_2$(dppf)·DCM (1.9 g, 2.3 mmol), bis(pinacolato) diboron (4.5 g, 18 mmol) and KOAc (5.0 g, 51 mmol) were dissolved in dry DMF (100 mL). The mixture was degassed using freeze-pump-thaw method and was then stirred at 80ºC under argon protection for 18 h. The mixture was cooled off and the DMF solvent was evaporated under vacuum. The residue was dissolved in DCM and filtered through cotton. The solvent was evaporated and the residue was separated with column chromatography (SiO_2) using hexane/EtOAc (4/1, v/v) as the eluent. The desired product was obtained as white powder (1.3 g, 33%). ^{1}H NMR (200 MHz, $CDCl_3$): δ = 9.28 (s, 1H), 8.55(d, *J* = 5.8 Hz, 1H), 8.35 (s, 1H), 7.97 (s, 2H), 7.68 (d, *J* = 5.8 Hz, 1H), 1.40 (s, 12H); ESI-MS MS+: m/z 256.2 ($[M+H]^+$, $C_{15}H_{19}BNO_2$ requires: 256.2).

Di-*tert*-butyl-phosphinoferrocene tetrafluoroboric acid complex[19]

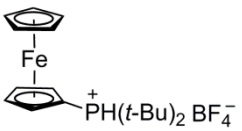

Ferrocene (2.1 g, 11 mmol) was dried under vacuum for over 3 h and replaced with argon. Dry THF (125 mL) was cannulated into the flask. *t*-BuOK (1.4 mL, 1.0 M in THF, 1.4 mmol) was added by syringe and the flask was put under dry ice-acetone bath. Under argon protection, *t*-BuLi (13 mL, 1.7 M in pentane, 22 mmol) was added slowly and the mixture was stirred for 1 h. The

flask was warmed by replacing the bath into ice-water bath. Di-*tert*-butylchlorophosphine (2.3 mL, 12.1 mmol) was added and the ice-water bath was removed. The mixture was stirred at room temperature overnight under argon protection. Tetrefluoroboric acid diethyl ether complex (3.0 mL, 22 mmol) was added into the mixture by syringe and the mixture was stirred under argon for 3 h. Water (26 mL) and methyl *tert*-butyl ether (26 mL) was added and the mixture was stirred for another 1 h and filtered through celite. The organic solvent was evaporated, leaving a mixture of crude product and water, which was dissolved by DCM and washed with water. The organic phase was dried by $MgSO_4$ and filtered. The solvent was evaporated and the crude product was dissolved with methyl *tert*-butyl ether/methanol (13/13 mL) solvent mixture at 50^{o}C under argon protection. *tert*-Butyl ether (13 mL) was added slowly into the solution at 50^{o}C and desired product slowly precipitated as the heating bath was removed. The mixture was stirred for 3 h and the precipitate was filtered. The precipitation process cannot give totally pure product and is often repeated for another 2 times. Desired product was obtained as orange powder (2.0 g, 42%).

^{1}H NMR (400 MHz, $CDCl_3$): δ = 6.85 (d, *J* = 493 Hz, 1H), 4.79 (d, *J* = 1.6 Hz, 2H), 4.65 (d, *J* = 1.6 Hz, 2H), 4.43 (s, 5H), 1.51 (d, *J* = 16.4 Hz, 18H); ^{31}P NMR ($CDCl_3$): δ = 40.3.

1,1'-Dibromoferrocene[20]

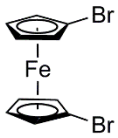

Ferrocene (9.3 g, 50 mmol) was dried under vacuum for 3 h in a 500 mL 3-neck round-bottom flask and the vacuum was replaced with argon. Dry hexane (50 mL) and dry tetramethylethylenediamine (TMEDA, 17.5 mL, 116 mmol) was added by syringe. The mixture was placed in ice-water bath. *n*-BuLi (43 mL, 2.5 M in hexanes, 0.11 mol) was added by syringe and the ice-water bath was removed. The mixture was stirred at room temperature under argon overnight and the precipitate was cannula-filtered and re-suspended in dry diethyl ether (150 mL). The suspension was placed under dry ice-acetone bath. 1,1,2,2-Tetrabromoethane (13 mL, 0.11 mmol) was dissolved in dry diethyl ether (50 mL) and the solution was slowly added into the suspension, while keeping the suspension at around -70ºC. The mixture was gradually warmed to room temperature and stirred overnight under argon. Water (20 mL) was added to quench the

reaction and the mixture was stirred for 20 min. The top dark-red layer containing the product was decanted and the solvent was evaporated. The residue was dried under high vacuum and dissolved in diethyl ether. The solution was washed with water to remove salts formed in the reaction and the solvent was evaporated. The residue was dissolved in hot methanol and then placed under -30ºC bath. The product was precipitated and filtered. The precipitation process cannot give totally pure product and is often repeated for another 2 times. Desired product was obtained as orange needle-like crystal (6.2 g, 36%).

^{1}H NMR (400 MHz, $CDCl_3$): δ = 4.42 (pseudo-t, 3H), 4.17 (pseudo-t, 3H); ^{13}C NMR (100 MHz, $CDCl_3$): δ = 78.3, 72.7, 70.0.

1,2-Dibromoferrocene[21]

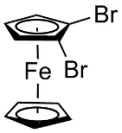

Under argon protection, 1,1'-dibromoferrocene (7.8 g, 23 mmol) was dissolved in dry THF (135 mL) and the solution was placed under -78ºC bath. *n*-BuLi (2.5 M in hexanes, 9.1 mL, 23 mmol) was slowly added and the mixture was stirred at -78ºC for 30 min. 2,2,6,6-Tetramethylpiperidine (TMP, 3.9 mL, 23 mmol) was added and the mixture was allowed to warm to -40ºC. The cold bath was controlled between -40ºC and -30ºC for 3 h as the reaction proceeded. The solution was again cooled to -78ºC and 1,1,2,2-tetrabromoethane (2.6 mL, 23 mmol) was added into the mixture. The mixture was stirred under argon protection overnight and was allowed to warm to room temperature. Water was added to quench the reaction and the crude product was extracted with diethyl ether. The solution was washed with water and the solvent was evaporated under vacuum. The residue was plugged through a short silica column with hexane, giving a mixture containing ferrocene, 1-bromoferrocene and the desired product. The mixture was separated by Kugelrohr distillation to give the product as dark yellowish solid (4.2 g, 54%).

^{1}H NMR (400 MHz, $CDCl_3$): δ = 4.44 (d, *J* = 2.4 Hz, 2H), 4.25 (s, 5H), 4.11 (t, *J* = 2.4 Hz, 1H).

1,2,3,4,5-Pentabromoferrocene[22]

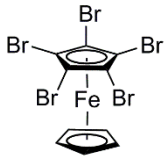

Under argon protection, 2,2,6,6-tetramethylpiperidine (TMP, 11 mL, 65 mmol) was dissolved in dry THF (85 mL) and placed under -30ºC bath. *n*-BuLi (2.5 M in hexanes, 26 mL, 65 mmol) was slowly added and the mixture was stirred at 0ºC for 15 min. 1,2-Dibromoferrocene (2.2 g, 6.5 mmol) was dissolved in dry THF (10 mL) and the solution was added into the freshly prepared LiTMP solution. The mixture was stirred under argon between -40ºC and -30ºC for 5 h. The solution was again cooled to -78ºC and 1,1,2,2-tetrabromoethane (7.6 mL, 65 mmol) was added into the mixture. The mixture was stirred under argon protection overnight and was allowed to warm to room temperature. Water was added to quench the reaction and the crude product was extracted with diethyl ether. The solution was washed with water and the solvent was evaporated under vacuum. The residue was plugged through a short silica column with hexane. The solvent was removed under vacuum to give the desired product as dark yellow solid (1.7 g, 45%).

^{1}H NMR (400 MHz, $CDCl_3$): δ = 4.31 (s, 5H); ^{13}C NMR (100 MHz, $CDCl_3$): δ = 80.77, 80.87.

4-[(Trimethylsilyl)ethynyl]pyridine[23]

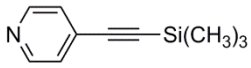

4-Bromopyridine hydrochloride (3.7 g, 19 mmol), $PdCl_2(PPh_3)_2$ (0.36 g, 0.52 mmol) and CuI (0.26 g, 1.3 mmol) were dissolved in dry THF (100 mL) and *i*-Pr_2NH (30 mL). The solution was degassed by freeze-pump-thaw method and saturated with argon. Trimethylsilyl acetylene (5.2 mL, 37 mmol) was added and the mixture was stirred at 45ºC for 20 h. The mixture was cooled to room temperature and the precipitate was filtered with silica. The mixture was purified by silica chromatography using petroleum ether/ethyl acetate (7/1, *v*/*v*) as the eluent. The product was obtained as light brown oil (2.3 g, 68%).

^{1}H NMR (400 MHz, $CDCl_3$): δ = 8.58 (s, 2H), 7.31 (d, *J* = 4.8 Hz, 2H), 0.26 (s, 9H).

4-Ethynylpyridine

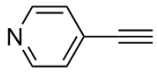

4-[(Trimethylsilyl)ethynyl]pyridine (6.5 g, 37 mmol) was dissolved in THF (190 mL) and the solution was cooled in dry ice-acetone bath. TBAF (65 mL, 1 M in THF, 65 mmol) was added and the mixture was stirred at -78ºC for 2 h. The reaction was quenched by pouring the mixture into water (2 L). The crude product was extracted with DCM and dried with $MgSO_4$. The solvent was evaporated and the mixture was separated by silica chromatography using petroleum ether/ethyl acetate (9/1 with polarity gradually increasing to 5/1, *v*/*v*) as the eluent. The product was obtained as white solid (1.6 g, 40%) which is sensitive to oxygen and should be stored under argon.

^{1}H NMR (400 MHz, $CDCl_3$): δ = 8.59 (dd, *J* = 5.4 Hz *J* = 1.6 Hz, 2H), 7.34 (d, *J* = 5.4 Hz *J* = 1.6 Hz, 2H), 3.29 (s, 1H).

6.3 Synthetic Procedures for Novel Compounds

4-Pyridinyl propanoic acid pentafluorophenol ester

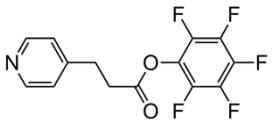

4-Pyridinyl propanoic acid (2.81 g, 18.8 mmol), pentafluorophenol (3.66 g, 19.9 mmol) and DCC (4.63 g, 22.4 mmol) were added into a 250 mL flask. The flask was evacuated and filled with N_2. THF (80 mL) was added under N_2 and the reaction mixture was stirred under N_2 protection at room temperature for 24 h. The solid generated was filtered and the solvent was evaporated. The residue was crystallized from petroleum ether to give the product as white solid (2.9 g, 49%).

^{1}H NMR (400 MHz, $CDCl_3$) δ = 8.58 (d, *J* = 6.0 Hz, 2H), 7.24 (d, *J* = 6.0 Hz, 2H), 3.17 – 3.10 (m, 2H), 3.10 – 3.03 (m, 2H); ^{19}F NMR (377 MHz, $CDCl_3$) δ = -152.62 (d, *J* = 17.1 Hz, 2F), -157.49 (t, *J* = 21.7 Hz, 1F), -161.98 (dd, *J* = 21.7, 17.1 Hz, 2F); ESI-HDMS+: *m/z* 318.0534 ($[M+H]^+$, $C_{14}H_9F_5NO_2$ requires: 318.0548).

Per-2,3-di-*O*-methyl-6-*O*-(*para*-pyridinyl)carboxyl-α-cyclodextrin T6*

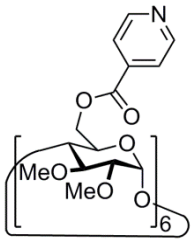

Per-2,3-di-*O*-methyl-α-cyclodextrin (120 mg, 0.106 mmol), 4-dimethylaminopyridine (DMAP, 230 mg, 1.88 mmol) and isonicotinic acid pentafluorophenyl ester (0.75 g, 2.6 mmol) were dried under vacuum for over 2 h, anhydrous pyridine (7.5 mL) was added. The mixture was stirred at 90°C for 24 h, at which point MALDI-MS analysis indicated the completion of the reaction. The reaction mixture was cooled and the solvent was evaporated under vacuum. The residue was dissolved in chloroform (120 mL) and washed with water (120 mL × 2). The solution was evaporated. Column chromatography (chloroform/MeOH, 20/1, *v*/*v*) of the residue gave the product as white powder (87 mg, 47%), R_f = 0.05.

^{1}H NMR (400 MHz, $CDCl_3$): δ = 8.76 (d, *J* = 5.8 Hz, 12H), 7.79 (d, *J* = 5.8 Hz, 12H), 4.98 (d, *J* = 3.3 Hz, 6H), 4.67 (d, *J* = 11.2 Hz, 6H), 4.48 (dd, *J* = 12.2, 3.7 Hz, 6H), 4.08 (d, *J* = 6.7 Hz, 6H),

3.68 (m, 18H), 3.65 – 3.58 (m, 6H), 3.52 (s, 18H), 3.18 (dd, *J* = 9.5, 3.2 Hz, 6H); ^{13}C NMR (100 MHz, $CDCl_3$): δ = 164.64, 150.99, 136.89, 122.96, 100.53, 82.69, 82.06, 81.53, 70.20, 64.41, 62.09, 58.75; MALDI-TOF MS+: *m/z* 1794.09 ($[M+Na]^+$, $C_{84}H_{102}N_6O_{36}Na$ requires: 1793.62).

Per-2,3-di-*O*-methyl-6-*O*-(*meta*-pyridinyl)carboxyl-α-cyclodextrin *meta*-T6*

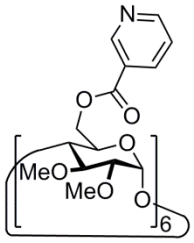

Per-2,3-di-*O*-methyl-α-cyclodextrin (0.10 g, 0.088 mmol), DMAP (190 mg, 1.55 mmol) and nicotinic acid pentafluorophenyl ester (0.62 g, 2.1 mmol) was dried under vacuum for over 2 h, anhydrous pyridine (6.0 mL) was added. The reaction mixture was stirred at 90°C for 24 h. MALDI-MS analysis of the reaction mixture indicated the completion of the reaction. The reaction mixture was cooled off and pyridine solvent was evaporated under vacuum. The residue was dissolved in chloroform (100 mL) and washed with water (100 mL × 2). The organic solution was evaporated to dryness. Column chromatography (chloroform/MeOH, 20/1, *v*/*v*) of the residue gave the product as white powder (95 mg, 61%), R_f = 0.05.

^{1}H NMR (400 MHz, $CDCl_3$): δ = 9.16 (s, 6H), 8.74 (d, *J* = 4.1 Hz, 6H), 8.36 – 8.05 (m, 6H), 7.38 (dd, *J* = 7.9, 4.9 Hz, 6H), 5.01 (d, *J* = 3.2 Hz, 6H), 4.69 (d, *J* = 11.3 Hz, 6H), 4.51 (dd, *J* = 12.2, 3.6 Hz, 6H), 4.11 (d, *J* = 6.2 Hz, 6H), 3.67 (s, 18H), 3.65 – 3.59 (m, 12H), 3.51 (s, 18H), 3.21 – 3.14 (m, 1H); ^{13}C NMR (100 MHz, $CDCl_3$): δ = 164.76, 153.89, 150.96, 137.32, 125.83, 123.64, 100.49, 82.77, 82.09, 81.45, 70.37, 64.13, 62.06, 58.61; MALDI-TOF MS+: m/z 1772.22 ($[M+H]^+$, $C_{84}H_{102}N_6O_{36}$ requires: 1771.64).

Per-2,3-di-*O*-methyl-6-*O*-(4-pyridinylethyl)carboxyl-β-cyclodextrin T7*

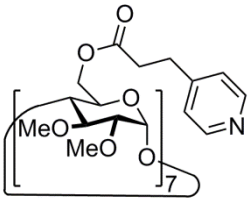

Per-2,3-di-O-methyl-β-cyclodextrin (88 mg, 0.066 mmol), 4-pyridinyl propanoic acid

pentafluorophenol ester (0.67 g, 2.1 mmol) and DMAP (0.16 g, 1.3 mmol) were dried under vacuum for over 2 h, then pyridine (7.0 mL) was added. The mixture was stirred at 90°C for 5 h. MALDI-MS analysis indicated the completion of the reaction. The reaction mixture was cooled and the solvent was evaporated under vacuum. The residue was dissolved in chloroform (100 mL) and washed with water (100 mL × 2). The organic solution was evaporated to dryness. Column chromatography (chloroform/MeOH, 20/1, gradually increasing the polarity to 20/1.6, *v/v*) washed off the excess pentafluorophenol ester. The column was then eluted with solvent of increasing polarity (chloroform/MeOH, 1/1, *v/v*) to give the product, along with impurities which do not dissolve in pure chloroform. The product was finally extracted from the residue using chloroform and evaporation of the solvent gave the product as light yellowish oily solid (137 mg, 92.1%).

^{1}H NMR (400 MHz, $CDCl_3$) δ = 8.39 (d, *J* = 5.9 Hz, 14H), 7.05 (d, *J* = 5.7 Hz, 14H), 4.86 (d, *J* = 3.5 Hz, 7H), 4.36 (d, *J* = 11.6 Hz, 7H), 4.20 (dd, *J* = 12.1, 3.7 Hz, 7H), 3.78 (d, *J* = 7.4 Hz, 7H), 3.55 (s, 21H), 3.44 (s, 21H), 3.43 – 3.37 (m, 14H), 3.05 (dd, *J* = 9.0, 3.3 Hz, 7H), 2.88 – 2.78 (m, 14H), 2.71 – 2.49 (m, 14H); ^{13}C NMR (100 MHz, $CDCl_3$) δ = 171.79, 149.75, 149.33, 123.70 , 99.09, 81.54, 81.47, 80.38, 69.56, 63.22, 61.32, 58.83, 34.00, 29.81; MALDI-TOF MS+: *m/z* 2263.90 ($[M]^+$, $C_{112}H_{147}N_7O_{42}$ requires: 2263.97).

c*-P6$_{t\text{-Bu}}$·T6

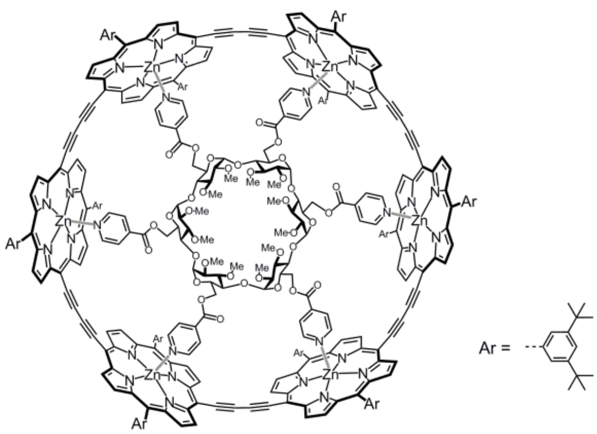

a) **T6*** (5.5 mg, 3.13 μmol) and ***l*-P2$_{t\text{-Bu}}$(H,H)** (20 mg, 12.5 μmol) were dissolved in chloroform (15 mL) and DIPA (0.2 mL). The solution was sonicated for 2 h and cooled to room temperature. A catalyst solution was prepared by dissolving $Pd(PPh_3)_2Cl_2$ (2.9 mg, 4.0 μmol), CuI (7.2 mg, 37 μmol) and 1,4-benzoquinone (5.4 mg, 50 μmol) in chloroform (15 mL) and DIPA (0.2 mL). The

catalyst solution was added to the mixture and stirred under air at room temperature overnight. The reaction mixture was passed through a plug of alumina using chloroform as eluent. The crude mixture was separated on size exclusion column (Biobeads SX-1, 200–400 mesh) using toluene as eluent to give the product as reddish-brown solid (12 mg, 59%).

b) **T6*** (5.5 mg, 3.13 μmol) and ***l*-P1$_{t\text{-Bu}}$(H,H)** (20 mg, 25 μmol) were dissolved in chloroform (15 mL) and DIPA (0.2 mL). The solution was sonicated for 2 h and cooled to room temperature. A catalyst solution was prepared by dissolving $Pd(PPh_3)_2Cl_2$ (2.9 mg, 4.0 μmol), CuI (7.2 mg, 37 μmol) and 1,4-benzoquinone (10.8 mg, 100 μmol) in chloroform (15 mL) and DIPA (0.2 mL). The catalyst solution was added to the mixture and the reaction was stirred under air at room temperature and UV-vis monitoring during the reaction process (0.5 h interval) indicated the reaction to completion at 6 h. The reaction mixture was passed through a plug of alumina using chloroform as eluent. The crude mixture was separated on size exclusion column (Biobeads SX-1, 200–400 mesh) using tolueneas eluent. Two major bands were collected from the column: the first band was collected for the following ***c*-P12$_{t\text{-Bu}}$·(T6*)$_2$** synthesis; the second band was collected, dried and precipitated using chloroform/methanolto give the product as reddish-brown solid (4.5 mg, 22%).

^{1}H NMR (700 MHz, $CDCl_3$): δ = 9.64 (d, *J* = 4.2 Hz, 6H), 9.56 (d, *J* = 4.2 Hz, 6H), 9.55 (d, *J* = 4.2 Hz, 6H), 9.51 (d, *J* = 4.2 Hz, 6H), 8.92 (d, *J* = 4.2 Hz, 6H), 8.84 (d, *J* = 4.2 Hz, 6H), 8.75 (d, *J* = 4.2 Hz, 6H), 8.73 (d, *J* = 4.2 Hz, 6H), 8.07 (s, 6H), 7.92 (s, 6H), 7.83 (s, 6H), 7.78 (s, 6H), 7.76 (s, 6H), 7.73 (s, 6H), 5.45 (d, *J* = 7.3 Hz, 12H), 3.37 (d, *J* = 2.8 Hz, 6H), 3.15 (d, *J* = 10.0 Hz, 6H), 3.06 (s, 18H), 2.86 (s, 18H), 2.78 (d, *J* = 11.0 Hz, 6H), 2.62 – 2.59 (m, 12H), 2.37 (d, *J* = 7.3 Hz, 12H), 2.32 (d, *J* = 10.0 Hz, 6H), 2.17 (dd, *J* = 10.0 Hz, *J* = 2.8 Hz, 6H), 1.51 (s, 108H), 1.50 (s, 54H), 1.46 (s, 54H); MALDI-TOF MS+: *m/z* 4775 ([M-**T6***]$^+$, $C_{312}H_{300}N_{24}Zn_6$ requires: 4778), 6544 ([M]$^{+\bullet}$, $C_{396}H_{402}N_{30}Zn_6O_{36}$ requires: 6549); UV-vis ($CHCl_3$): λ_{max} (ε) 483 (5.0×10^5), 772 (3.2×10^5), 808 (4.1×10^5), 848 (3.5×10^5).

***c*-P12$_{t\text{-Bu}}$·(T6*)$_2$**

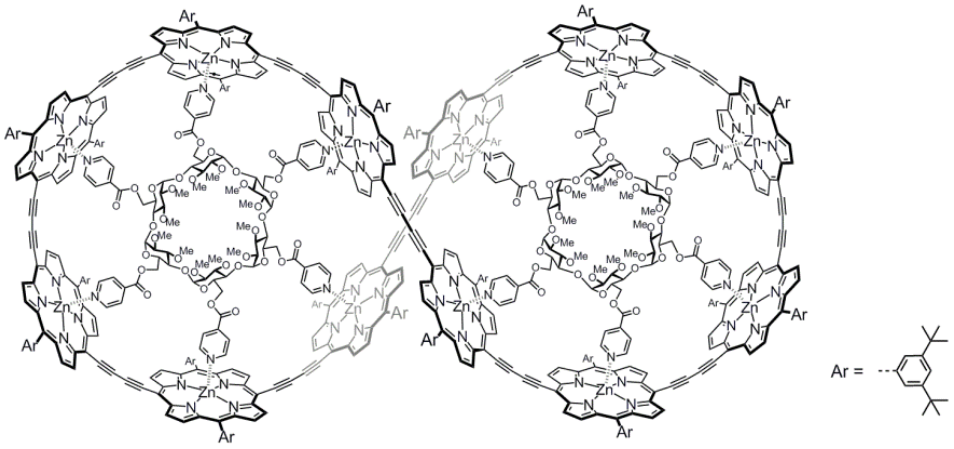

The mixture collected in the procedure (b) in the ***c*-P6$_{t\text{-Bu}}$·T6*** synthesis was separated on size exclusion column (Biobeads SX-1, 200–400 mesh) using chloroform/pyridine (10/1, *v*/*v*) to remove the template. Recycling GPC (Shimadzu recycling GPC system equipped with LC-20 AD pump, SPD-20A UV detector and a set of JAIGEL 3H (20 × 600 mm) and JAIGEL 4H (20 × 600 mm) columns in toluene/1% pyridine as eluent, flow rate 3.5 mL/min) gave the template-free ***c*-P12$_{t\text{-Bu}}$** intermediate (0.40 mg, 2.0%). ***c*-P12$_{t\text{-Bu}}$** (0.40 mg, 0.042 μmol) and **T6*** (0.20 mg, 0.11 μmol) were dissolved in chloroform (2 mL) and plugged through a short basic alumina column. The solvent was evaporated and the residue was precipitated using chloroform/methanol to give the product ***c*-P12$_{t\text{-Bu}}$·(T6*)$_2$** as black solid (0.39 mg, 70% from ***c*-P12$_{t\text{-Bu}}$**, 1.4% from ***l*-P1$_{t\text{-Bu}}$(H,H)**).

^{1}H NMR characterized by comparison of DOSY spectra of ***c*-P12$_{t\text{-Bu}}$·(T6)$_2$** (see SI in *Angew. Chem. Int. Ed.* **2014**, *53*, 7770–7773); MALDI-TOF MS+: *m/z* 11318 ([M-**T6***]$^+$, $C_{708}H_{702}N_{54}Zn_{12}O_{36}$ requires: 11327), 9543 ([M-2**T6***]$^+$, $C_{624}H_{600}N_{48}Zn_{12}$ requires: 9555). UV-vis ($CHCl_3$): λ_{max} (ε) 496 (8.1×10^5), 763 (3.1×10^5), 800 (3.8×10^5), 838 (4.3×10^5), 874 (6.7×10^5).

***c*-P7$_{t\text{-Bu}}$**

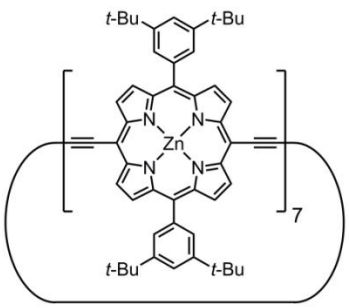

T7* (11.4 mg, 5.0 μmol) and ***l*-P1$_{t\text{-Bu}}$(H,H)** (40 mg, 50 μmol) were dissolved in chloroform (60 mL) and DIPA (1.0 mL). The solution was sonicated for 1 h. A catalyst mixture consisting of $Pd(PPh_3)_2Cl_2$ (5.8 mg, 8.0 μmol), CuI (15 mg, 75 μmol) and 1,4-benzoquinone (22 mg, 0.20 mmol) was added. The reaction was stirred under air at room temperature overnight, then the mixture was passed through a short plug of alumina using chloroform/pyridine (8/1, *v*/*v*) as eluent. The crude mixture was separated on size exclusion column (Biobeads SX-1, 200–400 mesh) using chloroform/pyridine (8/1, *v*/*v*) to remove the template. Recycling GPC (Shimadzu recycling GPC system equipped with LC-20 AD pump, SPD-20A UV detector and a set of JAIGEL 3H (20 × 600 mm) and JAIGEL 4H (20 × 600 mm) columns in toluene/1% pyridine as eluent, flow rate 3.5 mL/min) gave the product as dark brown solid (2.1 mg, 5.2%).

^{1}H NMR (400 MHz, $CDCl_3$): δ = 9.63 (d, *J* = 4.4 Hz, 28H), 8.78 (d, *J* = 4.4 Hz, 28H), 7.89 (d, *J* = 2.0 Hz, 28H), 7.70 (t, *J* = 2.0 Hz, 14H), 1.44 (s, 252H); MALDI-TOF MS+: *m/z* 5571, ($[M]^+$, $C_{364}H_{350}N_{28}Zn_7$ requires: 5575); UV-vis ($CHCl_3$): λ_{max} (ε) 458 (5.4×10^5), 494 (5.2×10^5), 772 (2.8×10^5).

c*-P7$_{t\text{-Bu}}$·T7

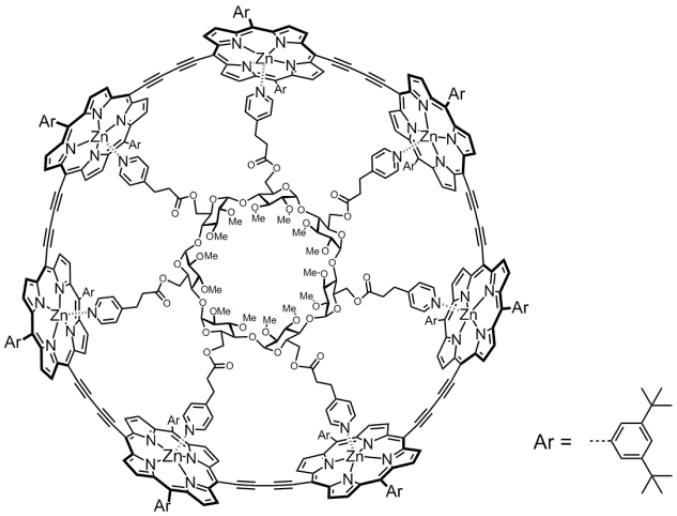

T7* (5.0 mg, 2.2 μmol) and ***c*-P7$_{t\text{-Bu}}$** (3.5 mg, 0.63 μmol) were mixed in chloroform and the solution was passed through a short basic alumina column using chloroform as the eluent. The compound was precipitated by dissolving in chloroform and adding methanol to give the product as dark brown solid (4.4 mg, 90% from ***c*-P7$_{t\text{-Bu}}$**, 4.7% from ***l*-P1$_{t\text{-Bu}}$(H,H)**).

^{1}H NMR (700 MHz, $CDCl_3$): δ = 9.73 (d, *J* = 1.8 Hz, 7H), 9.72 (d, *J* = 1.8 Hz, 7H), 9.66 (d, *J* = 4.2

Hz, 7H), 9.63 (d, *J* = 4.2 Hz, 7H), 8.88 (d, *J* = 4.2 Hz, 14H), 8.84 (d, *J* = 4.2 Hz, 7H), 8.81 (d, *J* = 4.2 Hz, 7H), 8.11 (s, 7H), 8.08 (s, 7H), 7.88 (s, 7H), 7.84 (s, 14H), 7.79 (s, 7H), 4.99 (d, *J* = 7.2 Hz, 14H), 4.04 (d, *J* = 3.0 Hz, 7H), 3.29 (d, *J* = 11.5 Hz, 7H), 3.21 (s, 28H), 3.05 (s, 21H), 2.91 (d, *J* = 7.2 Hz, 7H), 2.74 – 2.70 (m, 14H), 2.44 – 2.41 (m, 21H), 1.58 – 1.52 (m, 252H), 1.34 – 1.31 (m, 14H), 1.06 (t, *J* = 8.0 Hz, 14H); MALDI-TOF MS+: *m/z* 5569 ([M-**T7**]$^+$, $C_{364}H_{350}N_{28}Zn_7$ requires: 5575), 7829 ([M]$^{+\bullet}$, $C_{476}H_{497}N_{35}O_{42}Zn_7$ requires: 7837); UV-vis ($CHCl_3$): λ_{max} (ε) 464 (5.0 × 10^5), 509 (5.7 × 10^5), 767 (2.7 × 10^5), 807 (4.1 × 10^5), 853 (7.0 × 10^5).

***c*-P14$_{OOct}$**

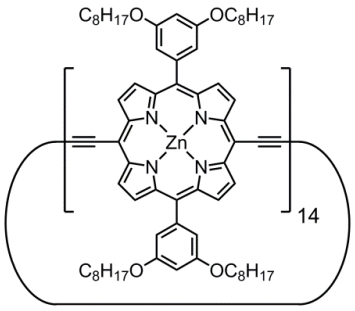

T7* (5.0 mg, 2.2 μmol) and ***l*-P2$_{OOct}$(H,H)** (26 mg, 12 μmol) were dissolved in chloroform (25 mL, obtained from solvent dalek) and dry DIPA (0.5 mL). $Pd(PPh_3)_2Cl_2$ (2.5 mg, 3.4 μmol), CuI (5.0 mg, 26 μmol) and 1,4-benzoquinone (2.5 mg, 23 μmol) was added into the mixture. The reaction proceeded under air at dark overnight at room temperature. Aliquot of the mixture was obtained and passed through size-exclusion column (Biobeads SX-1) using chloroform/pyridine (10/1, *v*/*v*) to remove the template. Recycling GPC (Shimadzu recycling GPC system equipped with LC-20 AD pump, SPD-20A UV detector and a set of JAIGEL 3H (20 × 600 mm) and JAIGEL 4H (20 × 600 mm) columns in toluene/1% pyridine as eluent, flow rate 3.5 mL/min) gave the product as dark brown solid (1.7 mg, 6.4%).

^{1}H NMR (400 MHz, $CDCl_3$): δ = 9.78 (d, 56H, *J* = 4.4 Hz), 8.99 (d, 56H, *J* = 4.4 Hz), 7.33 (d, 56H, *J* = 2.4 Hz), 6.85 (t, 28H, *J* = 2.4 Hz), 4.11 (s, 112H), 1.85 – 1.81 (m, 112H), 1.47 – 1.21 (m, 560H), 0.80 – 0.77 (m, 168H); MALDI-TOF MS+: m/z 15281 ([M]$^+$, $C_{952}H_{1148}N_{56}Zn_{14}O_{56}$ requires: 15187); UV-vis ($CHCl_3$): λ_{max} (ε) 503 (1.1 × 10^6), 797 (7.4 × 10^5), 839 (9.0 × 10^5).

1',2',3',4',5'-Pentakis(6-isoquinolinyl)ferrocenyl-di-*tert*-butylphosphine pre-T5

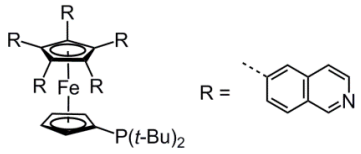

Di-*tert*-butyl-phosphinoferrocene tetrafluoroboric acid complex (0.12 g, 0.28 mmol), 6-bromoisoquinoline (0.70 g, 3.3 mmol), *t*-BuOK (0.30 g, 2.6 mmol), $Pd(OAc)_2$ (6.0 mg, 0.027 mmol) and PPh_3 (33 mg, 0.13 mmol) was dissolved in dry toluene (12 mL). The mixture was degassed using freeze-pump-thaw method and was then stirred vigorously at 107 ºC under argon protection for 2 days. The mixture was cooled and filtered through celite and the solvent was evaporated under vacuum. The residue was separated with column chromatography (SiO_2) using DCM/EtOH (80/11 gradually increasing polarity to 5/1, *v/v*) as the eluent. Pre-**T5** was obtained from the last dark red band as dark red solid (0.11 g, 40%).

^{1}H NMR (400 MHz, $CDCl_3$): δ = 9.19 (s, br, 5H), 8.43 (s, br, 5H), 7.69 (s, 5H), 7.65 (d, *J* = 8.5 Hz, 5H), 7.45 (dd, *J* = 8.5 Hz, *J* = 1.0 Hz, 5H), 7.26 – 7.24 (m, 5H), 4.78 (s, 2H), 4.64 (t, *J* = 1.6 Hz, 2H), 1.04 (d, *J* = 11.2 Hz, 18H); ^{13}C NMR (100 MHz, $CDCl_3$): δ = 152.2, 143.6, 137.4, 135.0, 131.8, 130.0, 126.5, 88.1, 78.4, 78.3, 76.6, 33.6 (d, *J* = 25 Hz), 31.1 (d, *J* = 13 Hz); ^{31}P{^{1}H} NMR ($CDCl_3$, 162 MHz): δ = 24.91; MALDI-TOF MS+: *m/z* 981.84 ($[M+O]^+$, $C_{63}H_{52}FeN_5PO$ requires: 981.33, showing the quick oxidization of pre-**T5** in the sample preparation process).

1',2',3',4',5'-Pentakis(6-isoquinolinyl)ferrocenyl-di-*tert*-butylphosphine oxide T5

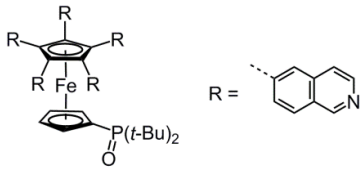

Pre-**T5** (0.10 g, 0.10 mmol) was dissolved in THF (20 mL). *N*-Methylmorpholine *N*-oxide monohydride (15 mg, 0.12 mmol) was added and the mixture was stirred at room temperature overnight. The solvent was evaporated and the residue was dissolved in DCM and the solution was washed with water and dried with $MgSO_4$. The DCM solvent was evaporated and the residue was precipitated by diffusion hexane into its solution in benzene. The product was obtained as bright red solid (84 mg, 84%).

^{1}H NMR (400 MHz, $CDCl_3$): δ = 9.14 (s, 5H), 8.41 (d, *J* = 5.8 Hz, 5H), 7.79 (s, 5H), 7.65 (d, *J* =

8.4 Hz, 5H), 7.37 (dd, *J* = 8.4 Hz, 1.6 Hz, 5H), 7.29 (d, *J* = 5.8 Hz, 5H), 5.08 (d, *J* = 1.6 Hz, 2H), 4.84 (d, *J* = 1.6 Hz, 2H), 0.96 (d, *J* = 14.2 Hz, 18H); ^{13}C NMR (100 MHz, $CDCl_3$): δ = 152.3, 143.8, 136.8, 135.3, 131.1, 130.4, 127.4, 127.0, 120.4, 88.8, 79.3, 79.2, 77.9 (d, *J* = 7.9 Hz), 77.7, 77.6, 37.0 (d, *J* = 60.7 Hz), 27.1; ^{31}P{^{1}H} NMR ($CDCl_3$, 162 MHz): δ = 62.27; MALDI-TOF MS+: *m/z* 981.22 ($[M]^+$, $C_{63}H_{52}FeN_5PO$ requires: 981.33).

***c*-P5$_{t\text{-Bu}}$·T5**

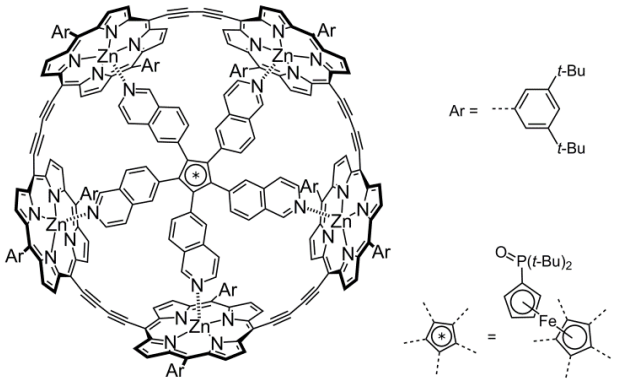

***l*-P1$_{t\text{-Bu}}$(H,H)** (31 mg, 38 μmol) and **T5** (7.5 mg, 7.7 μmol) were dissolved in toluene (700 mL). DIPA (7.5 mL) was added and the solution was stirred for 3 h. $PdCl_2(PPh_3)_2$ (70 mg, 0.10 mmol), CuI (75 mg, 0.19 mmol) and 1,4-benzoquinone (90 mg, 0.83 mmol) were added into the solution and the mixture was stirred at room temperature overnight. The mixture was filtered through basic Al_2O_3 and the solvent was evaporated. The residue was separated through size-exclusion column (Biobeads SX-1, 35 × 300 mm) and the second band was collected. The first (major) band was larger porphyrin nanorings and linear oligomers. The solvent was removed under vacuum and the residue was precipitated with DCM/MeOH to give the product as black solid (1.52 mg, 4.0%).

^{1}H NMR (500 MHz, CD_2Cl_2): 9.54 (d, *J* = 4.4 Hz, 10H), 9.52 (d, *J* = 4.4 Hz, 10H), 8.75 (d, *J* = 4.4 Hz, 10H), 8.73 (d, *J* = 4.4 Hz, 10H), 7.97 (t, *J* = 1.5 Hz, 5H), 7.91 (t, *J* = 1.5 Hz, 5H), 7.85 (t, *J* = 1.5 Hz, 5H), 7.79 (t, *J* = 1.5 Hz, 5H), 7.78 (t, *J* = 1.5 Hz, 5H), 7.70 (t, *J* = 1.5 Hz, 5H), 5.70 (s, 5H), 5.30 (d, *J* = 9.0 Hz, 5H), 5.01 (d, *J* = 9.0 Hz, 5H), 4.87 (d, *J* = 6.2 Hz, 5H), 3.24 (s, 2H), 2.80 (s, 2H), 2.69 (s, 5H), 1.86 (d, *J* = 6.2 Hz, 5H), 1.54 – 1.36 (m, 180H), -0.25 (d, *J* = 13.8 Hz, 18H); ^{31}P{^{1}H} NMR (CD_2Cl_2, 162 MHz): δ = 59.78; MALDI-TOF MS+: *m/z* 4953 ($[M]^+$, $C_{323}H_{302}FeN_{25}Zn_5PO$ requires: 4963), 3978 ($[M\text{-}\mathbf{T5}]^+$, $C_{260}H_{250}N_{20}Zn_5$ requires: 3982); UV-vis (toluene): λ_{max} (ε) 431 (2.5 × 10^5), 494 (4.0 × 10^5), 756 (2.2 × 10^5), 794 (2.2 × 10^5), 837 (1.8 × 10^5).

***c*-P5$_{t\text{-Bu}}$**

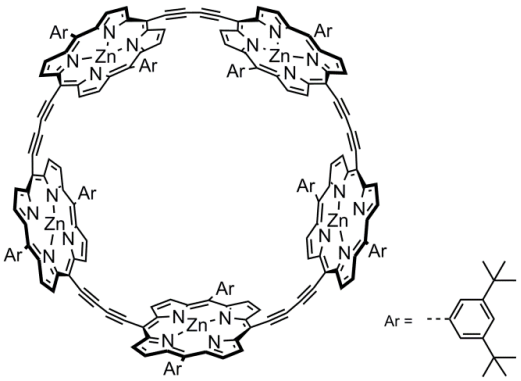

***c*-P5$_{t\text{-Bu}}$·T5** (2.0 mg, 0.40 μmol) was dissolved in toluene/pyridine (2/1, *v/v*) and the solution was applied through a size-exclusion column (Biobeads SX-1, 10 × 300 mm) with toluene/pyridine (2/1, *v/v*). The major band was collected and the solvent was evaporated. The desired product was obtained as black solid (1.5 mg, 94%).

^{1}H NMR (400 MHz, $CDCl_3$): δ = 9.49 (d, *J* = 4.5 Hz, 20H), 8.68 (d, *J* = 4.5 Hz, 20H), 7.81 (d, *J* = 1.6 Hz, 20H), 7.71 (d, *J* = 1.6 Hz, 10H), 1.44 (s, 180H); MALDI-TOF MS+: *m/z* 3974 ($[M]^+$, $C_{260}H_{250}N_{20}Zn_5$ requires: 3982); UV-vis (toluene): λ_{max} (ε) 430 (2.4×10^5), 489 (4.0×10^5), 719 (1.6×10^5), 747 (1.7×10^5).

***c*-P5$_{OOct}$·T5**

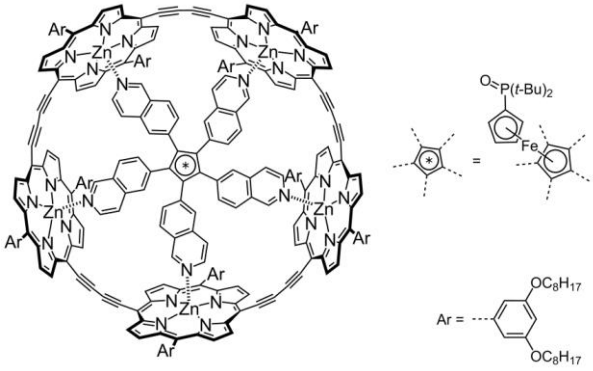

***l*-P1$_{OOct}$(H,H)** (42 mg, 38 μmol) and **T5** (7.5 mg, 7.7 μmol) were dissolved in toluene (700 mL). DIPA (7.5 mL) was added and the solution was stirred for 3 h. $PdCl_2(PPh_3)_2$ (70 mg, 0.10 mmol), CuI (75 mg, 0.19 mmol) and 1,4-benzoquinone (90 mg, 0.83 mmol) were added into the solution and the mixture was stirred at room temperature overnight. The mixture was filtered through basic Al_2O_3 and the solvent was evaporated. The residue was separated through size-exclusion column

(Biobeads SX-1, 25 × 1000 mm) to remove small molecules. Recycling GPC (Shimadzu recycling GPC system equipped with LC-20 AD pump, SPD-20A UV detector and a set of JAIGEL 3H (20 × 600 mm) and JAIGEL 4H (20 × 600 mm) columns in toluene/1% pyridine as eluent, flow rate 3.5 mL/min) gave the product as black solid (0.86 mg, 1.7%).

^{1}H NMR (500 MHz, CD_2Cl_2): 9.53 (d, *J* = 4.4 Hz, 10H), 9.50 (d, *J* = 4.4 Hz, 10H), 8.80 (d, *J* = 4.4 Hz, 20H), 7.16 – 7.09 (m, 20H), 6.83 (t, *J* = 1.5 Hz, 5H), 6.81 (t, *J* = 1.5 Hz, 5H), 5.68 (s, 5H), 5.28 (d, *J* = 9.0 Hz, 5H), 5.01 (d, *J* = 9.0 Hz, 5H), 4.88 (d, *J* = 6.2 Hz, 5H), 4.10 – 4.00 (m, 40H), 3.29 (s, 2H), 2.81 (s, 2H), 2.71 (s, 5H), 1.84 – 0.70 (m, 302H), -0.24 (d, *J* = 13.8 Hz, 18H); ^{31}P{^{1}H} NMR (CD_2Cl_2, 162 MHz): δ = 60.14; MALDI-TOF MS+: *m/z* 6404 ([M]$^+$, $C_{403}H_{462}FeN_{25}Zn_5PO_{21}$ requires: 6405), 5422 ([M-**T5**]$^+$, $C_{340}H_{410}N_{20}O_{20}Zn_5$ requires: 5424); UV-vis (toluene): λ_{max} (ε) 431 (2.4×10^5), 494 (4.0×10^5), 749 (2.2×10^5), 785 (2.2×10^5), 828 (1.9×10^5).

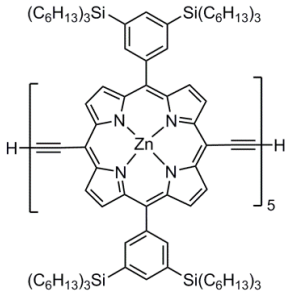

Zinc(II) 5,15-bis-(3,5-bis-trihexylsilyl)-10,20-bis-trihexylsilylethynylporphyrin pentamer *l*-P5$_{THS}$(H,H), **P5$_H$** in **Chapter 5**

Zinc(II) 5,15-bis-(3,5-bis-trihexylsilyl)-10,20-bis-ethynylporphyrin pentamer (***l*-P5$_{THS}$(THS,THS)**, 6.5 mg, 0.71 μmol) was dissolved in DCM (1.5 mL, 1% pyridine v/v). TBAF (1 M in THF, 12 μL, 12 μmol) was added into the solution and the mixture was stirred at r.t. for 15 min. MeOH (5 mL) was added to quench the reaction and stir continued for another 10 min to give the product as precipitate. The product was separated from the mixture by microfiltration; and was then plugged through silica with DCM, dried, washed with methanol and finally dried under high vacuum. ***l*-P5$_{THS}$(H,H)** was obtained as black powder (5.2 mg, 86%).

^{1}H NMR (400 MHz, $CDCl_3$/1% pyridine-d_5): δ = 9.83 – 9.81 (m, 16H), 9.61 (d, *J* = 4.6 Hz, 4H), 8.90 – 8.88 (m, 16H), 8.81 (d, *J* = 4.6 Hz, 4H), 8.25 (s, 12H), 8.21 (s, 8H), 7.97 (s, 5H), 7.94 (s, 5H), 4.12 (s, 2H), 1.46 – 0.81 (m, 780H); MALDI-TOF MS+: m/z 8519 ([M]$^+$, $C_{540}H_{852}N_{20}Si_{20}Zn_5$ requires: 8514).

6.4 References

[1] P. Neuhaus, A. Cnossen, J. Q. Gong, L. M. Herz, H. L. Anderson, *Angew. Chem. Int. Ed.* **2015**, *54*, 7344–7348.

[2] D. Lehnherr, J. Gao, F. A. Hegmann, R. R. Tykwinski, *Org. Lett.* **2008**, *10*, 4779–4782.

[3] J. K. Laha, S. Dhanalekshmi, M. Taniguchi, A. Ambroise, J. S. Lindsey, *Org. Process Res. Dev.* **2003**, *7*, 799−812.

[4] C. Brückner, J. J. Posakony, C. K. Johnson, R. W. Boyle, B. R. James, D. Dolphin, *J. Porphyrins Phthalocyanines* **1998**, *2*, 455–465.

[5] J. D. Megiatto, Jr., D. I. Schuster, S. Abwandner, G. de Miguel, D. M. Guldi, *J. Am. Chem. Soc.* **2010**, *132*, 3847–3861.

[6] S. G. DiMagno, V. S.-Y. Lin, M. J. Therien, *J. Am. Chem. Soc.* **1993**, *115*, 2513–2515.

[7] R. Chinchilla, C. Nájera*, Chem. Soc. Rev.* **2011**, *40*, 5084–5121.

[8] P. N. Taylor, H. L. Anderson, *J. Am. Chem. Soc.* **1999**, *121,* 11538–11545.

[9] J. Zhu, R. Beugelmans, S. Bourdet, J. Chastanet, G. Roussi, *J. Org. Chem.* **1995**, *60*, 6389–6396.

[10] P. B. Rheiner, D. Seebach, *Chem. Eur. J.* **1999**, *5*, 3221–3236.

[11] M. U. Winters, E. Dahlstedt, H. E. Blades, C. J. Wilson, M. J. Frampton, H. L. Anderson, B. Albinsson, *J. Am. Chem. Soc.* **2007**, *129*, 4291–4297.

[12] J. K. Sprafke, D. V. Kondratuk, M. Wykes, A. L. Thompson, M. Hoffmann, R. Drevinskas, W.-H. Chen, C. K. Yong, J. Kärnbratt, J. E. Bullock, M. Malfois, M. R. Wasielewski, B. Albinsson, L. M. Herz, D. Zigmantas, D. Beljonne, H. L. Anderson, *J. Am. Chem. Soc.* **2011**, *133*, 17262–17273.

[13] K. Takeo, K. Ueraura, H. Mitoh, *J. Carbohydr. Chem.* **1988**, *7*, 293–308.

[14] P. R. Ashton, E. Y. Hartwell, D. Philp, N. Spencer, J. F. Stoddart, *J. Chem. Soc., Perkin Trans. 2* **1995**, 1263–1277.

[15] C. S. Marvel, L. E. Coleman, G. P. Scott, *J. Org. Chem.* **1955**, *20*, 1785–1792.

[16] L. A. Babadzhanova, N. V. Kirij, Y. L. Yagupolskii, W. Tyrra, D. Naumann, *Tetrahedron* **2005**, *61*, 1813–1819.

[17] C. Genès, S. Michel, F. Tillequin, F.-H. Porée, *Tetrahedron* **2009**, *65*, 10009–10015.

[18] Q. Wang, E. Lucien, A. Hashimoto, G. C. G. Pais, D. M. Nelson, Y. Song, J. A. Thanassi, C. W. Marlor, C. L. Thoma, J. Cheng, S. D. Podos, Y. Ou, M. Deshpande, M. J. Pucci, D. D. Buechter, B. J. Bradbury, J. A. Wiles, *J. Med. Chem.* **2007**, *50*, 199–210.

[19] C. A. Busacca, M. C. Eriksson, N. Haddad, Z. S Han, J. C. Lorenz, B. Qu, X. Zeng, C. H. Senanayake, *Org. Synth.* **2013**, *90*, 316–326. (Checked by C. M. Reeves and B. M. Stoltz)

[20] M. S. Inkpen, S. Du, M. Driver, T. Albrecht, N. J. Long, *Dalton Trans.* **2013**, *42*, 2813–2816.

[21] I. R. Butler, *Inorg. Chem. Commun.* **2008**, *11*, 15–19.

[22] K. Sünkel, S. Bernhartzeder, *J. Organomet. Chem.* **2011**, *696*, 1536–1540.

[23] F. Hinderer, U. H. F. Bunz, *Chem. Eur. J.* **2013**, *19*, 8490–8496.

Appendix

S.1 Calculation of Statistical Factor[S1]

In a chemical process where A and B react to give C and D:

$$A + B \overset{K}{\rightleftharpoons} C + D$$

The observed equilibrium constant (K) can be expressed in terms of the partition functions (Q_i) of each species:

$$K = \frac{Q_C Q_D}{Q_A Q_B} = \frac{Q'_C Q'_D}{Q'_A Q'_B} \cdot \frac{\sigma_A \sigma_B}{\sigma_C \sigma_D} = K_{chem} \cdot K_\sigma \quad (S.1)$$

where $K_\sigma = \frac{\sigma_A \sigma_B}{\sigma_C \sigma_D}$

Statistical factor (K_σ) is the value connecting the observed equilibrium constants (K) with intrinsic equilibrium constants (K_{chem}, which is determined by the chemical nature of the process). K_σ can be calculated through the symmetry numbers (σ) of the species involved in the process.[S2,S3] The symmetry number of a species consists of two parts: internal symmetry number (σ_{int}) and external symmetry number (σ_{ext}).

$$\sigma = \sigma_{int} \cdot \sigma_{ext} \quad (S.2)$$

The internal symmetry number (σ_{int}) describes the symmetry of the molecule due to the rotation about internal bonds (without rotation of the molecule as a whole). It is the number of non-identical but indistinguishable positions generated in the course of 360° rotation of internal rotors.

The external symmetry number (σ_{ext}) describes the symmetry of the molecule due to the rotation of the molecule as a whole. It is determined by the point group, which is shown in **Table S.1**.[S1]

Table S.1 Symmetry point group and external symmetry number in this thesis.

Point group	σ_{ext}
C_s	1
C_n, C_{nv}	n
D_{nh}	$2n$
$C_{\infty v}$	1
$D_{\infty h}$	2

S.2 Calculation of 1:1 Binding Isotherm Model

For the formation of a 1:1 complex between ligand L and the porphyrin host P:

$$K_{\mathrm{L}} = \frac{[\mathrm{C}]}{[\mathrm{P}][\mathrm{L}]} \tag{S.3}$$

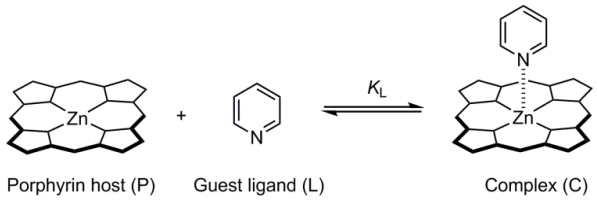

Figure S.1 Formation of a host-guest complex by a zinc-porphyrin (host) and pyridine (guest). The nitrogen atoms, double bonds and substituents are omitted for clarity.

Assume this is the only chemical reaction between the components:

$$[\mathrm{L}] = [\mathrm{L}]_0 - [\mathrm{C}] \tag{S.4}$$

$$[\mathrm{P}] = [\mathrm{P}]_0 - [\mathrm{C}] \tag{S.5}$$

where $[\mathrm{L}]_0$ and $[\mathrm{P}]_0$ are the total concentration of the guest ligand and the porphyrin host in the system and they are known in the titrations.

Substituting eq. (S.4) and (S.5) into eq. (S.3) and rearrangement gives:

$$K_{\mathrm{L}}[\mathrm{C}]^2 - (K_{\mathrm{L}}([\mathrm{L}]_0 + [\mathrm{P}]_0) + 1)[\mathrm{C}] + K_{\mathrm{L}}[\mathrm{L}]_0[\mathrm{P}]_0 = 0 \tag{S.6}$$

Solving the quadratic equation gives:

$$[\mathrm{C}] = \frac{(K_{\mathrm{L}}([\mathrm{L}]_0 + [\mathrm{P}]_0) + 1) \pm \sqrt{(K_{\mathrm{L}}([\mathrm{L}]_0 + [\mathrm{P}]_0) + 1)^2 - 4{K_{\mathrm{L}}}^2[\mathrm{L}]_0[\mathrm{P}]_0}}{2K_{\mathrm{L}}} \tag{S.7}$$

The site occupancy θ of the colored species is the proportion of bound porphyrin in the total concentration of porphyrin in the system.

$$\theta = \frac{[\mathrm{C}]}{[\mathrm{P}]_0} = \frac{(K_{\mathrm{L}}([\mathrm{L}]_0 + [\mathrm{P}]_0) + 1) \pm \sqrt{(K_{\mathrm{L}}([\mathrm{L}]_0 + [\mathrm{P}]_0) + 1)^2 - 4{K_{\mathrm{L}}}^2[\mathrm{L}]_0[\mathrm{P}]_0}}{2K_{\mathrm{L}}[\mathrm{P}]_0} \tag{S.8}$$

When θ = 0, the system is at the initial state of titration and all porphyrin species are at unbound state. At a specific wavelength, the absorption $A_{initial}$ can be calculated as:

$$A_{initial} = \varepsilon_{\mathrm{P}}[\mathrm{P}]_0 l \tag{S.9}$$

where ε_{P} is the extinction coefficient of unbound P at a specific wavelength, l is the length of measuring cuvette in the experiment.

When θ = 1, the system is at the final state of titration and all porphyrin species are at bound state. At the same wavelength as described in eq. (S.9), the absorption A_{∞} can be calculated as:

$$A_\infty = \varepsilon_C[P]_0 l \tag{S.10}$$

In the process of the titration, the absorption A can be calculated as:

$$A = \varepsilon_P[P]l + \varepsilon_C[C]l = \varepsilon_P([P]_0 - [C])l + \varepsilon_C[C]l \tag{S.11}$$

Rearrangement of eq. (S.11) and substituting into (S.8) gives:

$$\frac{A - A_{initial}}{A_\infty - A_{initial}} = \left(\frac{(K_L([L]_0 + [P]_0) + 1) \pm \sqrt{(K_L([L]_0 + [P]_0) + 1)^2 - 4K_L^2[P]_0[L]_0}}{2K_L[P]_0} \right) \tag{S.12}$$

Trial of the two equations in eq. (S.12) in the states (θ = 0 – 1) of the titration indicates the right one, which is the 1:1 binding isotherm model eq. (2.3):

$$\frac{A - A_{initial}}{A_\infty - A_{initial}} = \left(\frac{(K_L([L]_0 + [P]_0) + 1) - \sqrt{(K_L([L]_0 + [P]_0) + 1)^2 - 4K_L^2[P]_0[L]_0}}{2K_L[P]_0} \right) \tag{2.3}$$

$A_{initial}$ can be approximated to the first point of the titration; A_∞ can be approximated to the final point of the titration curve. Both $A_{initial}$ and A_∞ can be set as variables in the Origin software to give a better curve fitting result. It should be noted that the absorption used in the data processing procedure can also be the difference between two or even more wavelengths, which is frequently used since the method can eliminate baseline error in the calculation.[S4]

S.3 Calculation of *n*-Dentate Denaturation Isotherm Model

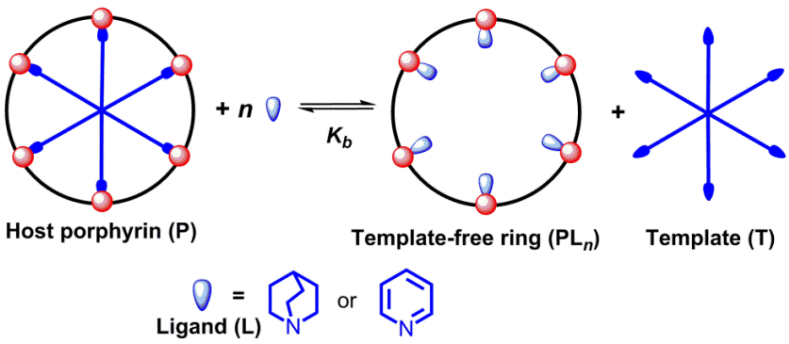

Figure S.2 Denaturation process of *n*-dentate template-nanoring complexes (*n* = 6 in this figure).

For the denaturation of the *n*-dentate ring-template complex (porphyrin host P) by ligand L:

$$K_b = \frac{[PL_n][T]}{[P][L]^n} \tag{S.13}$$

Assume there is no irreversible reaction between the components and that the starting ratio between P and T is exactly 1 to 1:

$$[\mathrm{PL}_n] = [\mathrm{T}] \tag{S.14}$$

The total concentration of porphyrin nanoring in the system $[\mathrm{P}]_0$ is:

$$[\mathrm{P}]_0 = [\mathrm{PL}_n] + [\mathrm{P}] \tag{S.15}$$

As the denaturation requires a large excess (> 1000 fold) of monodentate ligand L compared to the host porphyrin, it is reasonable to assume that the concentration of the ligand in the equilibrium is the concentration of ligand added into the system:

$$[\mathrm{L}] = [\mathrm{L}]_0 - n[\mathrm{PL}_n] \approx [\mathrm{L}]_0 \tag{S.16}$$

Substituting eq. (S.14), (S.15) and (S.16) into eq. (S.13) and rearrangement give:

$$[\mathrm{PL}_n]^2 + K_\mathrm{b}[\mathrm{L}]^n[\mathrm{PL}_n] - K_\mathrm{b}[\mathrm{L}]^n[\mathrm{P}]_0 = 0 \tag{S.17}$$

Solving the quadratic equation gives:

$$[\mathrm{PL}_n] = \frac{-K_\mathrm{b}{[\mathrm{L}]_0}^n \pm \sqrt{K_\mathrm{b}^2{[\mathrm{L}]_0}^{2n} + 4K_\mathrm{b}{[\mathrm{L}]_0}^n[\mathrm{P}]_0}}{2} \tag{S.18}$$

As before, the site occupancy θ of the colored species (porphyrin nanoring) can be calculated as:

$$\frac{A - A_{initial}}{A_\infty - A_{initial}} = \frac{[\mathrm{PL}_n]}{[\mathrm{P}]_0} = \left(\frac{-K_\mathrm{b}{[\mathrm{L}]_0}^n \pm \sqrt{K_\mathrm{b}^2{[\mathrm{L}]_0}^{2n} + 4K_\mathrm{b}{[\mathrm{L}]_0}^n[\mathrm{P}]_0}}{2[\mathrm{P}]_0} \right) \tag{S.19}$$

Trial of the two equations in eq. (S.19) in the states (θ = 0 – 1) of the titration indicates the right one, which is the *n*-dentate denaturation isotherm model eq. (2.4):

$$\frac{A - A_{initial}}{A_\infty - A_{initial}} = \left(\frac{-K_\mathrm{b}{[\mathrm{L}]_0}^n + \sqrt{K_\mathrm{b}^2{[\mathrm{L}]_0}^{2n} + 4K_\mathrm{b}{[\mathrm{L}]_0}^n[\mathrm{P}]_0}}{2[\mathrm{P}]_0} \right) \tag{2.4}$$

S.4 D_{5h} Symmetry Approximation of T5

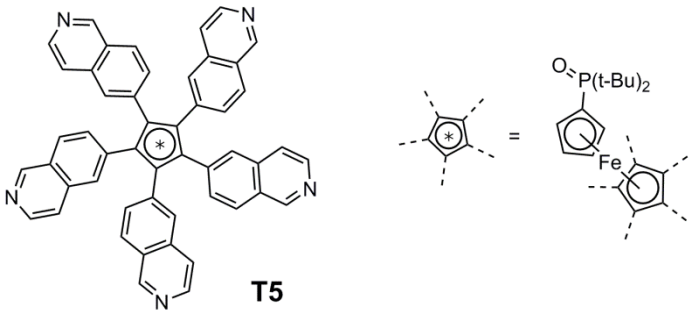

Figure S.3 The Chemical structure of **T5**.

As is shown in **Figure S.3**, only one of the two Cp rings is fully functionalized by 6-isoquinolinyl group. The other phosphine-functionalized Cp ring quickly rotates, as is revealed by the NMR spectra of **T5** (there are no differences between the signals of isoquinolinyl protons). The difference between the two faces of the template makes the symmetry of the molecule C_{5v}, as the molecule does not bear 5 perpendicular C_2 axes but there are 5 vertical reflection planes because of the fast rotation on the phosphine-functionalized Cp ring.

However, if **T5** is considered as C_{5v} symmetry in the calculation of statistical factors, many of the partially-bound complexes would be chiral. We use complex 3 (a partially-bound **P3·T5** complex with 2-site binding mode) as the example to illustrate the situation that an approximation is needed to simplify the calculation of statistical factors of the complexes in the host-guest systems.

As is shown in **Figure S.4**, the partially-bound **P3·T5** complex with 2-site binding mode has two isomers: complex 3a with green dot in the center of **T5** (representing the phosphine-functionalized Cp ring pointing up), and complex 3b with pink dot in the center of **T5** (representing the phosphine-functionalized Cp ring pointing down). Using this approach, the formation constant of complex 3 is the sum of the two isomers: $K_{f(complex\ 3)} = 80K_{chem2}$.

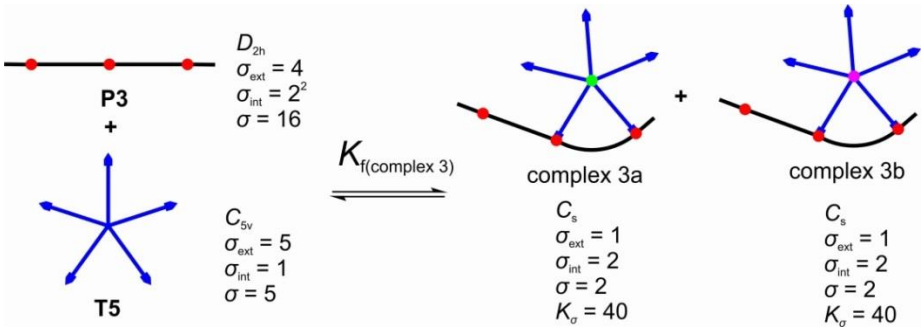

Figure S.4 Calculation of $K_{f(complex\ 3)}$ using the method with **T5** as C_{5v} symmetry.

If the phosphine-functionalized Cp ring is regarded as a single dot which does not give the difference between the two faces of **T5**, then the molecule bears 5 perpendicular C_2 axes as well as a horizontal reflection plane, making the molecule as D_{5h} symmetry. The calculation of $K_{f(complex\ 3)}$ has been shown in **Figure 5.15**; and the result is identical to the result shown in **Figure S.4**.

As the bindings are never affected by the phosphine-functionalized Cp ring, the approximation has generality in all the calculations of the statistical factors of the complexes in the host-guest systems.

S.5 References

[S1] C. A. Hunter, H. L. Anderson, *Angew. Chem. Int. Ed.* **2009**, *48*, 7488–7499.

[S2] S. W. Benson, *J. Am. Chem. Soc.* **1958**, *80*, 5151–5154.

[S3] W. F. Bailey, A. S. Monahan, *J. Chem. Educ.* **1978**, *55*, 489–493.

[S4] H. L. Anderson, S. Anderson, J. K. M. Sanders, *J. Chem. Soc., Perkin Trans. 1* **1995**, 2231–2245.